

Diss. ETH No. 25338

Carole Guggenheim

The Role of Copper for Methane-Oxidizing Bacteria in Lakes

Carole Selma Guggenheim

Dissertation ETH No. 25338

2018

DISS. ETH No. 25338

The Role of Copper for Methane-Oxidizing Bacteria in Lakes

A thesis submitted to attain the degree of
DOCTOR OF SCIENCES of ETH Zurich
(Dr. sc. ETH Zurich)

presented by
CAROLE SELMA GUGGENHEIM
M. Sc. Chemistry, University of Zurich

born on 27.07.1983
citizen of Zurich, Switzerland

accepted on the recommendation of
Prof. Dr. Bernhard Wehrli
Dr. Helmut Bürgmann
Prof. Dr. Laura Sigg
Prof. Dr. Martin Ackermann

2018

Book cover:

Rotsee Bathymetry, André Lotter, Dissertationes Botanicae, 1988

“Paläoökologische und paläolimnologische Studie des Rotsees bei Luzern.

Pollen-, grossrest-, diatomeen- und sedimentanalytische Untersuchungen“

This work is dedicated to my grandmothers

Rita Guggenheim-van Kollem and Clara Feinstein-Rosenberg,

who have always been moving spirits during different periods of my life.

Table of contents

Summary	i
Zusammenfassung	iii
Chapter 1 – Introduction	1
Introduction	2
Methane-oxidizing bacteria	5
The role of copper and iron	15
Objectives and outline	19
Analysing the link between copper and MOB	22
Chapter 2 – Aerobic methane oxidation under copper scarcity in a stratified lake	27
Chapter 3 – Environmental and microbial interactions shaping methane-oxidizing communities in a stratified sub-alpine lake	59
Chapter 4 – Activity of aerobic methane-oxidizing bacteria under nanomolar copper additions	105
Chapter 5 – Conclusions and outlook	133
Bibliography	145
Acknowledgements	157
Curriculum vitae	160

Summary

Aerobic methane-oxidizing bacteria (MOB) have the ability to thrive on methane, a potent greenhouse gas with critical climatic implications. They use methane as their sole source of carbon and energy. They phylogenetically mainly group as *Alpha*- and *Gammaproteobacteria*, as well as *Verrucomicrobia*. The metalloenzyme methane-monooxygenase (MMO) catalyses the initial oxidation step, the conversion of methane to methanol. The membrane-bound, particulate MMO (pMMO) is widespread among MOB, however, its atomic structure and active site composition remains a matter of debate. Nevertheless, it is generally agreed that pMMO is a copper-dependent enzyme.

Freshwater lakes are significant contributors to global natural methane emissions. However, MOB inhabiting their water column substantially reduce methane fluxes from the sediments to the atmosphere. MOB are commonly highly enriched at oxic-anoxic transition zones, but increasing evidence suggests that methane oxidation by MOB is also occurring at depths depleted in oxygen.

MOB ecology has been previously investigated in different lake systems, nevertheless field-based studies linking the structure of MOB and different enzymatic oxidation pathways with copper availability as a key driver are so far lacking. In addition, MOB possess several storage and extracellular copper acquisition mechanisms, which potentially play an important role to facilitate the pMMO methane oxidation pathway under copper limitation. The goal of this dissertation was to improve the understanding of the copper requirement of MOB and to clarify the role of copper as a controlling micronutrient in microbial methane oxidation in freshwater systems. Furthermore, additional physico-chemical and biological variables influencing MOB community assembly were explored *in-situ*. We conducted laboratory experiments with an axenic MOB culture, as well as spatio-temporal sampling campaigns on a freshwater lake, and applied a combination of geochemical techniques and molecular biology approaches.

In eutrophic Rotsee, we found overall low nanomolar concentrations of biological available and dissolved copper. Gammaproteobacterial MOB containing the gene for the pMMO oxidation pathway were highly accumulated at zones with assumed highest methane oxidation activity. At similar depths, bioavailable copper

concentrations were significantly reduced and particulate copper showed maximum values. Besides MOB, other biological processes and abiotic reactions have a profound effect on the distribution and availability of copper. Especially oxygenic phototrophs appeared to compete for copper in methane oxidation zones. Hence, MOB had to cope with copper scarcity, which may have furthered MOB to make use of their storage and copper acquisition strategies to maintain pMMO expression.

Copper storage mechanisms might play an important role in the conducted laboratory experiments with an axenic MOB culture. Therein, low bioavailable copper conditions did not limit MOB growth and methane consumption activity, which confirms the results of MOB being abundant at low *in-situ* copper concentrations. However, different copper amendments did not show significant influence on growth rates and methane oxidation, whereas biomass associated copper and deduced cellular elemental stoichiometry increased with higher copper addition. This indicates a copper storage mechanism in MOB, which probably acts as a “buffer” under scarce copper conditions.

Besides copper, methane and oxygen, other physico-chemical parameters, as well as the total bacterial community have a profound impact on MOB structuring in lacustrine systems. Anyway, isolated abiotic factors only explained a small percentage of MOB variability in Rotsee when analysed in conjunction with bacterial communities. MOB were well integrated into modular bacterial co-occurrence networks along the depth gradient. Positive bacterial interactions accounted for 22% of the MOB community structure. Considering both, physico-chemical and bacterial relationships, we could explain up to 60% of variance in MOB occurrence and diversity within the water column. Hence, in addition to geochemical parameters, microbial interactions are likely to play a considerable part in structuring the MOB community *in-situ*.

Altogether, the results of this thesis highlight the importance of copper as a relevant factor for aerobic methane oxidation, which needs to be included in future studies of MOB diversity and activity studies in environmental systems. MOB survival mechanisms should be further investigated to better understand MOB performance under low copper supply. Furthermore, additional knowledge of the complex interactions between MOB and their physico-chemical as well as biological environment is necessary to better value their crucial ecosystem service in the light of a continuously changing climate.

Zusammenfassung

Methan ist ein starkes Treibhausgas mit kritischen klimatischen Auswirkungen. Aerobe Methan oxidierende Bakterien (MOB) haben die Fähigkeit, Methan als einzige Kohlenstoff- und Energiequelle zu nutzen. Phylogenetisch werden sie hauptsächlich in *Alpha*- und *Gammaproteobakterien* sowie *Verrucomicrobia* eingeteilt. Das Enzym Methan-Monooxygenase (MMO) katalysiert den ersten Oxidationsschritt, die Umsetzung von Methan zu Methanol. Die membrangebundene, partikuläre MMO (pMMO) ist unter MOB weit verbreitet, jedoch sind seine chemische Struktur und die Zusammensetzung seines aktiven Zentrums weiterhin umstritten. Nichtsdestotrotz besteht ein allgemeiner Konsens, dass pMMO ein kupferabhängiges Enzym ist.

Süßwasserseen tragen wesentlich zu den globalen natürlichen Methanemissionen bei. Die in ihrer Wassersäule lebenden MOB konsumieren eine erhebliche Menge an Methan, welches aus den Sedimenten austritt, und andernfalls in die Atmosphäre gelangen würde. MOB findet man normalerweise stark angereichert in oxisch-anoxischen Übergangszonen, es gibt jedoch zunehmend Hinweise, dass Methanoxidation durch MOB auch in sauerstoffarmen Tiefen stattfindet.

Das Verhalten von MOB Gemeinschaften wurde bereits in verschiedenen Seen untersucht. Allerdings wurden noch keine Feldstudien durchgeführt, welche die Struktur von MOB mit verschiedenen enzymatischen Oxidationswegen in Zusammenhang mit der Kupferverfügbarkeit in Verbindung setzen. MOB besitzen Speicher- und extrazelluläre Kupferaufnahmemechanismen, welche möglicherweise eine wichtige Rolle für die Methanoxidation mittels pMMO bei tiefen Kupferkonzentrationen spielen. Das Ziel dieser Dissertation war es, unser Verständnis des Kupferbedarfs von MOB zu vertiefen und die Rolle von Kupfer als kontrollierenden Mikronährstoff in der mikrobiellen Methanoxidation in Seen zu klären. Darüber hinaus wurden weitere physikalisch-chemische und biologische Variablen untersucht, die die *in-situ* Struktur der MOB-Gemeinschaft beeinflussen. Laborexperimente mit einer MOB Reinkultur sowie räumlich und zeitlich aufgelöste Probenahmen in einem Süßwassersee wurden durchgeführt, und eine Kombination aus geochemischen und molekularbiologischen Ansätzen angewandt.

Im eutrophen Rotsee wurden insgesamt niedrige nanomolare Konzentrationen von biologisch verfügbarem und gelöstem Kupfer nachgewiesen. Gammaproteobakterielle MOB, die das Gen für den pMMO Oxidationsmechanismus enthalten, wurden in Bereichen mit höchsten Methanoxidationsaktivitäten gefunden. In ähnlichen Tiefen waren die bioverfügbaren Kupferkonzentrationen deutlich reduziert und partikuläres Kupfer zeigte maximale Werte. Neben MOB beeinflussen auch andere biologische Prozesse und abiotische Reaktionen die Verteilung und Verfügbarkeit von Kupfer. Besonders Sauerstoff freisetzende Phototrophe scheinen in den Methanoxidationszonen um Kupfer zu konkurrieren. Um die Kupferknappheit zu mildern, könnten MOB ihre Speicher- und Kupfererwerbsstrategien zur Aufrechterhaltung der pMMO Expression nutzen.

Kupferspeichermechanismen könnten auch eine wichtige Rolle in den durchgeführten Laborexperimenten mit einer MOB Reinkultur spielen. Dort haben niedrige bioverfügbare Kupferbedingungen das Wachstum von MOB und deren Methanverbrauchsaktivität nicht signifikant beeinflusst. Dies bestätigt die vorausgegangen Resultate, dass MOB bei niedrigen *in-situ* Kupferkonzentrationen reichlich vorhanden sind. Unterschiedliche Kupferzugaben zeigten jedoch keinen signifikanten Einfluss auf die Wachstumsraten und die Methanoxidation, während das in der Biomasse enthaltene Kupfer und die zelluläre Elementstöchiometrie bei höherer Kupferzugabe erheblich anstiegen. Dies deutet auf einen Kupferspeichermechanismus von MOB hin, der unter knappen Kupferbedingungen wahrscheinlich als "Puffer" fungiert.

Neben Kupfer, Methan und Sauerstoff haben andere physikalisch-chemische Parameter sowie die gesamte bakterielle Gemeinschaft einen starken Einfluss auf die Strukturierung von MOB in Süßgewässern. Abiotische Faktoren allein erklärten nur einen geringen Prozentsatz der MOB-Variabilität im Rotsee, wenn ihre Gesamtheit mit der bakteriellen Gemeinschaft betrachtet wird. MOB waren gehäuft in Netzwerken aus anderen Bakterien entlang des Tiefengradienten integriert. Positive bakterielle Interaktionen machten 22% der MOB-Gemeinschaftsstruktur aus. Betrachtet man aber physikalisch-chemische Faktoren in Zusammenhang mit der bakteriellen Gesamtgemeinschaft, können wir das Auftreten und die Diversität von MOB in der Wassersäule auf bis zu 60% erklären. Diese Ergebnisse deuten darauf hin, dass mikrobielle Interaktionen neben geochemischen Parametern eine wesentliche Rolle bei der *in-situ* Strukturierung von MOB Gemeinschaften spielen.

Die erzielten Ergebnisse konnten die Bedeutung von Kupfer als wichtigen Faktor für die aerobe Methanoxidation aufzeigen. In zukünftigen Studien sollte der Einfluss von Kupfer auf die Diversität und Aktivität von MOB in Umweltsystemen miteinbezogen werden. Überlebensmechanismen von MOB sollten weiter untersucht werden, um deren Leistung bei niedriger Kupferversorgung besser zu verstehen. Darüber hinaus ist zusätzliches Wissen über die komplexen Wechselwirkungen zwischen MOB und ihrer physikalisch-chemischen sowie biologischen Umgebung notwendig, damit Ökosystemleistungen von MOB angesichts eines sich ständig verändernden Klimas besser bewertet werden können.

Chapter 1

Introduction

Introduction

The earth's weather and climate system are mainly driven by the power of the sun. The solar energy reaching our planet is either reflected off clouds, absorbed by the atmosphere, or to a greater extent passes through and reaches the earth's surface. To balance this incoming radiation, the earth must emit a similar amount of energy back to space. Greenhouse gases within the atmosphere are able to absorb some of this radiation and reflect it back, which heats our planet. This greenhouse effect is a natural process, allowing life on earth to exist. However, atmospheric greenhouse gas concentrations have steadily increased over the past few decades, since the beginning of the industrial revolution, mainly due to anthropogenic activities [Salawitch *et al.*, 2017]. Consequently, the rapid intensification of the natural greenhouse effect causes global warming [Stocker *et al.*, 2013].

Methane is the most abundant organic gas in earth's atmosphere, and following carbon dioxide, it is the second most abundant greenhouse gas (in ppb, $\mu\text{g L}^{-1}$) [Montzka *et al.*, 2011]. Atmospheric levels of methane, reconstructed from measurements on ice cores, have more than doubled in the last 250 years, from 720 ppb in 1750 to 1834 ppb in 2015 [Stocker *et al.*, 2013; Dlugokencky, 2017], and have never been this high over the past 650'000 years [Loulergue *et al.*, 2008]. Due to its long wavelength absorption characteristics, methane manifests a strong global warming potential, a measure of the relative heat trapping ability per mass unit and atmospheric life span of a specific gas. Over a 100 year time horizon, methane shows a warming potential 28 times larger than that of carbon dioxide [Myhre *et al.*, 2013]. Hence, the drastic rise in atmospheric methane has a severe impact on global warming ($40 \times 10^{-4} \text{ }^{\circ}\text{C (Gt CH}_4\text{)}^{-1}$ for a 100 year time horizon) and climate change [Reisinger *et al.*, 2010]

Methane sources and sinks

Sources of methane are widespread over the globe, with natural and anthropogenic emissions each estimated to supply roughly 50% of the total global emissions (736 Tg methane yr^{-1} , bottom-up models, Figure 1) [Kirschke *et al.*, 2013; Saunio *et al.*, 2016]. However, the absolute contribution of individual sources is still a matter of debate [Nisbet *et al.*, 2014] and some sources have even not been evaluated yet. According to their

production process, methane sources can be grouped into three categories: thermogenic, pyrogenic and biogenic, each showing a distinct isotopic signature [Wuebbles *et al.*, 2002; Conrad, 2009; Sapart *et al.*, 2013; Saunio *et al.*, 2016]. The three categories involve both, anthropogenic and natural components, albeit transitions are blurry.

Thermogenic methane is generated on geological timescales by the breakdown of buried organic matter at high temperatures and pressures [Stolper *et al.*, 2014]. It is vented from the subsurface into the atmosphere through natural gas seeps or through the exploitation of coal, gas, and oil [Tissot and Welte, 1984; Etiope and Klusman, 2002]. At each step along the processing line of fossil fuels (mining, transmission, distribution, processing) some fractions of methane are released to the atmosphere. Pyrogenic methane is produced by the incomplete combustion of organic (non-fossil) material, by for example, burning of forests, savannas, agricultural wastes, as well as soil carbon and biofuel, and is mainly confined to the tropics [Hao and Ward, 1993; Lelieveld *et al.*, 1998]. In recent years, the global atmospheric methane budget is dominated by the increase of methane produced in the biosphere [Aronson *et al.*, 2013; Nisbet *et al.*, 2016; Schaefer *et al.*, 2016]. In general, the prevailing mechanism contributing to biogenic methane is methanogenesis, the breakdown of organic matter mediated by methanogenic archaea [Conrad, 2007; Hedderich and Whitman, 2013]. These microorganisms are strict anaerobes and tolerate only environments with low redox potentials [Conrad, 2007]. They are either able to disproportionate acetate or utilize carbon dioxide as terminal electron acceptor [Wetzel, 2001b]. The most important biogenic methane producing systems are wetlands, freshwaters and oceans, rice paddies, landfills, waste-water facilities, or animal digestive systems [Conrad, 2009; Kirschke *et al.*, 2013]. Freshwater ecosystems such as wetlands, lakes and ponds are among the largest natural contributors of atmospheric methane release (Figure 1). Lakes are responsible for about 6-16% of the total natural global methane emissions [Bastviken *et al.*, 2004, 2011; Holgerson and Raymond, 2016], even though they only cover less than 4% of earth surface [Downing *et al.*, 2006]. Oceans, despite their size, only account for 1-4% to the annual methane flux [Cicerone and Oremland, 1988], and more recent studies even suggest contributions of less than 1% [Rhee *et al.*, 2009].

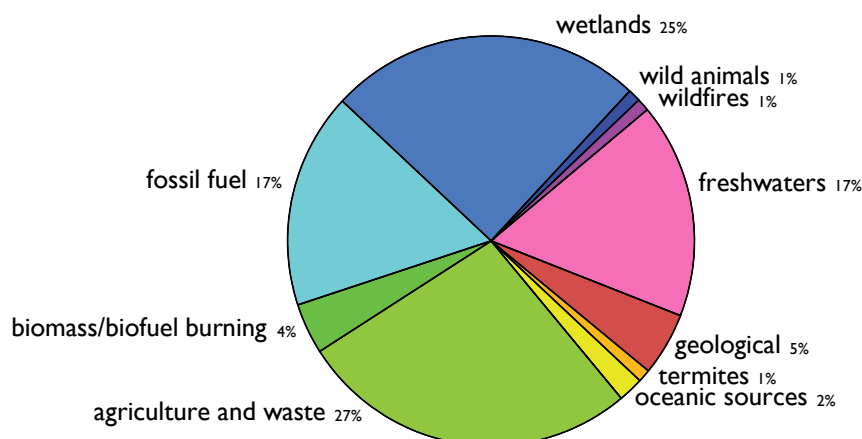


Figure 1. Global natural (right side) and anthropogenic (left side) methane emissions in per cent of the total atmospheric budget using the bottom-up model in [Saunio *et al.*, 2016].

The high abundance of oxygen in the atmosphere (21%) and its relatively high redox potential suggest that this gas is important for the oxidative removal of other gases. Nevertheless, direct reactions of molecular oxygen with gases such as methane are unimportant under atmospheric conditions, due to the large activation energy required. Instead, the primary natural sink for atmospheric methane is its partial oxidation by the highly reactive hydroxyl radical, which accounts for about 90% of the global methane removal [Ehhalt, 1974; Rigby *et al.*, 2017]. Other abiotic losses of methane are its reaction with chlorine and atomic oxygen radicals in the stratosphere [Cicerone and Oremland, 1988] or chlorine radicals deriving from sea salt in the marine boundary layer [Allan *et al.*, 2007]. The oxidation of methane in aerated soils by the activity of aerobic methanotrophic bacteria (also called methane-oxidizing bacteria and hereafter referred to as MOB) is the only known biotic sink for atmospheric methane [Curry, 2007]. Moreover, this specialized group of microorganisms is of particular importance in attenuating net fluxes of methane into the atmosphere in various ecosystems being sources of methane [Reeburgh, 2007; Conrad, 2009; Murrell, 2010; Semrau *et al.*, 2010; Knief, 2015]. For example within lacustrine systems, MOB act as an important natural methane filter and oxidize up to 90% of methane produced in these environments [Bastviken *et al.*, 2003, 2008]. Hence, due to the important role of lakes in the global methane cycle, investigating the involved organisms as well as understanding their driving forces is essential to better predict future climate change.

Methane-oxidizing bacteria

MOB are a diverse and a specialized group of prokaryotes [Hanson and Hanson, 1996; Kalyuzhnaya *et al.*, 2019]. They are a subset of the methylotrophic bacteria and have the unique ability to use methane as their sole source of carbon and energy [Chistoserdova and Kalyuzhnaya, 2018]. MOB growth efficiency is defined as the amount of biomass synthesized from methane being oxidized, and varies between 6-80% [Leak and Dalton, 1986a; King, 1992; Bastviken *et al.*, 2003]. The majority of extant MOB favour moderate conditions with pH values ranging from 5-8 (neutrophilic), temperatures between 20-37°C (mesophilic) and low salinity [Whittenbury *et al.*, 1970]. However, several species have been recently isolated from habitats featuring more extreme pHs (alkali-, acidophilic), temperatures (thermophilic) and salt concentrations (halophilic) [Trotsenko and Khmelenina, 2002; Trotsenko and Murrell, 2008; Op den Camp *et al.*, 2009; Nazaries *et al.*, 2013].

Taxonomy and phylogeny

MOB have been traditionally divided into two major groups (type I and type II) on the basis of their morphological and physiological characteristics [Whittenbury *et al.*, 1970]. Besides different carbon fixation pathways (ribulose monophosphate (RuMP) or serine pathway), they were distinguished by their internal membrane arrangement, their capability to fix nitrogen, the formation of resting stages, and to a certain degree on their predominant phospholipid fatty acid [Murrell, 2010].

Type X strains were previously considered a third group that included features from both other groups, but have been reclassified as being a subset of type I MOB [Bowman, 2006]. As the number of exceptional MOB increased during the last years, the initial concept by Whittenbury has no longer been useful to categorize all known MOB. It has even been proposed to abandon it [Op den Camp *et al.*, 2009; Semrau *et al.*, 2010]. Nevertheless, these terms are still frequently used, but have been further adapted to today's MOB diversity. Type I was subdivided into type Ia, Ib (previously described as type X), and Ic, type II into type IIa and IIb, respectively (Table 1) [Dumont *et al.*, 2014; Knief, 2015].

Phylogenetically MOB mainly belong to *Proteobacteria* and analyses of the 16S rRNA gene sequences have confirmed that type I and type X correspond to *Gammaproteobacteria* (γ -MOB), while type II group within the *Alphaproteobacteria* (α -MOB) [Rosenberg *et al.*, 2014a, 2014b]. Methane oxidizing *Gammaproteobacteria* consist of 18 cultivated genera within the families Methylococcaceae (type Ia and Ib) and Methylothermaceae (type Ic) and additional two genera so far only studied in natural enrichments (filamentous ‘*Candidatus* Clonothrix fucsa’ and ‘*Candidatus* Crenothrix polyspora’) [Vigliotta *et al.*, 2007; Oswald *et al.*, 2017]. The class of *Alphaproteobacteria* is less diverse with only five different genera within the families Methylocystaceae and Beijerinckiaceae [Rosenberg *et al.*, 2014a]. Methylobacterium might be genus number six, however, the ability of growing on methane must be treated with considerable scepticism as one of the species already lost this skill [Dedysh *et al.*, 2004; Gallego *et al.*, 2005; Kelly *et al.*, 2014]. Approximately 60 different species are referred to MOB in the phylum *Proteobacteria* [Knief, 2015].

MOB diversity was further expanded by the detection of species within the phylum *Verrucomicrobia* with two assigned genera in the family Methylacidiphilaceae [Op den Camp *et al.*, 2009; van Teeseling *et al.*, 2014; Knief, 2015]. They mostly lack the typical intracytoplasmic membranes and have distinct fatty acids. Verrucomicrobial MOB are often referred to as type III MOB. Cultured or sequenced representatives of the clade LD19 are still missing, however, a 16S-based phylogenetic analysis placed it as a sister group of Methylacidiphilaceae [Hugerth *et al.*, 2015]. The recently described ‘*Candidatus* Methylomirabilis oxyfera, sinica, and limnetica’ from the phylum NC10 are anaerobic methane-oxidizing bacteria [Knief, 2015]. They are assumed to use nitrite to internally generate oxygen to be able to oxidize methane via the conventional aerobic pathway [Ettwig *et al.*, 2010; He *et al.*, 2016].

Methane-oxidizing enzymes

Methane is one of the most difficult substrates to activate, with a C-H bond dissociation energy of 435 kJ mol⁻¹ [Culpepper and Rosenzweig, 2012]. MOB routinely carry out this reaction under ambient conditions by utilizing the methane monooxygenase (either soluble or particulate), which hydroxylates methane and initiates carbon assimilation (Figure 2) [Kroneck and Sosa Torres, 2015]. The oxidation of methane to methanol is followed by the formation of formaldehyde [Hanson and Hanson, 1996]. Roughly half of the carbon atoms

are then incorporated into cellular biomass either via the RuMP pathway or the serine cycle [Prior and Dalton, 1985; Trotsenko and Murrell, 2008]. The remainder is further oxidized to formate and ultimately ends up as carbon dioxide to generate reducing power for the initial oxidation of methane and for energy generation [Nazaries *et al.*, 2013]. Recently, a third pathway for carbon assimilation, the autotrophic fixation of carbon dioxide, commonly known as the Calvin-Benson-Bassham cycle, has been proposed for some proteobacterial and verrucomicrobial MOB, as well as for members in NC10 phylum [Khadem *et al.*, 2011; Rasigraf *et al.*, 2014].

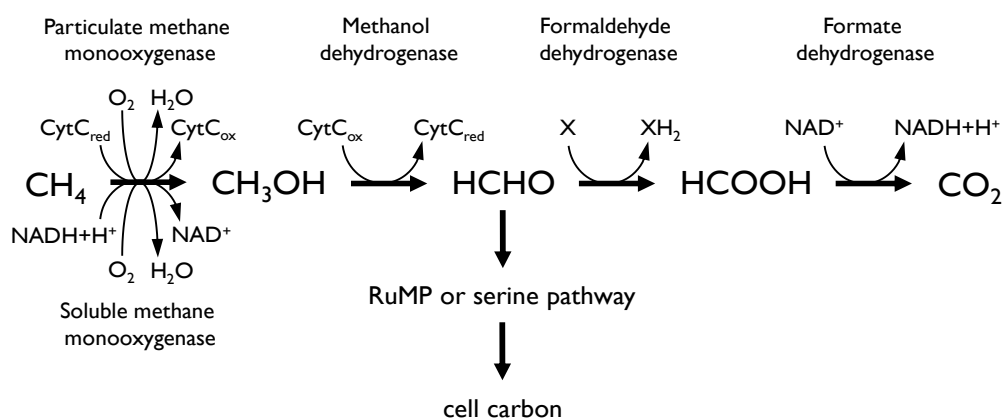


Figure 2. Enzymatic pathway of aerobic methane oxidation and carbon assimilation of proteobacterial methane-oxidizing bacteria. Adapted from [Nazaries *et al.*, 2013].

The methane monooxygenase (MMO) enzyme exists in two distinct forms, the transmembrane or particulate methane monooxygenase (pMMO) and the cytoplasmic or soluble methane monooxygenase (sMMO) [Ross and Rosenzweig, 2016]. pMMO appears to be widespread among MOB, whereas sMMO is only found in some organisms, typically in combination with pMMO (Table 1) [Murrell and Smith, 2010; Bowman, 2014]. The only known exception are members of the family *Beijerinckiaceae*, which solely possess sMMO [Dunfield *et al.*, 2003; Vorobev *et al.*, 2011; Marin and Ruiz Arahal, 2014].

Even though methane is the preferred substrate for MMOs, they also have the ability to oxidize other hydrocarbons [Colby *et al.*, 1977; Burrows *et al.*, 1984; Semrau, 2011; Sirajuddin and Rosenzweig, 2015]. sMMO can consume a wide range of hydrocarbons, including C1-C8 n-alkanes, alkenes, and larger substrates such as benzene, styrene, naphthalene, ethylbenzene, and cyclohexane and even halogenated hydrocarbons. pMMO has a narrower substrate range capable of oxidizing short chain alkanes, containing five or fewer

carbon atoms, and alkenes. Both enzymes demonstrate different methane affinities and kinetic behaviour. As pMMO is more specific and shows greater methane affinity, cells expressing pMMO display higher growth capabilities [Hanson and Hanson, 1996]. On the other hand, sMMO has a much higher methane turnover rate but lower affinity [Lee *et al.*, 2006].

Table 1. Taxonomic and physiological characteristics of aerobic and anaerobic methane-oxidizing bacteria.^a

Proteobacteria (p)	pMMO	sMMO	Proteobacteria (p)	pMMO	sMMO
<i>Gammaproteobacteria</i> (c)			<i>Alphaproteobacteria</i> (c)		
Methylococcaceae (f) - type Ia and Ib			Methylocystaceae (f) - type IIa		
<i>Methylobacter</i>	✓		<i>Methylocystis</i>	✓ ^b	(✓) some
<i>Methylocaldum</i>	✓	(✓) some	<i>Methylosinus</i>	✓ ^b	(✓) some
<i>Methylococcus</i>	✓	(✓) some	Beijerinckiaceae (f) - type IIb		
<i>Methylogaea</i>	✓		<i>Methylocapsa</i>	✓	
<i>Methyloglobulus</i>	✓		<i>Methylocella</i>		✓
<i>Methylomagnus</i>	✓	✓	<i>Methyloferula</i>		✓
<i>Methylomarinum</i>	✓		Methylobacteriaceae (f)		
<i>Methylomicrobium</i>	✓	(✓) some	<i>Methylobacterium</i> (lost ability to oxidize CH ₄)		
<i>Methylomonas</i>	✓	(✓) some			
<i>Methyloparacoccus</i>	✓		Verrucomicrobia (p)		
<i>Methyloprofundus</i>	✓		<i>Methylacidiphilae</i> (c) - type III		
<i>Methylosarcina</i>	✓		Methylacidiphilaceae (f)		
<i>Methylosoma</i>	✓		<i>Methylacidimicrobium</i>	✓	
<i>Methylosphaera</i>	✓		<i>Methylacidiphilum</i>	✓	
<i>Methylovulum</i>	✓	✓	LD19 (f) (probably lacks <i>pmoA</i>)		
<i>Candidatus Clonothrix fusca</i>	✓				
Methylothermaceae (f) - type Ic			Division NC10 (p)		
<i>Methylohalobius</i>	✓		<i>Candidatus Methyloirabilis oxyfera</i>	✓	
<i>Methylomarinovum</i>	✓		<i>Candidatus Methyloirabilis sinica</i>	?	?
<i>Methylothermus</i>	✓		<i>Candidatus Methyloirabilis limnetica</i>	✓	
Crenotrichaceae (f)					
<i>Candidatus Crenothrix polyspora</i>	✓	?			

^a Table was established applying information from the following literature: [Bowman, 2014; Marin and Ruiz Arahal, 2014; Webb *et al.*, 2014; Knief, 2015; He *et al.*, 2016; Graf *et al.*, 2018]. Description of taxonomic order was not included.

^b In some of these species the pMMO2 paralog has been detected [Baani and Liesack, 2008].

Recently, a novel particulate methane monooxygenase, the paralog pMMO2, has been discovered in *Methylocystis* and *Methylosinus* species, in addition to the conventional pMMO [Yimga *et al.*, 2003]. pMMO2 shows a distinct methane oxidation kinetic, and enables growth at very low methane mixing ratios down to atmospheric concentrations (10-100 ppmv) [Knief and Dunfield, 2005; Baani and Liesack, 2008]. In addition,

a pMMO homolog, the pXMO enzyme, has been detected in type I and type II MOB, however, its physiological function and substrate preference has not yet been identified by biochemical and genetic tests [Tavormina *et al.*, 2011]. However, it is hypothesized that pXMO may have evolved for catabolism of methane or ammonia.

Despite their similar function in the cell, sMMO and pMMO show no genetic and structural homology [Hakemian and Rosenzweig, 2007; Glass and Orphan, 2012; Sazinsky and Lippard, 2015; Sirajuddin and Rosenzweig, 2015]. sMMO is a well-characterized multicomponent enzyme, consisting of a hydroxylase, a reductase, and a regulatory protein for optimal activity, arranged as an $\alpha_2\beta_2\gamma_2$ dimer (Figure 3) [Waller and Lipscomb, 1996]. The alpha-subunit of the hydroxylase component bears the catalytic oxygen-bridged diiron complex, which functions as the active site for methane oxidation [Merkx *et al.*, 2001; Tinberg and Lippard, 2011]. sMMO is encoded by the six-gene cluster *mmoXYBZDC*, also entitled as *mmo* operon. Genes *mmoX*, *mmoY* and *mmoZ* are responsible for the expression of the alpha-, beta- and gamma-subunits of the hydroxylase. The reductase is encoded by *mmoC*, and the regulatory component by *mmoB* [Murrell, Gilbert *et al.*, 2000]. *mmoD* codes for a protein that was recently found to regulate the expression of pMMO and sMMO [Semrau *et al.*, 2013].

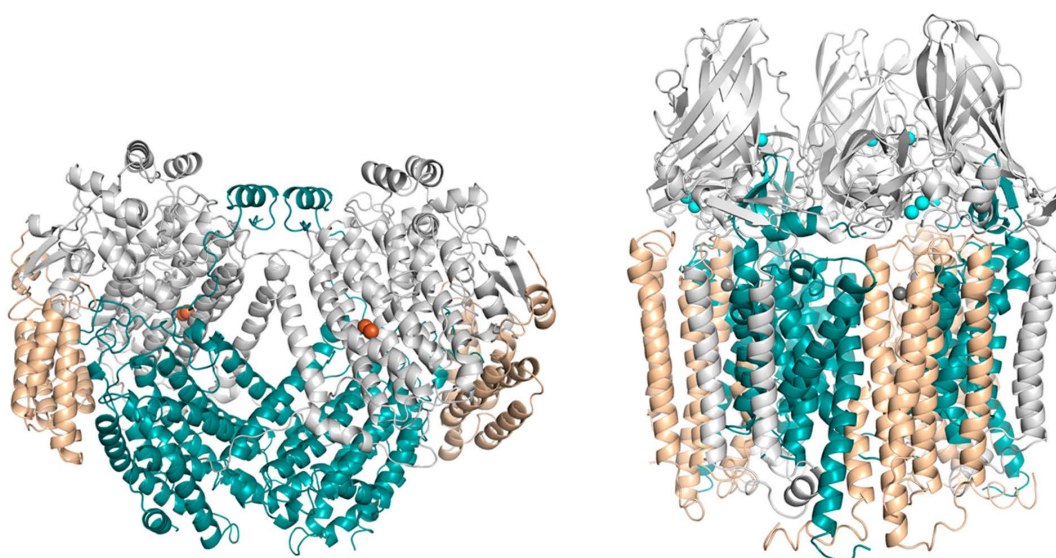


Figure 3. Three-dimensional ribbon structures of soluble methane-monooxygenase (sMMO, left). Alpha-subunits are shown in grey, beta-subunits in cyan, gamma-subunits in beige. Orange spheres depict the di-iron active sites. Particulate methane-monooxygenase (pMMO, right) consists of PmoB (grey), PmoC (beige), and PmoA (cyan) subunits. Copper ions are illustrated in turquoise [Sirajuddin and Rosenzweig, 2015].

In contrast, the pMMO oxidation chemistry is less understood due to difficulties in isolating the enzyme from the plasma membrane and purification for biochemical and physiological studies. The only known protein component of pMMO is the hydroxylase, referred to simply as pMMO [Ross and Rosenzweig, 2016]. pMMO comprises three major polypeptide chains, the alpha-subunit (PmoA), beta-subunit (PmoB), and gamma-subunit (PmoC), which are assembled into a homotrimer with an $(\alpha\beta\gamma)_3$ configuration (Figure 3) [Kitmitto *et al.*, 2005; Lieberman and Rosenzweig, 2005; Balasubramanian and Rosenzweig, 2007]. The different subunits are encoded by the genes *pmoA* (for PmoB), *pmoB* (for PmoA), and *pmoC* (for PmoC), summarized as the *pmo* operon [Semrau *et al.*, 1995]. Unlike sMMO, the structure of pMMO's active site has not been unambiguously identified yet. Over the years, different approaches by several research groups towards the biochemical and spectroscopic characterization of pMMO have generated much debate about the metal cofactors (copper versus iron), the number of copper ions, the nuclearity of the copper cofactors, and the active site location [Martinho *et al.*, 2007; Wang, Maji *et al.*, 2017; Cao *et al.*, 2018]. The discrepancies between the competing laboratories may have their origin in the difficulty of maintaining the activity of pMMO *in-vitro* and in dealing with labile metal cofactors, adventitious metal ions, and contamination from other metal-containing enzymes [Sazinsky and Lippard, 2015]. However, it is generally agreed that copper is an essential component of the PmoB subunit in pMMO, and reported values range from 2 to 15 copper ions per protomer [Semrau *et al.*, 2010; Glass and Orphan, 2012; Wang, Xia *et al.*, 2017].

Molecular markers and regulation of gene expression

By far the most used phylogenetic marker for studying microbial diversity is the 16S ribosomal RNA (16S rRNA) gene. Due to its conserved physiological function and its occurrence in all prokaryotes this gene provides an ideal target for phylogenetic studies [Amann *et al.*, 1995]. However, 16S rRNA phylogeny does not necessarily resolve the range of physiological properties precisely enough, as distinct metabolic pathways can be polyphyletic (i.e. can occur in organisms from different taxa). In addition, targeting only 16S rRNA genes makes it difficult to identify yet-undiscovered taxa from a specific bacterial guild. The use of functional genes, which encode key enzymes of unique metabolic pathways, is thus beneficial for molecular ecology studies.

To study the occurrence, activity and diversity of MOB species, examining the gene coding for pMMO has been well established. The well-conserved *pmoA* gene encodes for the β -subunit of pMMO and is present in almost all MOB (except some Beijerinckiaceae species) as well as in *Methylomirabilis* [Knief, 2015]. Its phylogenetic affiliation is largely congruent with those of the 16S rRNA gene, which makes it a suitable molecular marker in quantifying and characterizing MOB communities *in-situ* [Kolb *et al.*, 2003; McDonald *et al.*, 2008; Lüke and Frenzel, 2011; Dumont, 2014]. As pMMO expression is vital to the survival of most MOB, several characterized MOB species even possess multiple copies of the pMMO gene operon (*pmoCAB*), which appear to be nearly sequence identical [Stolyar *et al.*, 1999; Murrell, McDonald *et al.*, 2000]. Unlike pMMO, sMMO is found only in a subset of MOB and its presence often varies between species of the same genus [Knief, 2015]. Therefore, although highly specific for MOB, *mmoX*, the sMMO functional gene, is not often included in MOB ecology studies. Nevertheless, *mmoX* is a useful target, as it provides information regarding the catalytic diversity of MOB and it complements *pmoA* diversity studies, which do not detect MOB representatives lacking this gene [Chen *et al.*, 2007; Deng *et al.*, 2013; Liebner and Svenning, 2013].

A few alphaproteobacterial MOB (type II MOB) may also express the alternate form of pMMO, pMMO₂, which is encoded by the *pmoA2* gene. The gene is localized in the *pmoCAB2* operon and exhibits only 73% identity with the well-known *pmoA* gene at the nucleotide level, and 68.5% identity at the deduced amino acid level [Ricke *et al.*, 2004]. The pMMO homolog pXMO, has been found in several gammaproteobacterial MOB. *pxmA* sequences are only distantly related to characterized *pmoA* genes (53% identical and 73% similar on the amino acid level). Additionally, the operon structure shows an unusual non-canonical gene order *pxmABC* and its gene function is so far little understood [Tavormina *et al.*, 2011]. Verrucomicrobial MOB possess three phylogenetically distinct copies of the *pmoCAB* gene cluster, each encoding all three subunits of pMMO [Erikstad *et al.*, 2012]. The copies are all highly divergent from *pmoA* of proteobacterial MOB and different to each other [Op den Camp *et al.*, 2009]. *pmoA* is also present in “*Candidatus Methylomirabilis*” (NC10), albeit evolutionarily divergent from the conventional *pmoA* [Luesken *et al.*, 2011].

For MOB species capable of expressing sMMO and pMMO, copper availability plays a defining regulatory role in the activity of the respective enzyme, as their activation is reciprocally linked with respect to copper bioavailability [Stanley *et al.*, 1983]. When bioavailable copper exceeds a certain threshold relative to the cell biomass, pMMO is expressed and its activity is maintained by available copper, while sMMO translation is

expressed under copper-limited conditions [Prior and Dalton, 1985]. Experimental results suggest that copper concentrations above 5 μM enhances pMMO activity, whereas sMMO is expressed under copper-limited conditions ($< 1 \mu\text{M}$) [Choi *et al.*, 2003].

The mechanism of this “copper-switch” has not been fully explained yet, and many different models have been suggested within the last three decades [Nielsen *et al.*, 1997; Murrell, McDonald *et al.*, 2000; Stafford *et al.*, 2003; Lieberman and Rosenzweig, 2004; Scanlan *et al.*, 2009]. The most recent proposed hypothesis for the copper switch elucidated the role of the MmoD protein, whose functional gene resides on the *mmo* open [Semrau *et al.*, 2013]. The model suggests that in cells grown at low copper to biomass ratios, MmoD facilitates the expression of the *mmo* operon and the production of an extra-cellular copper acquisition peptide called methanobactin, while downregulating the *pmo* operon. Increase in methanobactin concentration additionally stimulates the expression of the *mmo* operon. In the case of high copper to biomass ratios, copper binds to methanobactin, leading to a reduction of *mmo* translation and production of methanobactin, and an enhancement of *pmo* expression. Additionally, MmoD interacts with copper, disabling it from binding to the *pmo* operon. However, the described model is under critical review by another research group, as, for example, the given results rely on gene knock-outs of major enzymes, which can cause significant metabolic rewiring [Dassama *et al.*, 2017; Kenney and Rosenzweig, 2018]. Instead, a second model has been proposed, which suggests that copCD, encoding for a periplasmic copper-binding protein and an inner-membrane protein, may be involved in copper uptake and/or the copper-switch in MOB [Kenney *et al.*, 2016]. Either way, the exact details of the copper-switch are much more complex than previously thought and more studies will be required to understand this mechanism.

MOB ecology and methane dynamics in lakes

Inland waters actively transform carbon and are significant sources of atmospheric methane [Bastviken *et al.*, 2004]. In lakes, methane is usually produced in anoxic sediments via methanogenesis, and reaches the atmosphere by ebullition (i.e. rising bubbles) or by vertical diffusion [Rasilo *et al.*, 2015; Bornemann *et al.*, 2016]. Methane flux can also be associated with plant-mediated transport in littoral zones [Knoblauch *et al.*, 2015]. In stratified lakes with methane being accumulated in the anoxic hypolimnion, mixing events can additionally lead to the release of high methane concentrations (i.e. storage flux) [Encinas Fernandez *et al.*,

2014]. Combining these flux pathways, freshwater lakes have been estimated to contribute 6-16% to the total non-anthropogenic methane emissions [Bastviken *et al.*, 2011]. Besides methane production in anoxic sediments, methanogenesis can also occur in the oxic epilimnion of lakes due to anoxic micro-niches [Grossart *et al.*, 2011; Bogard *et al.*, 2014]. Additionally, methane can be produced as a by-product of other microbes, which metabolize dimethylsulfoniopropionate (DMSP) [Tang *et al.*, 2016]. Nevertheless, atmospheric methane flux from freshwater systems is highly regulated by MOB within the water column, which are capable of oxidizing up to 90% of the produced methane [Bastviken *et al.*, 2008; Borrel *et al.*, 2011; Chistoserdova, 2015]. They are key players in transferring methane-derived carbon and energy to higher trophic levels of aquatic food webs while reducing greenhouse gas fluxes to the atmosphere [Bastviken *et al.*, 2003; Jones and Grey, 2011; Sanseverino *et al.*, 2012; Devlin *et al.*, 2015].

Previous studies have focused on MOB community structures in freshwater lakes and they reported high type I MOB occurrence responsible for aerobic methane oxidation [Sundh *et al.*, 2005; Schubert *et al.*, 2006, 2010; Blee *et al.*, 2014; Morana *et al.*, 2015; Oswald *et al.*, 2015; Zigah *et al.*, 2015]. MOB usually inhabit a narrow niche at oxic/anoxic transition zones, where opposite fluxes of oxygen and methane occur. In fully mixed lakes, when oxygen reaches the sediment-water interface, MOB are found close to the bottom. During summer stratification on the other hand, maximum amount of MOB is detected at the oxycline being located close to the metalimnion [Sundh *et al.*, 2005; Schubert *et al.*, 2010]. During these periods, methane oxidation appears to be less efficient in the oxic epilimnion, possibly due to inhibition by high light intensity [Murase and Sugimoto, 2005] and high oxygen concentrations [Rudd and Hamilton, 1975], or due to competition for oxygen with heterotrophs [van Bodegom *et al.*, 2001]. However, MOB cells containing the pMMO2 enzyme, which shows high methane affinity, would have a competitive advantage within these zones with low methane concentrations.

MOB were also detected in the anoxic hypolimnion of stratified lakes [Biderre-Petit *et al.*, 2011; Blee *et al.*, 2014; Chistoserdova, 2015]. In shallow lakes with light-penetration below the oxycline, aerobic methane oxidation can be supplied with oxygen produced by oxygenic photosynthesis [Milucka *et al.*, 2015; Oswald *et al.*, 2015]. In deeper lakes this mechanism is probably less relevant. There, the presence of MOB can be explained by the settlement of inactive cells [Schubert *et al.*, 2006], the downwelling of oxygen-rich water masses [Blee *et al.*, 2014], or active cells using a variety of other electron acceptors than oxygen. The coupling

of nitrate reduction and aerobic methane oxidation might play a relevant role under extreme hypoxia. Some MOB showed the ability to use nitrate and nitrite as electron acceptors under oxygen limitation [Kits, Campbell *et al.*, 2015; Kits, Klotz *et al.*, 2015]. Furthermore, bacteria related to *Methyloirabilis*, which perform this metabolism, appeared in anoxic hypolimnia [Graf *et al.*, 2018]. Closer to the sediments, methane oxidation linked to metal reduction could potentially play an important role [Crowe *et al.*, 2008; Oswald, Jegge *et al.*, 2016; Oswald, Milucka *et al.*, 2016].

It has been shown that different physico-chemical factors can affect MOB community structures and subsequent methane oxidation in lakes [Borrel *et al.*, 2011; Martinez-Cruz *et al.*, 2015; Samad and Bertilsson, 2017]. Besides physico-chemical parameters, recent studies additionally started to focus on inter-species interactions with other bacteria or even higher trophic organisms shaping MOB communities, and thus influence their important ecosystem service [Jones and Grey, 2011; Devlin *et al.*, 2015; Ho *et al.*, 2016; Bar-Or *et al.*, 2017].

The role of copper and iron

Copper and iron in lacustrine environments

The release of copper into the environment has been substantially increased due to its growing use in industrial activities [Nriagu and Pacyna, 1988]. Copper usually enters aquatic systems via fluvial and atmospheric input. Nevertheless, copper still counts as a trace metal and its concentration in most lake systems is below 50 nM [Wetzel, 2001a; Xue and Sigg, 2002; Mason, 2013]. As a micronutrient, copper is an essential cofactor in many microbial enzymatic pathways, such as denitrification, photosynthesis, ammonium and methane oxidation [Meyer and Cusanovich, 2003; Festa and Thiele, 2011; Glass and Orphan, 2012]. Due to its low abundance, copper availability is often limiting for the functioning of such pathways, although, paradoxically, high copper concentrations can also have an adverse or even toxic effect on various living organisms.

Cycling of copper in lakes is strongly governed by the physico-chemical, the hydrodynamic and the biological state of the water, and its biological availability is affected by many natural processes. Copper can exist in two oxidation states, with copper(II) being predominant. Copper(I) appears only in highly reductive environments, otherwise it is rapidly converted to copper(II) [Mansilla-Rivera and Nriagu, 1999]. Copper(II) reacts with a variety of ligands, as well as with many types of particulates to occur in a variety of chemical forms, such as soluble, colloidal, and particulate forms of copper (Figure 4) [Sigg and Stumm, 2011]. The dissolved phase contains free ions and copper complexed to different inorganic (e.g. hydroxide, carbonate) and organic ligands (e.g. amino acids, fulvic acids), which are usually smaller than 1 nm. The weaker complexes within this fraction are predominantly important for the uptake by organisms. However, copper(II) is normally strongly complexed by organic ligands, which leads to a rather small fraction directly available for organisms [Wetzel, 2001a; Xue and Sigg, 2002]. Colloidal copper particles range from few nanometres to one micrometre and sediment very slowly, but eventually aggregate into larger compounds. They consist of various organic (e.g. biopolymers, humic substances) and inorganic components (e.g. iron and manganese oxides). Particulate copper ($> 1 \mu\text{m}$) includes copper bound to the surface functional groups of particles (e.g. clay minerals) and in solid phases (e.g. with sulphide to form chalcopyrite in anoxic layers) [Hamilton-Taylor *et al.*, 2005]. It is

quickly transported to the sediments and may be released by resuspension or by chemical changes. Copper in various biological material additionally contributes to the particulate fraction. For example, phytoplankton within the surface layers of lakes take up copper, which can then settle to the sediment with the biogenic organic matter or be released as this organic matter is mineralized.

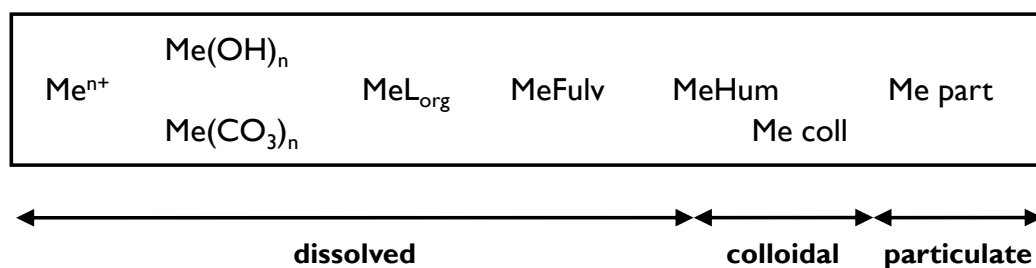


Figure 4. Metal species occurring in freshwater systems. Fulv = fulvic acid, Hum = humic acid, coll = colloidal, part = particulate. Adapted from [Sigg and Stumm, 2011].

During lake stratification, the anoxic conditions within the hypolimnion lead to the reductive dissolution of iron-oxide phases, and the release of iron into solution [Taillefert and Gaillard, 2002]. Most of the iron in the anoxic zone is in the dissolved fraction and likely present as iron(II). Dissolved concentrations increase substantially from 1 μM up to 150 μM iron(II) close to the sediments [Wetzel, 2001a; Mason, 2013]. These concentrations are orders of magnitude higher than in oxygenated surface waters, where reported values appear below 0.1 μM . In the presence of increasing sulphide during anoxia, precipitation of iron-sulphide (FeS) occurs, which decreases the dissolved iron fraction. In fall, physical disturbances lead to mixing of the water column. Dissolved iron in the epilimnion is oxidized to iron(III), which precipitates, and is removed from the water column by particle settling [Shaked *et al.*, 2004].

The uptake of metals by microorganisms strongly depends on their chemical speciation. Understanding the metal speciation as related to its bioavailability is essential to assess its effect on the productivity of aquatic organisms [Chi Fru, 2011]. In addition to the abiotic speciation, competition with other organisms can strongly reduce the available metal concentration and thus prevent metal uptake by certain species. However, some microorganisms can actively increase bioavailability of trace metals via the exudation of biochelators (e.g. siderophores, chalkophores). They solubilize the target metal from a mineral or organic nutrient source, and the formed metal-chelator complex is subsequently taken up by the organism [Kraemer *et al.*, 2015].

MOB copper acquisition and storage strategies

A possible route for uptake of unchelated copper by MOB is the diffusion of smaller solutes through porins [Nikaido, 2003; Balasubramanian *et al.*, 2011]. Hence, MOB can readily take up bioavailable copper. However, copper availability in natural environments is often strongly reduced [Morton *et al.*, 2000]. MOB need to overcome this limitation in order to satisfy their copper requirement for pMMO expression and they possess several mechanisms to obtain copper from non-biological available fractions.

In analogy to the iron-chelating siderophore, a copper-binding ligand, termed chalkophore (from the Greek *chalko-*, copper), has been detected in alphaproteobacterial MOB cells [Kim *et al.*, 2004; Balasubramanian and Rosenzweig, 2008; Kenney and Rosenzweig, 2018]. Today, this chalkophore is better known as methanobactin and there are many recent reviews available summarizing the current state of knowledge [DiSpirito *et al.*, 2016; Dassama *et al.*, 2017; Kenney and Rosenzweig, 2018]. Methanobactin is a ribosomally synthesized, post-translationally modified natural peptide with high copper affinity [Dassama *et al.*, 2017]. Although capable of binding copper(II), it has been identified that copper(I) ions are more favoured by methanobactin with affinities in the range of 10^{20} to 20^{21} M^{-1} [Hakemian *et al.*, 2005; Baslé *et al.*, 2018]. Upon binding of copper(II) by methanobactin, the reduction of copper(II) to copper(I) happens quickly, within 10 minutes, via a so far unknown mechanism. Under superstoichiometric copper conditions, a second copper ion can bind, albeit with lower affinity and without reduction.

Outside of the cell, methanobactin is able to scavenge copper from different soluble, mineral, and humic sources [Knapp *et al.*, 2007; Pesch *et al.*, 2012]. It can even mediate copper removal from borosilicate glasses [Kulczycki *et al.*, 2011]. The copper-loaded methanobactin is incorporated by an active uptake process via a specific transporter (TonB) [Balasubramanian *et al.*, 2011]. Genes encoding TonB-dependent transporters (TBDTs) are often associated with the methanobactin gene operon [Dassama *et al.*, 2016; Gu *et al.*, 2016]. TBDTs are outer membrane receptors already well known for their role in the uptake of siderophores [Noinaj *et al.*, 2010]. The copper release within the cell as well as methanobactin export is not yet well-characterized.

Some MOB, which lack the gene for methanobactin production, contain the copper binding proteins MopE or CorA. MopE has a high copper affinity, in the range as observed for methanobactin, and is expressed under copper limiting conditions [Ve *et al.*, 2012]. It is located on the cell surface, and its truncated form,

MopE*, is secreted into the growth medium to act as a copper chaperone. MopE* shares sequence resemblance to CorA, a copper repressible protein [Johnson *et al.*, 2014]. CorA is an outer-membrane protein and its synthesis is repressed by copper ions. Much smaller than MopE, CorA binds one copper ion at a time. Copper resistance proteins (CopCD) might be involved in the switch between sMMO and pMMO, however, they might also play a role in cellular copper homeostasis [Lawton *et al.*, 2016; Gu *et al.*, 2017]. CopC is a periplasmic copper binding protein and widely distributed among microbes. It is often present as a fusion protein together with CopD, an inner membrane protein, which functions in the uptake of copper and delivering it to the cytoplasm of the cell. Additional insight into how MOB handle their copper demand has been provided by the discovery of copper storage proteins, Csps [Lombardi, 2015; Vita *et al.*, 2015; Dennison *et al.*, 2018]. In *Methylosinus trichosporium* three Csps were detected, with each one binding a specific amount of copper ions. These proteins store copper for pMMO and provide an internal copper source when it becomes limiting. Under such conditions, methanobactin is produced and can readily remove Cu(I) ions from Csps. The possibility of making use of copper collecting and copper storage mechanisms are crucial for the survival of MOB in low-copper environments.

Objectives and outline

MOB perform an important ecosystem service in the global carbon cycle by mitigating emissions of methane, a potent greenhouse gas, from aquatic environments. Understanding the function and dynamic of MOB in these systems is important to estimate methane efflux to the atmosphere in times of ongoing climate change. Recent laboratory research has shown the importance of copper in the MOB metabolic pathway, the oxidation of methane to methanol, and demonstrated that its availability influences the expression and activity of the copper-dependent enzyme. Furthermore, copper storage mechanisms have been detected, which would allow MOB to metabolize methane using the copper-controlled enzymatic pathway within an environment of low copper concentrations. The role of copper in aerobic methane oxidation has been extensively investigated under controlled conditions, however, translating laboratory results to environmental systems is challenging due to MOB being embedded in complex biogeochemical networks that are difficult to simulate in laboratory set-ups. It remains uncertain to which degree copper as a micronutrient controls aerobic methane oxidation under natural conditions.

The overall objective of the herein presented project was to improve our understanding of MOB copper household with an emphasis on how copper availability is influencing lacustrine methane oxidation pathways. In addition, the investigations should shed light on the impact of general physico-chemical and biological interactions on MOB communities. To this end, a multidisciplinary approach was adopted throughout the course of this thesis by combining three specific objectives:

- How large are the pools of bioavailable copper along the water column of a stratified lake and is there evidence that copper conditions restrict MOB distribution and lacustrine methane oxidation pathways
- Apart from copper being a possible driving force of the MOB assembly, are there combined effects of microbial communities and other physico-chemical parameters shaping the MOB community in a stratified lake
- What are limiting copper conditions for MOB growth and copper-dependent methane oxidation, and can we infer an extended Redfield ratio (C:N:Cu) for MOB cells

In order to follow these hypotheses, we studied the dynamics of the MOB community structure, the concentration and speciation of copper and an extended set of physico-chemical parameters as well as correlations of MOB with the total bacterial community in space and time in a freshwater lake. Rotsee represents an excellent system to study methane oxidation as its hypolimnion is highly enriched in methane during summer stratification. A substantial amount of methane diffusing towards the lake surface is consumed by the activity of MOB at the oxic-anoxic transition zone and below. Additionally, we conducted laboratory experiments with an axenic MOB culture to improve the understanding of MOB copper requirement and its role as a micronutrient.

Chapter 2: Aerobic methane oxidation under copper scarcity in a stratified lake

MOB seem to be able to substantially reduce methane emissions from this system, although competition for copper by other organisms are likely. Therefore, we investigated the distribution of different copper species related to methane concentrations and the occurrence of MOB along the water column of Rotsee within four field campaigns. We made use of diffusive gradients in thin films to measure *in-situ* biological available copper concentrations. *pmoA* and *mmoX* functional genes were quantified to elucidate the potential of the respective methane oxidation pathway. Additionally, we explored the occurrence of different MOB species by 16S rRNA sequencing. Our goal was to shed light on how different copper species, in particular the bioavailable one, influence the copper-dependent enzymatic pathway. Furthermore, we tried to assess inter-species copper competition and how such competition can be circumvented by MOB.

Chapter 3: Environmental and microbial interactions shaping methane-oxidizing communities in a stratified sub-alpine lake

We studied the interrelationship of MOB and their physico-chemical environment as well as the total bacterial community, to determine additional potential drivers leading to MOB niche differentiation, adding to a more holistic understanding of MOB community dynamics in lake systems. The MOB community structure within Rotsee was analysed based on *pmoA* sequences, whereas bacterial communities were assessed by 16S rRNA sequences. Physico-chemical gradients included methane, oxygen, and copper, among others. We hypothesized

that MOB zonation within Rotsee is not solely determined by copper availability but also by interactive effects with other integral physico-chemical variables and bacterial players.

Chapter 4: Activity of aerobic methane-oxidizing bacteria under nanomolar copper additions

This laboratory study investigated the effect of different copper availabilities on the growth behaviour, methane consumption dynamics, and cellular elemental composition of a single MOB species (*Methylobacterium alcaliphilum*). Findings were evaluated in the context of the extended Redfield ratio variation. We suggested that MOB growth rates and methane consumption are accelerated by increasing copper concentrations. Furthermore, we assumed that the different experiments should reveal constant copper bound to biomass values as well as deduced extended elemental stoichiometries. Results would give insight into the potential of copper storage mechanisms in buffering different ambient copper concentrations.

The data generated in this thesis highlight the importance of copper as a micronutrient for aerobic methane oxidation in freshwater systems. Even though the bioavailable copper fraction within the water column of the investigated lake is rather low, within the nanomolar range, and MOB are possibly exposed to a setting of high copper competition with other organisms, they efficiently reduce methane emissions to the atmosphere. The data reveal that copper collecting and storage mechanisms might play an important role for MOB performance *in-situ*. In addition, MOB are integrated in complex physico-chemical and bacterial networks, and it seems that microbial interactions have so far gained an underappreciated role in structuring the MOB community.

The results of this project can serve as a foundation for future research, either in the direction of *in-situ* copper-dependent methane oxidation or the inter-connectivity of MOB with the total bacterial community and their environment. A more profound comprehension of the role of MOB within freshwater ecosystems will help to better understand the carbon cycle in the context of ongoing global change.

Analysing the link between copper and MOB

Study site

Field investigations were conducted in Rotsee, a monomictic lake located in Central Switzerland at an altitude of 436 m (Figure 5). Rotsee is about 1 km² in size (2.4 km long, 0.4 km wide) and shows a maximum depth of 16 m. The Reuss River feeds Rotsee via the Reuss-Rotsee canal with a drainage area of 4.6 km². Its wind-shielded location allows a stable summer stratification from approximately May to November, with an oxycline usually located between 8 and 11 m depths [Schubert *et al.*, 2010]. Rotsee became highly eutrophic in the mid 1800s due to anthropogenic nutrient enrichment. In 1920 the lake has been classified as polytrophic [Stadelmann, 1980; Kohler *et al.*, 1984]. Although its trophic state has improved through the introduction of an interceptor sewer in 1969 and a sewage treatment plant in 1974 [Bloesch, 1974], Rotsee is still classified as eutrophic [Schubert *et al.*, 2010]. During stratification, Rotsee exhibits an anoxic hypolimnion with high accumulation of methane. Methane oxidation activity in the water column of Rotsee has been investigated in previous studies [Schubert *et al.*, 2010; Oswald *et al.*, 2015] and was found to be highest at and below the oxycline with aerobic gammaproteobacterial MOB being the main methane consumers. Aerobic methane oxidation at depths depleted in oxygen was fuelled by light-dependent oxygenic photosynthesis [Oswald *et al.*, 2015; Brand *et al.*, 2016]. Nevertheless, regardless of the strong MOB activity, the epilimnion of Rotsee is still oversaturated with methane compared to the atmosphere and thus serves as a source of methane [Schubert *et al.*, 2010].

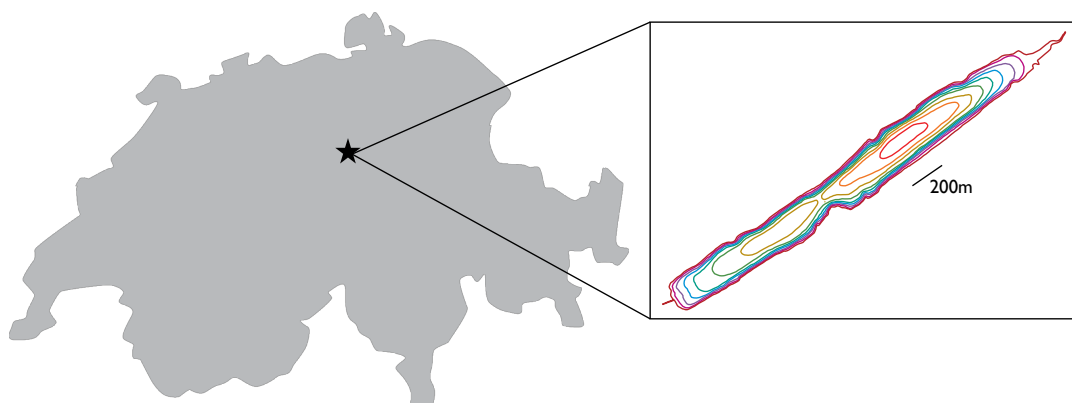


Figure 5. Bathymetric map of Rotsee [Lotter, 1988] and its location in Switzerland.

***In-situ* profiling and sampling**

High-resolution geochemical profiling and sampling were performed with an in-house built profiler for *in-situ* analysis (PIA) [Kirf *et al.*, 2014], equipped with a multi-parameter probe for measurements of conductivity, turbidity, depth, temperature and pH. Profiles of dissolved oxygen concentrations down to trace levels were obtained from two micro-optodes (125 and 20 nM detection limit). Chlorophyll a was measured with a fluorescence probe. Photosynthetically active radiation (PAR) was recorded with a spherical quantum sensor with detection limit of $0.1 \mu\text{mol m}^{-2} \text{s}^{-1}$. Water for chemical analysis was sampled using an integrated rosette syringe sampler (12 x 60 ml syringes), which was attached to PIA and could be triggered on board during profiling at specific depth intervals. Samples included anions, cations, nutrients (nitrite, nitrate, ammonium, total sulphide, sulphate, phosphate), dissolved in-/organic carbon, total dissolved nitrogen, and dissolved and total metals. Lake water for methane and molecular analysis was collected with a Niskin bottle or via pumping with a gas tight tubing attached to PIA. Chemical analysis of relevant species was performed according to standard protocols.

Diffusive gradients in thin films

In order to obtain information of the biological available fraction of copper and other trace metals, Diffusive Gradients in Thin film (DGT) samplers were deployed within the water column of Rotsee. DGT is a passive sampling technique based on diffusion characteristics and dissociation kinetics of different metal chemical species [Davison and Zhang, 1994; Davison, 2016]. Hence, it allows analysis of low molecular weight compounds such as simple inorganic and labile organic complexes, as well as free metal ions over a typical time period.

The core of a DGT unit consists of three layers with different functions (Figure 6). The uppermost layer is a simple membrane filter (0.2 or 0.45 μm pore size), which provides a protective surface for the layers below. Underneath the membrane, the diffusive gel layer allows unimpeded diffusion of the solutes due to its well-defined open structure. The ion transport through the diffusive gel occurs by molecular diffusion, which makes this layer usually controlling the overall rate of mass transport, irrespectively of the hydrodynamics in the bulk solution. The diffusive boundary layer (DBL) is a stationary region in the bulk solution that forms

adjacent to the filter membrane. Transport of species through DBL is by diffusion (and not convection), which makes this layer an extension of the diffusive layer. The thickness of DBL is generally considered to be negligible for well-mixed lakes [Scully *et al.*, 2006]. The binding gel lies below the diffusive layer and consists of an adsorbent (resin) immobilized in a hydrogel. Rapid and irreversible binding of analytes to the resin ensures that concentration gradients are quickly established.

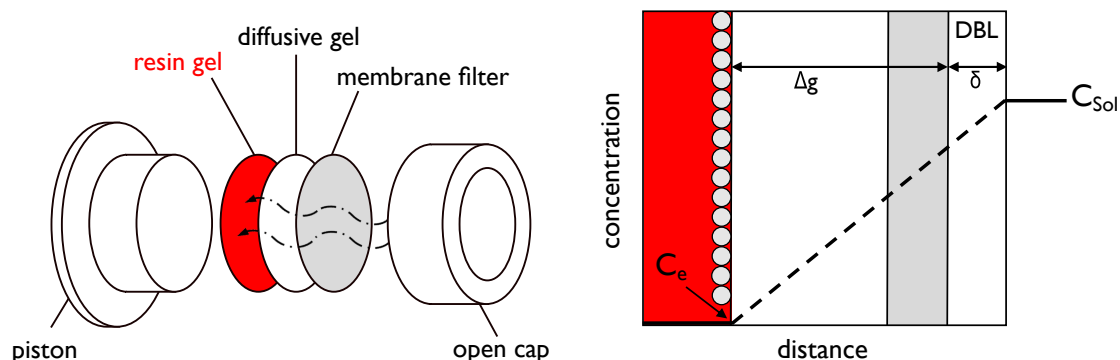


Figure 6. Schematic representation of a single DGT unit and the concentration gradient of a metal species through a DGT assembly.

The bold/dashed line in the schematic on the right represents the concentration gradient of the analyte, C_{sol} is the concentration in the bulk solution, C_e the concentration of the analyte at the binding layer. Δg and δ are the thickness of diffusive gel and the diffusive boundary layer (DBL), respectively. Adapted from [Davison, 2016].

This diffusion and accumulation process mimics metal uptake by microorganisms and results from DGT are hence a good indicator for metal bioavailability [Menegário *et al.*, 2017]. However, DGT results might underestimate the bioavailable fraction, as it is a passive sampling method and provides time-integrated metal concentrations. Furthermore, metals loosely bound to larger complexes will have different diffusion coefficients, which are not considered in the measurements. The DGT unit consists of the three mentioned layers and a plastic holding device. The piston works as a support for the gel-layers, which are placed on top. The closing cap tightly fits and allows the transport of ions from the bulk solution to the inner layers through a specific defined exposure window.

Assembling of the DGT units was performed according to [Odzak *et al.*, 2002]. In field, DGT samplers were attached to a rope at distinct water depth intervals and deployed 2-3 days. After retrieving, resin gels were eluted and metal concentrations were analysed by Inductively Coupled Plasma Mass Spectrometry (ICP-MS).

The accumulated mass of analyte in the resin gel (M) was calculated using the following equation [Zhang and Davison, 1995]:

$$M = \frac{C_e (V_{HNO_3} + V_{gel})}{f_e}$$

where C_e denotes the concentration in the elution solution, V_{HNO_3} is the added eluent volume, V_{gel} is the volume of the resin gel and f_e is the elution efficiency for each metal (ratio of eluted to bound metal [Zhang and Davison, 1995]), typically 0.8. By knowing M , the mean free metal concentration at the surface of the DGT device (C_{DGT}) can be obtained as:

$$C_{DGT} = \frac{M \Delta g}{D t A}$$

where t is the overall deployment time, Δg is the diffusive layer thickness (diffusion gel + filter, usually 0.093 cm) and D is the diffusion coefficient of the free metal ion [Zhang and Davison, 2015]. 3.14 cm^2 was used for A as exposed surface area, and the negligible thickness of the DBL was disregarded [Warnken *et al.*, 2006; Davison and Zhang, 2012].

Molecular biological methods

Molecular biological methods were used to investigate the total bacterial community, as well as the MOB community structure and the functional gene distribution within the water column of Rotsee. Therefore, water samples from discrete depths were collected, and filtered onto $0.2 \text{ }\mu\text{m}$ filters. DNA was extracted using a DNA extraction kit. Quantitative polymerase chain reaction (qPCR) was applied to quantitatively detect 16S rRNA genes of the total bacterial community using the primer combination 349f-805r [Herlemann *et al.*, 2011]. The abundance of *pmoA* and *mmoX*, the functional marker genes of pMMO and sMMO, respectively, were additionally quantified via qPCR. For *pmoA* analysis, the primer set A189f-mb661 was applied [Costello and Lidstrom, 1999] with qPCR conditions adapted from [Henneberger *et al.*, 2015]. For *mmoX* detection we used the primer pair 536f-898r [Fuse *et al.*, 1998] and an self-developed thermal cycler program. In addition to quantitative measurements, we applied the Illumina MiSeq sequencing technique to get additional qualitative information about the total bacterial and MOB communities. 16S rRNA sequencing (total bacterial community) was performed by Microsynth AG (Balgach, Switzerland). In-depth investigation of the

MOB community structure was revealed by sequencing the *pmoA* gene, which was partly conducted by the Genomics Facility Basel (Basel, Switzerland). Sequencing data were analysed by the Genomic Diversity Centre (GDC, Zurich, Switzerland).

***In-vitro* growth experiments**

Laboratory-based incubations were performed to investigate the role of copper as a limiting factor in bacterial methane oxidation, and to increase our understanding of MOB copper handling. Therefore, an axenic MOB culture (*Methylobacterium alcaliphilum*) was grown under different copper amendments. Growth behaviour, methane consumption, biomass associated copper, and intracellular elemental stoichiometries were investigated. Some literature is available on copper incubation experiments with axenic MOB cultures. Early studies were conducted in the 80s [Stanley *et al.*, 1983; Prior and Dalton, 1985], where they found that copper stress underlies the intracellular location of MMO. Later, most research focused on the atomic characterization of pMMO [Balasubramanian *et al.*, 2010] and on the switchover of sMMO and pMMO, which depends on the copper-to-biomass ratio [Zahn and DiSpirito, 1996]. Today many research groups perform incubation studies with axenic cultures to better understand the copper binding capacity of methanobactin and its competition with other trace metals [Semrau *et al.*, 2013; Kalidass *et al.*, 2015], or to test different carbon sources on MOB growth behaviour [Im *et al.*, 2011; Farhan Ul-Haque *et al.*, 2017]. This is just a small list of the recent literature, however, most of the reviewed studies conducted experiments with excess copper, which do not reflect natural environmental conditions.

Chapter 2

Aerobic methane oxidation under copper scarcity in a stratified lake

Carole Guggenheim

Andreas Brand

Helmut Bürgmann

Laura Sigg

Bernhard Wehrli

Published in *Scientific Reports*

DOI: 10.1038/s41598-019-40642-2

Abstract

Aerobic methane-oxidizing bacteria (MOB) substantially reduce methane fluxes from freshwater sediments to the atmosphere. Their metalloenzyme methane monooxygenase (MMO) catalyses the first oxidation step converting methane to methanol. Its most prevalent form is the copper-dependent particulate pMMO, however, some MOB are also able to express the iron-containing, soluble sMMO under conditions of copper scarcity. So far, the link between copper availability in different forms and biological methane consumption in freshwater systems is poorly understood. Here, we present high-resolution profiles of MOB abundance and pMMO and sMMO functional genes in relation to copper, methane and oxygen profiles across the oxic-anoxic boundary of a stratified lake. We show that even at low nanomolar copper concentrations, MOB species containing the gene for pMMO expression are present at high abundance. The findings highlight the importance of copper as a micronutrient for MOB species and the potential usage of copper acquisition strategies, even under conditions of abundant iron, and shed light on the spatial distribution of these microorganisms.

Introduction

Aerobic methane-oxidizing bacteria (MOB) are phylogenetically diverse and mainly group among the *Alpha*- and *Gammaproteobacteria* (α -MOB and γ -MOB) and the *Verrucomicrobia*. They efficiently mitigate the emission of methane (CH_4) generated in freshwater systems while utilizing CH_4 as their sole carbon and energy source [Chistoserdova, 2015]. The enzyme methane monooxygenase (MMO) plays a key role for this process by catalysing the first oxidation step, the conversion of CH_4 to methanol under ambient conditions. Two forms have been described, the soluble MMO (sMMO) and the membrane-bound, particulate MMO (pMMO) [Sirajuddin and Rosenzweig, 2015]. Whereas most known MOB express pMMO, sMMO production has been characterized in only a few organisms [Knief, 2015]. The conserved gene segments *mmoX* and *pmoA* encode subunits of sMMO and pMMO, respectively, and serve as biological markers to track MOB in environmental samples [Knief, 2015]. sMMO has a well-characterized di-iron catalytic centre [Sirajuddin and Rosenzweig, 2015], but the atomic structure of the pMMO active site is still a matter of debate. Several competing models with different metals and different numbers of metal atoms at the active site of pMMO have been proposed [Martinho *et al.*, 2007; Wang, Maji *et al.*, 2017; Cao *et al.*, 2018]. However, it is generally agreed that pMMO is a copper-dependent enzyme. Copper (Cu) has a regulatory effect on MOB activity, especially on the biosynthesis of the pMMO and sMMO enzymes and switching between these in cells able to express both [Semrau *et al.*, 2010]. According to experiments with axenic cultures, sMMO expression occurs under low Cu to biomass levels ($< 1 \mu\text{M}$), whereas pMMO is predominant at concentrations above $5 \mu\text{M}$ [Stanley *et al.*, 1983; Sirajuddin and Rosenzweig, 2015]. Nevertheless, in cells grown under sMMO expressing conditions, low but detectable levels of pMMO transcription have been measured [Stolyar *et al.*, 2001; Choi *et al.*, 2003]. Well-defined incubation experiments with environmental samples documented the influence of Cu on the MOB community structure and abundance and composition of functional gene transcripts [Ho, Lücke, *et al.*, 2013; Cantera *et al.*, 2016]. Cu addition stimulated *pmoA* gene transcription and promoted growth of MOB, which mostly lacked *mmoX*. Some MOB utilize special mechanisms to regulate their Cu homeostasis, also in response to Cu toxicity at high levels. The chalkophore methanobactin, the extracellular component of a Cu acquisition system, binds Cu with high affinity and specificity and is able to increase the bioavailable Cu

fraction by dissolving Cu from soluble, mineral, and humic sources, but open questions about its role still remain [Chi Fru, 2011; Kenney and Rosenzweig, 2018]. It has recently been proposed that methanobactin works in concert with a protein called MmoD to modulate the Cu-switch of sMMO and pMMO [Semrau *et al.*, 2013], however, other proteins are also involved in the Cu or Cu-methanobactin uptake and/or the Cu-switch in MOB [Ve *et al.*, 2012; Johnson *et al.*, 2014; Gu *et al.*, 2016; Lawton *et al.*, 2016; Dennison *et al.*, 2018].

The hypothesis that Cu acts as a controlling variable for the distribution of MOB with different enzymatic pathways has not yet been tested under *in-situ* conditions in aquatic systems. Many studies have assessed the role of growth substrates and physical parameters on MOB activity [Semrau *et al.*, 2010; Borrel *et al.*, 2011; Farhan Ul-Haque *et al.*, 2017], but it remains unclear if bioavailable Cu limits the distribution of MOB and affects the dominant enzymatic pathways of CH₄ oxidation in natural systems [Semrau *et al.*, 2010; Chi Fru, 2011; Glass and Orphan, 2012]. We make a first attempt to reduce this uncertainty by combining trace metal speciation measurements with marker-gene based analysis of MOB in the water column of a stratified lake. We explore the hypothetical link between the depth distribution patterns of different Cu fractions and the abundance of MOB and their functional genes.

Results

Copper and methane oxidation in the water column of Rotsee

In order to improve our understanding of CH₄ and Cu dynamics *in-situ*, we studied seasonally stratified Rotsee, a small freshwater lake (1 km²) with pronounced sedimentary CH₄ production and aerobic CH₄ oxidation in its water column [Schubert *et al.*, 2010]. We conducted four field campaigns at the early stage (June 2013), peak (August 2013), and end of stratification before the lake overturns (September 2014 and September 2015). CH₄ concentrations were highest close to its production site in the sediment (270-710 µM) and steadily decreased towards the oxycline where CH₄ was predominantly consumed (Figure 1a,e,i,m). The low residual CH₄ concentration (0.12-1.07 µM) detected in the oxic epilimnion during all campaigns indicated that CH₄ removal within the water column of Rotsee was highly efficient. Nevertheless, surface water was still oversaturated in CH₄ relative to the atmosphere and thus Rotsee was a source of CH₄. For all campaigns, we found that oxygen (O₂) concentrations dropped from ~400 µM at the surface to below detection limit (< 20 nM) at the oxycline, which varied in depth between 6 to 9 m across sampling dates (Figure 1a,e,i,m). Measurements of photosynthetically active radiation (PAR) showed light penetrating throughout the oxycline and into the anoxic zones (Figure 1a,e,i,m). These findings are consistent with the work of Brand *et al.* [Brand *et al.*, 2016], who reported oxygenic primary production in anoxic zones, and Oswald *et al.* [Oswald *et al.*, 2015], who showed MOB activity consuming O₂ in these same layers. This indicates that aerobic CH₄ oxidation might be coupled to oxygenic photosynthesis in the macroscopically anoxic hypolimnion of Rotsee.

We focused our field sampling on depths with the greatest potential for active CH₄ oxidation: from where CH₄ first begins to accumulate in the water column, down to where PAR falls below detection limit (grey shaded areas in all profiles, Table 1). Previous work also showed that within these zones, CH₄ isotopic signatures became substantially heavier, indicative of intense biological CH₄ oxidation (August 2013, September 2014) [Oswald *et al.*, 2015, 2017]. Further, isotopic CH₄ values also showed slight increases in the anoxic, dark hypolimnion of Rotsee, which implies that some CH₄ is already oxidized at these depths. O₂ was completely consumed in the upper part of the specified zones, except for June 2013 where O₂ and CH₄ gradients did not show any overlap and thus no O₂ was measured in the potential CH₄ oxidation zone.

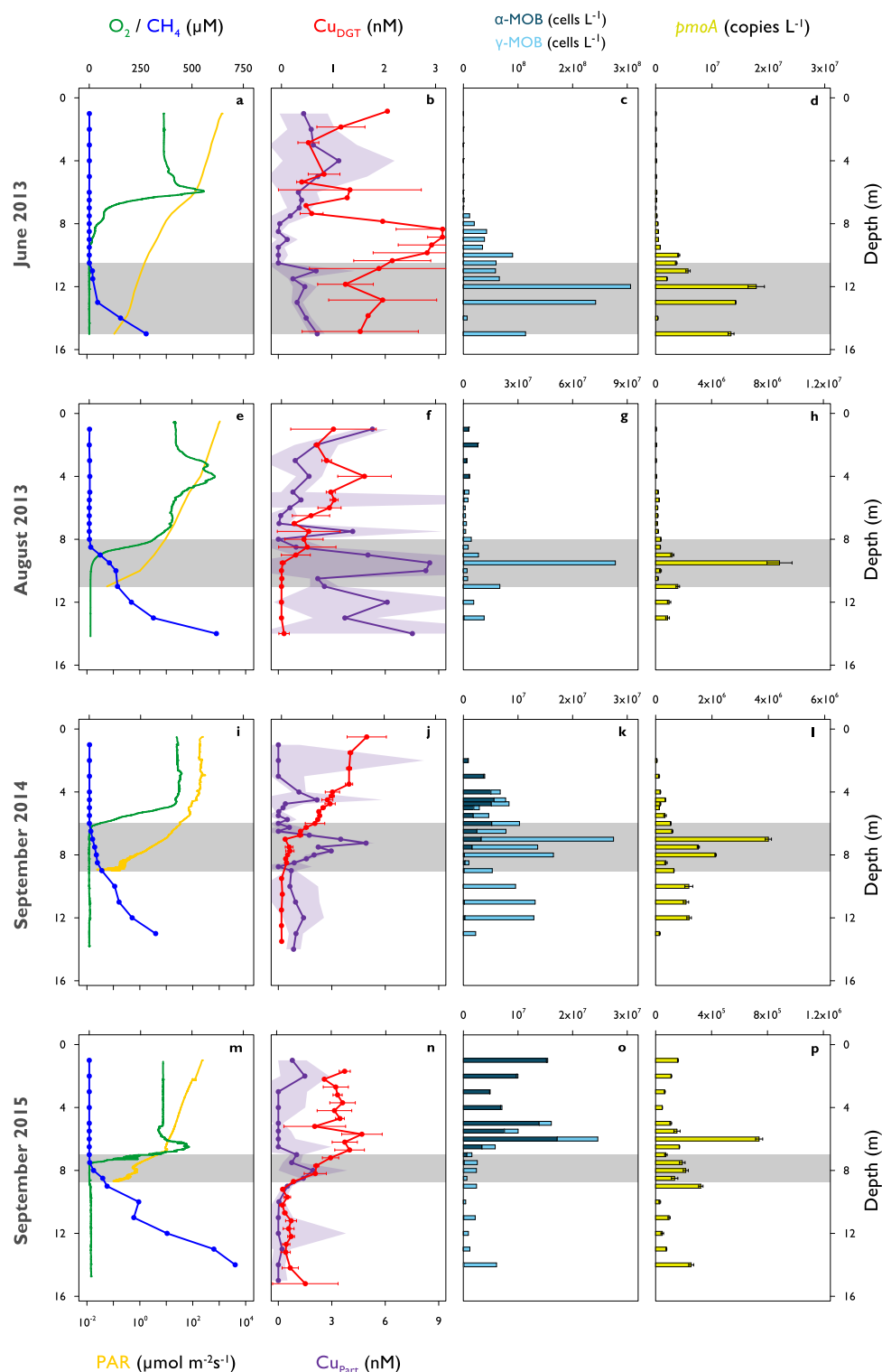


Figure 1. Depth profiles of biogeochemical parameters in Rotsee.

(a-d) June 2013. (e-h) August 2013. (i-l) September 2014. (m-p) September 2015. Grey shaded areas denote the depth range of potential methane oxidation (availability of methane above epilimnetic background concentration and availability of oxygen or light). (a,e,i,m) Oxygen (O_2 , normal optode, green) and methane (CH_4 , blue) concentrations, photosynthetically active radiation (PAR, deep yellow, logarithmic scale). (b,f,j,n) Bioavailable copper (Cu_{DGT} , red) and particulate copper concentrations (Cu_{Part} , purple). Red error bars and purple shaded areas represent standard deviations ($n = 3$ or $n = 4$, error propagation for Cu_{Part}). (c,g,k,o) Absolute abundances of methane oxidizing bacteria (MOB) separated into α -MOB (deep blue) and γ -MOB (light blue). (d,h,l,p) Absolute quantity of *pmoA* gene copy numbers (yellow). Error bars indicate standard deviations from triplicate qPCR amplification of one sample. Note the different x-axes for (c,g,k,o) and (d,h,l,p).

To assess the biogeochemical role of Cu on CH₄ oxidation, several metal fractions were quantified throughout the water column. We determined bioavailable metals by deploying diffusive gradients in thin-film (DGT) samplers at 0.25-1 m resolution. The DGT technique is based on the diffusion characteristics of different metal chemical species [Davison, 2016]. The samplers allow low molecular weight compounds such as simple inorganic and labile organic complexes as well as free metal ions to diffuse across a diffusive layer to be sorbed at an ion exchange layer. This accumulation process mimics uptake of dissolved metals by organisms. Previous studies showed that the DGT measurement is a good indicator for *in-situ* metal bioavailability [Menegário *et al.*, 2017]. However, the results might underestimate bioavailable Cu as DGT provides a time-integrated concentration and Cu may be bound to large complexes with low diffusion coefficients. Some MOB possess specific uptake pathways such as the ligand methanobactin [Chi Fru, 2011; Kenney and Rosenzweig, 2018], which may increase the bioavailable Cu fraction.

Maximum bioavailable Cu (Cu_{DGT}) concentrations were usually found within the oxic zone of Rotsee (1.6-3.1 nM, Figure 1b,f,j,n, Supplementary Figure S1, Supplementary Table S1, Kruskal-Wallis: $p < 0.001$). The concentrations were about a factor of ten lower than dissolved Cu (Cu_{Diss}), which reached concentrations in the low nM range (11.1-17.7 nM, Figure 2a-d, Supplementary Figure S1). Cu_{DGT} is expected to be highest where Cu_{Diss} is high. This is typically in the surface layers where Cu originating from river water or surface runoff enters the lake. In addition, concentrations in the epilimnion can be increased due to degradation of organic matter and the release of organically bound Cu. Differences between Cu_{DGT} and Cu_{Diss} might arise due to the bonding of Cu with strong organic complexes, which can pass the 0.45 µm pore size filter and diffuse through the diffusive layer, but cannot be captured by the resin inside the DGT sampling unit [Odzak *et al.*, 2002; Menegário *et al.*, 2017]. Dissolved organic carbon (DOC) profiles were quite homogeneous throughout the water column and do not elucidate any Cu-binding capacity therein (Supplementary Figure S2). Both Cu fractions clearly decreased from the epi- to the hypolimnion and profiles followed typical patterns previously observed at lower resolutions in other subalpine lakes in Switzerland [Xue *et al.*, 1997; Odzak *et al.*, 2002]. MOB need to acquire Cu to build and activate pMMO. They can either directly incorporate bioavailable Cu (Cu_{DGT}) or enlarge this fraction by the use of different Cu uptake mechanisms [Ve *et al.*, 2012; Gu *et al.*, 2016; Kenney and Rosenzweig, 2018]. These auxiliary peptides collect Cu and bind it with high affinity, hence, they are not included in the Cu_{DGT} fraction, and only measured as Cu_{Diss}. We monitored strong Cu_{DGT} and Cu_{Diss}

gradients towards the CH₄ oxidation zones where concentrations were depleted (Figure 1b,f,j,n, Figure 2a-d). Calculated particulate Cu concentrations ($Cu_{part} = Cu_{tot} - Cu_{diss}$) showed maximum values within the CH₄ oxidation zones (1.9-8.5 nM, Figure 1b,f,j,n, Supplementary Figure S1, Supplementary Table S1, Kruskal-Wallis: $p < 0.05$), which matches well with the decreases in Cu_{DGT} and Cu_{Diss} . Cu_{part} showed some additional local peaks within the other zones (Figure 1b,f,j,n, Supplementary Figure S1).

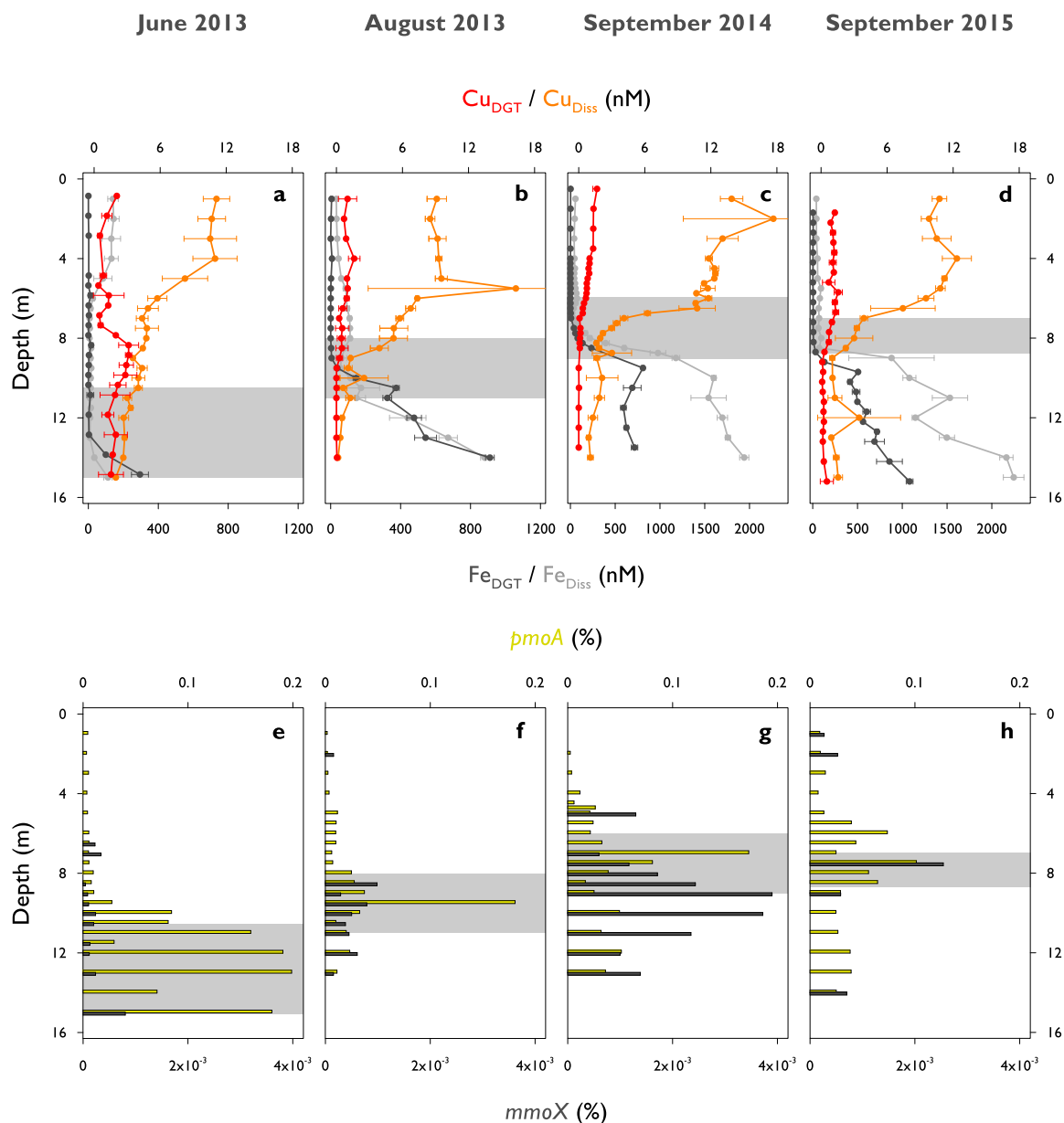


Figure 2. Bioavailable and dissolved metal concentrations and relative methane monooxygenase functional gene abundances in Rotsee.

(a,e) June 2013. (b,f) August 2013. (c,g) September 2014. (d,h) September 2015. The grey boxes show the depth range of potential highest methane oxidation (see Figure 1). (a-d) Depth profiles of bioavailable and dissolved copper (Cu_{DGT} in red, Cu_{Diss} in orange) and iron (Fe_{DGT} in dark grey, Fe_{Diss} in light grey) concentrations. Cu_{DGT} concentrations are identical to Figure 1. Error bars represent standard deviations ($n = 3$ or $n = 4$). (e-h) Relative abundances of *pmoA* (considering two *pmoA* genes per MOB, yellow) and *mmoX* (dark grey).

MOB zonation and functional gene distributions

To link physico-chemical conditions with microbial CH₄ consumption dynamics, we quantified bacterial 16S rRNA and functional gene (*pmoA* and *mmoX*) distributions in Rotsee down to 0.5 m resolution. 16S rRNA sequencing yielded a total number of 3679 Operational Taxonomic Units (OTUs). In-depth analysis of the OTU data set revealed a total of 15 OTUs belonging to γ -MOB and one α -MOB OTU (Supplementary Table S2). *Verrucomicrobia* were also detected and were represented by 5 OTUs. 3 of the 5 OTUs were assigned to potentially methanotrophic clades ($p \leq 0.85$) while the remaining two belonged to a family known not to contain any MMO (LD19), which hence probably lack the ability of oxidizing CH₄ [Hugerth *et al.*, 2015]. As the applied primer pair for *pmoA* detection did not cover verrucomicrobial *pmoA* sequences, and genomic investigations of freshwater *Verrucomicrobia* implicated them as (poly)saccharide degraders [He *et al.*, 2017], the verrucomicrobial OTUs were not included in the further analysis of the data.

MOB diversity was highest in September 2014 and 2015, when richness peaked at 15 OTUs, whereas in June and August 2013, the MOB community consisted of 10 and 11 OTUs, respectively (Supplementary Table S2). The single α -MOB OTU was found in all campaigns, but with variable abundance. This OTU appeared primarily in the epilimnion and was therefore unlikely to participate in the dominant CH₄ oxidation process in Rotsee (Figure 1c,g,k,o). The MOB community was dominated by γ -MOB, which is in agreement with previous studies on Rotsee and other (sub)alpine lakes, suggesting that γ -MOB play an important role in freshwater CH₄ cycling [Schubert *et al.*, 2010; Milucka *et al.*, 2015; Oswald *et al.*, 2015, 2017; Oswald, Milucka, *et al.*, 2016]. Although most so far characterized γ -MOB are obligate aerobes, we could detect them in suboxic and anoxic layers throughout the campaigns. We found maximum absolute MOB cell numbers (10^6 - 10^7 cells L⁻¹) directly below the oxycline in August 2013 and September 2014 (Figure 1g,k), which supports our assumption that MOB abundance peaks at depths where physico-chemical profiles indicate active aerobic CH₄ oxidation. Within the CH₄ oxidation zones the proportion of MOB reached 1.2-3.4% of the total bacterial abundance.

In June 2013, most MOB (10^8 cells L⁻¹) were found in deeper layers where neither O₂ nor oxygenic phototrophs were detected (Figure 1c) [Brand *et al.*, 2016]. Several mechanisms may allow MOB to persist under these conditions. It is possible that some MOB from the oxic period during the winter mixing remained

in the deeper parts of the lake or that they are settling from upper, oxygenated water layers. MOB could potentially be inactive under anoxic conditions, as it is known that MOB can enter a state of anaerobic dormancy for extended periods of O₂ starvation [Roslev and King, 1994]. However, the methodology applied in this study cannot determine the activity of the cells. Some MOB species in the dark, anoxic layers of Rotsee may be able to survive O₂-limiting conditions while using fermentation as their main metabolic strategy [Kalyuzhnaya *et al.*, 2013]. MOB may live mixotrophically or use other reduced carbon compounds as alternative energy sources (facultative MOB) [Semrau *et al.*, 2011]. Or, they could be involved in anaerobic oxidation of CH₄ (AOM) and use O₂ or other electron acceptors provided by different reaction pathways [Kits, Klotz, *et al.*, 2015; Bar-Or *et al.*, 2017]. Anaerobic methanotrophic archaea could also play a role in oxidizing CH₄ at depths depleted in O₂ [Cui *et al.*, 2014], however, in this study DNA was only screened for bacteria. MOB distribution in September 2015 showed an abundance maximum above the oxycline with a majority of α -MOB (10⁷ cells L⁻¹, Figure 1o). There is evidence that littoral sediments can act as additional source of MOB in the water column [Hofmann *et al.*, 2010]. Alternatively, MOB may accumulate due to *in-situ* CH₄ production in the oxygenated epilimnion, a phenomenon that has been frequently observed [Donis *et al.*, 2017].

The potential involvement of particulate and soluble MMO was identified by the quantitative detection of *pmoA* and *mmoX*, respectively. As most MOB contain *pmoA*, these results can independently confirm MOB abundance evaluated from 16S rRNA sequencing data. Real time quantitative polymerase chain reaction (qPCR) yielded *pmoA* copy numbers between 10⁴-10⁷ copies L⁻¹ (Figure 1d,h,l,p). The depth-distribution of *pmoA* counts correlated well with MOB concentrations from 16S rRNA based community analysis, resulting in R²-values of 0.89 (June 2013), 0.98 (August 2013), 0.87 (September 2014) and 0.40 (September 2015). However, absolute numbers suggested by *pmoA* analysis were on average a factor of ~30 lower than those derived from 16S rRNA gene analysis, possibly a result of methodical biases. Correspondingly, the calculated proportion of cells containing copies of *pmoA* was between 0.002-0.2% (Figure 2e-h).

Relative abundances of *mmoX* were on average 160 times lower compared to *pmoA* and remained below the limit of quantification for some samples (Figure 2e-h). This indicates that we never observed a population with *mmoX* becoming a numerically important part of the MOB community. It has been reported that cells expressing pMMO have a higher growth yield and greater affinity for CH₄ than cells relying on the sMMO

mechanism [Leak and Dalton, 1986b; Hanson and Hanson, 1996], which suggests that pMMO is the more efficient system. *mmoX* was usually found in the hypolimnion of Rotsee. The highest relative abundance of *mmoX* was observed in September 2014 (Figure 2g), and this was the only time a clear *mmoX* peak was observed ~2 m below the *pmoA* maximum, towards the lower end of the CH₄ oxidation zone. This coincided with minimum Cu and highest iron availability (Fe_{DGT} and Fe_{Diss}, Figure 2a-d) and could support the notion that MOB populations with this gene grow under Cu limited conditions at this specific time point. However, correlations between MOB and *mmoX* distributions were rather low over all campaigns ($R^2 = 0.00-0.54$). We propose that sMMO-mediated CH₄ oxidation is of minor importance in Rotsee at the investigated sampling dates, although additional studies are needed to confirm this.

Having a closer look on the specific CH₄ oxidation zones of August 2013 and September 2014, the concentrations of *pmoA* genes rapidly increased at the upper boundary of the zones in which they showed highest abundances (Figure 1h,l). Their concentrations increased in parallel with Cu_{Part} (Figure 1f,j). In September 2014 the correlation between *pmoA* and Cu_{Part} within the CH₄ oxidation zone was high ($R^2 = 0.85$), however, R^2 -values for the other three campaigns were much lower (June 2013: 0.22, August 2013: 0.30, September 2015: 0.06) indicating that MOB did not constitute the main component of the Cu_{Part} concentration.

Biogeochemical fluxes and competition for copper in the methane oxidation zone

We computed fluxes of various solutes into the CH₄ oxidation zones from measured concentration gradients and a site-specific coefficient for turbulent diffusion (Supplementary Table S3). Dissolved O₂ concentrations in the epilimnion of Rotsee gradually decreased towards the oxycline (Figure 1a,e,i,m). O₂ downward fluxes showed the largest change, from lowest values in June 2013 when stratification was still in its early stage (3.4 mmol m⁻² d⁻¹), to about tenfold higher ones in the other three campaigns (27.6-42.9 mmol m⁻² d⁻¹). These O₂ flux estimates do not account for potential oxygenic photosynthesis within the seemingly anoxic CH₄ oxidation zone [Brand *et al.*, 2016]. Theoretical CH₄ fluxes out of the sediment were about half to one order of magnitude lower than for O₂ (2.7-13.3 mmol m⁻² d⁻¹), except for June 2013 (10.2 mmol m⁻² d⁻¹), which indicates O₂ is being consumed by additional processes, like mineralization and oxidation of other reduced substances. Dissolved and bioavailable Cu fluxes from the lake's surface down to where they are depleted were

in the $\text{nmol m}^{-2} \text{d}^{-1}$ range, with values for Cu_{Diss} being about ten times higher than for Cu_{DGT} (Table 1). The Cu_{Part} pool integrated over the CH_4 oxidation zones ranged from 2.4 to $13.1 \mu\text{mol m}^{-2}$ (Table 1). As Rotsee typically starts to re-stratify in April [Brand *et al.*, 2016], it has been stratified for approximately 60 d in June 2013, 120 d in August 2013 and 160 d in September 2014 and 2015. We calculated a rough estimate of the Cu_{Part} build-up times based on Cu_{Diss} fluxes (6-39 d, Table 1) and the results indicate that Cu_{Part} build-up would have required much less time than the stratification period. Thus, organisms or particle formation processes either cannot access the Cu_{Diss} fraction, or else Cu_{Part} settling rates are extremely high. In contrast, accumulation times estimated for Cu_{DGT} fluxes (212-433 d, Table 1) were much longer than the time elapsed since the onset of stratification (with exception of September 2015 with 60 d). This indicates that either organisms in the CH_4 oxidation zones established mechanisms to mobilize Cu from other not directly available sources, or that the bioavailable Cu values measured by the DGT method were underestimating the true bioavailable concentrations.

Table 1. Methane-oxidizing bacterial cell numbers, copper pools, fluxes, and resulting accumulation times in Rotsee's methane oxidation zones.

Parameter		June 2013 (10.5 - 15 m)	August 2013 (8 - 11 m)	September 2014 (6 - 9 m)	September 2015 (7 - 8.7 m)
Integrated relative MOB	(%)	6.0	1.4	1.7	0.9
Integrated absolute MOB	(cells m^{-2})	3.8×10^{11}	5.5×10^{10}	6.6×10^{10}	2.8×10^9
Cu_{Part} pool contributed by MOB	(nmol m^{-2})	14	2	1	0.1
Cu_{Part} pool in Rotsee	(nmol m^{-2})	4100	13'100	5200	2400
Cu_{DGT} flux	($\text{nmol m}^{-2} \text{d}^{-1}$)	19	30	20	40
Cu_{Diss} flux	($\text{nmol m}^{-2} \text{d}^{-1}$)	195	336	828	394
Accumulation time (Cu_{DGT})	(d)	212	433	254	60
Accumulation time (Cu_{Diss})	(d)	21	39	6	6

Numbers in parentheses denote the depth range of the defined methane oxidation zones (grey zones in Figures 1 and 2). Absolute and relative methane-oxidizing bacterial (MOB) cell numbers as well as particulate copper (Cu_{Part}) concentrations were integrated over the methane oxidation zones. Cu_{Part} stemming from MOB was calculated using MOB cell counts and the MOB copper content ($4 \times 10^{-20} \text{ mol Cu cell}^{-1}$) developed from literature values. Accumulation times were estimated by applying bioavailable copper (Cu_{DGT}) or dissolved copper (Cu_{Diss}) fluxes calculated into the zones on the measured Cu_{Part} pool in Rotsee.

In order to assess whether MOB are an important contributor to Cu_{part} in Rotsee's CH_4 oxidation zones, we calculated an extended Redfield stoichiometry (Cu:C) for a single MOB cell. The Redfield ratio stands for the specific elemental composition (C:N:P) of a cell reflecting the conditions under which it grows [Redfield, 1934]. Assuming an average MOB spherical cell diameter of $2\ \mu\text{m}$, the biovolume of a single cell ($\mu\text{m}^3\ \text{cell}^{-1}$) can be converted into biomass (mol carbon cell^{-1}) by applying a carbon (C) conversion factor of $6.4\ \text{fmol C}\ \mu\text{m}^{-3}$ [Oswald *et al.*, 2015]. This results in a C content of $0.03\ \text{pmol C}\ \text{cell}^{-1}$. Considering the studies focusing on the type and number of Cu ions in pMMO's metal centre, we choose a range of 2-15 Cu ions per pMMO [Wang, Maji *et al.*, 2017]. Accepting the estimate of Nihous by which cell membrane walls are able to bind between 1000-4000 pMMO enzymes [Nihous, 2010], a single MOB organism contains between 2000-60'000 Cu atoms in pMMO, which amounts to a mean of $4 \times 10^{-20}\ \text{mol Cu}\ \text{cell}^{-1}$. Putting this value in relation to the calculated C content, we obtained an averaged proportion for Cu:C of 10^{-6} . This ratio is more likely to be an under- than an overestimate since MOB cells contain Cu acquisition and storage proteins and use Cu also for other enzymes besides pMMO [Glass and Orphan, 2012; Ve *et al.*, 2012; Johnson *et al.*, 2014; Lawton *et al.*, 2016; Dennison *et al.*, 2018; Kenney and Rosenzweig, 2018]. Nevertheless, based on these cellular Cu contents we calculated a contribution of MOB to Cu_{part} that underestimates the actually measured *in-situ* Cu_{part} concentrations by a factor of 10^2 - 10^4 (Table 1). Even though MOB have an overall stronger Cu demand than other organisms (~ 10 times) [Semrau *et al.*, 2010; Chi Fru, 2011; Glass and Orphan, 2012], and we saw agreement in the distributions of MOB, *pmoA* and Cu_{part} at expected CH_4 oxidation zones, we conclude that they contributed only a small part of the measured Cu_{part} in Rotsee.

Cu holds an important role in the photosynthetic and respiratory electron transport in phytoplankton [Meyer and Cusanovich, 2003]. Extended Redfield ratios of marine and freshwater phytoplankton centre around a total Cu content of 10^{-16} - $10^{-18}\ \text{mol cell}^{-1}$ and a Cu:C ratio of $\sim 10^{-6}$ [Knauer *et al.*, 1997; Ho *et al.*, 2003; Wang, Xia *et al.*, 2017]. This Cu:C ratio is similar to the theoretical stoichiometric ratio of a MOB cell, but phytoplankton, being significantly larger than MOB, contains much more Cu per cell (factor 10^2 - 10^4). With the exception of June 2013, Cu_{part} concentrations showed distinct peaks within the defined CH_4 oxidation zones, which coincided well with chlorophyll a (Chl-a) maxima and turbidity (Turb) measurements (Supplementary Figure S3), both suitable proxies for phytoplankton abundance. As primary producers were present in similar numbers as MOB in Rotsee ($\sim 10^7\ \text{cells L}^{-1}$) [Brand *et al.*, 2016], we suggest that the difference

in Cu content between MOB and phytoplankton explains most of the observed discrepancy between measured Cu_{Part} and the calculated Cu_{Part} contribution of MOB within the defined zones (Figure 3). In June 2013, lower Cu_{DGT} concentrations in the epilimnion might illustrate the uptake by phytoplankton at ~ 6.5 m (Figure 1b, Supplementary Figure S3). This corresponded to the slight decrease in Cu_{Diss} at similar depths (Figure 2a). However, a second distinct Chl-a increase at deeper depths was missing, indicating an overall weaker Cu-consumption by primary producers, which resulted in elevated Cu_{DGT} concentrations.

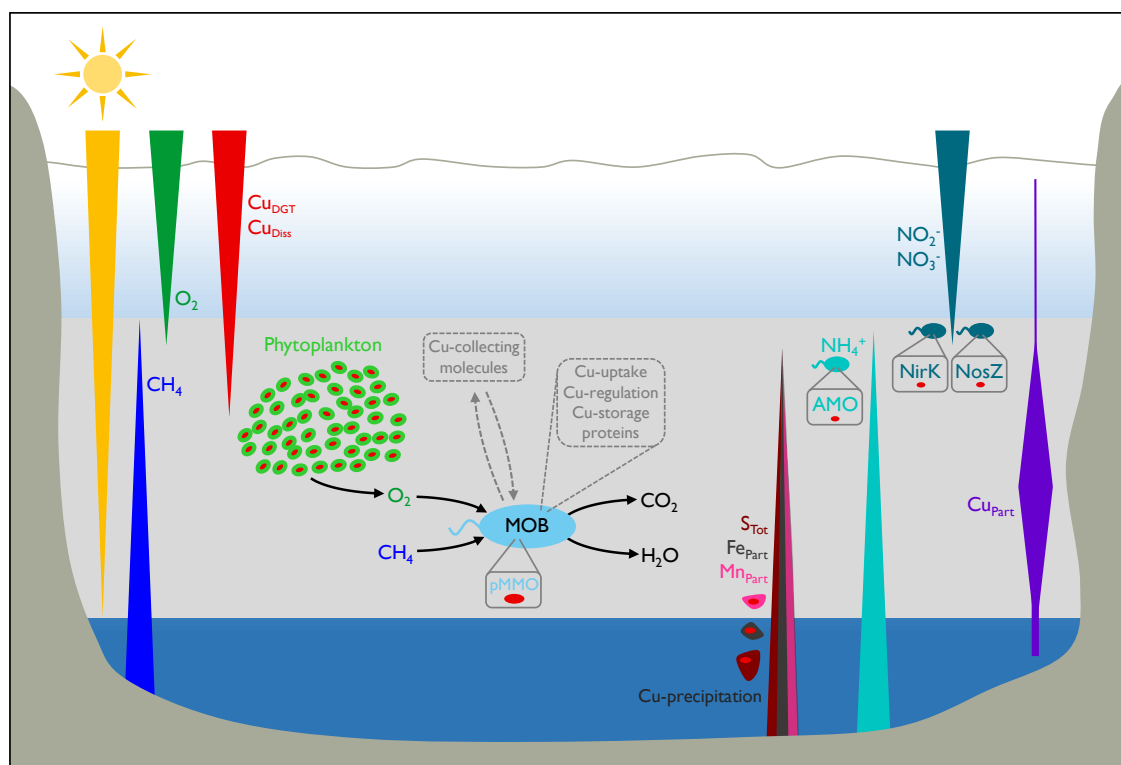


Figure 3. Conceptual model of the biogeochemistry of copper within the methane oxidation zone in Rotsee.

Long triangles depict concentration gradients of different parameters across the water column. Bioavailable and dissolved copper (Cu_{DGT} , Cu_{Diss}) diffuse into the methane (CH_4) oxidation zone (grey bar) and are depleted by different processes, which contribute to elevated particulate copper (Cu_{Part}). Methane-oxidizing bacteria (MOB) are highly abundant in the CH_4 oxidation zone and need to compete for Cu, the fundamental micronutrient for their major enzyme particulate methane monooxygenase (pMMO). Phytoplankton is the main constituent of Cu_{Part} and the main competitor for Cu. However, its presence is at the same time crucial for MOB as it provides O_2 under low light conditions in anoxic depths, which is used by MOB. Cu can also be incorporated into other bacteria, for example ammonia-oxidizing bacteria and bacteria involved in denitrification. They use Cu for their central enzymes ammonia monooxygenase (AMO) and nitrite reductase (NirK)/nitrous oxide reductase (Nos). Further, Cu can be captured by rising sulphide (S_{Tot}) and precipitate to the sediment as CuS or Cu can be scavenged by precipitating iron and manganese oxides (Fe_{Part} , Mn_{Part}). Therefore, MOB probably make use of Cu scavenging mechanisms, i.e. the release of Cu-collecting molecules (methanobactin or MopE*) and the involvement of Cu-uptake (CorA), Cu-regulation (CopCD) and Cu-storage proteins (Csp).

These findings lead to the conclusion that MOB are strongly enriched within highest CH₄ oxidation zones despite low bioavailable Cu supply and co-occurrence of large numbers of oxygenic primary producers, which possibly create a setting of Cu competition. MOB cannot escape the Cu scarcity as in the study system they also rely on oxygenic primary production for O₂ supply (Figure 3) [Oswald *et al.*, 2015; Brand *et al.*, 2016]. The low Cu availability may at first glance appear as an impediment to the growth of MOB. Nevertheless, it has been suggested that the competitiveness of MOB in terms of Cu acquisition may in fact favour their growth [Chang *et al.*, 2018]. Cu is also an essential element for many other bacteria and organisms [Festa and Thiele, 2011]. Enzymes involved in the denitrification process, in particular the nitrite reductase (NirK) and the nitrous oxide reductase (Nos), are Cu-rich proteins [Glass and Orphan, 2012]. Nitrite (NO₂⁻) and nitrate (NO₃⁻) concentrations in Rotsee were low (max. 30 µM) and it seems that the organisms containing these proteins potentially only make a small contribution to Cu_{part} (Supplementary Figure S4). In addition, some MOB species also contain the gene for the nitrite reduction process (NirK) [Oswald *et al.*, 2017]. The closely related pMMO homologue, ammonia monooxygenase (AMO), belongs to the Cu-containing membrane-bound monooxygenase (CuMMO) superfamily and catalyses the initial ammonia (NH₃) oxidation step [Lawton *et al.*, 2015]. Inferred sites of NH₄⁺ oxidation or uptake by primary producers in Rotsee only weakly overlapped with Cu_{part} maxima (Supplementary Figure S5).

Alternative mechanisms for Cu_{part} formation might include abiotic reactions, such as iron and manganese oxide scavenging or precipitation with sulphide (Figure 3) [Hamilton-Taylor *et al.*, 2005], but we found little evidence that any of these processes are dominant in Rotsee. Profiles of particulate iron (Fe_{part}) and manganese (Mn_{part}) did not appear to be strongly related to the Cu_{part} profiles (Supplementary Figure S6). Sequencing data of sulphur oxidizing bacteria (SOB) showed highest relative abundances at the upper hypolimnion where light was still measurable (Supplementary Figure S7). We assume that total sulphide (S_{Tot}) is continuously consumed by SOB during the day during which sampling campaigns were conducted [Kohler *et al.*, 1984] and thus resulting Cu_{part} precipitation with S_{Tot} would be minimal.

Discussion

Our findings have important implications for CH₄ oxidation in lakes and specifically for Cu-dependent MOB activity. During stratification, MOB in Rotsee were abundant within a zone with CH₄ supply from the sediment and O₂ release from oxygenic photosynthesis (Figure 3). Most of the CH₄ generated in the sediment was oxidized at this oxic-anoxic boundary. CH₄ concentrations could have additionally been reduced within the hypolimnion of the lake, however, in this study we did not specifically assess the potential for anaerobic oxidation of CH₄. Bioavailable and dissolved Cu concentrations were in the nanomolar range and showed strong depletion in the zone of CH₄ oxidation. Far higher *pmoA* copy numbers, coding for the Cu-containing enzyme, compared to *mmoX* were found in the whole water column at all times. The dominant MOB species therefore had to cope with Cu scarcity and they were not the only competitors. Other organisms, particularly oxygenic phototrophs, possibly competed for Cu in the CH₄ oxidation zones (Figure 3). However, MOB could have used several mechanisms to deal with low Cu supply conditions to maintain pMMO production. The chalkophore methanobactin is able to dissolve Cu from soluble, mineral, and humic sources [Chi Fru, 2011; Kenney and Rosenzweig, 2018]. MopE is a membrane-bound Cu binding protein, and its truncated form (MopE*) is secreted into the environment to collect Cu [Ve *et al.*, 2012]. MopE* shares sequence resemblance to the CorA (copper repressible) protein. CorA is located on the cell surface and it is postulated to be involved in the uptake of Cu into the cell [Johnson *et al.*, 2014]. A copper resistance protein-mediated (CopCD) Cu uptake may play a role for delivering Cu to the cytosol of the cell [Lawton *et al.*, 2016]. Additional insight in how MOB manage their Cu demand has also been provided by the recent discovery of a new family of Cu storage proteins (Csp) [Dennison *et al.*, 2018]. Such mechanisms are likely to be crucial for MOB ecology in low-Cu environments such as Rotsee.

This detailed *in-situ* study of Cu and CH₄ oxidation reveals that MOB species containing the gene for a potential Cu-dependent enzymatic pathway are abundant despite low bioavailable Cu concentrations and excess of Fe. We provide evidence that other biological processes and abiotic reactions could have a profound impact on the availability of Cu in the water column, which may in turn have consequences for the ecology of CH₄ oxidation, a critical process in the global carbon cycle. Since Rotsee is representative for mid-latitude,

nutrient-rich lakes in terms of topography and chemical cycling, we expect that the observed distribution of Cu species as well as the vertical zonation of MOB and phytoplankton is typical for such lakes. Therefore, the proposed Cu competition and inferred mechanisms of MOB adaptation to Cu scarcity may be common in numerous other lakes.

Methods

Study site

Rotsee is a small (1 km²), eutrophic subalpine lake in Switzerland with a maximum depth of 16 m. Rotsee exhibits a stable summer stratification from approximately April-November with an oxycline between 6 m and 9 m depth [Schubert *et al.*, 2010; Brand *et al.*, 2016]. Large amounts of CH₄ are released from the sediments reaching concentrations up to 1 mM before winter overturn [Schubert *et al.*, 2010].

In-situ profiling and sampling, chemical analysis

Four sampling campaigns were conducted (June 2013, August 2013, September 2014, September 2015) near the deepest part of Rotsee (47°04.259'N, 8°18.989'E). A custom built device (Profiler for *In-situ* Analysis, PIA) [Kirf *et al.*, 2014] was used for high resolution profiling and sampling: conductivity, turbidity, depth, temperature and pH were monitored with a CTD multi-parameter probe and Chl-a with an ECO-FL fluorescence probe (Wetlabs). Profiles of dissolved oxygen (O₂) concentrations were obtained from two needle-type optodes (PSt1 and TOS7, PreSens) with detection limits of 125 nM (normal) and 20 nM (trace), respectively. Photosynthetically active radiation (PAR) was recorded with a spherical quantum sensor (LI-190 SB, LI-Cor). Detection limit of PAR sensing photon flux was 0.1 μmol m⁻² s⁻¹. Water for chemical analysis was taken using an integrated rosette syringe sampler (12 x 60 ml syringes), which could be triggered remotely during profiling. Sampling was carried out across the whole water column with high resolution in the oxycline (0.25-0.5 m) and in one-meter steps otherwise. Aliquots for sulphate (SO₄²⁻), nitrite (NO₂⁻), nitrate (NO₃⁻) and ammonium (NH₄⁺) were filtered (0.22 μm cellulose acetate syringe filters) and analysed on the same day by ion chromatography (881 Compact IC pro, 882 Compact IC plus, 761 Compact IC, Methrom AG) and flow-injection analysis (SAN++, Skalar, Procon AG). Samples for total sulphide (S_{Tot}) detection were immediately fixed with zinc acetate (final concentration: ~1.3%) and determined spectrophotometrically [Cline, 1969]. Equipment for metal sampling and filtering was acid-washed and rinsed with nanopure water before use. Triplicate samples for dissolved (< 0.45 μm cellulose acetate syringe filters)

and total metals (Cu_{Diss} , Cu_{Tot} , Fe_{Diss} , Fe_{Tot} , Mn_{Diss} , Mn_{Tot}) were acidified on-site to a final concentration of 0.1 M HNO_3 and analysed with inductively coupled plasma mass spectrometry (ICP-MS, Element2, Thermo). Particulate metal species (Cu_{Part} , Fe_{Part} , Mn_{Part}) were calculated as $\text{Cu}_{\text{Part}} = \text{Cu}_{\text{Tot}} - \text{Cu}_{\text{Diss}}$. Cu_{Part} errors were estimated by standard deviation propagation from dissolved and total metal measurements. Aliquots for dissolved organic carbon (DOC) analysis were filtered (0.22 μm , Millex-GP polyethersulfone syringe filters) into pre-combusted glass vials and acidified with 2 M HCl (final concentration: 20 mM) and measured on a total carbon analyser (TOC-L_{CSH/CPH}, Shimadzu) equipped with a non-dispersive infrared detector. Outliers of triplicate samples were removed applying Grubbs' outlier test. Methane (CH_4) samples were collected with a Niskin bottle or via pumping with a gas tight tubing (PVC Solaflex, Maagtechnic) attached to PIA. 120 ml serum bottles were filled anoxically, poisoned with NaOH ($\text{pH} > 12$) or Cu(I)Cl , and sealed with butyl-rubber stoppers and aluminium crimps. In the laboratory, a 20 ml nitrogen (N_2) headspace was inserted. After overnight equilibration at room temperature, CH_4 was measured by headspace injection using a gas chromatograph (GC, Agilent 6890N, Agilent Technologies) equipped with a Carboxen 1010 column (30 m x 0.53 mm, Supelco) and a flame ionization detector (detection limit: ~ 10 nM). Vertical diffusive fluxes of dissolved compounds into the CH_4 oxidation zones (Supplementary Table S3) were calculated from the chemical concentration gradients determined by linear regression and a vertical turbulent diffusion coefficient of $10^{-6} \text{ m}^2 \text{ s}^{-1}$ [Schubert *et al.*, 2010; Oswald *et al.*, 2015; Brand *et al.*, 2016].

Diffusive Gradients in Thin film gels (DGT)

DGT preparations were performed in a clean room (except for June 2013). All plastic devices, containers and membrane filters were soaked in diluted HNO_3 for 24 h and rinsed with nanopure water before use. Acrylamide (40%, Sigma Aldrich), agarose cross-linker (2%, DGT Research Ltd.) and nanopure water were used to generate diffusive and resin hydrogels according to Odzak *et al.* [Odzak *et al.*, 2002]. To initiate chemical polymerisation freshly mixed ammonium persulfate (10%, Sigma Aldrich) and TEMED (N,N,N',N' -Tetramethylenediamine, 99%, Sigma Aldrich) were added. The resin hydrogel contained additional ion-exchange resin (Chelex-100, 200-400 mesh, Na^+ form, Bio-Rad). The gels were hydrated and cleaned with nanopure water and stored in 0.01 M NaNO_3 . Each piston was loaded with a resin gel, a diffusive gel (0.8 mm thickness), a protective filter (0.13 mm thickness, $< 0.45 \mu\text{m}$ cellulose nitrate, Sartorius) and a plastic cap (2 cm

diameter exposure window, Supplementary Figure S8). 3-4 DGTs were placed into a plastic stripe and attached to a rope. Deployment time was 2-3 days. Some DGTs were left in the laboratory as controls. After deployment, resin gel layers were eluted in 1 M HNO₃ for 1-2 days. After dilution (to 0.1 M HNO₃), bioavailable trace metal concentrations (Cu_{DGT}, Fe_{DGT}, Mn_{DGT}) were analysed via ICP-MS. The accumulated mass of the analytes was calculated following Davison [Davison, 2016] with published diffusion coefficients (accessed May 2016, <http://www.dgtresearch.com/diffusion-coefficients/>). The negligible thickness of the diffusive boundary layer was disregarded. Significant outliers were determined based on Grubbs' outlier test.

DNA extraction and sequencing of 16S rRNA

Water samples were pre-filtered (< 5.0 µm) and subsequently filtered onto 0.2 µm polycarbonate membranes. Filters were packed into plastic bags, immediately frozen in liquid N₂ and stored at -80°C until DNA was extracted using a PowerWater DNA Isolation Kit (MoBio Laboratories). Extracted DNA was quantified using a NanoDrop 1000 Spectrophotometer (Thermo Fisher). Illumina MiSeq sequencing technology was performed on amplicons obtained with bacterial primers 341f (5'-CCTACGGGNGGCWGCAG-3') and 805r (5'-GACTACHVGGGTATCTAATCC-3') [Herlemann *et al.*, 2011]. 16S rRNA gene PCRs, library preparation and sequencing were conducted by Microsynth. Sequence data was analysed by the Genomic Diversity Centre (ETH Zurich), which clustered the sequences into operational taxonomic units (OTUs) with a cut-off value of 97% similarity using the Uparse workflow with usearch (v8.1.1812_i86linux64). Taxonomic identity was classified via UTX based on the GreenGene database (May 2013, <http://greengenes.lbl.gov/>). Narrowing the data set gave a final alignment of 1 α-MOB, 15 γ-MOB, and 5 potential verrucomicrobial MOB (Supplementary Table S2, Supplementary xlsx-file "16S rRNA sequences_MOB"). These taxonomic assignments were confirmed against SILVA SSU database (release 123) using RDP classifier (confidence level of 80%) as well as by NCBI megaBLAST against GenBank numbers (<https://blast.ncbi.nlm.nih.gov/Blast.cgi>). OTUs of sulphur oxidizing bacteria (SOB) were chosen based on the assignments to phylum *Chlorobi* and orders *Chromatiales* and *Legionellales*, and were checked with literature [Rosenberg *et al.*, 2014b] (Supplementary xlsx-file "16S rRNA sequences_SOB").

Quantification of 16S rRNA, *pmoA* and *mmoX* genes

For analysing 16S rRNA and methane monooxygenase (MMO) functional genes, the limit of detection (LOD) was set as the highest crossing point (Cp-value) determined in PCR or extraction blanks. A sample was considered not detectable if either its Cp-value was \geq Cp-value LOD or if no clear, or multiple, melting temperature (Tm) peak(s) were detected in comparison to the positive control. The limit of quantification (LOQ) was the concentration of the lowest quantifiable standard dilution with a standard deviation of quadruplicate Cp-values < 0.5 . Samples above LOD were described not quantifiable when Cp-values of replicates differed more than 0.5, Cp-values were $> \text{LOQ}$, or when 2 out of 3 replicates were $< \text{LOD}$. However, some sample concentrations were estimated using standard curve extrapolation below LOQ. qPCR efficiency was calculated from the slope of the standard curve ($E = 10^{-1/\text{slope}}$). Product lengths were additionally verified by gel electrophoresis (1.5% agarose gel). All samples were run on a Roche Light Cycler 480 (Roche Diagnostics).

16S rRNA-qPCR reactions were adapted from Takai and Horikoshi [Takai and Horikoshi, 2000] (Supplementary Table S4). 16S rRNA gene copies were used as a proxy for the size of the bacterial community and for translating relative MOB abundances into absolute cell numbers by applying specific amounts of 16S rRNA copies per genome (5.8 for *Gammaproteobacteria*, 2.2 for *Alphaproteobacteria*, 4.2 for other bacteria [Větrovský and Baldrian, 2013]). Copy numbers of *pmoA* were measured using an adjusted protocol from Henneberger et al. [Henneberger *et al.*, 2015] (Supplementary Table S4). qPCR measurements of *mmoX* were performed following the conditions listed in Supplementary Table S4. To determine the calibration curves, plasmids containing amplifiable fragments of each target gene were serially diluted in AE buffer (5×10^7 - 5×10^0 copies per reaction). All standards were run in quadruplicates, all samples in triplicates. Genomic DNA of several axenic culture strains served as positive and negative controls (Supplementary Table S5). *pmoA* and *mmoX* gene copy numbers were both normalized with bacterial 16S rRNA gene copies [Větrovský and Baldrian, 2013], assuming 2 copies per MOB cell for *pmoA* [Murrell, McDonald *et al.*, 2000].

Statistical analysis

The water column of Rotsee was divided into three zones (oxic zone, methane oxidation zone, anoxic zone) to apply statistical testing using the Past3.18 statistic software (<http://folk.uio.no/ohammer/past/>). Normality of the data was tested by the Shapiro-Wilk test. Differences between the three zones were evaluated using the Kruskal-Wallis test followed by the Mann-Whitney pairwise test if normality was not met. Else, a one-way ANOVA following a Tukey's HSD test was performed. p-values < 0.05 were considered significant. Tests were conducted for all seasons, and for single seasons each (Supplementary Table S1).

Nucleotide sequence accession number

The gene sequences obtained in this study are publicly archived on the ENA database (accession number PRJEB28460).

Acknowledgements

We would like to thank Niksa Odzak for mentoring support in DGT preparation. Christian Dinkel, Kirsten Oswald, Hannah Bruderer and Tanja Beck are thanked for their help during field campaigns. We appreciate the assistance of Carsten Schubert, Serge Robert, Gijs Nobbe (R.I.P.), David Kistler and Patrick Kathriner in ICP-MS, GC, IC and FIA analysis. We greatly acknowledge the help of Karin Beck, Karolin Kleffel and Magdalena Mayr for PCR and qPCR development. We thank Ruth Henneberger for constructive discussions and providing pure MOB cultures. We are grateful to Kirsten Oswald and Rohini Athavale for making several methane, nutrients, ammonium and sulphide profiles available. Jean-Claude Walser (Genetic Diversity Centre, ETH Zurich) and Feng Ju are appreciated for their collaboration and help with analysis of next-generation sequencing data. Comments from Remo Freimann and Scott Winton improved the manuscript. This work was supported by the Swiss National Science Foundation (no. 153091).

Supplementary information

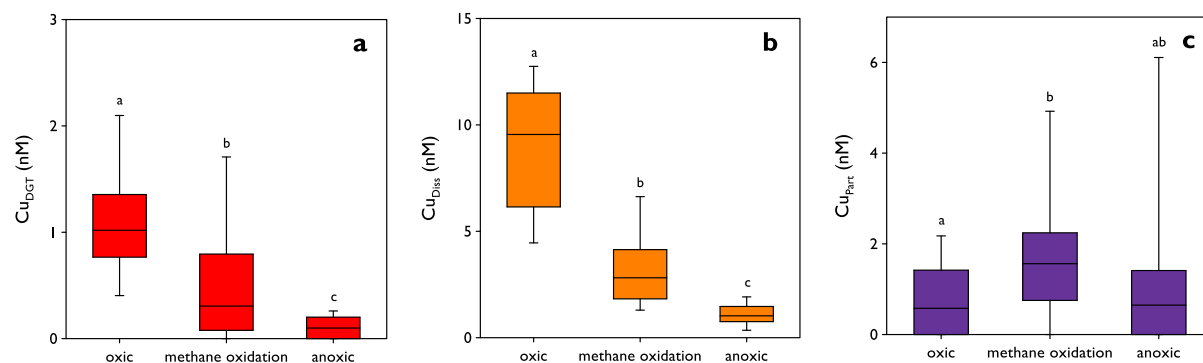


Figure S1. Box-Whisker plots of different copper species subdivided into three zones (oxic zone, methane oxidation zone, anoxic zone).

(a) Cu_{DGT} . (b) Cu_{Diss} . (c) Cu_{part} . Plots combine data from all four field campaigns (June 2013, August 2013, September 2014, September 2015). Boxes denote median and lower/upper quartiles, Whiskers represent 10/90 percentiles. Note the different y-axis ranges.

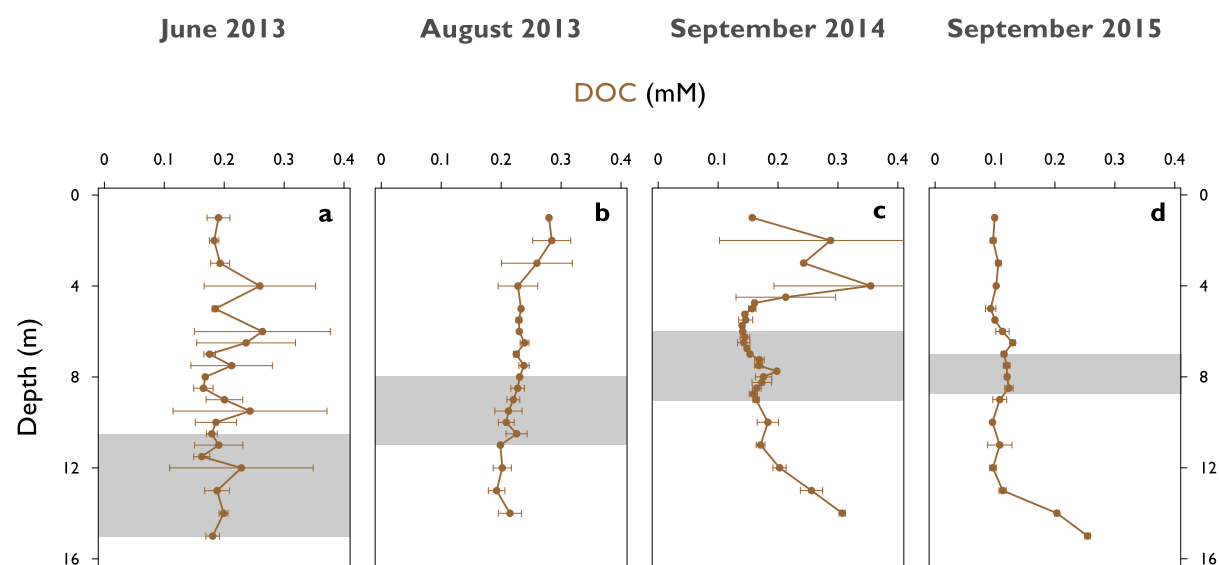


Figure S2. Depth profiles of dissolved organic carbon (DOC) in Rotsee

(a) June 2013. (b) August 2013. (c) September 2014. (d) September 2015. Grey areas represent potential methane oxidation zones. Error bars indicate standard deviations ($n = 3$).

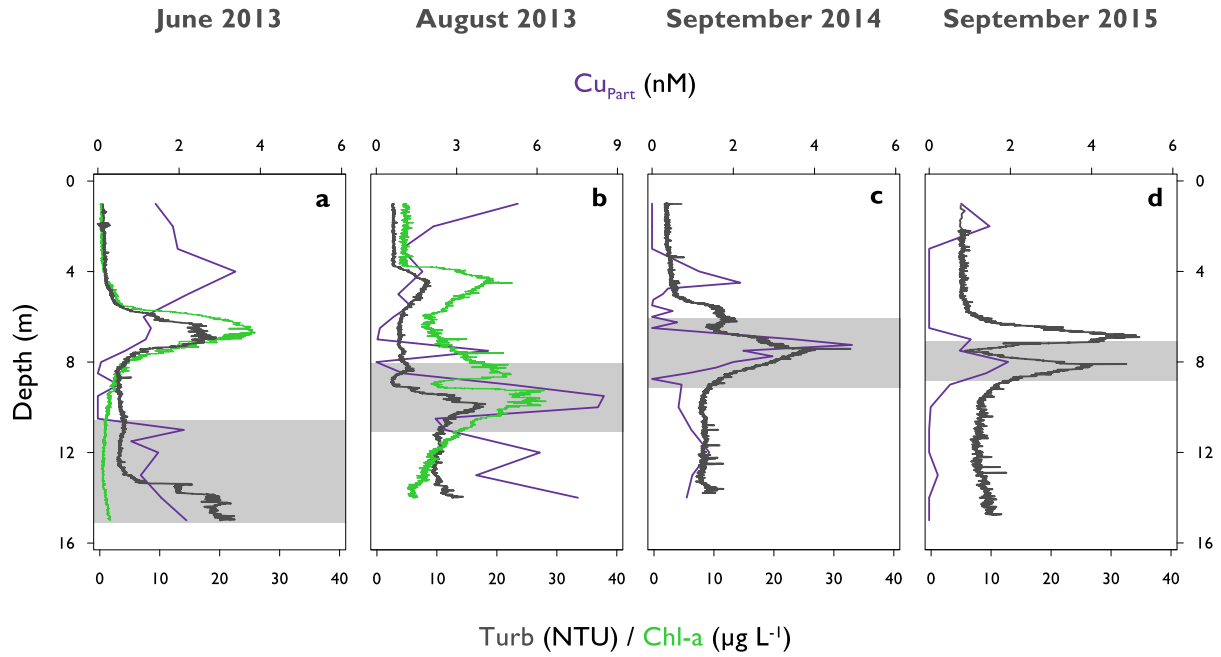


Figure S3. Turbidity, chlorophyll a and particulate copper profiles in Rotsee.

(a) June 2013. (b) August 2013. (c) September 2014. (d) September 2015. (a,b) Chlorophyll a (Chl-a) measurements are shown in grass green. No Chl-a data are available for September 2014 (c) and September 2015 (d), respectively. (a-d) Turbidity (Turb) is drawn in deep green, particulate copper (Cu_{Part}) in purple. Grey bars represent potential methane oxidation zones. Note the different x-axis scale for Cu_{Part} in August 2013 (b).

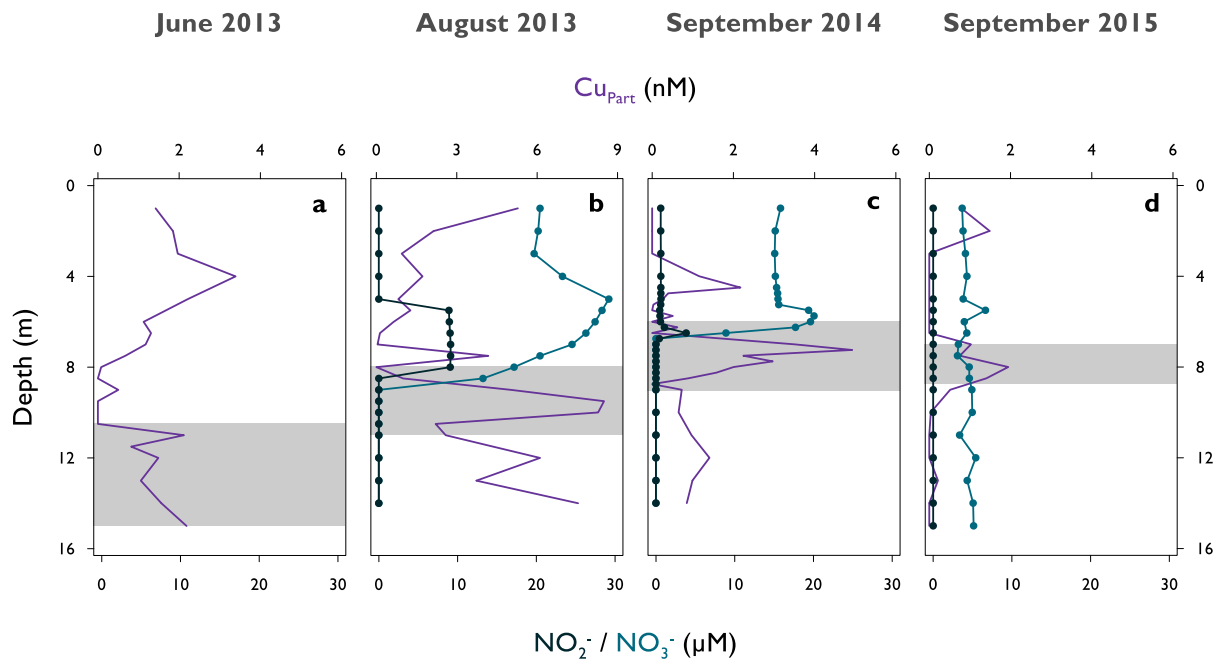


Figure S4. Water column profiles of nitrite, nitrate and particulate copper.

(a) June 2013. (b) August 2013. (c) September 2014. (d) September 2015. Particulate copper (Cu_{Part}) is shown in purple, nitrite (NO_2^-) in dark turquoise, nitrate (NO_3^-) in turquoise. Grey bars represent potential methane oxidation zones. Note the different x-axis scale for Cu_{Part} in August 2013 (b).

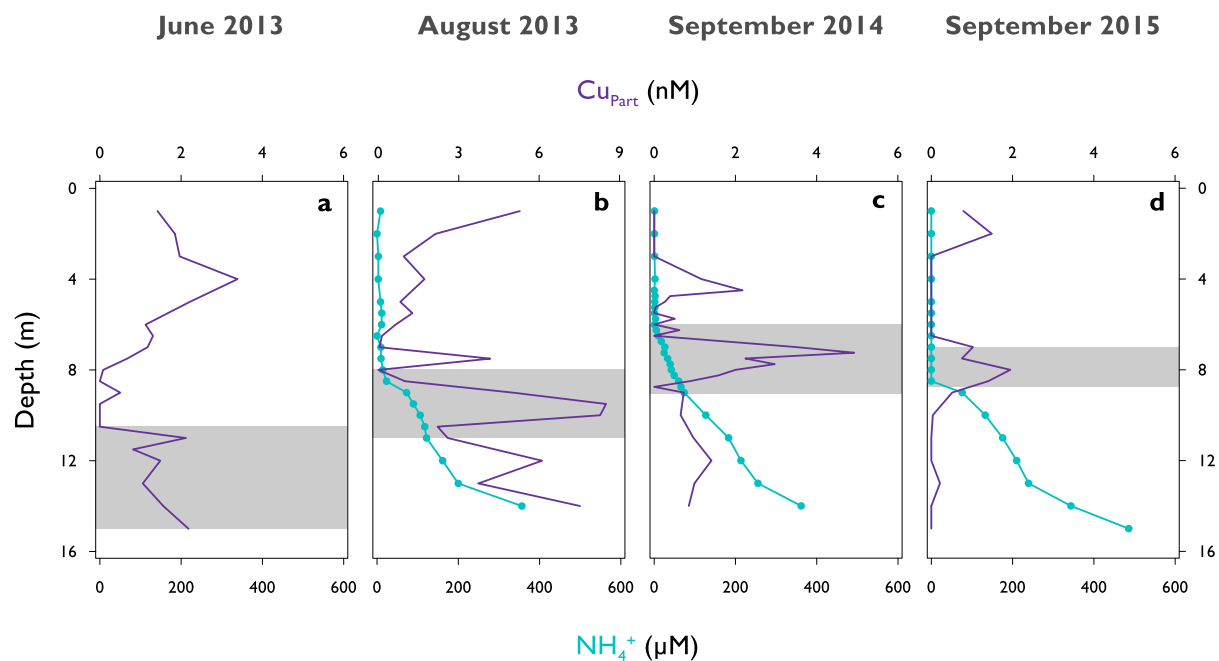


Figure S5. Ammonium and particulate copper concentrations in Rotsee.

(a) June 2013. (b) August 2013. (c) September 2014. (d) September 2015. Ammonium (NH_4^+) in light turquoise, particulate copper (Cu_{Part}) in purple. Grey areas denote potential methane oxidation zones. Note the different x-axis scale for Cu_{Part} in August 2013 (b).

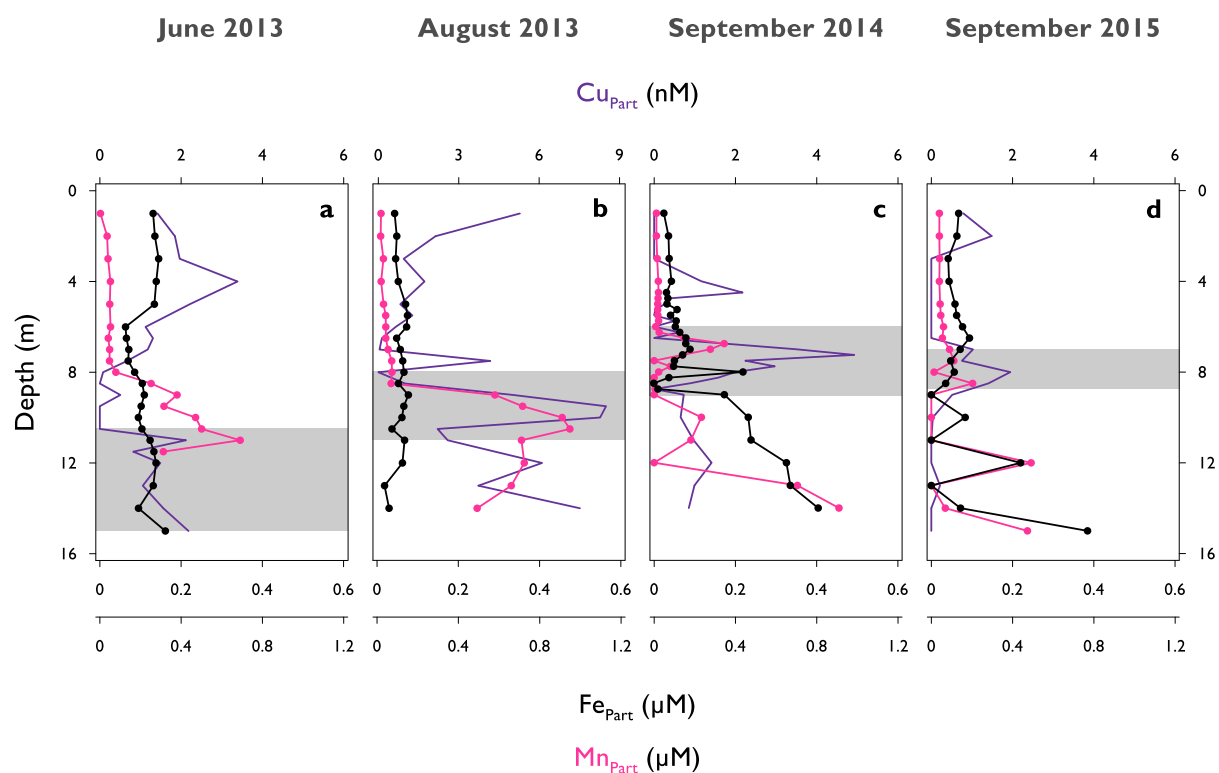


Figure S6. Depth profiles of particulate iron, manganese and copper in Rotsee.

(a) June 2013. (b) August 2013. (c) September 2014. (d) September 2015. Particulate iron (Fe_{Part}) in black, particulate manganese (Mn_{Part}) in pink, particulate copper (Cu_{Part}) in purple. Grey areas denote potential methane oxidation zones. Missing data in Mn_{Part} profiles in the hypolimnion of June 2013 (a) are due to undiluted concentrations exceeding ICP-MS maximum detection limit. Note the different x-axis scale for Cu_{Part} in August 2013 (b).

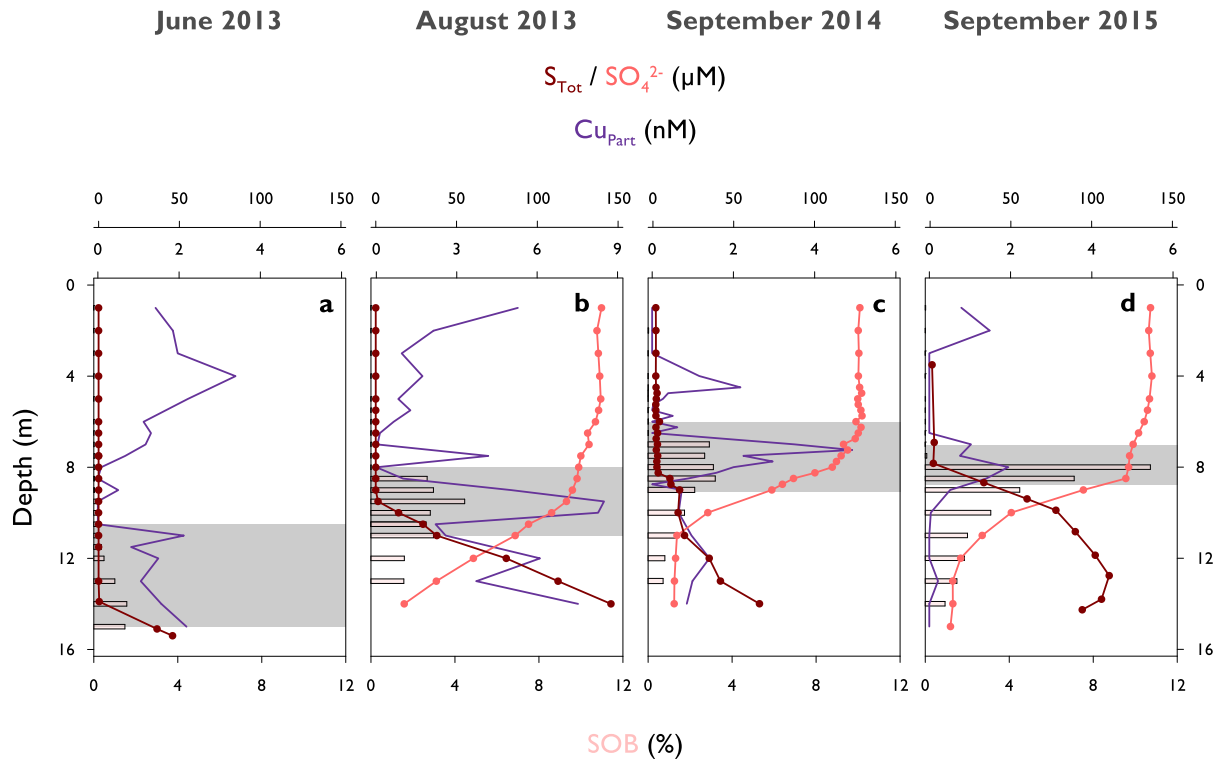


Figure S7. Total sulphide, sulphate, sulphur oxidizing bacteria and particulate copper profiles in Rotsee.

(a) June 2013. (b) August 2013. (c) September 2014. (d) September 2015. Total sulphide (S_{Tot}) is shown in deep red, sulphate (SO_4^{2-}) in light red, particulate copper (Cu_{Part}) in purple. Relative abundance of sulphur oxidizing bacteria (SOB) are represented by the bar plot (see txt-file "16S rRNA sequences_SOB" for corresponding sequences). Grey areas denote potential methane oxidation zones. Note the different x-axis scale for Cu_{Part} in August 2013 (b).

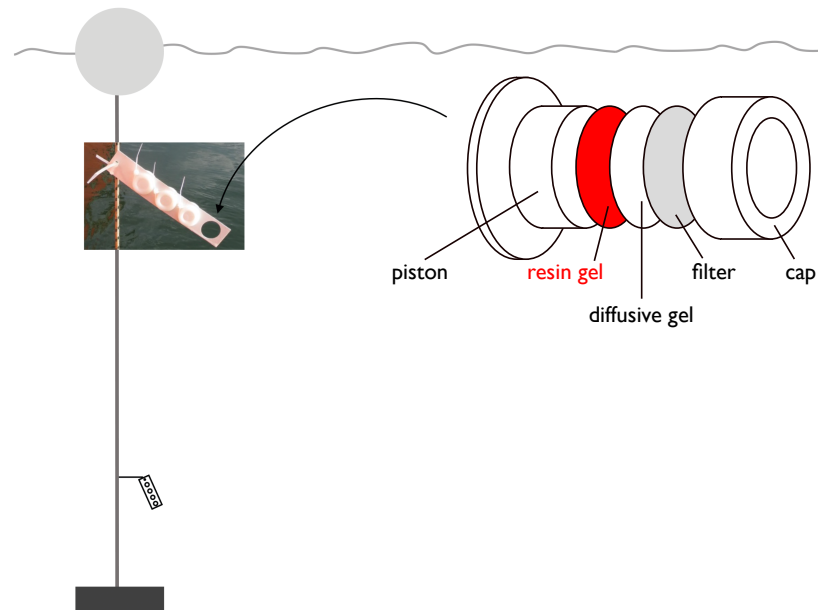


Figure S8. Diffusive Gradients in Thin film (DGT) samplers installation in Rotsee.

The DGT parts consisted of a plastic piston, layered with a resin gel (red), a diffusive gel (white) and a protective filter (light grey), and were covered with an open plastic cap. 3-4 DGT samplers were placed in a plastic stripe and attached to a rope, which was loosely connected to a floating buoy on top to place it in a straight condition.

Table S1. Statistical tests describing bioavailable (Cu_{DGT}), dissolved (Cu_{Diss}), and particulate (Cu_{Part}) copper distributions within Rotsee.

Parameter	All	June 2013	August 2013	September 2014	September 2015
Cu_{DGT}					
Sample size (n)	284	54	73	81	75
Normality	$p < 0.001$	$p < 0.01$	$p < 0.001$	$p < 0.001$	$p < 0.001$
Kruskal-Wallis	$p < 0.001$	$p = 0.6$	$p < 0.001$	$p < 0.001$	$p < 0.001$
Mann-Whitney					
oxic - methane oxidation	$p < 0.001$		$p < 0.001$	$p < 0.001$	$p < 0.001$
oxic - anoxic	$p < 0.001$		$p < 0.001$	$p < 0.001$	$p < 0.001$
methane oxidation - anoxic	$p < 0.001$		$p < 0.05$	$p < 0.001$	$p < 0.001$
Cu_{Diss}					
Sample size (n)	260	60	60	83	57
Normality	$p < 0.001$	$p < 0.001$	$p < 0.001$	$p < 0.001$	$p < 0.001$
Kruskal-Wallis	$p < 0.001$	$p < 0.001$	$p < 0.001$	$p < 0.001$	$p < 0.001$
Mann-Whitney					
oxic - methane oxidation	$p < 0.001$	$p < 0.001$	$p < 0.001$	$p < 0.001$	$p < 0.001$
oxic - anoxic	$p < 0.001$		$p < 0.001$	$p < 0.001$	$p < 0.001$
methane oxidation - anoxic	$p < 0.001$		$p < 0.001$	$p < 0.001$	$p < 0.001$
Cu_{Part}					
Sample size (n)	88	21	20	28	19
Normality test	$p < 0.001$	$p = 0.21$	$p < 0.05$	$p < 0.001$	$p < 0.001$
Kruskal-Wallis / ANOVA	$p < 0.05$	$p = 0.66$	$p = 0.07$	$p = 0.07$	$p < 0.05$
Mann-Whitney / Tukey's HSD					
oxic - methane oxidation	$p < 0.01$				$p < 0.05$
oxic - anoxic	$p = 0.76$				$p = 0.84$
methane oxidation - anoxic	$p = 0.09$				$p < 0.01$

The water column was divided into three zones (oxic, methane oxidation, anoxic). Normality of the data was assessed by the Shapiro-Wilk test. Differences between zones were tested by one-way ANOVA followed by Tukey's HSD. When normality was not met, differences were tested by the Kruskal-wallis test followed by the Mann-Whitney pairwise test. p-values < 0.05 were considered significant.

Table S2. Relative abundances and phylogenetic affiliations of methane-oxidizing bacterial operational taxonomic units (OTUs) in Rotsec.

OTU	Taxonomy	OTU abundance (%)			
		June 2013	August 2013	September 2014	September 2015
OTU_129	α -MOB	0.018	0.394	1.144	5.542
OTU_56	γ -MOB	6.266	2.172	2.277	6.067
OTU_68	γ -MOB	8.713	0.753	2.941	2.993
OTU_141	γ -MOB	8.599	1.162	0.011	0.868
OTU_319	γ -MOB	0.024	0.006	1.175	0.050
OTU_433	γ -MOB	0.049	0.241	0.279	0.203
OTU_575	γ -MOB	1.440	0.846	0.081	0.364
OTU_614	γ -MOB	0.003	0.004	0.178	0.055
OTU_663	γ -MOB	0.002	0.143	0.048	0.074
OTU_821	γ -MOB	-	-	0.236	0.015
OTU_917	γ -MOB	-	0.002	0.072	0.020
OTU_931	γ -MOB	0.630	0.089	0.093	0.158
OTU_2276	γ -MOB	-	-	0.015	0.008
OTU_2426	γ -MOB	-	-	0.005	0.002
OTU_3248	γ -MOB	-	-	-	0.005
OTU_3421	γ -MOB	-	-	0.005	-
OTU_112	Methylacidiphilae	0.687	7.471	3.668	8.796
OTU_566	Methylacidiphilae	0.351	0.070	0.030	0.396
OTU_1479	Methylacidiphilae	0.013	-	0.012	0.016
OTU_1541	Methylacidiphilae	0.002	-	0.022	-
OTU_1686	Methylacidiphilae	0.005	0.003	0.020	0.006

γ -MOB: methane-oxidizing bacteria belonging to *Gamma*proteobacteria, α -MOB: methane-oxidizing bacteria belonging to *Alpha*proteobacteria. *Methylacidiphilae* group within *Verrucomicrobia*. After transforming absolute OTU reads to relative abundances, single OTUs are listed as sums of the water column for each campaign. See Supplementary txt-file "16S rRNA sequences_MOB" for sequences corresponding to each OTU.

Table S3. Upward and downward fluxes of dissolved species in the water column of Rotsee.

Parameter		June 2013	August 2013	September 2014	September 2015
		(10.5-15 m)	(8-11 m)	(6-9 m)	(7-8.7 m)
O ₂	(mmol m ⁻² d ⁻¹)	3.4 ± 1%	31.3 ± 3%	27.6 ± 1%	42.9 ± 1%
NO ₂ ⁻	(mmol m ⁻² d ⁻¹)	n.a.	1.6 ± 0%	0.7 ± 45%	0.0 ± 0%
NO ₃ ⁻	(mmol m ⁻² d ⁻¹)	n.a.	1.5 ± 31%	3.0 ± 0%	0.0 ± 0%
SO ₄ ²⁻	(mmol m ⁻² d ⁻¹)	n.a.	0.3 ± 18%	0.9 ± 10%	0.4 ± 8%
Cu _{DGT}	(nmol m ⁻² d ⁻¹)	19 ± 24%	30 ± 21%	20 ± 8%	40 ± 9%
Cu _{Diss}	(nmol m ⁻² d ⁻¹)	195 ± 8%	336 ± 20%	828 ± 25%	394 ± 16%
CH ₄	(mmol m ⁻² d ⁻¹)	-10.2 ± 3%	-13.3 ± 25%	-2.7 ± 17%	-9.2 ± 9%
Fe _{DGT}	(μmol m ⁻² d ⁻¹)	-13 ± 20%	-13 ± 25%	-47 ± 5%	-12 ± 11%
Fe _{Diss}	(μmol m ⁻² d ⁻¹)	-4.5 ± 29%	-19 ± 9%	-62 ± 13%	-24 ± 24%
Mn _{Diss}	(μmol m ⁻² d ⁻¹)	-52 ± 21%	-22 ± 49%	-136 ± 5%	-87 ± 5%
NH ₄ ⁺	(mmol m ⁻² d ⁻¹)	n.a.	-6.4 ± 27%	-3.9 ± 4%	-4.2 ± 11%
S _{Tot}	(mmol m ⁻² d ⁻¹)	-2.6 ± 1%	-3.1 ± 5%	-1.1 ± 16%	-1.8 ± 14%

Oxygen: O₂, nitrite: NO₂⁻, nitrate: NO₃⁻, sulphate: SO₄²⁻, bioavailable copper/iron: Cu_{DGT}/Fe_{DGT}, dissolved copper/iron/manganese: Cu_{Diss}/Fe_{Diss}/Mn_{Diss}, methane: CH₄, ammonium: NH₄⁺, total sulphide: S_{Tot}. The depth ranges in brackets define the methane oxidation zones (grey bars in figures). Fluxes were calculated from the chemical concentration gradients determined by linear regression and the same vertical diffusion coefficient for all substances. n.a.: not analysed. Note the different units between the parameters.

Table S4. Primer pairs and amplification conditions for quantitative detection (qPCR) of 16S rRNA and MMO functional genes (*pmoA* and *mmoX*).

Gene	Primer	Sequence (5' to 3')	Reagents	Thermal profile & Quantification analysis	Efficiency
16S rRNA ^a	349f	AGAGTTTGATCMTGGCTCAG	1 x master mix (LightCycler® 480 Probes Master, Roche)	Initial denaturation: 95°C, 10 min	1.822
	806r	GGACTACCAGGGTATCTAAT	0.9 µM primers (Microsynth)	45 cycles: 95°C, 40 sec; 53°C, 40 sec; 72°C, 1 min	
			0.3 µM TaqMan probe (Bac516F FAM; Microsynth)	Fluorescent reading after each cycle at 72°C for 1 min	
			2 µl DNA (1:100 diluted in AE)	Absolute Quantification/2 nd Derivative Maximum method	
			10 µl final volume		
<i>pmoA</i> ^b	A189f	GGNGACTGGGACTTCTGG	1 x master mix (LightCycler® 480 SYBR® Green I Master, Roche)	Initial denaturation: 95°C, 10 min	1.868
	mb661r	CCGGMGCAACGTCYTTACC	0.2 µM primers (Eurofins Genomics)	10 touchdown cycles: 95°C, 10 sec; 62-53°C, 30 sec (-1°C/cycle); 72°C, 30 sec	
			2 µl DNA (1:10 diluted in AE)	30 cycles: 95°C, 10 sec; 52°C, 30 sec, 72°C, 30 sec	
			10 µl final volume	Fluorescent reading after each cycle at 79°C for 30 sec	
				Melting curve analysis after last cycle from 65-97 °C (0.11°C/sec)	
<i>mmoX</i> ^c	536f	CGCTGTGGAAGGGCATGAAGCG	1 x EvaGreen (Biotium)	Initial denaturation: 95°C, 5 min	2.018
	898r	GCTCGACCTTGAACCTTGGAGCC	1 x PCR buffer (Promega)	38 cycles: 95°C, 1 min; 63°C, 1 min; 72°C, 40 sec	
			2 mM MgCl ₂ (Promega)	Fluorescent reading after each cycle at 72°C for 40 sec	
			0.2 mM dNTP (Qiagen)	Melting curve analysis after last cycle from 65-97°C (0.11°C/sec)	
			0.25 mg ml ⁻¹ BSA (Sigma Aldrich)	Fit Points method	
			0.27 µM primers (Microsynth)		
			0.025 U Taq polymerase (Go Taq G2 Flexi DNA Polymerase, Promega)		
			2 µl DNA (undiluted)		
			10 µl final volume		

^a [Takai and Horikoshi, 2000]^b [Holmes *et al.*, 1995; Costello and Lidstrom, 1999]^c [Fuse *et al.*, 1998]

Table S5. Taxonomic and physiological characteristics of axenic methane-oxidizing bacterial cultures.

Class	Species	Collection	<i>pmoA</i> / <i>mmoX</i>
α -MOB	<i>Methylocapsa aurea</i>	DSM 22158	y / n
	<i>Methylocystis heyeri</i>	DSM 16984	y / y
	<i>Methylocystis hirsuta</i>	R. Henneberger	y / y
	<i>Methylocystis rosea</i>	DSM 17261	y / n
	<i>Methyloferula stellata</i>	DSM 22108	n / y
	<i>Methylosinus sporium</i>	DSM 17706	y / y
	<i>Methylosinus trichosporium</i>	R. Henneberger	y / y
γ -MOB	<i>Methylococcus capsulatus</i>	R. Henneberger	y / y
	<i>Methylobacterium alcaliphilum</i>	DSM 19304	y / n

α -MOB and γ -MOB are abbreviations for methane-oxidizing bacteria (MOB) belonging either to *Alpha*- or *Gammaproteobacteria*. Axenic cultures were either ordered from DSMZ (Deutsche Sammlung von Mikroorganismen und Zellkulturen) or received from R. Henneberger. y = organism contains respective functional gene, n = organism does not contain respective functional gene.

Chapter 3

Environmental and microbial interactions shaping methane-oxidizing communities in a stratified sub-alpine lake

Running title: Mechanisms shaping methanotrophs in lakes

Carole Guggenheim

Remo Freimann

Magdalena J. Mayr

Karin Beck

Bernhard Wehrli

Helmut Bürgmann

Under review in *The ISME Journal*

Abstract

Methane is an important greenhouse gas, which is produced in anoxic environments such as lake sediments. In stratified lakes, methane-oxidizing bacteria (MOB) are mitigating methane fluxes to the atmosphere by consuming large amounts of methane entering the water column from the sediment. Previous studies have indicated that MOB communities in lakes are diverse and vertically structured, but their temporal dynamics as well as the physico-chemical and biological drivers of the community assembly have not been explored. Here, we present a detailed investigation in a shallow, seasonally stratified, sub-alpine lake applying high-resolution profiling of physico-chemical parameters and of MOB and bacterial community compositions. Amplicon sequencing of *pmoA* and 16S rRNA genes was applied to capture MOB and bacterial community structures under different conditions during the stratified period. Non-randomly assembled MOB communities were detected in all compartments and during various stages of development of the stratified water column. We could identify methane and oxygen gradients and several other physico-chemical parameters (light, pH, available Cu and Fe and total dissolved N) as important drivers of the MOB community structure. MOB were also well integrated into modular bacterial co-occurrence networks. In combination, a network of physico-chemical variables and bacteria explained up to 84% of MOB occurrence within the lake's depth profile. Spatio-temporal MOB community changes were 51% congruent with shifts in the total bacterial community and 22% of variance in MOB occurrence could be explained exclusively by the bacterial community composition, indicating that microbial interactions may play an underappreciated role in structuring the MOB community.

Introduction

Atmospheric concentrations of methane (CH_4), a potent greenhouse gas, have steadily increased since the pre-industrial era [Ciais *et al.*, 2013]. Freshwater lakes are important natural CH_4 sources, as CH_4 is produced primarily in their sediments by anaerobic mineralization of organic matter [Bastviken *et al.*, 2004, 2011; Kirschke *et al.*, 2013]. To a smaller extent CH_4 production can also occur in the oxic epilimnion of lakes via different suggested pathways (e.g. anoxic micro-niches or CH_4 as by-product) [Grossart *et al.*, 2011; Bogard *et al.*, 2014; Tang *et al.*, 2016]. Nevertheless, CH_4 flux to the atmosphere is under strong control of aerobic-methane oxidizing bacteria (MOB), which use CH_4 as carbon and energy source [Bastviken *et al.*, 2008; Chistoserdova, 2011]. In lakes MOB mainly belong to *Gamma*- and *Alphaproteobacteria*, and are often referred to as type I and type II MOB, respectively [Hanson and Hanson, 1996; Chistoserdova and Lidstrom, 2013; Knief, 2015]. Different MOB genera show distinct life strategies, enabling them to predominate under different environmental conditions [Ho, Kerckhof, *et al.*, 2013].

Temperate lakes usually develop a strong thermal stratification during summer, and anoxia may develop in the bottom waters. Anoxic conditions in the hypolimnion allow large amounts of CH_4 to accumulate [Schubert *et al.*, 2012]. Highest MOB activity is detected at the bottom part of the oxycline where CH_4 and O_2 counter gradients meet [Bastviken *et al.*, 2002; Sundh *et al.*, 2005; Borrel *et al.*, 2011]. Such CH_4 oxidation zones migrate within the water column as stratification progresses [Carini *et al.*, 2005].

Despite their apparently simple substrate requirements, MOB in the water column of lakes are known to be diverse. Currently it is not clear which traits govern the ecological success of MOB in lake water columns. Competitiveness under specific O_2 and CH_4 concentrations can be a factor leading to niche differentiation [Knief, 2015]. This is thought to be partially coupled to the properties of the expressed methane monooxygenases (MMO) [Jones and Lennon, 2009]. This enzyme initiates the CH_4 oxidation process and exists in two main forms: particulate (pMMO) and soluble (sMMO) methane monooxygenase [Sirajuddin and Rosenzweig, 2015]. pMMO is a copper (Cu) dependent enzyme and appears to be almost ubiquitous among MOB [Semrau *et al.*, 2010; Wang, Maji *et al.*, 2017]. It generally has a higher CH_4 affinity than sMMO, but shows a narrower substrate range and a slower CH_4 turnover rate [Lee *et al.*, 2006]. sMMO uses iron (Fe)

in its active centre and is only found in some MOB, typically in combination with pMMO [Merckx *et al.*, 2001; Tinberg and Lippard, 2011]. The availabilities of Cu, Fe, O₂, and CH₄ have been shown to affect MOB community characteristics and performances [Begonja and Hrsak, 2001; Chidambarampadmavathy *et al.*, 2017; Guggenheim *et al.*, 2019]. In addition, other physico-chemical variables can shape the MOB community structure. For instance, low water temperature and nitrogen-rich (NH₄NO₃) conditions favour growth of type I over type II MOB [Tsutsumi *et al.*, 2011; He *et al.*, 2012; Siljanen *et al.*, 2012], or, some MOB are able to use nitrate or nitrite to save O₂ under hypoxic conditions [Kits, Campbell, *et al.*, 2015].

Apart from physico-chemical parameters, co-occurring organisms can also influence the MOB community composition. For example, MOB can form mutualistic interactions with oxygenic phototrophs in light penetrated anoxic layers, enabling CH₄ oxidation while potentially providing carbon dioxide in return [Milucka *et al.*, 2015; Oswald *et al.*, 2015]. Indeed, MOB play an integral part in transferring CH₄-derived carbon and other metabolites to the microbial pool and higher trophic levels of the food web [Jones and Grey, 2011; Sanseverino *et al.*, 2012]. There is also evidence that CH₄ oxidation by MOB under O₂ limitation is connected to the reduction of alternative terminal electron acceptors (e.g. such as metal-oxides) by themselves or by archaea [Crowe *et al.*, 2011; Bar-Or *et al.*, 2017]. Heterotrophic richness has been shown to enhance CH₄ oxidation activity by MOB as accompanying organisms can either remove inhibiting (e.g. formaldehyde) or produce stimulating substances (e.g. cobalamin) [Stock *et al.*, 2013; Ho *et al.*, 2014; Iguchi *et al.*, 2015]. On the other hand, MOB select for certain heterotrophs by providing organic metabolites (e.g. acetate) or by removing toxic compounds (e.g. trichloroethylene) [Morris *et al.*, 2013; van der Ha *et al.*, 2013; Oshkin *et al.*, 2015; Gilman *et al.*, 2017; Xing *et al.*, 2018].

In order to facilitate predictions of MOB based ecosystem functioning (i.e. CH₄ removal) under varying conditions, we need to improve our understanding of the combined effects of microbial communities and the physico-chemical environment shaping MOB community assemblies [Comte *et al.*, 2016; Ho *et al.*, 2016]. We hypothesized that investigating the MOB community in the context of spatial (depth gradient) and temporal (different sampling campaigns representing different stages of the developing stratification) variation in a single lake was the most promising approach to identify driving factors using multivariate ecostatistical analysis. Hence, we assessed the interdependencies of MOB inhabiting the water column of a eutrophic, seasonally stratified, sub-alpine lake (Rotsee) with the total bacterial community (characterized by amplicon

sequencing) and a large set of physico-chemical variables. The system was probed four times during the stratification period along the entire depth of the water column. The spatio-temporal fluctuations of physico-chemical variables and the bacterial community composition within the lake enabled identification of potential drivers of the MOB community structure. In particular, our results indicate that variation in the MOB community structure is not solely driven by substrate fluxes, but by a complex network of physico-chemical variables and different bacterial players.

Methods

Site description, *in-situ* profiling, sample collection and analysis

Rotsee is a well-studied small (0.5 km²), eutrophic lake located in central Switzerland with a maximum depth of 16 m. Its wind-shielded position allows a stable stratification from spring until mid to late autumn with an oxycline usually formed between 6 and 9 m depth. Its sediment releases CH₄ into the anoxic water column, where it accumulates and reaches concentrations up to 1 mM. However, MOB substantially consume CH₄ at the oxic-anoxic interface [Schubert *et al.*, 2010; Oswald *et al.*, 2015]. The reliable stratification, high CH₄ production and oxidation as well as the proximity to our institute make Rotsee an ideal site for the purpose of this study.

Sample collection was conducted close to the deepest point of the lake during three consecutive years at the beginning of stratification (June 2013), during peak stratification (August 2013) and shortly before the lake overturns (September 2014, September 2015). Detailed methods of physico-chemical profiling, sampling, and analysis are reported partially in [Guggenheim *et al.*, 2019] and in the Supplementary information. In short, we recorded or sampled and analysed the following parameters: conductivity (Cond), turbidity (Turb), depth (pressure), temperature (T), pH, O₂, photosynthetically active radiation (PAR, herein to be equated as light), chlorophyll a (Chl-a), total sulphide (S_{Tot} = H₂S, HS⁻, S²⁻), dissolved organic carbon (DOC), total dissolved nitrogen (TDN), dissolved inorganic carbon (DIC), nitrite (NO₂), nitrate (NO₃), ammonium (NH₄), sulphate (SO₄), phosphate (PO₄), CH₄, ¹³C/¹²C isotopic ratio of CH₄ (δ¹³C-CH₄), dissolved (M_{Diss}) and total (M_{Tot}) metals (Cu, Fe, manganese (Mn), zinc (Zn), chromium (Cr)). Particulate metal (M_{Part}) concentrations were obtained by subtracting dissolved from total metal concentrations. Bioavailable metal fractions (Me_{DGT}) were measured via the Diffusive Gradients in Thin film (DGT) technique.

DNA sampling and extraction, *pmoA* qPCR, library preparation, sequencing

DNA sampling and processing was conducted by [Guggenheim *et al.*, 2019] and is reported in the Supplementary information. 16S rRNA and the *pmoA* gene served as marker genes for total bacterial

community and MOB detection, respectively [Dumont, 2014]. Quantitative polymerase chain reaction (qPCR) on the *pmoA* gene was conducted using the primer pair A189f and mb661r (5'-GGNGACTGGGACTTCTGG-3', 5'-CCGGMGCAACGTCYTTACC-3', Eurofins Genomics, Ebersberg, Germany), which covers most alpha- and gammaproteobacterial MOB (see Supplementary information) [Costello and Lidstrom, 1999]. *pmoA* amplicon libraries were prepared using the above-mentioned primers with Illumina Nextera overhang sequences at the 5'-end (Microsynth AG, Balgach, Switzerland) (see Supplementary information). Amplicons were purified using AMPure XP beads (BeckmanCoulter Inc., Fullerton, CA, USA). Indexing and sequencing (MiSeq platform, Illumina Inc., San Diego, CA, USA) were conducted by the Genomics Facility Basel (Basel, Switzerland). Library preparation and Illumina sequencing for 16S rRNA were performed by Microsynth AG (Balgach, Switzerland). 16S rRNA genes were amplified using the primers S-D-Bact-0341-b-S-17 (5'-CCTACGGGNGGCWGCAG-3', 341F) and S-D-Bact-0785-a-A-21 (5'-GACTACHVGGGTATCTAATCC-3', 805R) [Herlemann *et al.*, 2011].

Sequence processing, phylogenetic analysis, data deposition

16S rRNA and *pmoA* sequencing data were analysed by the Genomic Diversity Centre (GDC, Zurich, Switzerland). Raw data were quality controlled using FastQC (v0.11.4) and MultiQC (v0.7). 16S rRNA low quality ends of reads were trimmed with PRINSEQ-lite (v0.20.4) and merged using usearch (v8.1.1812_i86linux64). *pmoA* reads were trimmed and merged using usearch (v9.2.64_i86linux 64) and FLASH (v1.2.11), respectively. Merged reads were primer-site trimmed by cutadapt v1.5 and v1.12, respectively. PRINSEQ-lite (v0.20.4) was used to filter and size-select the amplicons. Sequences were clustered into operational taxonomic units (OTUs) at a cutoff level of 97% similarity using the uparse (16S rRNA) and unoise (*pmoA*) workflow with usearch. Taxonomic assignment of the representative sequences was set using the UTX classifier together with the GreenGene database (May 2013) for 16S rRNA, and the SINTAX classifier with the database published for *pmoA* in [Wen *et al.*, 2016]. A phylogenetic tree based on *pmoA* sequences was calculated using muscle (v3.8.1551) and MEGA X [Kumar *et al.*, 2018] applying the Maximum Parsimony method with 10000 bootstrap replications. The Maximum Parsimony tree was obtained using the Subtree-Pruning-Regrafting algorithm [Nei and Kumar, 2000]. All sequence data have been deposited at the ENA database under the accession numbers PRJEB28460 (16S rRNA) and PRJEB28505 (*pmoA*).

Depth zones, statistical analysis

We divided the water column into four zones with contrasting environmental conditions. The “oxic” zone ranged from the surface to depths where O_2 started to decrease, and where CH_4 remained stable at low concentrations, but epilimnetic CH_4 sources might be present [Hofmann *et al.*, 2010; Donis *et al.*, 2017]. This zone was followed by the “oxycline” zone where O_2 is being reduced, but CH_4 remained low. The lower boundary of the oxycline zone ended where CH_4 accumulation began. The main “oxidation zone”, in which CH_4 was consumed, was thus the zone where either O_2 was present at measurable concentrations, or where it was below detection but *in-situ* photosynthetic O_2 production could be assumed based on available light measured as PAR [Oswald *et al.*, 2015]. Therefore, this zone ended where PAR fell below detection limit. The dark bottom water was defined as the “anoxic” zone, where O_2 for aerobic methane oxidation was lacking (Supplementary Figure S1).

Statistical analysis was performed within the R statistical software environment (version 3.4.3) using the *vegan*, *phyloseq*, *mixOmics*, *EcoSimR*, *igraph* and *picante* packages [Csárdi and Nepusz, 2006; Kembel *et al.*, 2010; McMurdie and Holmes, 2013; Gotelli *et al.*, 2015; Rohart *et al.*, 2017; Oksanen *et al.*, 2018]. 16S rRNA (total bacterial community) and *pmoA* (MOB) reads occurring less than 3 or 50 times in at least 3 samples, respectively, were removed from the OTU tables. To compare relative OTU abundances, reads were standardized to the mean sequencing depth. 16S rRNA data assigned to MOB species was excluded in models incorporating also the *pmoA* data set. Alpha diversity measures were calculated (richness, Shannon). To obtain profiles for comparison and for co-linearity assessment a number of missing values were imputed using the *missMDA* package (10 complete profiles for NO_2 , NO_3 , NH_4 , SO_4 , PO_4 , DIC (all June 2013), Chl-a (September 2014 and 2015), $\delta^{13}C-CH_4$ (June 2013, September 2015), and 8 missing values for pH in September 2014) (Supplementary Figure S1). Except for pH, imputed profiles were not incorporated in the statistical models, but are discussed in the context of their co-linearity with non-imputed variables. Predicted values were tested by multiple- and overimputation (Supplementary Figure S2, Supplementary Figure S3). A principal component analysis (PCA) with the environmental variables was performed to summarize the changes in physico-chemical variables along the depth gradients during temporal succession. Pearson correlations with Holmes-corrected p-values of physico-chemical parameters were calculated to assess the

influence of single physico-chemical variables on specific MOB species. Non-metric multidimensional scaling (NMDS) was used to visualize temporal succession dynamics in community structure by using the Bray-Curtis dissimilarity matrix of the square root transformed Wisconsin standardized OTU table. The mvabund package was used to test environmental, total bacterial and MOB community structure differences between different depth zones [Wang *et al.*, 2012]. To assess the environmental influence on the MOB community structuring we applied canonical correlation analysis (CCA) based on selected environmental parameters (forward, backward, and both, incorporating variables that were chosen at least in two selection strategies). Variables with variance inflation factors (VIFs) > 10 were removed prior model selection and significance was assessed by permutation tests (9999 permutations). Randomness in co-occurrence of MOB and total bacterial community was tested with C-score metric and quasiswap algorithm in a null model using the EcoSimR package [Gotelli and Ulrich, 2012; Gotelli *et al.*, 2015]. To determine if phylogenetically related species cluster within specific sites in different depth zones, we assessed the standardized (z-score) effect size (SES) of mean pairwise distances (MPD) and the mean nearest taxon distances (MNTD) [Webb *et al.*, 2002]. SES were compared to a null model (“richness” null model, 999 randomizations of the phylogenetic tree) and differences between zones SES were assessed by ANOVA followed by Tukey’s HSD. MPD is sensitive to differences in phylogenetically more distant taxa whereas MNTD is sensitive to differences of phylogenetically more closely related taxa (i.e. tip of a phylogenetic tree). Overall similarity of MOB and the total bacterial community was assessed by Procrustes analysis of the first two dimensions of the respective NMDS plots. Significance was estimated by a correlation-like statistic based on the squared m12 algorithm (9999 permutations) [Peres-Neto and Jackson, 2001].

A network analysis was conducted based on Spearman’s rank coefficients (false discovery rate adjusted, Benjamini-Hochberg, 0.7 correlation and $p < 0.05$ cut-off) of most abundant bacteria (> 5% of all reads and in 10% of the samples present) and MOB [Spearman, 2010; Weiss *et al.*, 2016]. Visualization of the network clustering (Luovain Modularity) and structuring of most abundant bacterial phyla were performed in Gephi 0.9.2 using the Fruchterman Reingold algorithm [Bastian *et al.*, 2009]. To visualize the bacterial network distribution within the water column, we assigned network modularity classes (MCs) to the 16S rRNA based NMDS plot. To evaluate the inter-correlations of total community, MOB and environmental variables explaining the different depth zonation we used the supervised N-integration discriminant analysis with

DIABLO from the mixOmics package in R. Optimal sparsity parameters were determined by computing M-fold cross-validation scores. The relative influence of inter-correlations of the selected environmental variables and bacterial community members on MOB at an association relevance level > 0.5 was assessed by partial Bray-Curtis dissimilarity-based redundancy analysis using Hellinger standardized 16S rRNA and *pmoA* data and scaled and centred environmental data. Variables having a VIF > 5 (environmental data) and VIF > 3 (16S rRNA) were stepwise removed and selected (forward, backwards, and both) prior to analysis. The results of the DIABLO approach were analysed by building relevance networks visualized with Gephi using the Yifan Hu algorithm. Non-randomness of the networks was tested by comparing the network to 10'000 random Erdős-Rényi networks with similar numbers of edges and nodes [Ju *et al.*, 2014; Weiss *et al.*, 2016]. The network GML files are available as Supplementary files. See Supplementary information for a more detailed description of statistical analyses.

Results

Limnological conditions and zonation

The depth zones over all four field campaigns were consistently different from each other in terms of their overall physico-chemical properties (mvabund: Likelihood Ratio Test (LRT) = 778.8, $p < 0.001$) and sampling time contributed considerably to the variability in the dataset (Figure 1). Vertical profiles of physico-chemical parameters are summarized in Supplementary Figure S1. The annual T-driven stratification during summer months results in a narrowing of the oxycline and the oxidation zones as the season progresses (Supplementary Figure S1). The surface water was always well-oxygenated, and O_2 concentrations fell below detection limit usually in the upper half of the oxidation zone. The anoxic zone was substantially enriched with CH_4 , while only small amounts of CH_4 (0.12-1.07 μM) were detected in the oxic zone, which, however, was still oversaturated relative to the atmosphere [Schubert *et al.*, 2010]. In September 2015, the oxycline was combined with the oxidation zone as CH_4 profiles already slightly increased where O_2 decreased. In June 2013, light was detected almost to the sediment, therefore an anoxic zone was not defined (Supplementary Figure S1). Turbidity (Turb) maxima were mostly congruent with Chl-a throughout the water column as profiled in June and August 2013 (Supplementary Figure S1). The anoxic zone exhibited substantial concentrations of TDN, PO_4 , DIC and reduced substances ($Fe_{DGT/Diss}$, $Mn_{DGT/Diss}$, S_{Tot} , NH_4). Cu_{DGT} , Cu_{Diss} , and Cu_{Tot} were found to be highest at the lake's surface, and decreased strongly in the lower oxic zone and in the oxycline, whereas Cu_{Part} concentrations usually peaked within the oxidation zone. Some variables exhibited pronounced co-linearity (Figure 1, Supplementary Figure S2).

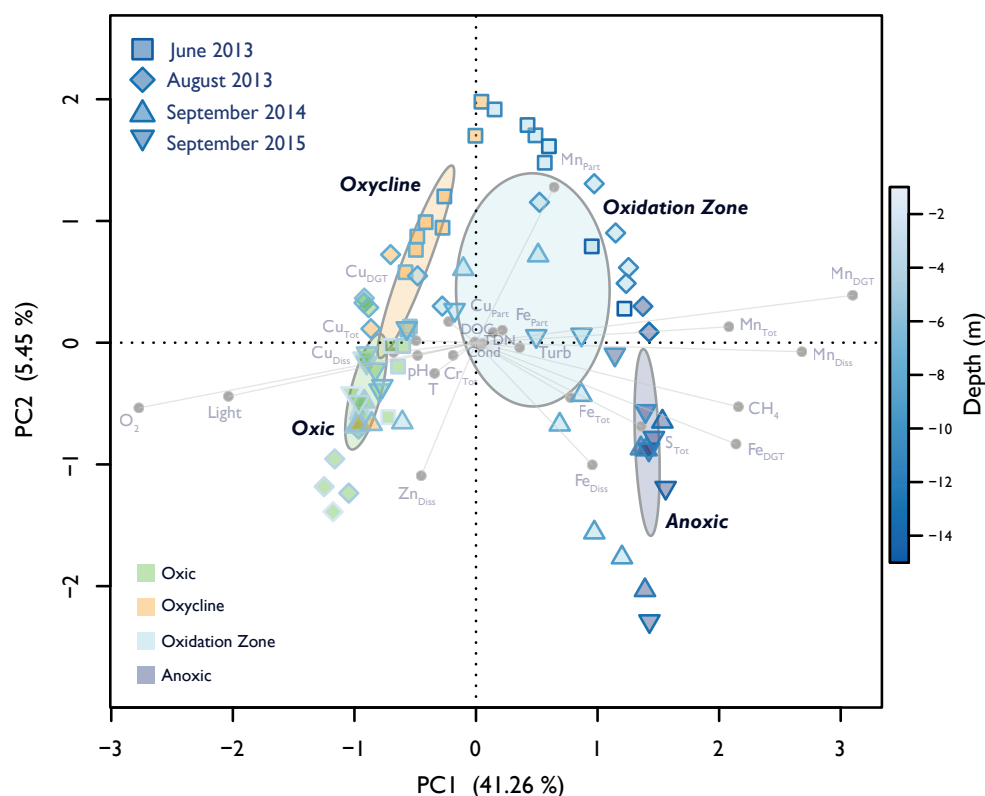


Figure 1. Principal component analysis (PCA) of physico-chemical variables.

Dispersion ellipses depict the standard error of weighted average scores of depth zone groupings (confidence limits = 0.95). Symbols show scores of individual samples. They indicate the sampling date and are coloured according to assigned depth zones. The colour of the symbol outline illustrates depth of the respective sample according to the depicted colour gradient. Environmental variable loadings are depicted in light grey. Explained variance of PC1 and PC2 are given in parenthesis.

Microbial community structure (16S rRNA)

An average of 41951 reads per sample were assigned to 1829 unique bacterial OTUs after filtering. Alpha diversity over all campaigns increased from around 400 OTUs in the surface water to approximately 1000 OTUs close to the sediment (Supplementary Figure S4A). *Actinobacteria*, *Bacteroidetes*, *Proteobacteria* and *Verrucomicrobia* dominated the communities during all campaigns (Supplementary Figure S5). *Cyanobacteria* were abundant in the oxic zone and oxyclyne in September 2015, and present in lower proportions in the other three campaigns. *Firmicutes* were detected in the oxidation and anoxic zone. OD1 were highly abundant during peak and late stratified periods in the oxidation and anoxic zone. *Planctomycetes* inhabited the oxic zone and oxyclyne mainly in August 2013. Microbial community structures were different between the sampling dates (mvabund: LRT = 29741, $p < 0.001$), and not randomly distributed among depths over all campaigns (C-score = 14.16, $p < 0.001$, SES = 24.75). Bacterial communities were further structured

along the depth gradient during all campaigns and were significantly different between the depth zones (mvabund: LRT = 45650, $p < 0.001$, Supplementary Figure S6). In summary, microbial communities were thus found to be clearly structured with depth and in time.

MOB community structure (*pmoA*)

We obtained an average of 89816 *pmoA* reads per sample, which resulted in 3662 unique MOB OTUs and 121 OTUs remaining after removing sparse OTUs. Alpha diversity increased with depth from 21 OTUs in the surface waters to 110 OTUs in deeper waters (Supplementary Figure S4B). Sequences from type I (*Gammaproteobacteria*) and type II (*Alphaproteobacteria*) MOB were identified (Supplementary Figure S5). Type I related to *Methylobacter*, *Methylomonas*, *Methylosoma*, and various environmental clusters (typeIa, typeIb), whereas type II comprised only *Methylocystis*. MOB communities were structured along the depth gradient and differed between the depth zones and campaigns (mvabund: LRT = 3134 / 2900, $p < 0.001$, Figure 2).

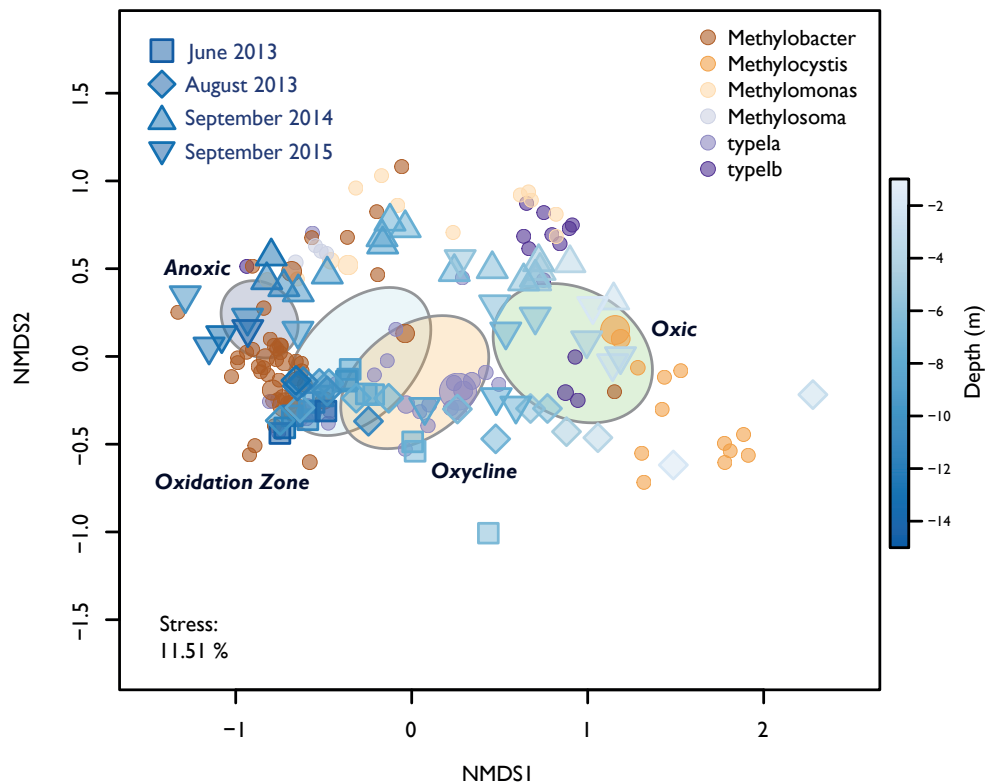


Figure 2. Non-metric multidimensional scaling (NMDS) of the MOB (*pmoA*) community structure.

Blue symbols indicate scores of individual samples obtained at different sampling dates. The fill colour illustrates the depth of the respective sample. MOB OTU scores are depicted as points coloured by taxonomic affiliation. The diameter of the dots is relative to the square root of the sums of the read counts standardized to the mean sequencing depth. Dispersion ellipses represent the standard error of weighted average scores of depth zone groupings (confidence limits = 0.95). The stress of the NMDS ordination is declared.

June 2013 was dominated by *Methylobacter* and typeIa (herein we refer to typeIa excluding *Methylobacter*, *Methylomonas* and *Methylosoma*) predominantly inhabiting the lower oxycline and the oxidation zone (Supplementary Figure S5). *Methylobacter* was abundant in August 2013 in the oxidation and anoxic zone, whereas typeIa occurred from the oxycline on downwards. In September 2014 and 2015, *Methylobacter* was also detected within anoxic waters. *Methylocystis* was found mainly in the oxic part of the lake, with highest abundance in September 2015. *Methylomonas* and *Methylosoma* were most abundant in the CH₄ oxidation zone of September 2014. TypeIb MOB were detected in low numbers in August 2013 in the lower part of the oxic zone and could also be found more dispersed within the oxic zone and the oxycline in September 2014 and 2015. Statistical testing confirmed that MOB communities were not randomly distributed within the water column (C-score = 118.93, $p < 0.001$, SES = 98.4) and showed phylogenetic relatedness higher than expected by chance in each sample within the different zones (SES MPD < 0, SES MNTD < 0, Supplementary Figure S7). Phylogenetic relatedness changed at higher node levels between specific samples in the oxycline compared to the anoxic zone (ANOVA $F(3,66) = 3.70$, $p < 0.05$, Tukey's HSD < 0.01), whereas phylogenetic relatedness at the tree-tip level (i.e. lower node levels) was highest within the oxidation and anoxic zone (ANOVA $F(3,66) = 7.17$, $p < 0.001$, Tukey's HSD < 0.01). This indicates that MOB clades that are phylogenetically highly similar coexist within specific sites in the oxycline whereas phylogenetically less similar MOB are mutually exclusive. Inversely, sites within the anoxic zone have a narrower phylogenetic structuring but highly similar MOB tend to be mutually exclusive (see also Tangle tree, Figure 3, Supplementary Figure S7).

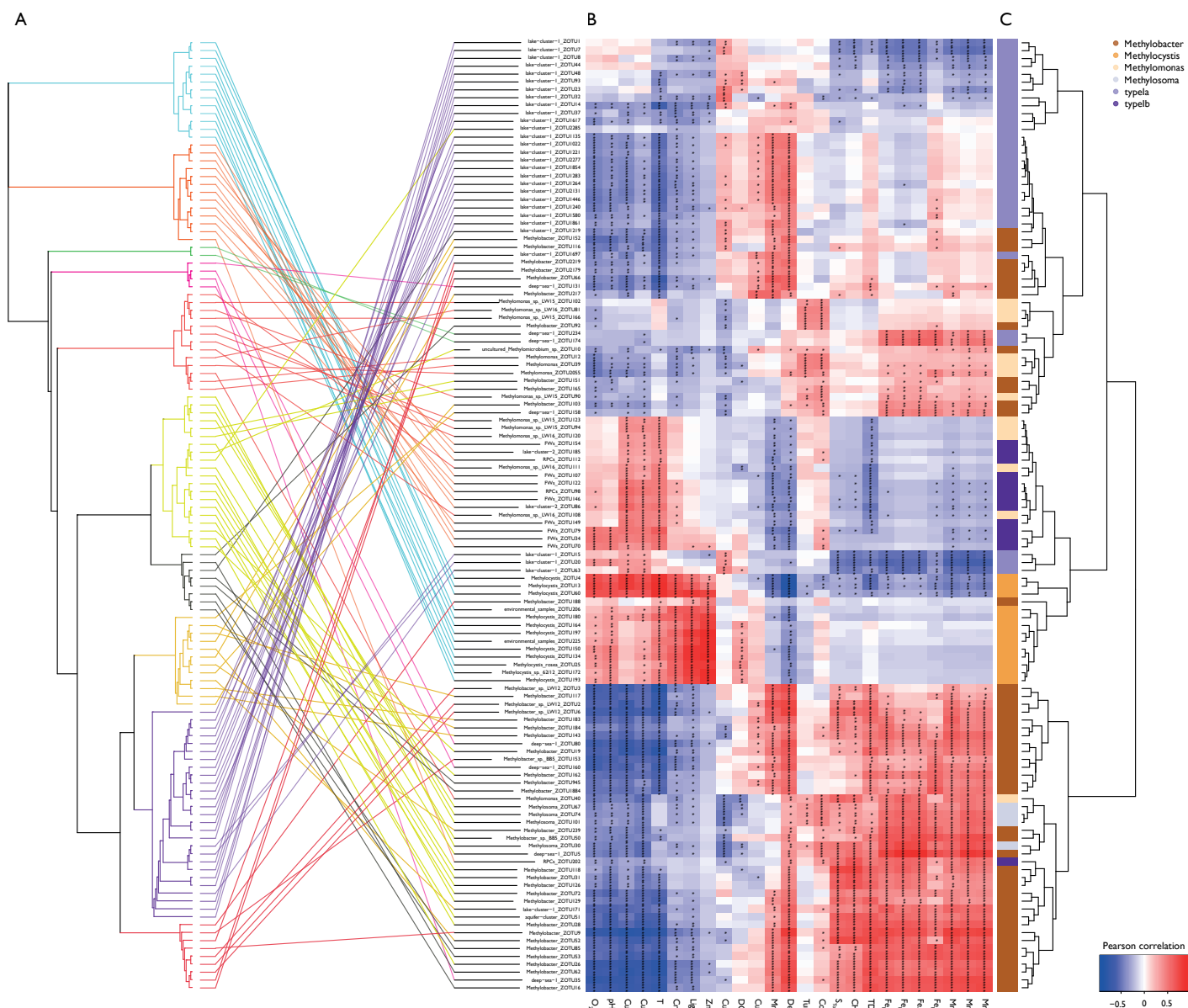


Figure 3. Tanglegram linking MOB (*pmoA*) phylogeny to physico-chemical variables (Heatmap)

(A) The phylogenetic Maximum Parsimony tree (see Supplementary Figure S8) is clustered into coloured clades with their tips being connected to their relative position in the heatmap (B) The heatmap of the Pearson correlation of specific MOB abundance with physico-chemical variables is ordered by its column and row means. Asterisks indicate levels of Holmes corrected p-values (* = $p < 0.05$, ** = $p < 0.01$, *** = $p < 0.001$). (C) A hierarchical environmental clustering dendrogram of MOB and their colour coding according to their taxonomic affiliation are depicted on the right.

MOB communities in the context of environmental and microbial variations

Clustering MOB according to their correlation pattern with different sets of environmental variables suggested phylogenetic groupings according to habitat preferences (Pearson correlation, Figure 3). Broad phylogenetic correlation with environmental structuring can be seen, but some MOB show environmental preferences that are distinct from their phylogenetic relatives (Tangle tree, Figure 3, Supplementary Figure S8).

A CCA based on selected environmental variables explained 69% of the MOB community structure over all campaigns (Figure 4). CH_4 and O_2 were the expected strong antipodal drivers. Light, Cu_{Diss} , pH, Fe_{DGT} , and TDN also contributed to the first canonical axis. Procrustes rotation showed 51% similar structuring of MOB and bacterial community along the lake gradients over all sampling dates (Procrustes correlation = 0.51, $p < 0.001$, Mantel $r = 0.41$, $p < 0.001$, Supplementary Figure S9) indicating biological interactions or similar niche preferences.

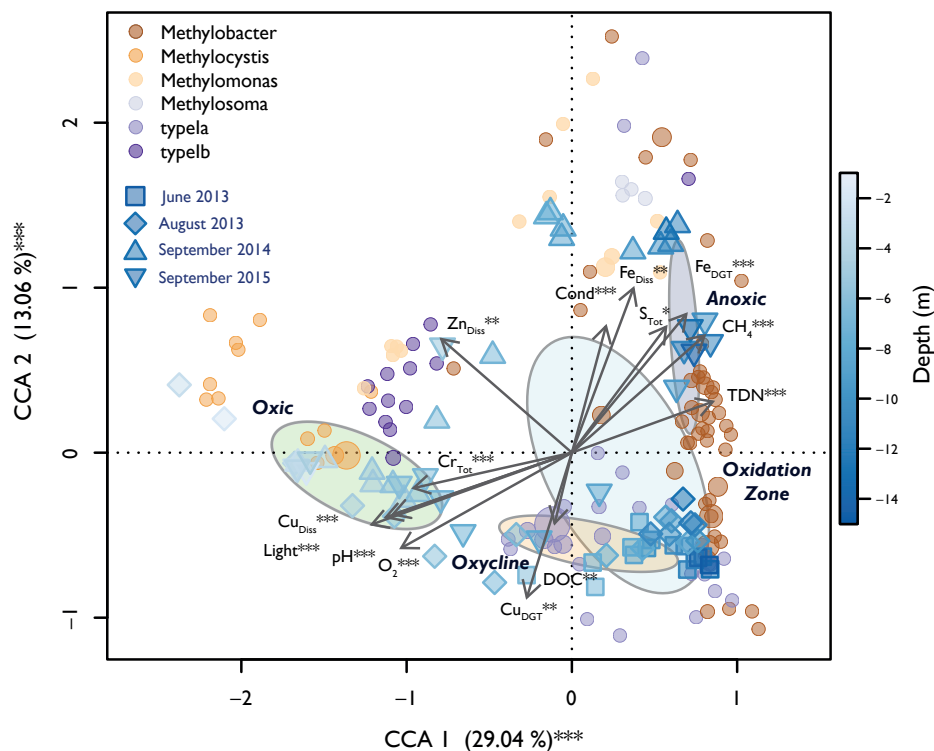
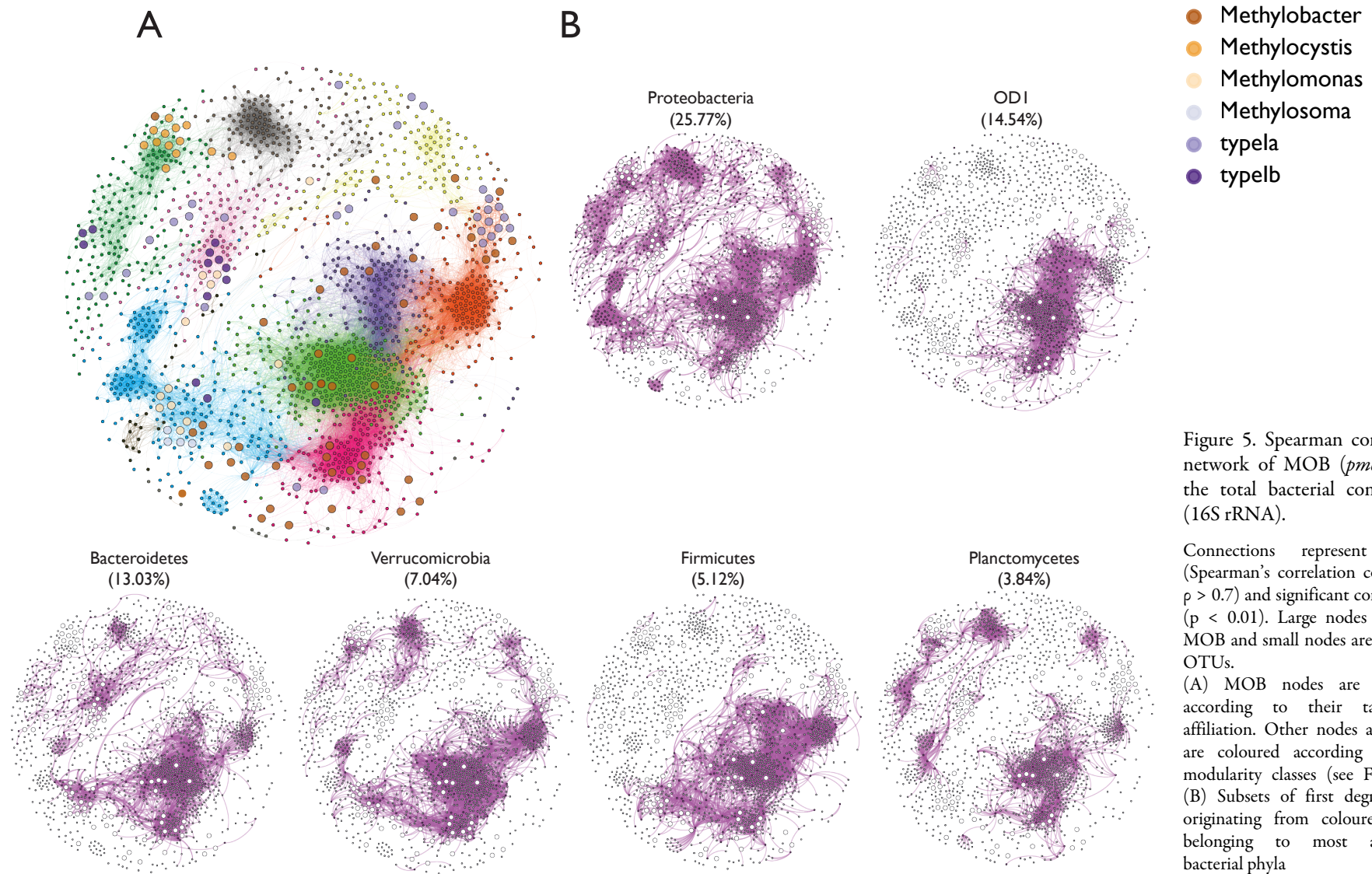


Figure 4. Canonical correspondence analysis (CCA) biplot of relative MOB (*pmoA*) abundance.

Dots indicate specific MOB OTUs and are coloured according to their taxonomic affiliation. The diameter of the dots is relative to the square root of the sums of the read counts standardized to the mean sequencing depth. Squares and triangles depict scores of specific sampling depths during different sampling dates. The fill colour declares the depth of the respective sample according to the depicted colour gradient. Dispersion ellipses show standard errors of weighted average scores of depth zones (confidence limits = 0.95). Environmental variables are fitted as arrows and the explained variance for CCA axes 1 and 2 are given. Asterisks represent significance of permutational ANOVAS of the single variables and axes (** = $p < 0.01$, *** = $p < 0.001$).

We therefore analysed co-occurrence patterns of MOB and bacteria via Spearman correlation based network analysis (Figure 5A, Supplementary Table S1). The network was dominated by the following phyla: *Proteobacteria* (25.77% relative abundance), OD1 (14.54%), *Bacteroidetes* (13.03%), *Verrucomicrobia* (7.04%), *Firmicutes* (5.12%), and *Planctomycetes* (3.84%) (Figure 5B, Supplementary Figure S10). OTUs of specific MOB genera tended to be embedded into similar regions of the network (Figure 5A). The structure of the network was analysed further by clustering the network into tightly connected subnetworks, i.e. modularity classes (MCs, Figure 6A). 15 MCs could be identified from which five had less than four members, thus were not further analysed. The defined MCs were distributed along the depth gradient and corresponded to the defined depth zones (Figure 6). Several bacterial phyla were part of multiple MCs (i.e. *Proteobacteria*, *Bacteroidetes*, *Verrucomicrobia*, *Planctomycetes*) whereas others were tied more closely to specific MCs (i.e. OD1, *Firmicutes*) (Figure 5, Supplementary Figure S10). Some MOB genera were similarly embedded into several MCs (i.e. *Methylobacter*, *Methylomonas*), whereas others were mostly related to one MC (i.e. *Methylocystis*, *Methylosoma*) (Figure 6D). Part of the typeIa and typeIb MOB showed strong clustering within the network MCs (i.e. MC0 or MC8).



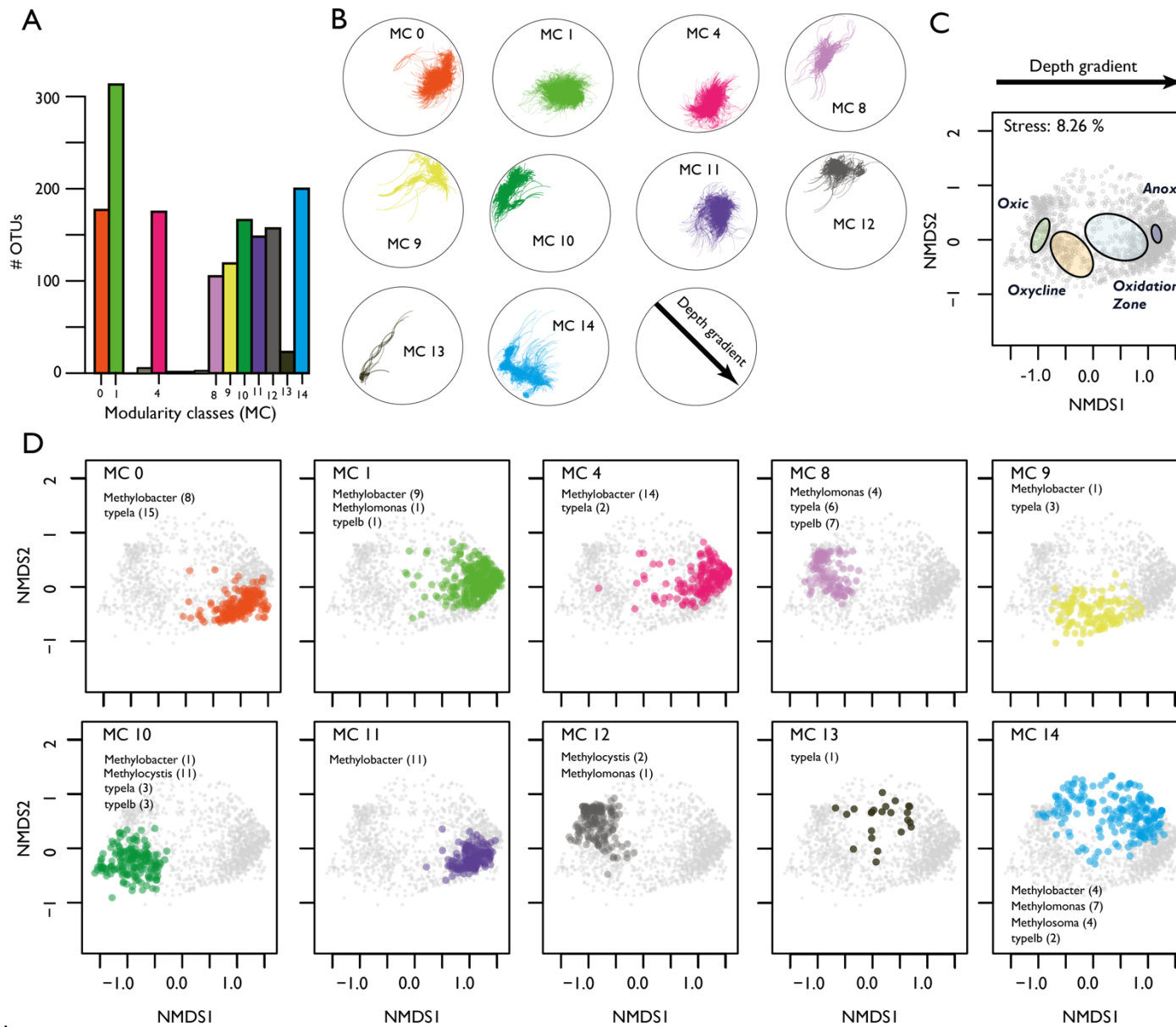


Figure 6. Representation of the Spearman correlation network (Figure 5) modularity classes (MCs).

(A) Numbers of bacterial OTUs affiliated with each MC.

(B) Location of the MCs within the network.

(C) NMDS of the bacterial community (16S rRNA). Grey dots represent bacterial OTUs present in the correlation network. Dispersion ellipses depict standard errors of weighted scores of depth zone groupings of samples (confidence limits = 0.95) and thus indicate the depth gradient present in the OTUs distribution.

(D) Projection of the bacterial OTUs embedded within specific network MCs on the total bacterial NMDS plot. Numbers of MOB genera present within the respective MC are indicated.

We constructed a relevance network to analyse the connection of MOB, bacteria and physico-chemical variables altogether (Figure 7A, Table S1). 59 MOB, 17 physico-chemical variables and 271 bacterial OTUs formed 5 MCs, which discriminated the depth zonation in Rotsee (Figure 7B, 7C), confirming that the originally hypothesized zonation can be broadly reconstructed from the dataset. The network architecture showed inter-correlation of *Methylobacter* with a larger set of bacteria (MC0, MC1) and physico-chemical variables (Mn_{Diss} , CH_4 , Fe_{Diss} , TDN, S_{Tot} , Fe_{DGT} , Mn_{DGT} ,) within greater depths. MC2 consisted mainly of typeIa, was associated with Cu_{part} and Turb, and situated within the oxidation zone. MC3 in the oxidation zone and oxycline solely consisted of typeIa and was connected with Mn_{part} and Cu_{DGT} . MC4 represents the surface waters and showed association with *Methylocystis*, O_2 , Cu_{Diss} , light, pH, T, and Zn_{Diss} . MC0, MC1 and MC4 showed more bacterial connections compared to MC2 and MC3.

We used partial redundancy analysis to distinguish the relative contributions of physico-chemical variables and bacterial interactions on the variance of MOB abundance. According to this analysis, out of a total of 84% of explained variance in MOB occurrence, 22% can be explained exclusively by bacterial interactions, but only 2% exclusively by environmental drivers (Figure 7D). Interestingly, most of the explained variance is shared by physico-chemical variables and the bacterial community (60%). Specific bacterial OTUs affiliated with MOB in the network analysis are illustrated in the Gephi files (Supplementary files).

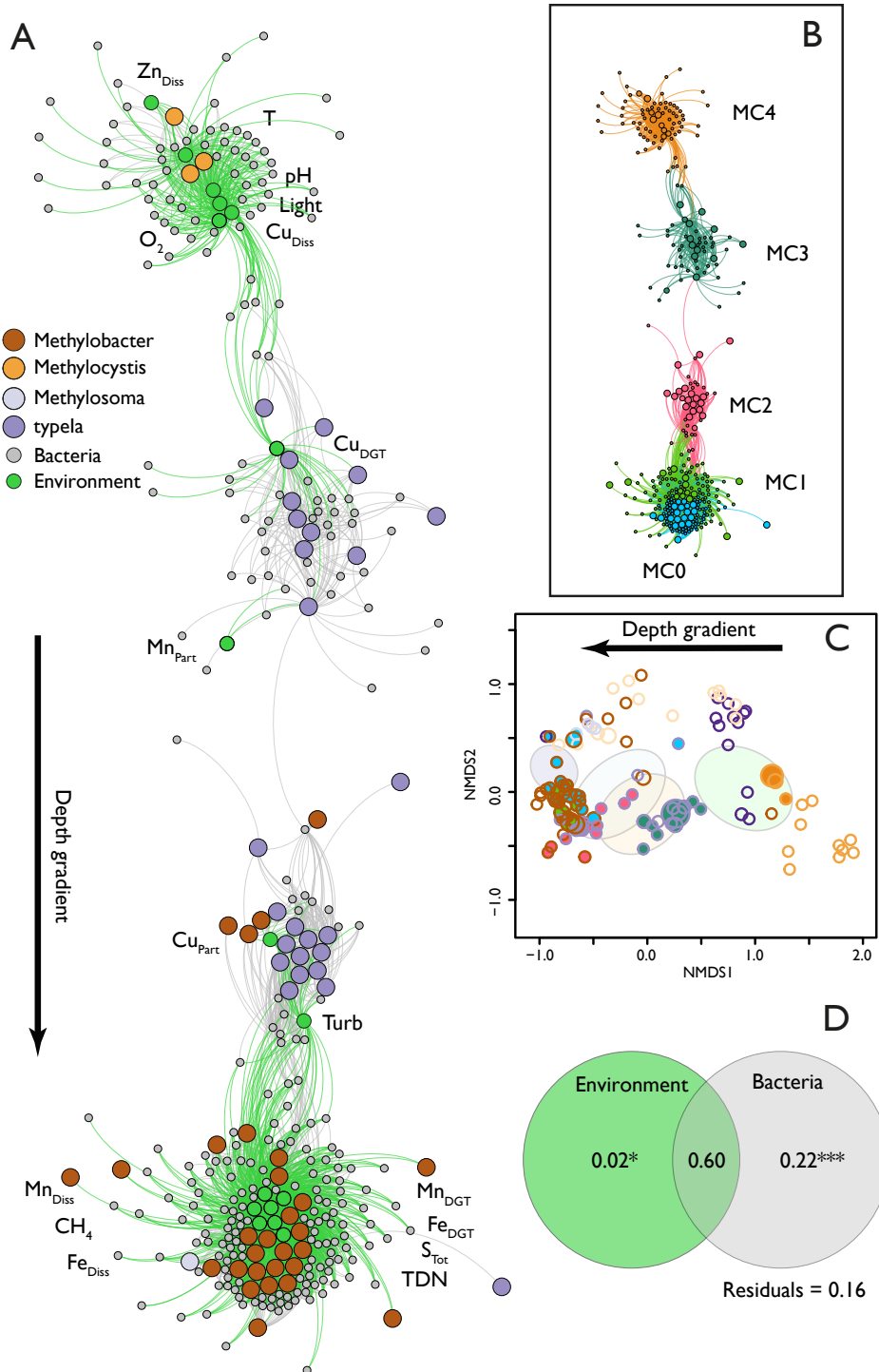


Figure 7. Relevance network based on N-integration discriminant analysis.

(A) Network of positive correlations between MOB, bacteria and physico-chemical variables. Connections represent association relevance > 0.5 . Nodes and edges are coloured according to their source group. MOB nodes are depicted larger than physico-chemical and bacterial nodes. Environmental variables are annotated. (B) MCs of the relevance network are illustrated in different colours (edges and nodes). (C) NMDS showing species scores of MOB (see also Figure 2). Filled circles are MOB present in the relevance network and are coloured according to their modularity class (MC). Unfilled circles represent OTUs from the NMDS that were not assigned to MCs. Outline of the circles denote their taxonomic affiliation according to the legend shown in (A). Dispersion ellipses represent the standard error of weighted average scores of depth zone sample groupings (confidence limits = 0.95) and thus indicate the depth gradient present in the MOB distribution. (D) Partial redundancy analysis of associated network variables (bacteria and physico-chemical variables) assessing influence on MOB occurrence. Significance levels of testable fractions are annotated (*** = $p < 0.001$).

Discussion

Although MOB play a dominant role in mitigating CH₄ emissions to the atmosphere, there is little knowledge regarding the interactive effects of the physico-chemical and microbial environment on MOB occurrence and linked ecosystem services within lake systems (i.e. effect on CH₄ removal capacity) [Semrau *et al.*, 2010; Borrel *et al.*, 2011; Ho *et al.*, 2016]. A better ecological understanding of the underlying mechanisms is important to estimate the impact on mass fluxes under dynamic environmental conditions.

Physicochemical gradients driving MOB community structure

MOB throughout the water column of Rotsee play a prominent role in mitigating CH₄ emissions to the atmosphere [Schubert *et al.*, 2010; Oswald *et al.*, 2015]. Our defined depth zones, based on coarse physico-chemical characteristics (CH₄, O₂, and light availability), broadly classify MOB habitat preferences. A general MOB structuring along the depth zones could be seen during all investigated sampling dates (Figure 2, Supplementary Figure S5). The dominance of type I MOB (*Methylobacter*, *Methylomonas*, *Methylosoma*, typeIa, typeIb) over type II MOB (*Methylocystis*) is consistent with previously reported patterns, indicating our findings may also apply to other freshwater systems [Borrel *et al.*, 2011; Bornemann *et al.*, 2016].

The MOB community composition was correlated with a set of environmental gradients along the water column of Rotsee, and the results are in agreement with the postulated importance of the O₂ and CH₄ counter gradient (Mayr *et al.*, unpublished). It is worth emphasizing that, except for September 2015, the population maximum of MOB was found below the oxycline, and that MOB were always detected throughout the water column (Supplementary Figure S5). We found Rotsee to have a highly structured and phylogenetically determined MOB distribution, with phylogenetic relatedness being present even within relatively small spatial scales of our defined depth zones (SES of MPD and MNTP < 0). All these findings clearly indicate that MOB are not simply linked to the nadir of the counter gradient, and at best passively dispersed into other zones as often assumed. Our results suggest that each of the zones exhibit dynamically overlapping physico-chemical gradients, which influence MOB communities even on small scales. Additional parameters, in particular light,

Cu- and Fe-species, pH and TDN played a significant role in further structuring MOB communities (Figure 4).

Co-occurrences and interactions of MOB with the bacterial community

Interestingly, spatio-temporal shifts in the MOB community were highly congruent with the total bacterial community change (OTU level, 51%). The bacterial community changed along the depth gradient with phylogenetically closely related OTUs being predominant at specific depths during specific time points within the sampling dates (Supplementary Figure S7A). The microbial distribution in Rotsee is consistent with other lake water studies that suggest anoxic communities to be more diverse than the ones in the epilimnion (Supplementary Figure S4A) [Schmidt *et al.*, 2016; Hengy *et al.*, 2017; Morrison *et al.*, 2017]. The restrictive and congruent localization of MOB and bacterial OTUs throughout the stratified periods suggests similar niche preferences based on similar inter-correlated physico-chemical preferences and/or biological interactions.

Our network analysis revealed the embedment of MOB into distinctive bacterial co-occurrence groups (Figure 6). It is noteworthy that positive bacterial interactions explain a relevant part of MOB occurrence (22%, Figure 7). However, when taking the inter-correlation of physico-chemical parameters and the bacterial community into account, we could see that they jointly explain a substantial proportion of the variation in MOB occurrence (60%). Mechanistically, this could be explained by an interactive effect of the environment influencing bacteria that themselves constrain MOB occurrence. Alternatively, bacterial taxa may also depend on physico-chemically constrained MOB. Additionally, it might also be that a niche overlap is present where co-existence is possible without a direct functional link between the correlated taxa. In the following, we discuss some potential mechanisms that either directly or indirectly influence MOB community structures.

Mechanisms of direct and indirect constraints on MOB

The following interpretations are based on our observations and existing literature, and provide a set of hypotheses that can be tested in future more detailed investigations.

T is one of the variables that positively correlated with *Methylocystis*, a type II MOB, which is often found in warmer waters (Figure 3, Figure 7) [Borrel *et al.*, 2011; Tsutsumi *et al.*, 2011]. It is suggested that high T selects for type II over type I MOB [Sundh *et al.*, 2005]. The absence of type II MOB in June 2013 within the oxic zone may thus be explained by lower T (Supplementary Figure S1).

The availability of Cu as a co-factor of pMMO's active site can restrict enzymatic activity in MOB communities and thus limit their anabolic potential [Semrau *et al.*, 2010]. We observed positive correlations of Cu_{Diss} with a wide range of MOB OTUs (*Methylocystis*, *Methylobacter*, typeIb) (Figure 3, Figure 7). Certain MOB are able to use Cu acquisition mechanisms based on complexing agents to deal with low Cu supply conditions [Dassama *et al.*, 2017]. Such auxiliary peptides could mobilize Cu from part of the non-bioavailable Cu_{Diss} fraction within the oxic zone of Rotsee. *Methylocystis* can indeed contribute to CH₄ consumption in the oxic zone, as most members of this taxon possess a second, high CH₄ affinity pMMO isozyme, which oxidizes CH₄ at trace atmospheric concentrations [Baani and Liesack, 2008]. MOB in the oxic zone might also be in a dormant state, as indicated by their low abundance, since high light intensity and O₂ concentrations are likely to inhibit CH₄ oxidation [Roslev and King, 1994; Murase *et al.*, 2005].

In-situ studies focussing on the influence of Cu on MOB community structures are rare, but it has been recently elucidated that MOB able to express pMMO thrive even under very low bioavailable Cu conditions (< 50 nM) [Cantera *et al.*, 2016; Guggenheim *et al.*, 2019]. Cu_{DGT}, which is thought to be the bioavailable Cu fraction, seems to be an integral variable shaping MOB community structures in Rotsee (Figure 3, Figure 4). Its distribution correlated specifically with the large typeIa MOB cluster (MC3) situated in the oxycline (Figure 7), where CH₄ oxidation can take place. The relevance network is less dense within MC3, which could indicate that MOB are more autonomous here in their central niche, and hence less dependent on interactions with other organisms.

Some *Methylobacter* and typeIa clusters (MC2) tend to be positively correlated to Cu_{Part}, an indication for Cu being incorporated into biomass (Figure 3, Figure 7) [Guggenheim *et al.*, 2019]. They were mostly present

within the oxidation zone. Part of this community correlated with Turb, a possible indicator for primary producers as Turb and Chl-a show strong co-linearity (Supplementary Figure S1, Supplementary Figure S2). It seems likely that these MOB clusters are the main CH₄ consumers as the main CH₄ oxidation process in Rotsee during stratification might be predominantly coupled to oxygenic primary production [Oswald *et al.*, 2015; Brand *et al.*, 2016].

Bioavailable and dissolved Fe (Fe_{DGT}, Fe_{Diss}) were correlated with most *Methylobacter* species in the CH₄ rich anoxic zone of Rotsee (Figure 3, Figure 4). Cultivated representatives of *Methylobacter* are not able to express the iron-dependent sMMO [Knief, 2015]. It is however possible that these MOB rely on Fe for other enzymatic pathways (e.g. formate dehydrogenase) [Glass and Orphan, 2012]. In addition, there is evidence for anaerobic methane oxidation proceeding via Fe(III) (or Mn(IV)) reduction, which could explain the increase in Fe_{Diss} (and Mn_{Diss}) (Supplementary Figure S1) and the correlation with MOB (Figure 7) [Oswald, Milucka, *et al.*, 2016].

Methylobacter were strongly embedded into the bacterial network structures (MC0, MC1) and showed many inter-correlations with bacteria as well as several additional physico-chemical variables (e.g. TDN, S_{Tot}) (Figure 7). This indicates that bacterial community feedback loops possibly constrain *Methylobacter* more than physico-chemical variables. Furthermore, it has previously been postulated that PO₄ availability can reduce type I CH₄ oxidation activity in boreal lakes as they are outcompeted by fast growing heterotrophs using PO₄ for energy and biomass production [Denfeld *et al.*, 2016]. In Rotsee, PO₄ was co-linear with Fe_{Diss} and with *Methylobacter* (Supplementary Figure S2). This implies that PO₄ concentrations were high enough to sustain growth of *Methylobacter* species and other heterotrophs at the same time. Possibly, secondary effects mediated by PO₄ on the bacterial community also influence *Methylobacter*.

Conclusions

The investigation of the MOB community in Rotsee during the build-up and progression of stratification throughout different years was a successful approach to unravel interactive microbial and environmental effects. Our results provide a first insight into potential driving forces shaping MOB community composition within stratified freshwater lakes and indicate that MOB community assembly was unexpectedly complex and sensitively linked to environmental conditions and the greater bacterial community. We see a distinct zonation of MOB throughout the water column, which is partly driven by the expected chemical gradients of CH_4 and O_2 . However, MOB occurrence appears to be also influenced by other physico-chemical drivers, such as T, Cu, Fe, Mn and PO_4 . 69% of MOB structuring (according to CCA) can be explained by environmental variability (Figure 4). Importantly, interactions with the bacterial community play an important role in shaping the MOB community distribution (Figure 5). Herein, we focused on positive inter-correlations, which means that we track species co-existence driven by synergism (i.e. win-win situation) and mutualism (i.e. cooperation) (bacterial fraction in Figure 7D), as well as similar niche preferences (shared fraction in Figure 7D) [Faust and Raes, 2012; Ho *et al.*, 2016]. Furthermore, positive correlations could also arise from positive feedback loops mediated via physico-chemical variables affecting the bacterial community structuring, which subsequently influences the MOB community by synergistic and/or mutualistic effects (shared fraction in Figure 7D). Especially in the surface layers and the hypolimnion of the lake, bacterial and physico-chemical inter-connectivities were more complex. Considering the three-way relation of MOB, bacteria and environment, our analysis revealed that bacteria alone could explain significantly more of the MOB structure (22%) than the isolated physico-chemical variability (2%). Taking into account both, physico-chemical and biological variability, we see up to 60% explained variance. However, the mode of action underlying the correlations could not be unambiguously determined. Understanding these mechanisms of bacterial interactions would help to predict the responses of community functioning under diverse conditions. Future studies with a strong focus on microbial interdependency and incorporating metabolic and anabolic analysis of community players might help to disentangle the mode of action.

Acknowledgements

We are grateful to Andreas Brand, Christian Dinkel, Kirsten Oswald, Hannah Bruderer, Tanja Beck, and Rohini Athavale for their help during field and lab work. We wish to thank Laura Sigg and Niksa Odzak for mentoring support in DGT preparation and interpretation of its results. David Kistler, Serge Robert, Gijs Nobbe (R.I.P), and Patrick Kathriner are thanked for their assistance in ICP-MS, GC, IC and FIA analysis. Special thanks goes to Kirsten Oswald and Rohini Athavale for making several methane, nutrients, ammonium, and total sulphide profiles available. We appreciate the help of the Genetic Diversity Centre, particularly Jean-Claude Walser, in preparing and analysing next-generation sequencing data. We thank Christian Beisel from the Genomics Facility Basel for his help with *pmoA* library preparation and sequencing. Feng Ju is acknowledged for giving input on co-occurrence analysis. This study was made possible through a research grant (no. 153091) by the Swiss National Science Foundation.

Supplementary information

Profiling and physico-chemical analyses

Sample collection was conducted close to the deepest point of Rotsee (47°04.259'N, 8°18.989'E) during three consecutive years at the beginning of stratification (June 2013), during peak stratification (August 2013) and shortly before lake overturn (September 2014, September 2015). A custom-built 'Profiler for *In-situ* Analysis' (PIA) was deployed for high-resolution depth profiling and deployment of different sensors and sampling devices [Kirf *et al.*, 2014]. A multi-parameter probe (XRX 620, RBR, Ottawa, ON, Canada) recorded conductivity (Cond), turbidity (Turb), depth (pressure), temperature (T) and pH. Dissolved oxygen (O₂) was measured with normal and trace micro-optodes (types PSt1 and TOS7, Presens, Regensburg, Germany; detection limits: 125 and 20 nM). A spherical quantum sensor (LI-190 SB, LI-Cor, Lincoln, NE, USA) provided data of photosynthetically active radiation (PAR) with a detection limit of 0.1 $\mu\text{mol m}^{-2} \text{s}^{-1}$. Chlorophyll a (Chl-a) was measured in June and August 2013 using an ECO-FL fluorescence probe (Wetlabs, USA) attached to PIA.

The following variables were sampled via a rosette syringe sampler (12 x 60 ml syringes). Aliquots for total sulphide ($S_{\text{Tot}} = \text{H}_2\text{S}, \text{HS}^-, \text{S}^{2-}$) measurements were immediately fixed with zinc acetate (~1.3% final concentration) and determined by spectrophotometric analysis following the procedure of Cline [Cline, 1969]. Dissolved organic carbon (DOC) and total dissolved nitrogen (TDN) samples were analysed on a total carbon analyser (TOC-L_{CSH/CPH}, Shimadzu, Tokyo, Japan) after filtration (< 0.22, Millex-GP polyethersulfone (PES) membrane, Millipore, Zug, Switzerland) and acidification (2 M HCl; final concentration: 20mM). Dissolved inorganic carbon (DIC) samples (August 2013, September 2014 and 2015) were filtered (< 0.22 μm) on-site and measured on the same TOC-analyser. Except for June 2013, samples for nitrite (NO₂), nitrate (NO₃), ammonium (NH₄), sulphate (SO₄), and phosphate (PO₄) were immediately filtered (< 0.22 μm) and measured by ion chromatography (881 Compact IC pro, 882 Compact IC plus, 761 Compact IC, Methrom AG, Zofingen, Switzerland) and flow-injection analysis (SAN++, Skalar, Procon AG, Burgdorf, Switzerland), respectively. Dissolved ($M_{\text{Diss}} < 0.45 \mu\text{m}$) and total (M_{Tot}) metal samples (copper (Cu),

iron (Fe), manganese (Mn), zinc (Zn), chromium (Cr)) were acidified and quantified via inductively coupled plasma mass spectrometry (Element2, Thermo-Fisher Scientific, Reinach, Switzerland). All metal sampling equipment was acid-washed and rinsed with nanopure water before use. Particulate metal concentrations (M_{Part}) were calculated by subtracting dissolved from total concentrations. The diffusive gradient in thin film (DGT) technique was applied to receive information about the bioavailable metal fractions (M_{DGT}) [Davison, 2016; Menegário *et al.*, 2017]. M_{DGT} data were obtained from [Guggenheim *et al.*, 2019].

Samples for dissolved methane (CH_4) concentrations were either collected with a Niskin bottle or via pumping with a gas tight tubing (PVC Solaflex, Maagtechnic, Dübendorf, Switzerland) attached to PIA. 120 ml serum bottles were filled anoxically allowing water to overflow. CH_4 oxidation was stopped by adding NaOH (pH > 12) or Cu(I)Cl and bottles were crimped airtight. Headspace injection of 20 ml N_2 was used for equilibrium and CH_4 was measured on a gas chromatograph (Agilent 6890N, Agilent Technologies, Santa Clara, CA, USA) equipped with a Carboxen 1010 column (30 m x 0.53 mm, Supelco, Bellefonte, PA, USA) and a flame ionization detector (detection limit $\sim 0.01 \mu\text{M}$). CH_4 concentrations in the water phase were calculated using Henry's law [Wiesenburg and Guinasso Jr., 1979]. The same headspace was used to determine the $^{13}\text{C}/^{12}\text{C}$ isotopic ratio of CH_4 ($\delta^{13}\text{C}-\text{CH}_4$) (August 2013, September 2014) using isotope ratio mass spectrometry with a trace gas instrument (T/GAS PRE CON, Micromass UK Ltd., Wilmslow, UK) coupled to a mass spectrometer (GV Instruments, Manchester, UK; Isoprime, Stockport, UK). Data were obtained from [Oswald *et al.*, 2015, 2017]. Isotopic ratios are given in the conventional δ -notation normalized to the Vienna Pee Dee Belemnite (VPDB) reference standard.

DNA sampling and extraction, *pmoA* qPCR and limited cycle PCR, amplicon purification

Water samples were collected either via a Niskin bottle or via pumping and were prefiltered (5.0 μm polycarbonate) and subsequently run through 0.2 μm polycarbonate membrane filters. Filters were frozen in liquid N_2 and stored at -80°C until DNA was extracted from the 0.2 μm filters using the PowerWater® DNA Isolation Kit (MoBio Laboratories, Carlsbad, CA, USA) following the manufacturer's instructions. DNA was quantified with a NanoDrop 1000 Spectrophotometer (Thermo-Fisher Scientific, Wilmington, DE, USA).

pmoA gene numbers were quantified using the primer pair A189f (Eurofins Genomics, Ebersberg, Germany; 5'-GGNGACTGGGACTTCTGG-3') and mb661r (Eurofins Genomics, Ebersberg, Germany;

5'-CCGGMGCAACGTCYTTACC-3') [Holmes *et al.*, 1995; Costello and Lidstrom, 1999] according to a protocol adapted from [Henneberger *et al.*, 2015]. The qPCR reaction mixture consisted of 1 × master mix (LightCycler® 480 SYBR® Green I Master), 0.2 µM of each primer, and 2 µl of template DNA (1:10). Samples were run using the following thermal program: initial denaturation (95°C, 10 min), 10 touchdown cycles (denaturing: 95°C, 10 sec; annealing: 62-53°C (-1°C per cycle), 30 sec; extension: 72°C, 30 sec), followed by 30 cycles (denaturing: 95°C, 10 sec; annealing: 52°C, 30 sec; extension: 72°C, 30 sec). Fluorescent readings were taken at 79°C for 30 sec and melting curves at 65-97°C (0.11°C/sec). Results were analysed with the Absolute Quantification/2nd Derivative Maximum method. qPCR efficiency (E) yielded in 1.868.

For *pmoA* library preparation, triplicate PCR reactions (20 µl) were set up for each sample containing: primers (0.3 µM each, A189f, mb661r), 1 × Nebnext Q5 Hot Start HiFi PCR Master Mix (New England BioLabs, Frankfurt, Germany), and undiluted DNA extracts of the respective sample (3 µl). Cycle conditions were as follows: initial denaturation (30 sec, 98°C), 27 cycles of denaturation (10 sec, 98°C), annealing (35 sec, 54°C) and elongation (35 sec, 65°C); and final extension (5 min, 65°C). Genomic DNA from an axenic culture strain (*Methylocystis rosea* received from DSMZ, Braunschweig, Germany) served as positive control. Parallel reactions were combined and purified using AMPure XP Beads (BeckmanCoulter Inc., Fullerton, CA, USA) according to the protocol.

Additional statistical analysis

Shapiro-Wilk test was performed to assess normality of physico-chemical variables, which were subsequently log transformed if test criteria were not met. Absolute MOB abundances were calculated by applying relative abundances to *pmoA* copy numbers obtained from qPCR measurements. Differences in beta diversity among depth zones were assessed by multivariate homogeneity of dispersions [Anderson *et al.*, 2006]. Thereby, Bray-Curtis distances between samples within the depth zones are reduced to principal coordinates and distances of zone members to the zones centroid are calculated and compared by type III ANOVAs followed by Tukey's HSD (honest significant difference) test. Overall similarity of MOB and the total bacterial community was assessed by Procrustes and additionally by a mantel test (9999 permutations). The Spearman correlation

network had 1079 nodes and 41'977 edges (Table 1). The DIABLO relevance network at an association relevance level > 0.5 included 347 nodes and 3099 edges.

Additional results

Light radiation was attenuated with depth and detectable down to the anoxic zones. CH₄ isotopic signatures usually became heavier from the anoxic zone towards the oxycline and shifted again to lighter signatures within the oxycline and the oxic zone (measured in August 2013, September 2014). pH decreased from the oxic to the anoxic zone and Cond slightly increased. DOC, NO₂, NO₃, SO₄, Cr_{Tot}, Zn_{Diss} either decreased from the epi- to the hypolimnion or were more or less stable throughout. Fe_{Part} and Mn_{Part} concentrations were low compared to their soluble concentrations.

16S rRNA beta diversity over all campaigns was smallest in the anoxic zone, and highest within the oxidation zone (ANOVA $F(3,71) = 5.50$, $p < 0.01$) reflecting a distinct community turnover within this zone (Supplementary Figure S11A). Bacteria in a sample within a specific depth zone were phylogenetically more related than expected by chance (SES MPD < 0, SES MNTD < 0, Supplementary Figure S7A), which shows the presence of ecological niches within the zonation. 16S rRNA based SES was highest in the anoxic zone (ANOVA $F(3,71) = 23.27 / 30.52$, $p < 0.001$, Tukey's HSD < 0.01), which indicates lower phylogenetic relatedness within a specific site within this zone compared to the other zones. *pmoA* beta diversity did not differ between the depth zones over all sampling dates ($F(3,66) = 0.07$, $p = 0.98$, Supplementary Figure S11B) indicating a relative steady community turnover throughout the specific zones.

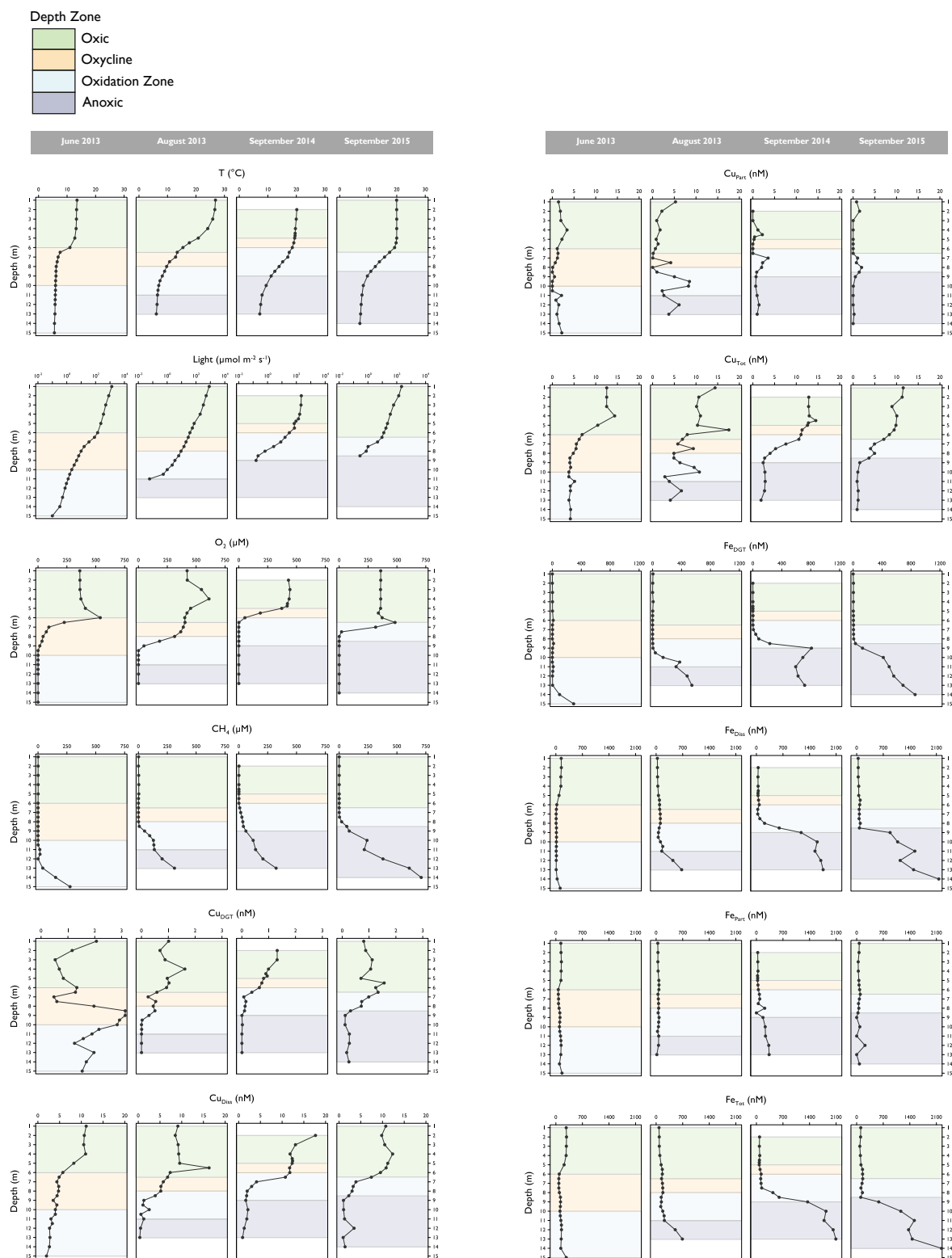
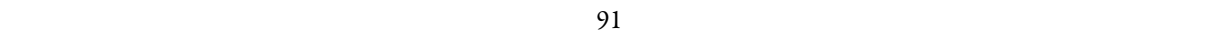
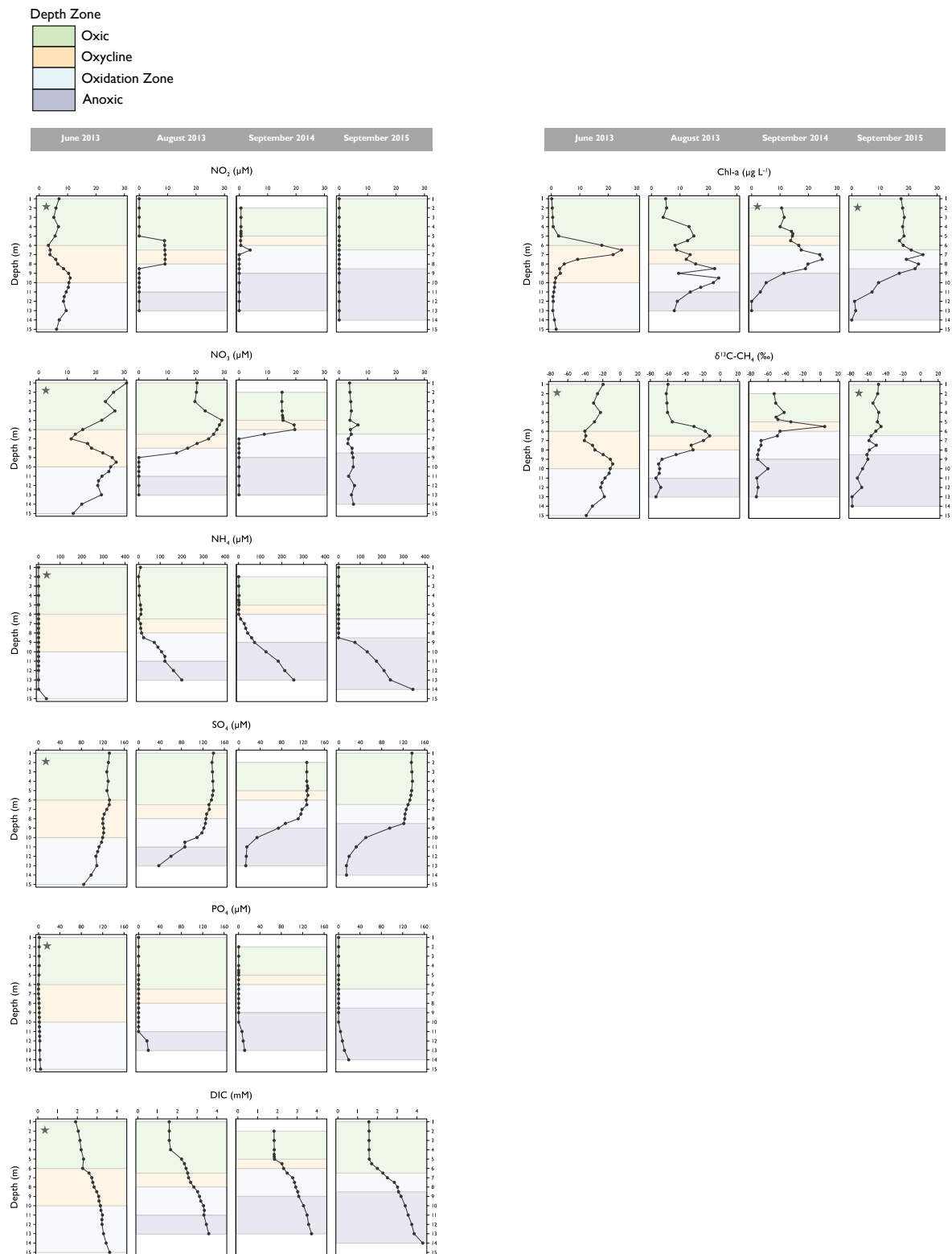


Figure S1. Gradients of physical and chemical parameters in Rotsee.

First panel of each plot shows June 2013, second panel August 2013, third panel represents September 2014, and the fourth panel September 2015. Background colours refer to the different depth zones (green = oxic zone, yellow = oxycline, blue = oxidation zone, dark blue = anoxic zone). A star indicates complete imputed profiles, except for pH where data points from 6.5 m onwards were imputed.





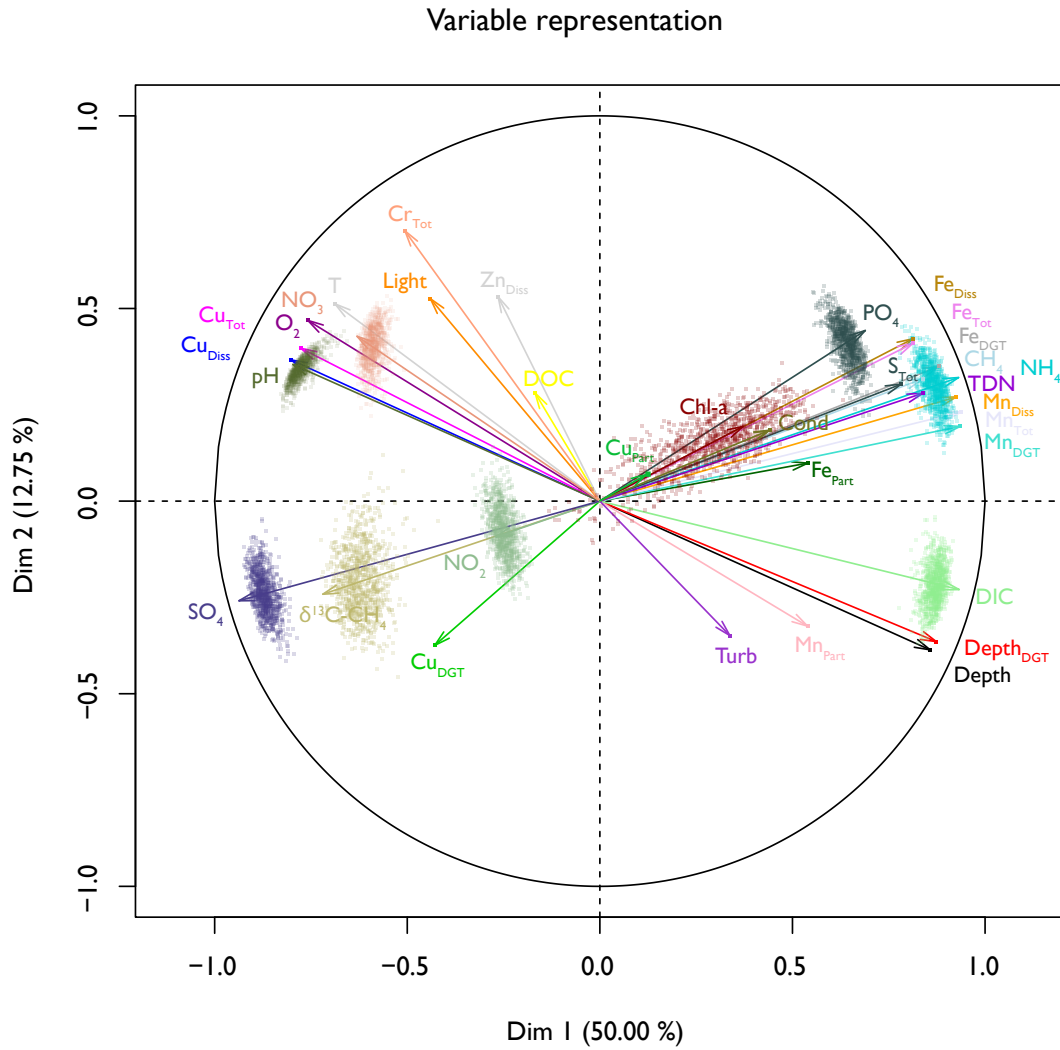


Figure S2. PCA of 10000 boot imputed datasets from the physico-chemical variables.

Observed values are the same from one dataset to the others whereas imputed values change. The variation of the point cloud of imputed values reflects the variability with which missing values can be predicted. The PCA shows also the co-linearity (i.e. similar directionality of arrows) for the measured variables.

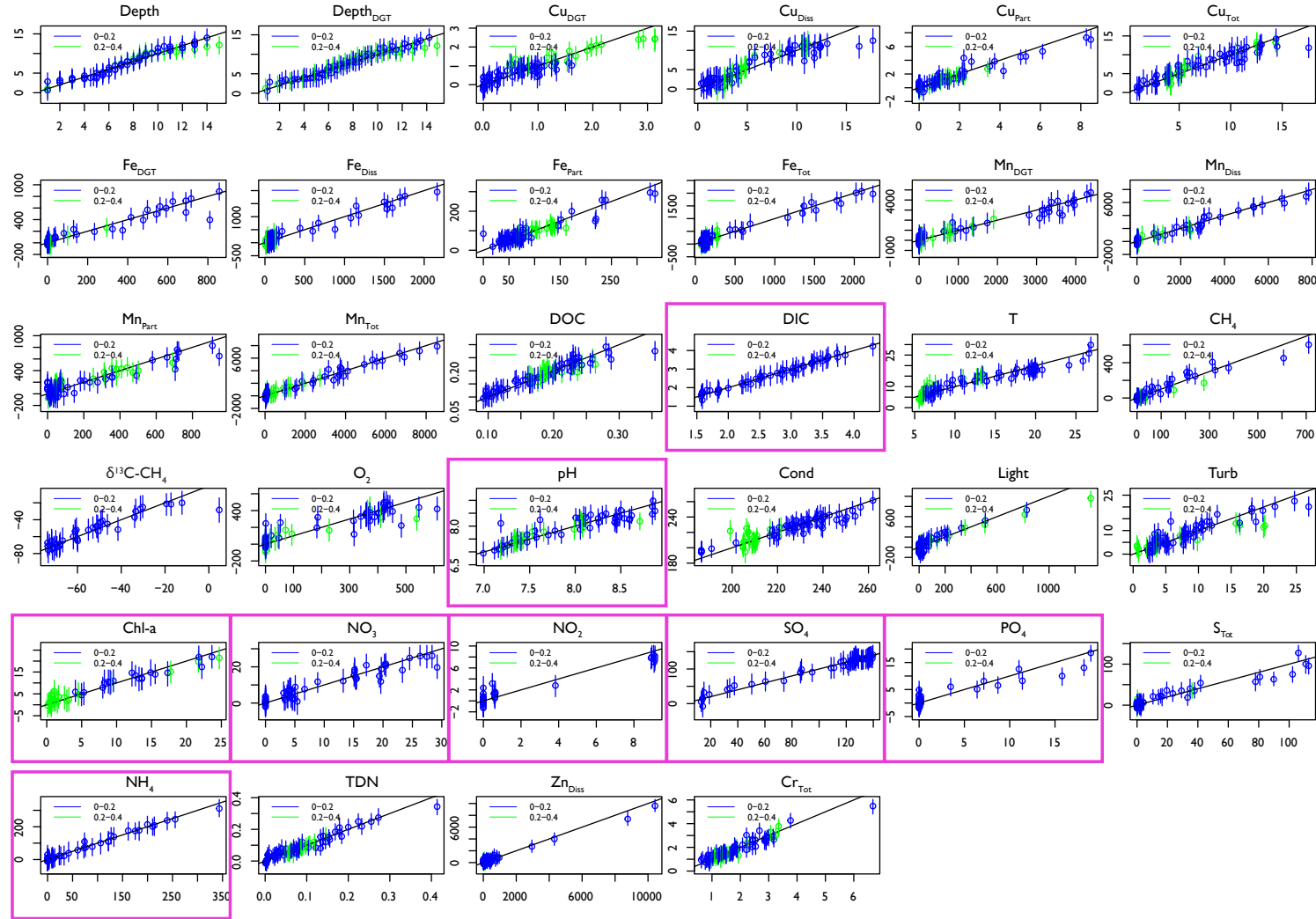


Figure S3. Overimputation to assess the fit of the predictive distribution.

10000 imputations for each observed value from each variable were produced and a 90% confidence interval for each observed value is constructed using the quantiles of the overimputed values.

The proportion of the other values that were missing for that observation in the original data are indicated in blue and green. Purple frames indicate variables that have missing values in the original data. Black lines show the 1:1 ratio. Units of the variables can be found in Supplementary Figure S1.

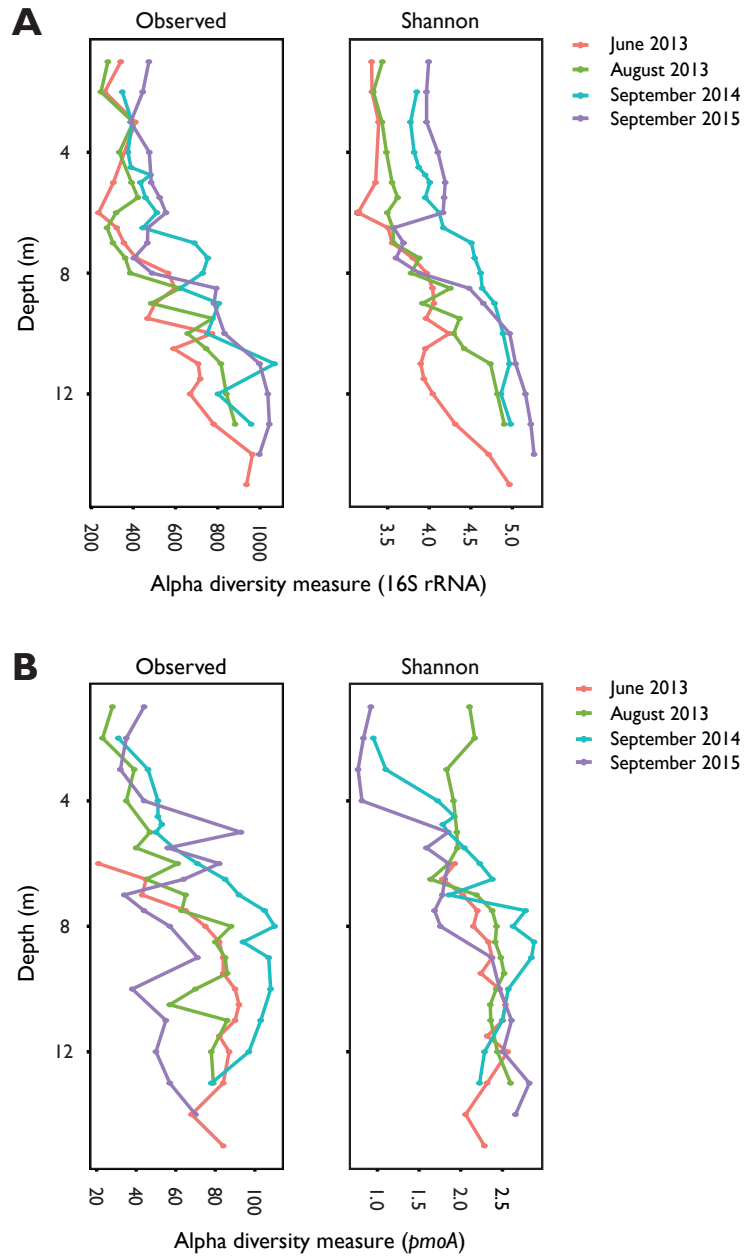


Figure S4. Alpha diversity measures of 16S rRNA based bacterial community data (A) and *pmoA* based MOB data (B).

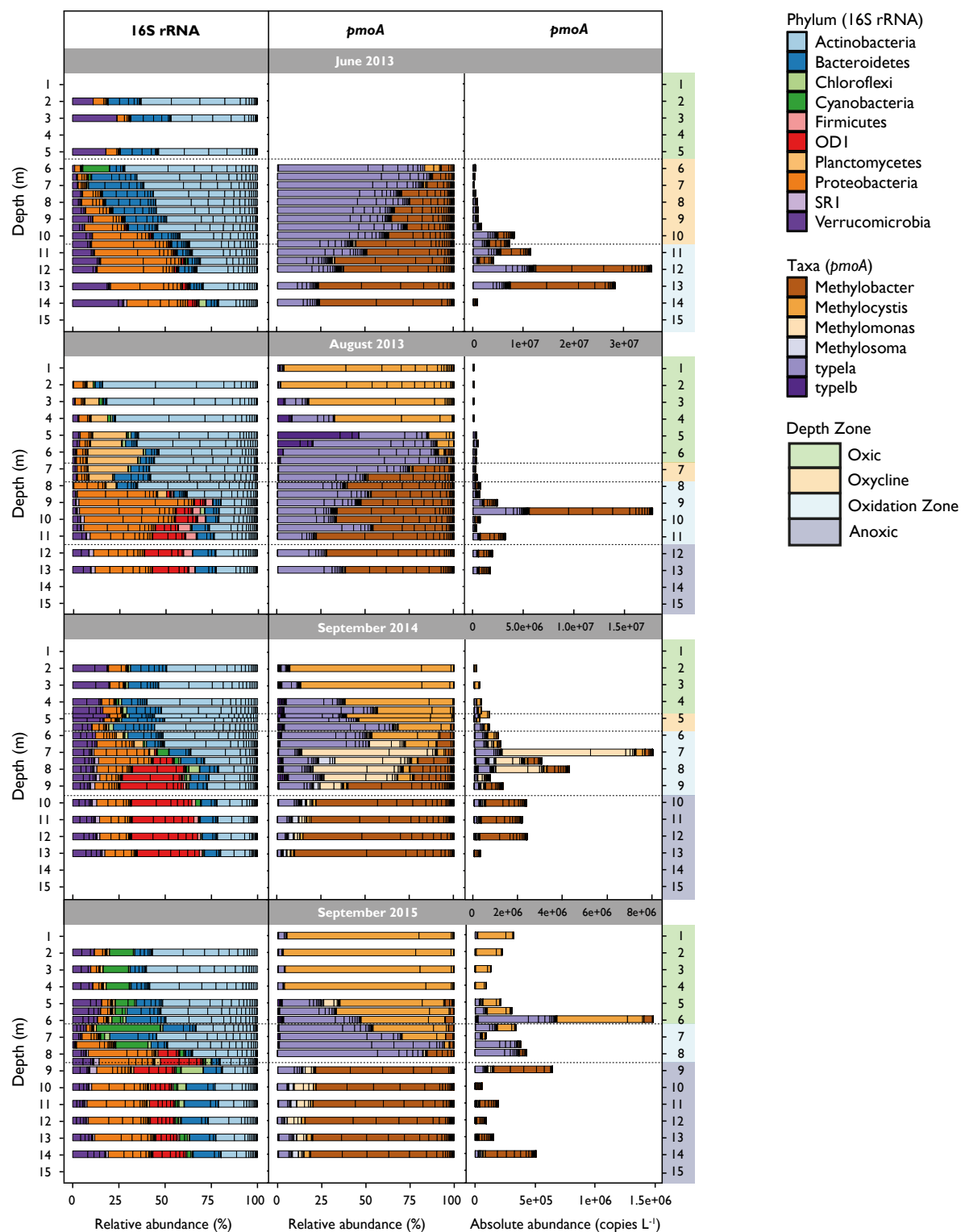


Figure S5. Relative abundance of most abundant bacterial phyla (16S rRNA) and MOB (*pmoA*) genera along the depth gradient during the different sampling dates.

Bacteria phyla represent sequence reads that occur at least in 10% of the samples and represent at least 1% of total read counts. Bacterial and MOB relative abundances are standardized to the mean sequencing depth. MOB absolute abundances are calculated as relative abundance multiplied by *pmoA* copy numbers per litre determined by qPCR.

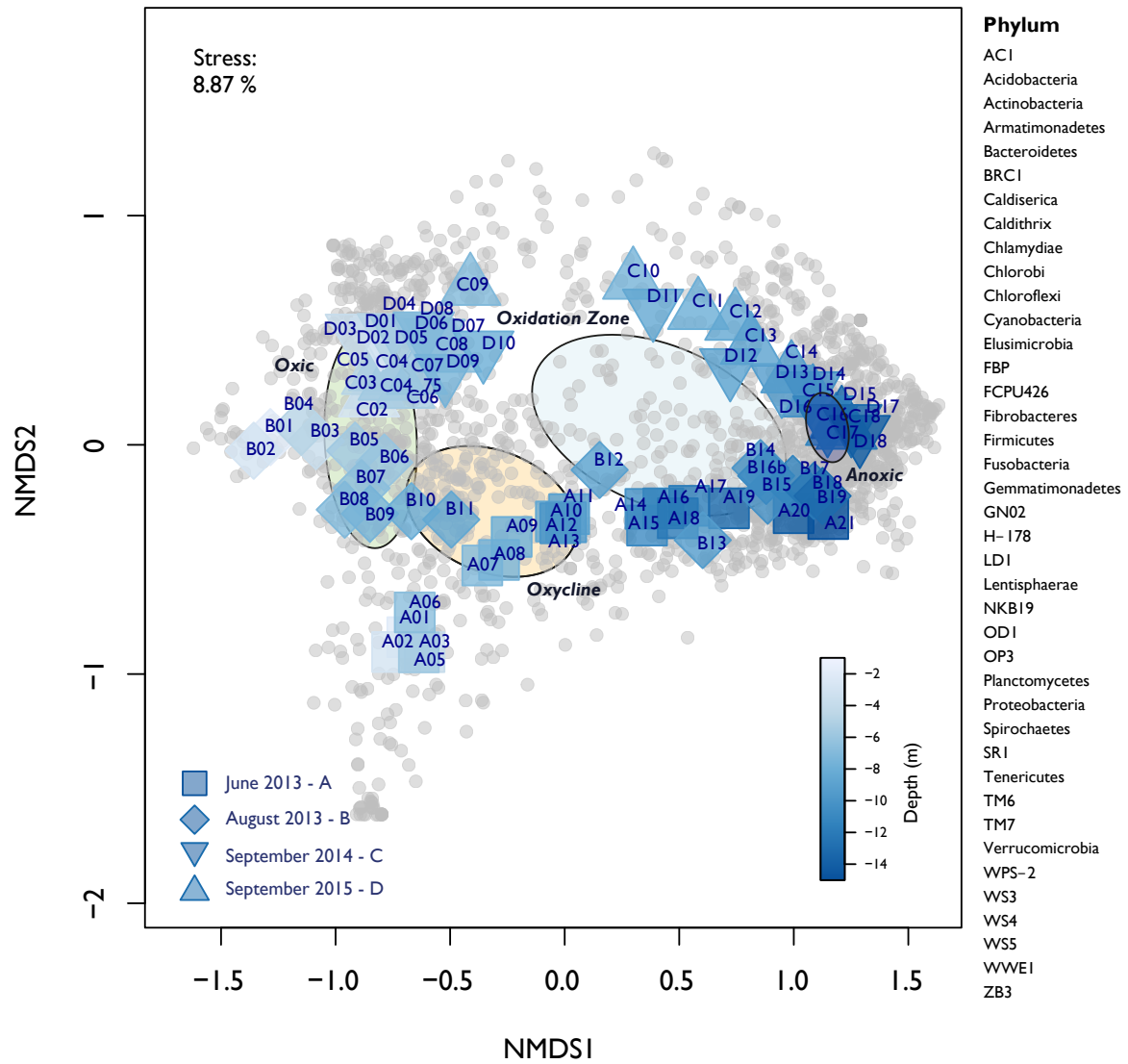


Figure S6. NMDS of total bacterial community structure during all sampling dates.

Grey dots depict species score of 40 detected bacterial phyla. Annotated blue squares and triangles indicate scores of individual sampling depths during different sampling campaigns (e.g. A01 – D18). Fill colour represents the depth of the respective sample according to the colour gradient. Dispersion ellipses depict the standard error of weighted average scores of depth zone groupings (confidence limits = 0.95). The stress of the NMDS ordination is stated.

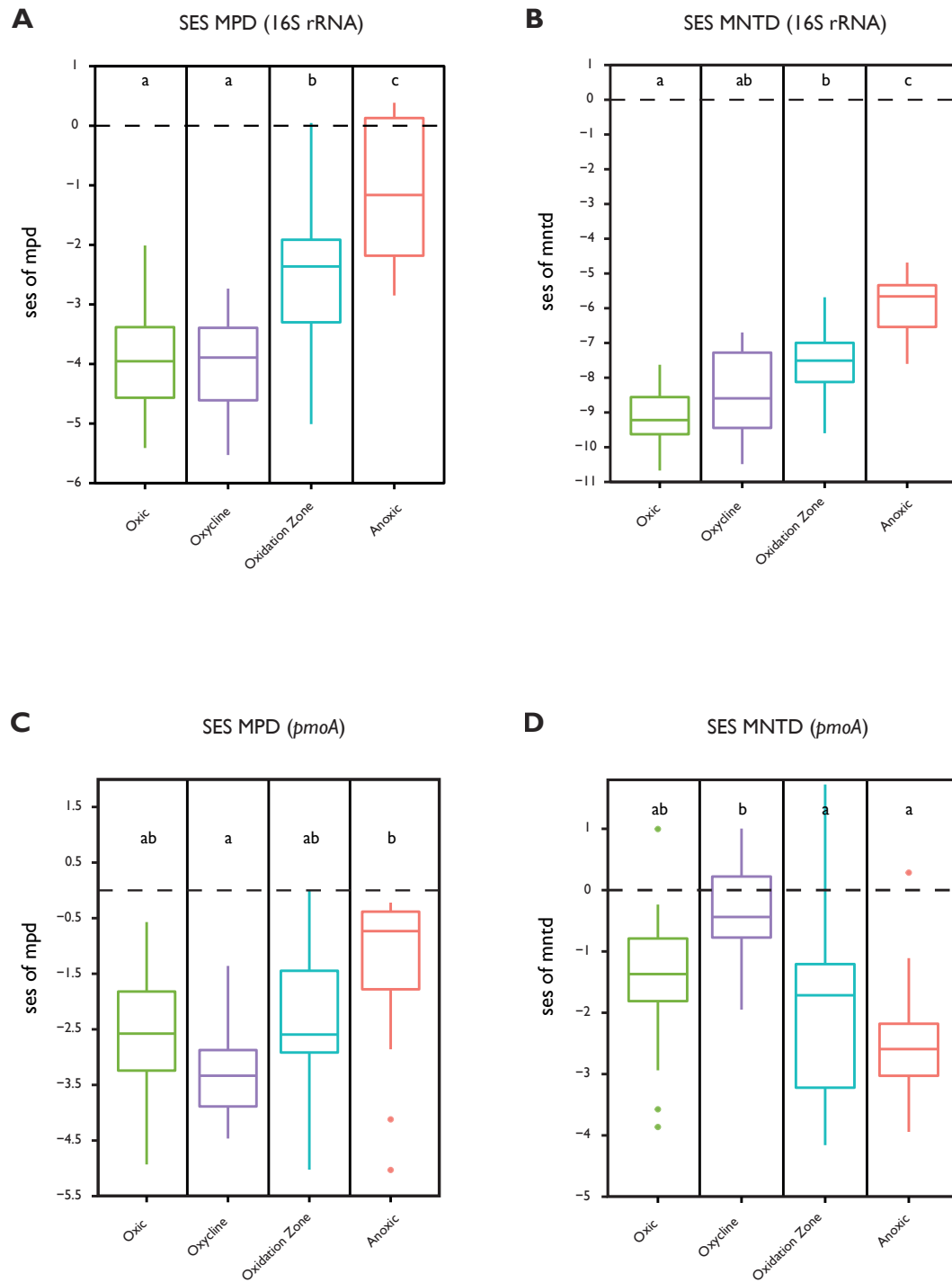


Figure S7. Boxplots of Standard Effect Size (SES) of Mean Pairwise Distance (MPD) and Mean Nearest Taxon Distance (MNTD).

SES are compared to a null model with randomized ($n = 999$) tree structuring. SES-MPD and SES-MNTD of bacteria (A,B) and MOB (C,D) communities within the different depth zones. Differences in SES were tested by ANOVA followed by Tukey's HSD. Negative SES values indicate phylogenetic clustering (i.e. higher degrees of phylogenetic relatedness among species in the habitat than expected by chance) whereas positive values would represent overdispersion. MPD is more sensitive to patterns over the complete phylogenetic tree, whereas MNTD is more sensitive to clustering and evenness of tree tips.

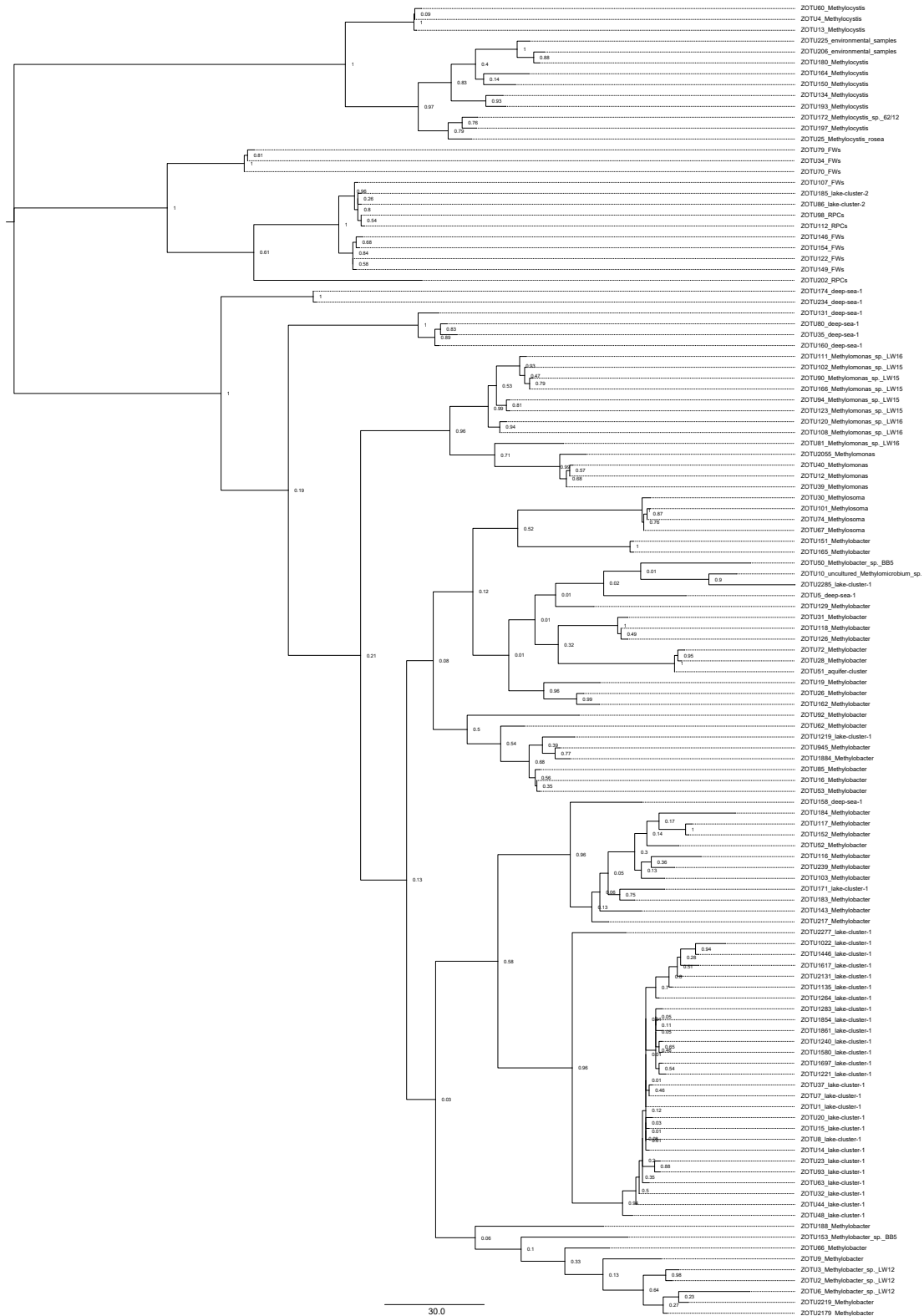


Figure S8. Maximum Parsimony Tree of *pmoA*.

The evolutionary history was inferred using the Maximum Parsimony method. The most parsimonious tree with length 1857 is shown. The percentage of replicate trees in which the associated taxa clustered together in the bootstrap test (1000 replicates) are shown next to the branches. The Maximum Parsimony tree was obtained using the Subtree-Pruning-Regrafting (SPR) algorithm with search level 1 in which the initial trees were obtained by the random addition of sequences (10 replicates). The analysis involved the 121 *pmoA* sequences with the lowest taxonomic resolution annotated based on the Wen database 2016 [Wen *et al.*, 2016]. The tree is used in Figure 3.

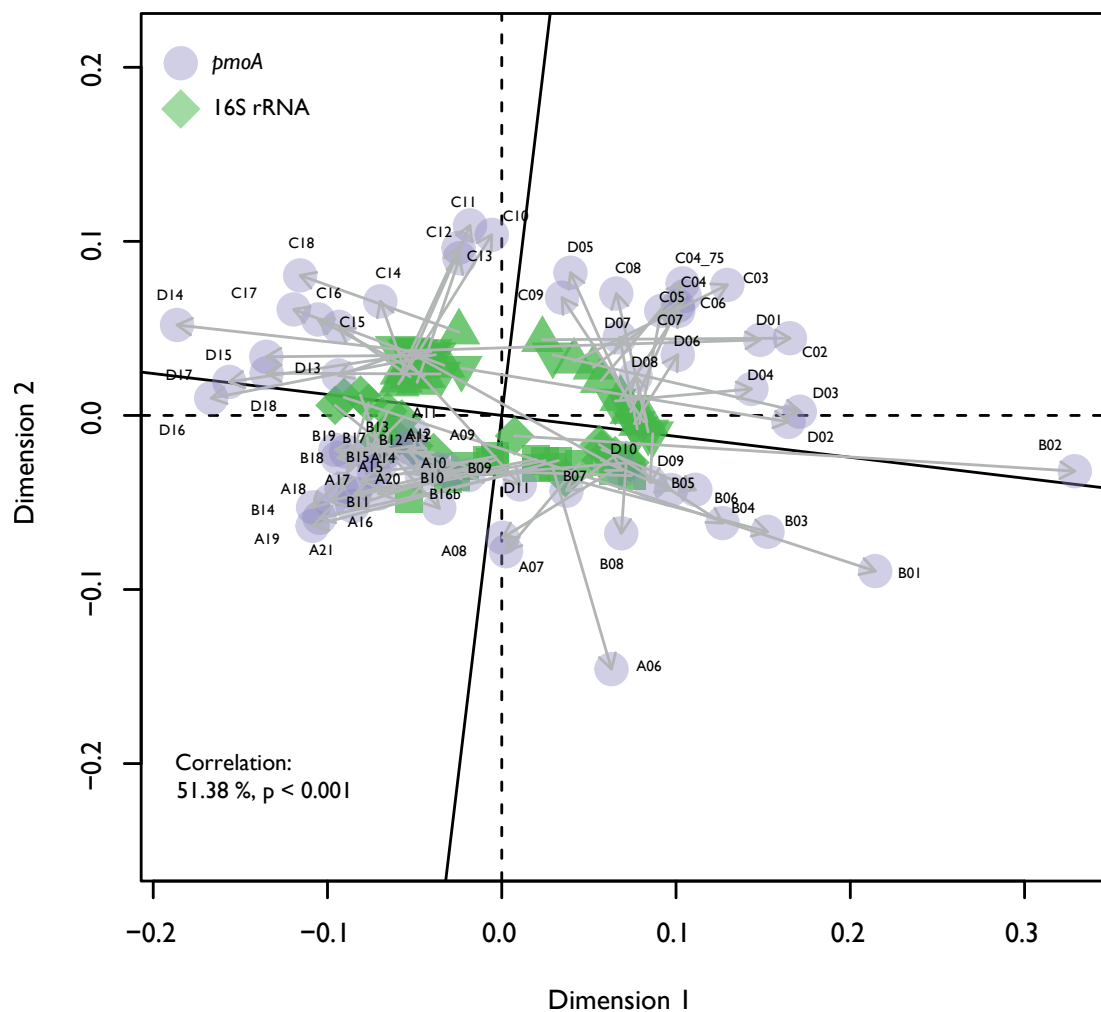


Figure S9. Procrustes rotation of the first two dimensions of the NMDS of total bacterial and MOB community structures.

Green and blue coloured symbols indicate site scores of total bacterial and MOB communities, respectively. Scores of the same samples are connected with grey arrows. Overall correlation and significance levels are given.

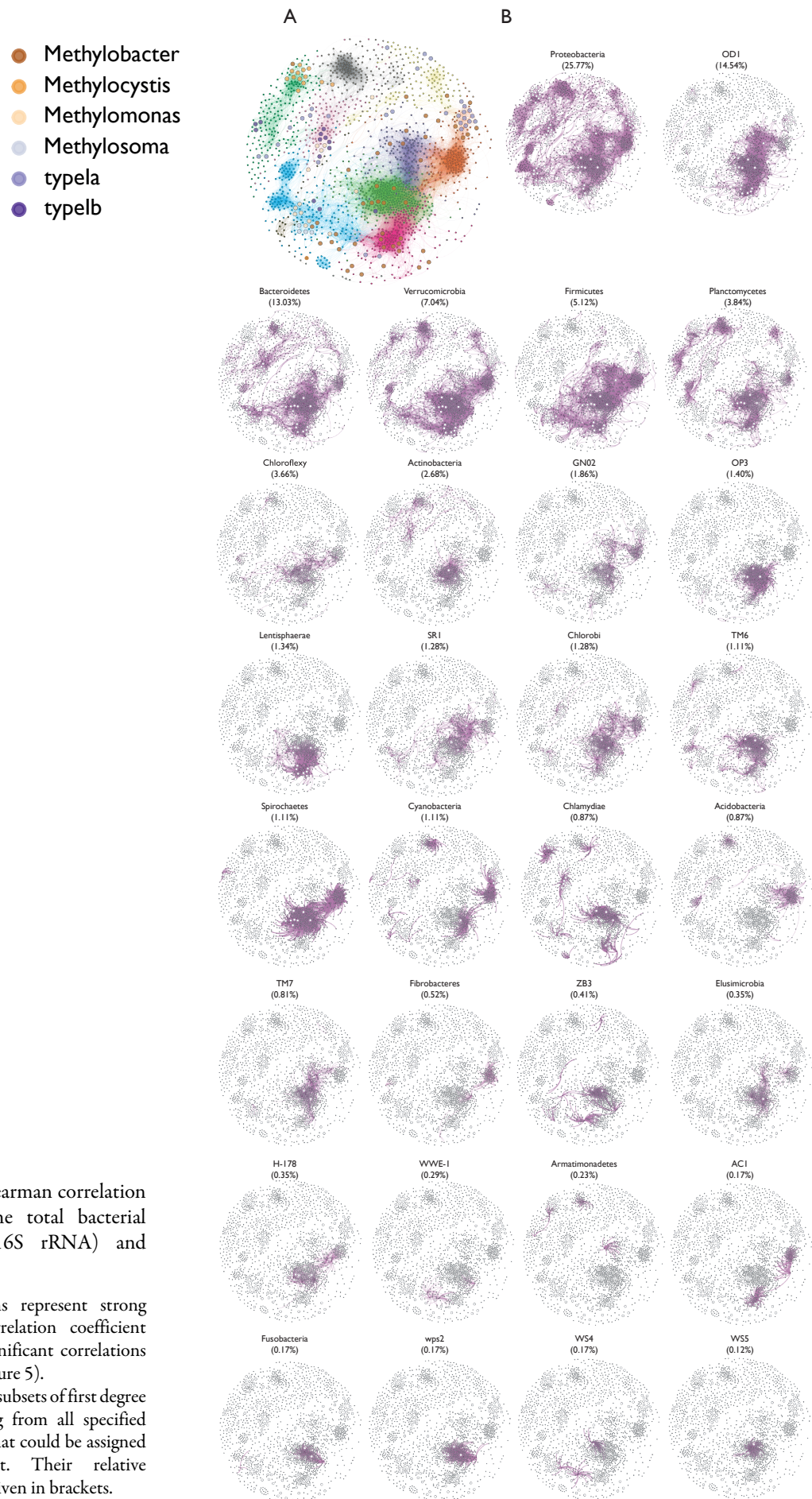


Figure S10. Spearman correlation network of the total bacterial community (16S rRNA) and MOB (*pmoA*).

(A) Connections represent strong (Spearman's correlation coefficient $\rho > 0.7$) and significant correlations ($p < 0.01$, see Figure 5).

(B) Depicted are subsets of first degree edges originating from all specified bacterial phyla that could be assigned in the dataset. Their relative abundances are given in brackets.

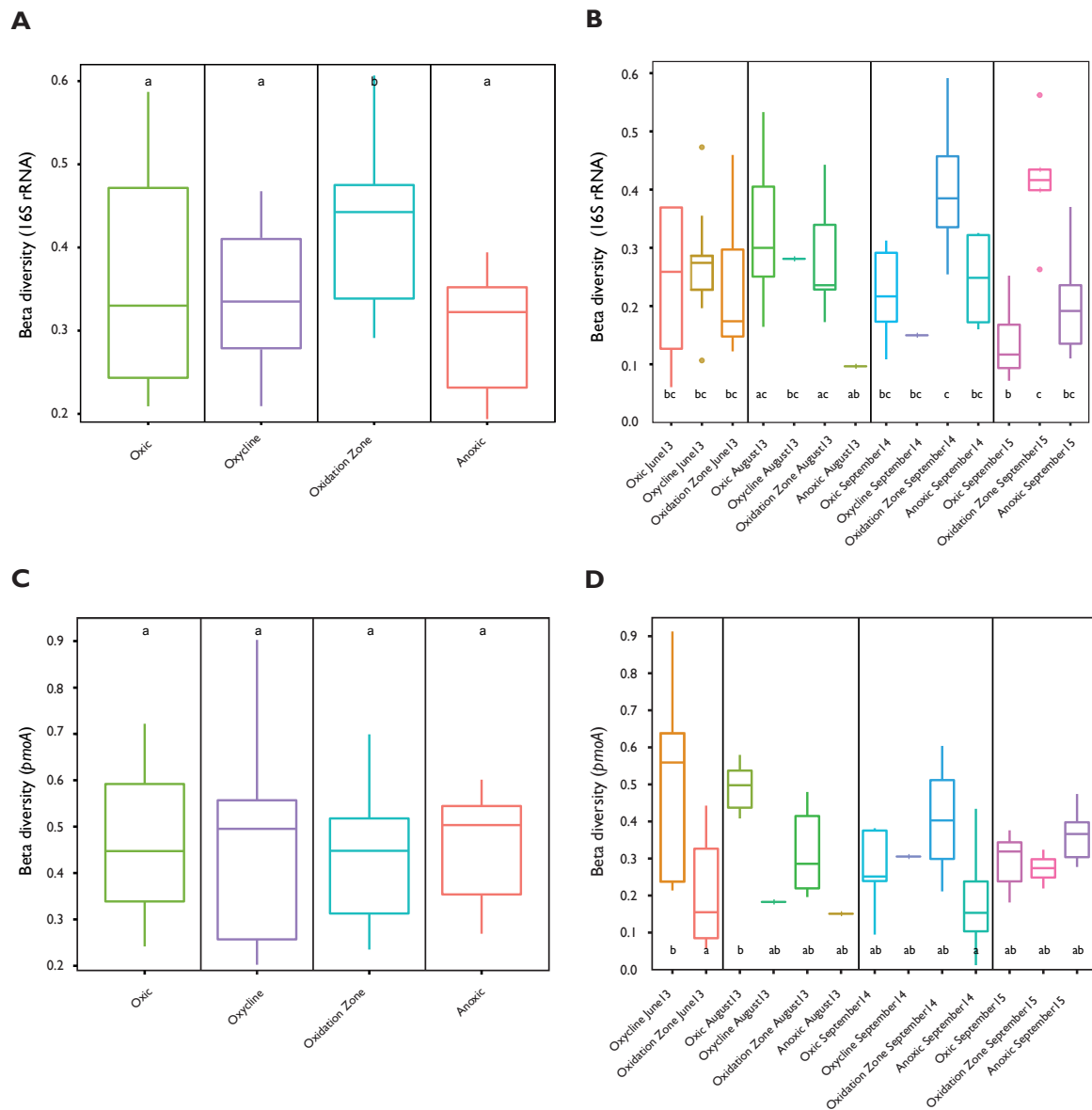


Figure S11. Boxplots of beta diversity measured as distance to group centroids of principal coordinates of original distances (multivariate homogeneity of group dispersions).

Beta diversity of bacteria (A,B) and MOB (C,D) communities within the different depth zones (A,C) and within the depth zones during the different sampling campaigns (B,D). Differences in diversity were tested by ANOVA followed by Tukey's HSD.

Table S1. Properties of the co-occurrence (Spearman, DIABLO) networks compared to similarity sized Erdős-Rényi random networks.

Network characteristics (cut off)	Spearman (0.7) / Radom	DIABLO (0.5) 7 Random
Nodes	1079	347
Edges	41'977	3'099
Average degree	48.8 / 77.8	17.9 / 17.8
Diameter	16 / 3	12 / 4
Average path length	5.36 / 1.93	4.77 / 2.33
Modularity	0.65 / 0.06	0.43 / 0.17
Modularity classes	15	5
Density	0.028 / 0.07	0.05 / 0.05
Average cluster coefficient	0.62 / 0.07	0.29 / 0.05
Small world coefficient	3.19	2.83

Chapter 4

Activity of aerobic methane-oxidizing bacteria under nanomolar copper additions

Carole Guggenheim

Laura Sigg

Helmut Bürgmann

Carsten J. Schubert

Bernhard Wehrli

In preparation for submission to *PLoS ONE*

Abstract

Aerobic methane-oxidizing bacteria (MOB) substantially reduce methane emissions to the atmosphere. Copper is an essential micronutrient for the production and activation of the particulate methane monooxygenase enzyme that catalyses the first oxidation step, the conversion of methane to methanol. In order to clarify the role of copper as a limiting micronutrient in microbial methane oxidation and to analyse the copper requirements of MOB, we conducted laboratory experiments with an axenic MOB culture. *Methylobacterium alcaliphilum* species were first grown under vanishingly low concentrations of copper and starved for several generations before being exposed to various copper environments ranging from 0 to 500 nanomolar copper. We studied the effects of copper on the growth behaviour, methane consumption dynamics, and cellular elemental stoichiometries of *Methylobacterium alcaliphilum* species. The results revealed that copper does not significantly limit bacterial growth rates and methane turnover even at low nanomolar copper concentrations. Different Cu:C ratios after very similar starvation phases and increasing ratios at higher copper additions indicate that recently discovered copper storage mechanisms might play an important role in buffering conditions of low dissolved copper environments.

Introduction

Atmospheric methane (CH_4) concentrations have dramatically increased since pre-industrial times [Nisbet *et al.*, 2014; Salawitch *et al.*, 2017] and the global budget is determined by several different natural sources (e.g. lakes, oceans, wetlands) [Kirschke *et al.*, 2013]. However, large amounts of produced CH_4 are readily reduced by the activity of aerobic methane-oxidizing bacteria (MOB) [Conrad, 2009]. These microorganisms act as a natural filter capturing CH_4 before it reaches the atmosphere [Borrel *et al.*, 2011; Chistoserdova, 2011; Knief, 2015]. MOB own the ability to thrive on CH_4 as a carbon and energy source [Chistoserdova and Lidstrom, 2013] and are preferably located at the interface between oxic and anoxic zones [Hanson and Hanson, 1996]. Their metalloenzyme methane monooxygenase (MMO) uses oxygen to convert CH_4 to methanol under ambient conditions. MMO exists in two structurally and biochemically distinct forms [Ross and Rosenzweig, 2016]. The soluble MMO (sMMO) is a cytoplasmic enzyme complex and uses a di-iron active centre [Tinberg and Lippard, 2011; Sirajuddin and Rosenzweig, 2015]. By contrast, pMMO is the membrane-associated or particulate MMO and its active site composition is still a matter of debate [Martinho *et al.*, 2007; Wang, Maji *et al.*, 2017; Cao *et al.*, 2018]. However, it is generally agreed that copper (Cu) is an essential component of pMMO, even though recent studies dispute the exact number of Cu atoms associated with the functional enzyme [Wang, Maji *et al.*, 2017]. While pMMO is the predominant aerobic CH_4 oxidation catalyst and present in virtually all known MOB, only a subset of MOB can additionally express sMMO [Knief, 2015]. Only a small number of MOB organisms are limited to the gene for sMMO [Chen *et al.*, 2010; Vorobev *et al.*, 2011].

Cu has a significant physiological role in MOB as its availability regulates the nature and level of expression of the two MMOs as well as their switchover [Murrell, McDonald *et al.*, 2000; Semrau *et al.*, 2010; DiSpirito *et al.*, 2016]. Prior studies have explored the effects of different Cu concentrations on MOB species (mainly *Methylococcus capsulatus* and *Methylosinus trichosporium*) [Prior and Dalton, 1985; Knapp *et al.*, 2007; Semrau *et al.*, 2013; Kalidass *et al.*, 2015]. It was revealed that a high Cu-to-biomass ratio stimulates pMMO expression and represses sMMO. Cu availability is critical for MOB that only contain the gene for pMMO production [Martin and Murrell, 1995; Lontoh and Semrau, 1998; Lloyd *et al.*, 1999; Semrau *et al.*, 2013].

In a field study in a stratified lake, we have recently shown that active MOB communities thrive with bioavailable Cu concentrations in the nanomolar range and most likely oxidize CH₄ via the pMMO pathway [Guggenheim *et al.*, 2019]. It is possible that in some MOB Cu acquisition is mediated by the chalkophore methanobactin, a high-affinity Cu-binding peptide [DiSpirito *et al.*, 2016; Kenney and Rosenzweig, 2018]. Furthermore, several Cu uptake mechanisms and Cu storage proteins have been identified to be present in several MOB species [Ve *et al.*, 2012; Johnson *et al.*, 2014; Kenney *et al.*, 2016; Lawton *et al.*, 2016; Dennison *et al.*, 2018]. Such coping strategies are essential for MOB at zones with high CH₄ turnover.

The concept of constant carbon:nitrogen:phosphorus (C:N:P) ratios in plankton and seawater has been introduced in oceanography by Albert Redfield [Redfield, 1934, 1958], and the ecological stoichiometry as a biochemical basis has been investigated in more detail [Geider and La Roche, 2002; Sterner and Elser, 2002]. Recent surveys of marine and freshwater microbes revealed detailed information regarding their stoichiometric flexibility or specificity [Cotner *et al.*, 2010; Grob *et al.*, 2013]. An “extended Redfield stoichiometry”, which includes micronutrients such as iron, copper, and zinc, has been proposed by Morel [Morel, 2008] and explored in detail for marine phytoplankton [Ho *et al.*, 2003; Quigg *et al.*, 2003; Twining and Baines, 2013]. Developing extended Redfield ratios for different microorganisms using field data is hampered by the presence of co-occurring living and abiotic particles in the same size range [Ho and Lee, 2007]. Therefore, an alternative solution for estimating trace-metal compositions in distinct bacteria is the use of axenic culture studies.

Despite the importance of Cu for MOB species, there is little knowledge regarding their cellular stoichiometric ratio. The typical Cu:C and Cu:N ratios for MOB under different Cu conditions would be indicative for its role as a micronutrient ultimately influencing the carbon cycle. Here, we investigate the effect of Cu availability on the elemental composition of *Methylobacterium alcaliphilum* (*M. alcaliphilum*) strain, a gammaproteobacterial MOB [Knief, 2015]. *M. alcaliphilum* contains the functional gene for pMMO, but lacks the one for sMMO [Vuilleumier *et al.*, 2012; Akberdin *et al.*, 2018]. We designed the present study to test two main hypotheses. First, with Cu as an essential micronutrient, increasing Cu concentrations should accelerate cell growth and CH₄ turnover. Second, pMMO as the main Cu containing enzyme should define a rather constant extended Redfield ratio of C:N:Cu. To this end, Cu-starved cells were supplemented with medium containing different Cu amendments, ranging from 0 nM to 25 nM, reflecting *in-situ* surface water Cu concentrations [Mason, 2013; Guggenheim *et al.*, 2019], to a maximum of 500 nM dissolved Cu.

Cell counts were measured daily in order to assess the growth efficiency of the culture, and CH₄ consumption rates were estimated. At the beginning and end of the incubations, bacteria were harvested for particulate C, N and Cu analysis. Based on these controlled experiments, the study addresses the questions whether growth of MOB directly depends on Cu availability and how Cu:C and Cu:N ratios will be affected when Cu addition varies over two orders of magnitude. The obtained results facilitate the interpretation of the biogeochemical role of MOB and their enzymatic pathways under a range of realistic Cu concentrations.

Methods

Growth conditions

M. alcaliphilum 20Z (No. 19304) was obtained from the Deutsche Sammlung von Mikroorganismen und Zellkulturen (DSMZ) and maintained in the suggested medium (No. 1180) applying slight modifications (Supplementary Table S1). Only chemicals of analytical grade and membrane-purified and deionized water were used. Cultures were kept in 120 ml serum bottles with a headspace/liquid space ratio of ~1:10. An ICP-MS Cu standard solution (1000 mg Cu L⁻¹ prepared from Cu(NO₃)₂ in 0.5 M HNO₃, Merck) was used to precisely adjust the amount of Cu within the medium. We added glass beads to enhance bacterial growth over the incubation time. The atmosphere consisted of 10% [v/v] CH₄ in air. After autoclaving, buffer solutions and cells (2% of medium) were inoculated into fresh medium. Serum bottles were incubated at 25°C on a rotary shaker at 150 rpm. Grown cells (~2% [v/v]) were transferred after respective growth to opaque density (after 4-6 days).

Inoculum and growth experiments

Trace metal-clean protocols were applied requiring all glass and plastic ware being soaked in diluted HNO₃ (0.1-0.01 M) for at least 24 hours and thoroughly rinsed with nanopure water prior to use. All experiments were undertaken in gastight glass serum bottles (120 ml, 0.5 L, 1.2 L) sealed with butyl rubber stoppers (Geo-Microbial Technologies, Inc.) and solution handling was carried out under a laminar flow clean hood. To avoid carryover of any residual Cu of the inoculum to the incubation set-ups, *M. alcaliphilum* was initially exposed to a Cu-depleted medium (i.e. addition of trace element solution lacking Cu(NO₃)₂, Supplementary Table S1) for 2-3 generations in 120 ml serum vials (starved culture in Supplementary Figure S1). The last transition was set up into a 0.5 L bottle to guarantee enough starting material for the following growth experiments. For the main incubation experiments, serum bottles (1.2 L) were filled with the medium prepared following Supplementary Table S1 with upscaling to the specific volume. A headspace air volume of 10-15% was exchanged with CH₄, and the starved culture enrichment (~2% [v/v]) was used as inoculum in

the form of a suspension with on average $\sim 5 \times 10^4$ cells ml^{-1} (Supplementary Figure S1). We performed three separate growth experiments (Exp5, Exp25, Exp50) with three different Cu-amendment concentrations, which were adjusted by specific addition of $\text{Cu}(\text{NO}_3)_2$ standard to the trace element solution (Supplementary Table S1). 500 nM Cu was set as the maximum Cu concentration for all three experiments, while it was intended to work with zero Cu addition (0 nM) as lowest concentration. The middle concentration, however, was altered between the three experiments (5 nM, 25 nM, 50 nM, i.e. experiments name). All treatments were run in triplicate bottles and one additional bottle per concentration, which did not receive any bacteria, served as control (except for 5 nM in Exp5 where no control bottle was included). A bottle filled with nanopure water instead of medium was used as analytical blank to detect any Cu, C or N contamination during the experimental handling (except for Exp5 where nanopure water filled in a beaker was used as analytical blank for Cu measurements). Each set-up was prepared for two time points (t_{Zero} , t_{End}), where we harvested *M. alcaliphilum* cells and investigated chemical parameters. Zero-time bottles (t_{Zero}) were analysed immediately after culture addition whereas end-point incubation bottles (t_{End}) were measured at the end of the incubation experiments. Incubations lasted between 3.4 (Exp25) and ~ 4.4 (Exp5, Exp50) days.

Growth monitoring and cell counts

During the incubation experiments, 2 ml samples were removed daily from t_{End} bottles in a clean and sterile manner for cell growth monitoring (Supplementary Figure S1). At t_{End} , bottles were also sampled for cell count measurements in order to calculate elemental quotas. Microbial abundance was measured by flow cytometry (FC). To this end, samples containing bacterial cells were diluted to reach appropriate cell densities measurable by the instrument (maximum 3000 events s^{-1}). Samples from control bottles were measured without dilution. For total cell counts, samples were stained with SYBR® Green I (Invitrogen), while for membrane intact cell counts, samples were additionally stained with propidium iodide (Invitrogen). After 13 min of incubation at 37°C in the dark, samples were analysed on a BD Accuri C6 flow cytometer (BD Biosciences) [Berney *et al.*, 2007; Hammes *et al.*, 2008]. We attempted to harvest t_{End} cells in their late exponential or stationary phase for chemical analysis. FC plots were gated (P3 in Supplementary Figure S2) to distinguish intact bacterial cells from background signals and damaged cells using the BD Accuri C6 software. Specific bacterial growth rate

constants were calculated from the slope of the linear regression of ln-transformed cell counts over time during the exponential phase (Figure 1, stars indicate values not considered for rate calculations).

Methane consumption

Headspace samples for CH₄ measurements were removed from t_{End} bottles at the beginning and at the end of the incubation periods (Supplementary Figure S1). As supplemented CH₄ concentrations were high (between 20-100 mM) to prevent CH₄ being the limiting factor for MOB cell growth, CH₄ samples had to be diluted before analysis. Duplicate or triplicate headspace samples (0.5-1 ml) of each bottle were transferred into anoxically filled 120 ml N₂-bottles, which were subsequently measured on a gas chromatograph (GC, Agilent 6890N, Agilent Technologies) equipped with a Carboxen 1010 column (30 m x 0.53 mm, Supelco) and a flame ionization detector (detection limit: ~10 nM). CH₄ concentrations were deduced from standard curves and amounts dissolved in the medium were calculated using Henry's law [Wiesenburg and Guinasso Jr., 1979]. The absolute differences of CH₄ within the bottles were corrected with values from control bottles that had no added bacterial cells. CH₄ consumption rates were calculated by dividing the differences to the specific incubation period ($\mu\text{M CH}_4 \text{ h}^{-1}$). Statistical tests were performed using the Past3.18 statistic software (<http://folk.uio.no/ohammer/past/>). One-way ANOVA followed by a Tukey's HSD pairwise test was applied to determine any significant differences in the CH₄ consumption between the incubation treatments (Supplementary Table S2), whereas $p < 0.05$ was considered significant.

Measurement of copper fractions

Subsamples of each incubation bottle (t_{Zero} and t_{End}) were taken to measure total, particulate and dissolved Cu fractions (Supplementary Figure S1). All plastic material and filters were pre-washed with diluted HNO₃ and nanopure water before sampling. Each fraction was sampled in triplicate from a single treatment bottle. Aliquots (4 ml) for total Cu (Cu_{Tot}) were directly filled into Falcon tubes and acidified to a concentration of 5 M HNO₃. After digestion in Teflon containers using an UltraClave 4 digester (MLS GmbH) with concentrated H₂SO₄, the digests were diluted with nanopure water to 0.1 M HNO₃ and analysed by inductively coupled plasma mass spectrometry (ICP-MS, Element2, Thermo). Particulate Cu (Cu_{Part}) values

were received through filtering the samples (5 ml) on a cellulose nitrate filter ($< 0.45 \mu\text{m}$, Sartorius). Filters were soaked in diluted HNO_3 (5 M), digested by applying the same procedure as for Cu_{Tot} , and diluted to an appropriate concentration of 0.1 M HNO_3 for ICP-MS analysis. The dissolved Cu fraction (Cu_{Diss}) was collected from filtering the samples (8 ml) through a cellulose acetate syringe filter ($< 0.45 \mu\text{m}$, VWR), and the filtrate was measured in a 0.1 M HNO_3 matrix via ICP-MS.

Carbon and nitrogen in biomass

Samples for particulate carbon (C_{Part}) and nitrogen (N_{Part}) analysis were subducted at the beginning (t_{Zero} bottles) and at the end (t_{End} bottles) of the respective incubation experiment (Supplementary Figure S1). Triplicate samples were obtained by concentrating 15-40 ml of culture onto 25 mm pre-combusted (4 h at 450°C) and pre-weight glass fibre filters (GF/F, Whatman) under a gentle vacuum. The filters were dried overnight at 70°C and stored in a desiccator until further processing. After weighing, filters were packed as a whole in tin caps (10x10 mm). Relative values of organic carbon and nitrogen on the filters were analysed by flash combustion in an automated CHN-elemental analyser (EA) connected to an IRMS (Vario Pyro Cube connected to GV Instrument or Flash 2000 coupled to Delta V Advantage with Conflow IV interface). Resulting data were standardized to a reference material (Acetanilide, Indiana University). Median data for C_{Part} , N_{Part} and Cu_{Part} (see above section) from t_{End} time point were related to each other to verify molar elemental ratios (C:N, Cu:C, Cu:N). Elemental quotas of cells ($\text{C}_{\text{Biomass}}$, $\text{N}_{\text{Biomass}}$, $\text{Cu}_{\text{Biomass}}$ in mol cell^{-1}) in t_{End} bottles were computed as the median particulate values divided by the average cell density.

Microbial contamination

In order to test for bacterial contamination, t_{End} bottles of the first (Exp5) and last experiment (Exp50) were analysed for microbial biomass intruding from the sample handling during the incubation period. To do so, *M. alcaliphilum* cells were collected by gentle centrifugation and DNA was extracted from the pellet using Chelex®-100 reagents (BioRad Laboratories). 100 μl of sample was transferred to 100 μl of Chelex suspension (50 mg ml^{-1} in nuclease free water) and boiled at 99°C for 10 min using a thermal cycler. After centrifugation (2250 g, 5°C , 10 min), the supernatant was diluted (1:2) and stored at -20°C until further processing. For PCR

amplification of the bacterial 16S rRNA gene we used the primer set S-D-Bact-0008-d-S-20 (5'-AGAGTTTGTATCMTGGCTCAG-3') (27F) and S-D-Arch-1492-a-A-19 (5'-GGCTACCTTGTTAC GACTT-3') (1492R) [Lane, 1991]. The final reaction volume of 25 μ l contained 5 μ l of 5 x PCR buffer (Promega), 3 mM MgCl₂ (Promega), 0.2 μ M forward and reverse primer (Microsynth), 0.8 mM dNTPs (Promega), 1 mg ml⁻¹ bovine serum albumin (New England BioLabs), 0.3 U μ l⁻¹ GoTaq G2 Flexi DNA polymerase (Promega) and 4 μ l template DNA. Applied PCR conditions were as follows: initial denaturation at 94°C for 5 min, 40 cycles (denaturation at 94°C for 30 s, annealing at 60°C for 1 min, and extension at 72°C for 1.3 min), final extension at 72°C for 5 min. Aliquots of amplicons were checked by electrophoresis on a 0.8% agarose gel. Subsequently, PCR products were purified using the Wizard® SV Gel and PCR Clean-Up System (Promega) and quantified on a NanoDrop 1000 Spectrophotometer (Thermo Fisher). The PCR samples were sequenced at Microsynth, Switzerland. The NCBI BLAST search tool (<http://www.ncbi.nlm.nih.gov/BLAST/>) was used to compare the obtained DNA sequences with nucleotide sequences from the NCBI database.

Results

Bacterial growth and methane consumption

Cell counts of *M. alcaliphilum* increased over the periods of incubation in all experiments and with all supplemented Cu concentrations (Figure 1). Control bottles did not show any bacterial growth (Supplementary Figure S2). Average cell densities at time zero of t_{End} bottles ranged from 2.8×10^4 – 5.7×10^5 cells ml^{-1} and bottles in Exp5 started with the lowest number of MOB (Figure 1a). Minimal cell numbers were measured in the 0 nM Cu treatment over the whole time span of the incubations. The 500 nM Cu amendments reached highest cell densities between 7.4×10^6 – 2.5×10^8 cell ml^{-1} at the end of the experiments. Overall, lag phases were short but were most prominent in Exp25 (Figure 1b). The other incubations usually started directly with the exponential growth phase, and some set-ups even reached the stationary or death phase by the end of the incubation time (5 nM and 500 nM in Exp5, 0 nM in Exp25, 50 nM in Exp50).

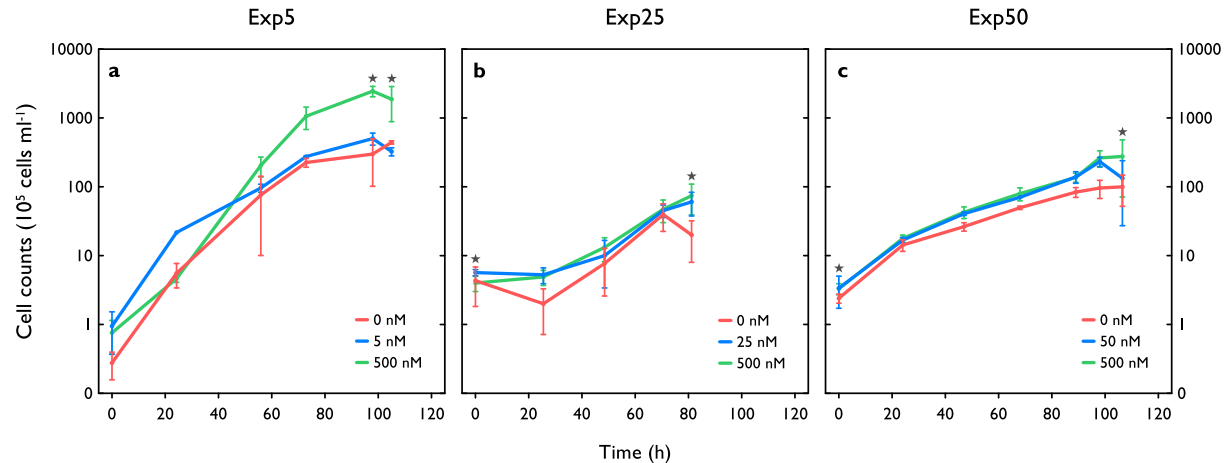


Figure 1. Growth curves of *Methylobacterium alcaliphilum*.

The increase of *Methylobacterium alcaliphilum* cells exposed to different copper amendments in three experiments (Exp5, Exp25, Exp50; a,b,c) was evaluated daily by flow-cytometry. Colours depict different copper growth conditions (red = 0 nM, blue = 5 / 25 / 50 nM, green = 500 nM). Note the logarithmic scale (log₁₀) for the y-axis (cell counts). Data points are means of single samples of triplicate bottles. Error bars represent standard deviation (n = 3). Stars denote values not considered for growth rate constant calculations.

In general, bacterial growth rates were quite similar at 0.026–0.102 h^{-1} for the broad range of Cu amendments from 0 nM to 500 nM (Table 1). The 5 nM Cu treatment initially showed distinct cell growth that flattened at half time and approached growth behaviour of 0 nM Cu (Figure 1a). 25 nM as well as 50 nM treatments

showed similar growth rates as their 500 nM counterparts (Figure 1b,c, Table 1). Exp5 exhibited highest cell increase over time compared to Exp25 and Exp50 with growth rates varying between 0.091-0.102 h⁻¹ (Table 1). Lowest end point cell numbers were found in Exp25 (Supplementary Table S4). Anyway, this experiment was aborted earlier as cell densities started to decrease or became stationary. Nevertheless, growth rates of Exp25 were higher than in Exp50 (Table 1). At the end of the incubation experiments all sequencing results matched with DNA sequences from *Methylobacterium alcaliphilum* strain 20Z (99% identity) implying no bacterial contamination during the course of the incubations.

The CH₄ consumption rates varied only within an order of magnitude (14-160 µM CH₄ h⁻¹) for the broad range of Cu amendments (Figure 2, Table 1). The 0 nM incubation of Exp25 was the notable exception showing no significant consumption (Figure 2b). Highest rates were detected in Exp5 (Figure 2a, Table 1), which goes in line with highest cell growth. Even the rate in the 0 nM set-up exceeded most values within the other two experiments (except 500 nM in Exp50). Consumption rates were similar between 0 nM and 5 nM (Tukey's HSD, $p = 0.91$, Supplementary Table S2), and between all set-ups in Exp50 (ANOVA, $p = 0.09$). In Exp25, CH₄ consumption rate of the 500 nM amendment was neither different to the 0 nM nor the 25 nM amendment (Tukey's HSD, $p = 0.18$, $p = 0.56$). Lowest decrease of CH₄ over time was detected in Exp25.

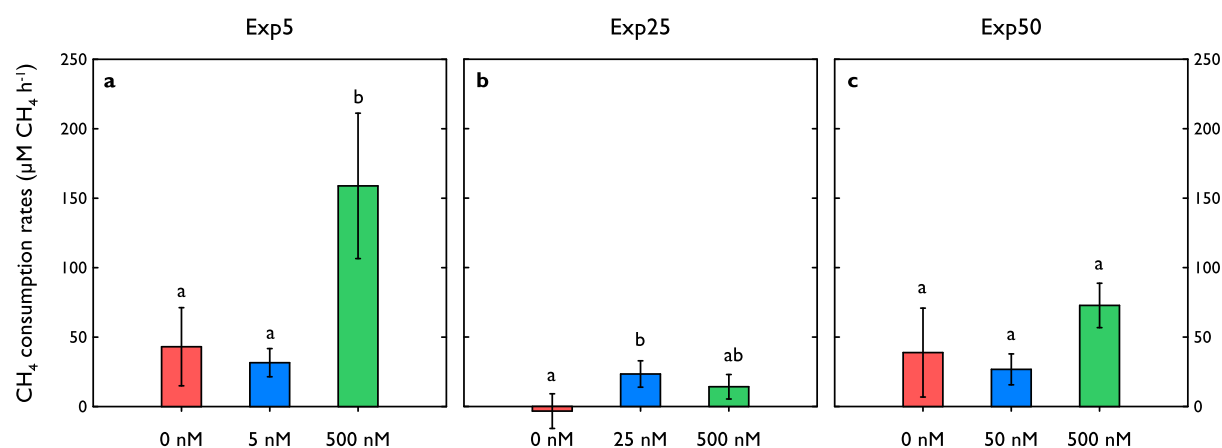


Figure 2. Methane consumption rates of *Methylobacterium alcaliphilum*.

CH₄ consumption rates (blank-corrected CH₄ values) of each incubation experiment (Exp5, Exp25, Exp50; a,b,c) are given as absolute CH₄ changes per hour. Colours indicate different copper amendments (red = 0 nM, blue = 5 nM / 25 nM / 50 nM, green = 500 nM). All data are means of duplicate or triplicate samples of triplicate bottles. Error bars represent standard deviation of triplicate bottles ($n = 3$). Letters emerge from statistical analysis and show differences between treatments ($p < 0.05$, Supplementary Table S2).

Table 1. Average and median values for growth rates (over the course of the experiments), CH₄ consumption, biomass stoichiometry, cellular elemental contents and ratios in t_{End} bottles.

Set-up		Growth rate (h ⁻¹)	CH ₄ consumption (μM CH ₄ h ⁻¹)	C _{Biomass} (mol cell ⁻¹)	N _{Biomass} (mol cell ⁻¹)	Cu _{Biomass} (mol cell ⁻¹)	Cu:C (μmol mol ⁻¹)	Cu:N (μmol mol ⁻¹)	C:N (mol mol ⁻¹)
Exp5	0 nM	0.091	43 ± 28	1.5 × 10 ⁻¹⁴	2.7 × 10 ⁻¹⁵	1.9 × 10 ⁻¹⁹	12	69	5.7
	5 nM	0.074	32 ± 10	2.8 × 10 ⁻¹⁴	4.5 × 10 ⁻¹⁵	3.5 × 10 ⁻¹⁹	12	77	6.2
	500 nM	0.102	159 ± 52	2.3 × 10 ⁻¹⁴	1.5 × 10 ⁻¹⁵	9.5 × 10 ⁻¹⁹	41	642	16
Exp25	0 nM	0.066	-3 ± 12	8.5 × 10 ⁻¹⁴	1.5 × 10 ⁻¹⁴	4.5 × 10 ⁻¹⁸	52	297	5.7
	25 nM	0.048	23 ± 9	3.8 × 10 ⁻¹⁴	1.0 × 10 ⁻¹⁴	2.7 × 10 ⁻¹⁸	69	265	3.8
	500 nM	0.050	14 ± 9	4.1 × 10 ⁻¹⁴	8.1 × 10 ⁻¹⁵	6.1 × 10 ⁻¹⁸	150	752	5.0
Exp50	0 nM	0.026	39 ± 32	3.4 × 10 ⁻¹⁴	8.0 × 10 ⁻¹⁵	4.2 × 10 ⁻¹⁸	122	520	4.3
	50 nM	0.034	27 ± 11	5.0 × 10 ⁻¹⁴	9.2 × 10 ⁻¹⁵	6.6 × 10 ⁻¹⁸	133	719	5.4
	500 nM	0.034	73 ± 16	2.4 × 10 ⁻¹⁴	4.6 × 10 ⁻¹⁵	8.1 × 10 ⁻¹⁸	346	1755	5.1

CH₄ consumption rates were calculated from blank-corrected values, other parameters were evaluated from raw values. Average (growth rate and CH₄ consumption) or median values of triplicate samples of triplicate incubation bottles are listed. Elemental quotas (C_{Biomass}, N_{Biomass}, Cu_{Biomass}) and elemental ratios (Cu:C, Cu:N, C:N).

Intracellular elemental composition and stoichiometry

Throughout all three experiments, C_{part} , N_{part} and C_{part} concentrations usually increased during the course of the incubations starting usually with low levels in the t_{zero} bottles to higher concentrations in the t_{end} bottles (see difference between grey and coloured dots in Figure 3). It is important to note that each experiment involved triplicate incubations that were analysed each three times. As concentration data can vary strongly in these experiments, median values were calculated and are reported in Supplementary Table S4. Overall, lowest particulate end values (t_{end} bottles) were detected within the 0 nM amendments, and highest within the 500 nM set-ups. Consistent with its fastest microbial growth (Figure 1) and CH_4 consumption rates (Figure 2), Exp5 experienced the largest absolute elemental shift towards particulate species (C_{part} , N_{part} , C_{part}) during the incubation period (Figure 3a,d,g). It resulted in high end-concentrations for the 500 nM treatments. By contrast, Exp25 showed the lowest concentrations in all three fractions and smallest concentration differences between the set-ups (Figure 3b,e,h, note the differences in scale). As growth stopped earlier in this experiment, bacterial cells had less time to grow (Figure 1), resulting in lower biomass.

In the case of Cu, we observed the highest uptake in the 500 nM incubations of Exp5 and Exp50. Again, the slow-growing Exp25 lags behind. As expected, C_{part} concentrations were usually lowest in t_{zero} and highest in t_{end} bottles. However, initial incubation values, blanks and control bottles of Exp5 showed highly scattered and elevated values, probably due to contamination during sampling (Figure 3a, Supplementary Table S3). Theoretically, dissolved Cu (C_{diss}) concentrations should decrease over the incubation period as microorganisms take up Cu. This was generally observed (Supplementary Figure S3a-c). Again Exp25 stands out, as very little uptake occurred in the 500 nM incubations. Total Cu (C_{tot}) concentrations remained more or less stable in most experiments (Supplementary Figure S3d-f).

Comparing end values for C_{part} from 500 nM treatments in t_{end} bottles depicted a large range with median values between 0.32-4.61 mM (Figure 3d-f, note the different x-axis, Supplementary Table S4). Apart from initial C_{part} concentrations at the beginning of the incubations (t_{zero} bottles, Supplementary Table S3), lowest C_{part} was measured in the 0 nM t_{end} bottles in Exp25 (0.15 mM). N_{part} end-concentrations of all treatments showed values between 0.03-0.27 mM (Supplementary Table S4), and were approximately one magnitude

lower than C_{Part} . N_{Part} data similarly increased over all treatments and experiments (Figure 3g-i, note the different x-axis).

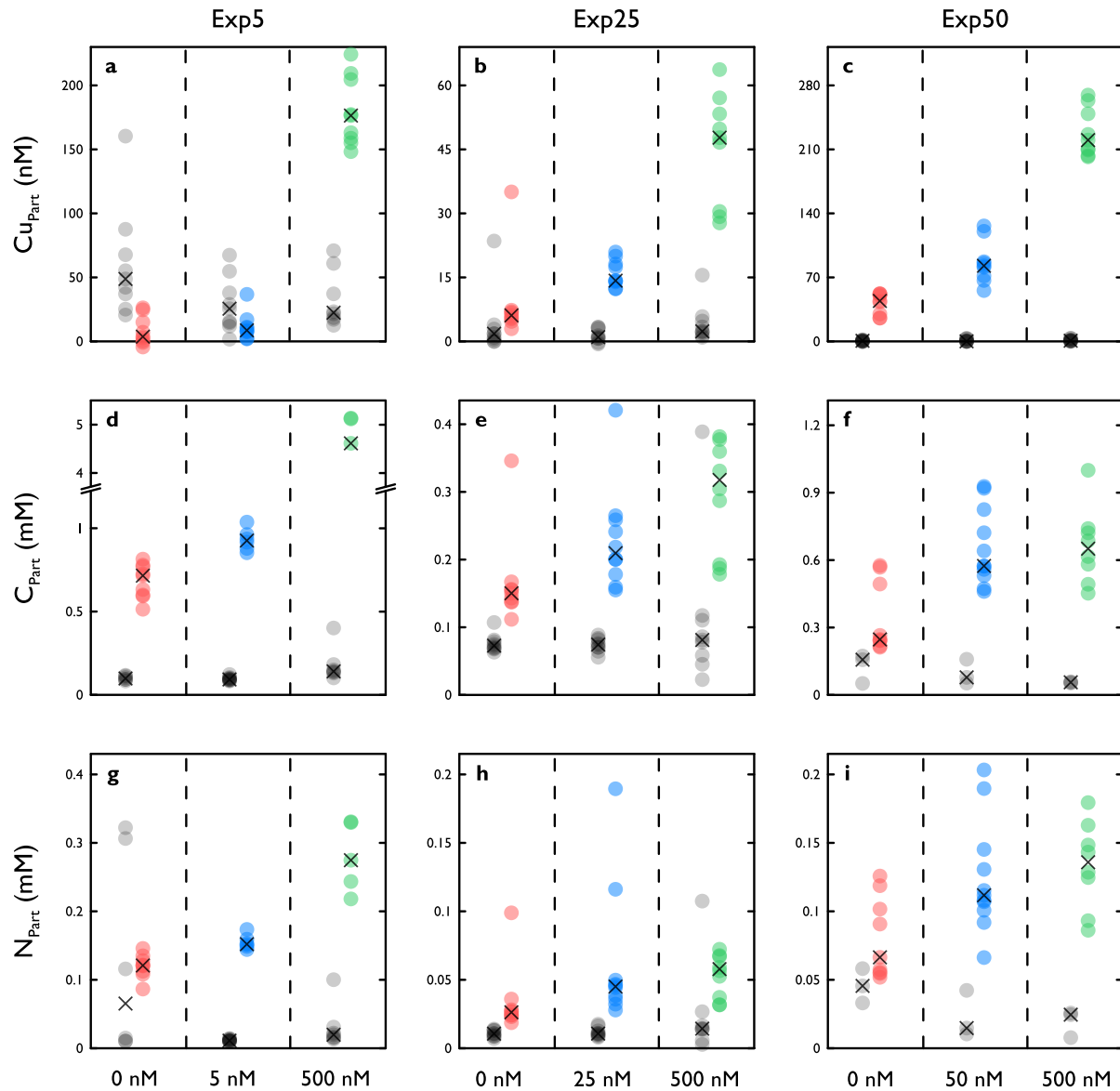


Figure 3. Measured particulate carbon, nitrogen and copper concentrations within incubation set-ups

Measured particulate concentrations of copper (Cu_{Part} , a,b,c), carbon (C_{Part} , d,e,f), and nitrogen (N_{Part} , g,h,i) at the beginning (t_{Zero} bottles, grey dots) and at the end (t_{End} bottles, coloured dots) of the respective incubation treatment (Exp5, Exp25, Exp50). Each column of the respective scatter plot belongs to a certain copper amendment (red = 0 nM, blue = 5 nM / 25 nM / 50 nM, green = 500 nM) and shows all measured samples of each incubation bottle. X represents median values. Note the different y-axis range for each plot.

Even though the absolute increase of C_{Part} was dissimilar between the three experiments, carbon values per cell (C_{Biomass}) did not show any distinct development with addition of Cu and varied between 1.5×10^{-14} – 8.5×10^{-14} mol C cell⁻¹ (Table 1). Lowest C quotas were measured in Exp5. Nitrogen incorporated

into the cells (N_{Biomass}) revealed more variation, with an overall change of one order of magnitude ranging from 1.5×10^{-15} – 1.5×10^{-14} mol N cell⁻¹ (Table 1). With the exception of one high value in Exp5, the C:N ratio was usually between 3.8–6.2 mol C mol⁻¹ N (Table 1). Highest biomass associated Cu ($\text{Cu}_{\text{Biomass}}$) was measured in Exp50 with addition of 500 nM Cu (8.1×10^{-18} mol Cu cell⁻¹, Table 1). Lowest values were detected in Exp5 (1.9×10^{-19} – 9.5×10^{-19} mol Cu cell⁻¹), which were almost up to two orders of magnitude lower compared to the other two experiments. Overall, Cu:C and Cu:N proportions were usually smallest within the 0 nM Cu set-ups and strongly increased with increasing Cu addition (500 nM, Figure 4, Table 1). Especially the Cu:N ratio in Exp5 highly increased, however, maximum values were still smaller than corresponding treatments in Exp25 and Exp50.

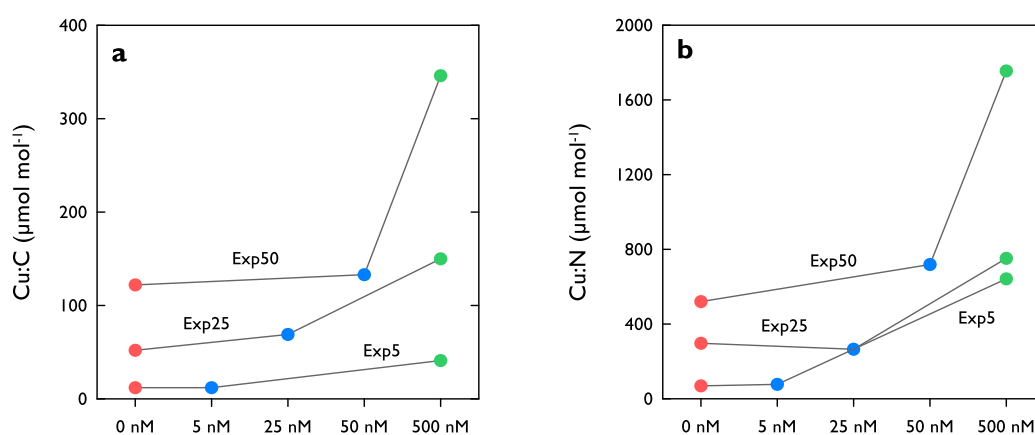


Figure 4. Intracellular copper to carbon and copper to nitrogen ratios between different copper additions at t_{End} .

Copper to carbon (Cu:C, a) and copper to nitrogen (Cu:N, b) stoichiometries of each copper treatment of the different incubation experiments (Exp5, Exp25, Exp50). Data show the ratios of the respective median values of the particulate elemental concentrations.

Discussion

In the following paragraphs, we first address some of the limitations of the incubations with nanomolar Cu additions. Then we revisit the hypothesis of Cu as a limiting micronutrient for MOB. Finally, we discuss the different Cu:C ratios in the experiments and their implications for microbial stoichiometry and Cu storage mechanisms.

Limitation of incubation set-up

In order to mimic natural conditions, the experimental Cu additions were kept in the nanomolar range. Therefore, preparing, sampling and quantifying the different trace metal fractions was challenging and required clean working conditions and cross-checks with blanks. Most published incubation studies, which tested the effect of Cu on MOB and their enzymatic activity, applied higher amounts of Cu (30 nM up to 80 μ M) [Kalidass *et al.*, 2015], or they failed to provide any information about the background concentrations in their Cu deficient set-ups [Choi *et al.*, 2003; Knapp *et al.*, 2007; Fergala *et al.*, 2018].

In setting-up the incubations, only Cu-free chemicals of analytical grade were used. Even though all utilized incubation equipment was thoroughly acid-washed before the experiments, contamination due to the handling procedure could provide additional Cu sources for MOB growth. Especially while working under low Cu concentrations such as the 0 nM and 5 nM set-ups, unintentional Cu sources could have entered the system and modified the expected results, as shown by the elevated Cu concentrations in blanks as well as low nanomolar Cu treatments at both time points (t_{Zero} , t_{End} , Supplementary Figure S3, Supplementary Tables S3 and S4).

Total and dissolved Cu (Cu_{Tot} and Cu_{Diss}) fractions were analysed to add additional information about the actual MOB growth conditions (Supplementary Figure S3, Supplementary Tables S3 and S4). An ICP-MS Cu standard was used to precisely adjust the Cu_{Diss} concentrations, the fraction available for organisms in the growth medium. As expected, the analysis of Cu_{Diss} usually revealed decreasing concentrations between t_{Zero} and t_{End} . The incubations with 50 nM and 500 nM Cu, however, showed significantly lower t_{Zero} Cu concentrations than expected, which points to either fast Cu uptake by MOB after culture injection or to

adsorption of dissolved Cu to the container walls. This is also observed in the control bottles (i.e. no bacteria injected), which show significantly lower Cu concentrations than expected (Supplementary Table S3). Average Cu_{Diss} background concentration over all experiments calculated from the blank bottles was ≤ 10 nM (Supplementary Tables S3 and S4). This is lower than most values reported in other incubation studies [Choi *et al.*, 2010; Kalidass *et al.*, 2015; Xing *et al.*, 2018]. In theory, Cu_{Diss} and Cu_{Part} concentrations should add up to Cu_{Tot} , the concentration of which should match at the beginning and the end of the experiments (Supplementary Figure S3, Supplementary Table S3 and S4). Overall lower Cu_{Tot} values could point to loss of Cu_{Diss} or Cu_{Part} (i.e. bacteria) to the wall of the containers. Obtained higher results than theoretically expected, such as t_{Zero} values in Exp5 and Exp25 as well as t_{End} values in Exp50, demonstrate signs of contamination (Supplementary Figure S3). Such contamination effects can be traced back from the results of the blank bottles (Supplementary Table S3 and S4).

In order to improve the reproducibility of these experiments, it will be appropriate to perform all the work in a clean room. Additionally, stringent protocols of sample recovery should be adopted to account for a full Cu balance. This includes the difficult task to grow MOB reliably under Cu-starving conditions and tracking their change of Cu:C ratios over the whole period of the experiments.

Effects of copper on cell growth

Optimal growth conditions for *M. alcaliphilum* cells were reported to be 5-10 μM Cu [Akberdin *et al.*, 2018]. In our experiments, concentrations were 100-1000 times lower. Growth rates of *M. alcaliphilum* cells varied rather randomly within only a factor of four. This is largely irrespective of the two orders of magnitude in Cu additions and similar total cell yields at the end of the incubations, except for the 500 nM addition in Exp5 (Figure 1, Table 1, Supplementary Table S4). Considerable growth was also detected at low nanomolar dissolved Cu concentrations (0 nM set-ups) even though *M. alcaliphilum* cannot circumvent diminishing Cu availability by switching to sMMO [Kalyuzhnaya *et al.*, 2008]. However, growth rates were about one to five times lower than reported literature values of *M. alcaliphilum* grown in batch and continuous cultures with excess Cu [Akberdin *et al.*, 2018]. The results corroborate our recent field study, which documented that proteobacterial MOB potentially using the pMMO pathway are able to thrive at low nanomolar Cu concentrations in lake waters [Guggenheim *et al.*, 2019].

The consumption rates of CH₄ within a single experiment were generally not correlated with the amount of Cu added. Only the 500 nM addition in Exp5 led to a significantly faster oxidation rate (Figure 2, Supplementary Table S2). The range of the calculated CH₄ oxidation rates (27-159 $\mu\text{M CH}_4 \text{ h}^{-1}$, Table 1) in this study were roughly 100 times higher than reported estimates in methane-oxidation zones of freshwater lakes [Martinez-Cruz *et al.*, 2015; Oswald, Jegge, *et al.*, 2016; Oswald, Milucka, *et al.*, 2016]. However, the amount of CH₄ added to the incubations in these studies was much lower (5-50 μM) than applied here (20-100 mM), which explains the difference in the observed rates. Notice that our laboratory incubation experiments started with 2.8×10^4 - 5.7×10^5 cells ml^{-1} , which corresponds to the *in-situ* cell counts of the cited studies.

The observed microbial growth corresponds qualitatively with the observed increase in particulate C and N between t_{Zero} and t_{End} of the incubations (Figure 1, Figure 3). Particulate concentrations increased with raising amounts of added Cu and goes in-line with rising cell numbers. Highest cell counts corresponded to highest particulate concentrations. Taken together, the observations of cell growth, CH₄ consumption and particulate C and N accumulation reveal surprisingly constant activities of Cu starved MOB in incubations with 0 nM to 500 nM Cu. Only small effects were observed for the highest Cu additions. This indicates that MOB like *M. alcaliphilum* are well adapted to operate in environments with only nanomolar available Cu such as at the oxic-anoxic boundary of lakes [Guggenheim *et al.*, 2019]. There are some MOB studies claiming that pMMO's active site contains a diiron centre [Martinho *et al.*, 2007; Wang, Maji *et al.*, 2017]. Iron is highly available in the incubation settings herein (Supplementary Table S1), hence it could be an important factor regulating cell growth and CH₄ oxidation dynamics. Nevertheless, the obtained results cannot be correlated to different iron concentrations, as in this study we did not alter the iron amendments for the incubation set-ups.

Effects of copper on elemental composition

Biomass carbon (C_{Biomass} in mol cell^{-1}) remained remarkably constant in the different Cu treatments (Table 1). Average C_{Biomass} was 3.8×10^{-14} mol C cell^{-1} , which agrees well with the theoretical value (3×10^{-14} mol C cell^{-1}) calculated by [Guggenheim *et al.*, 2019]. With an average N_{Biomass} from all experiments of 7.1×10^{-15} mol N cell^{-1} we obtained a C:N ratio for *M. alcaliphilum* of 6.3, which is close to the elemental proportion of C:N = 5.6 reported recently for this species [Akberdin *et al.*, 2018]. By contrast, $\text{Cu}_{\text{Biomass}}$ showed an increasing

trend with higher Cu amendments (Table 1). The $\text{Cu}_{\text{Biomass}}$ values ranged from 1.9×10^{-19} to 8.1×10^{-18} mol Cu cell⁻¹, which is one to two orders of magnitude higher than the theoretical estimate of 4×10^{-20} mol Cu cell⁻¹ by [Guggenheim *et al.*, 2019], who considered only Cu bound to the pMMO enzyme.

A comparison of Cu:C and Cu:N ratios in the three experimental runs reveals significant differences of the Cu starved incubations in the 0 nM Cu treatments. The Cu:C ratios for Exp5, Exp25 and Exp50 were about 12, 52, and 122 $\mu\text{mol Cu mol}^{-1} \text{C}$ (Table 1). The respective elemental ratios increased with higher amounts of added Cu (Figure 4). Cellular Cu ratios evaluated in this study ranged over several orders of magnitude from 12 to 346 $\mu\text{mol Cu mol}^{-1} \text{C}$, and from 69 to 1755 $\mu\text{mol Cu mol}^{-1} \text{N}$, increasing with the corresponding Cu amendment. The Cu:C ratios cover a wide range of elemental compositions, whereas minimum values were about ten times higher than the ones reported in [Guggenheim *et al.*, 2019]. At high Cu abundance, maximum ratios even exceeded values for phytoplankton by two orders of magnitude [Ho *et al.*, 2003; Annett *et al.*, 2008]. This illustrates the importance of Cu for MOB species, which have an atypically high Cu demand being approximately 10-times higher than of other microorganisms [Semrau *et al.*, 2013].

The broad range of Cu quotas at 0 nM Cu addition, and the fact that MOB develop different cellular Cu ratios depending on the Cu supply could be explained by recently discovered and characterized Cu storage proteins (Csp) [Lombardi, 2015; Vita *et al.*, 2015]. Besides the role of Cu-supply to the cell, which could also happen by passive equilibration with the concentration of the medium [Balasubramanian *et al.*, 2011], Csp provide protection for MOB against Cu-induced toxicity [Vita *et al.*, 2016]. Csp were first detected in *Methylosinus trichosporium* species, whereas today several homologues (Csp1, Csp2, Csp3) with different Cu capacities have been identified. They each form a tetramer of four-helix bundles. Csp1 binds 12-14 Cu(I) ions per monomer, Csp3 up to 18 Cu(I) ions, and Csp2 is less studied due to its high sequence similarity to Csp1 [Dennison *et al.*, 2018]. The gene for Csp1 expression in *Methylosinus trichosporium* was significantly upregulated in the presence of Cu, which indicates that the organism actively controls its Cu homeostasis [Gu and Semrau, 2017]. Csp homologues are widespread in MOB, and Csp3 is found in *M. alcaliphilum* [Dennison *et al.*, 2018]. It is therefore plausible that similar Cu storage mechanisms were in use during the starvation phases of *M. alcaliphilum* species, but were also responsible for the different Cu:C ratios of *M. alcaliphilum* incubation experiments, for the potential rapid uptake of dissolved Cu and the variability

observed with different Cu additions. Therefore, the concept of a reliable constant extended Redfield ratio based on the Cu demand of the pMMO enzyme must be rejected.

This study sought to reveal the stoichiometry of MOB under diverse Cu concentrations and analyse limiting effects of Cu on MOB activity. The results support recent findings that specific Cu storage complicates the determination of Cu:C ratios and probably acts as a “buffer” against Cu scarcity [Lombardi, 2015; Vita *et al.*, 2015, 2016; Gu and Semrau, 2017; Dennison *et al.*, 2018]. The incubations with total Cu concentrations in the range of a few nmol Cu did not show any signs of Cu limitation. This corroborates field observations of active MOB communities thriving in the nanomolar Cu range [Guggenheim *et al.*, 2019]. A few obstacles have to be addressed before these conclusions can be generalized: expanding this work to sub-nanomolar Cu concentrations will require rigorous clean-room protocols - in our study, we did not achieve Cu_{Diss} starting concentrations below 2 nM. Including other MOB species as well as more explicitly analysing their mechanisms for Cu uptake and storage will help bridging the gap between laboratory and field studies.

Acknowledgements

We thank Marc Dumont for his constructive suggestions in culturing *Methylobacterium alcaliphilum*. Benjamin Stern and Nora Minas are greatly acknowledged for their help in the lab before, during and after the incubation experiments, and for data analysis. We are grateful for the technical and analytical assistance of Serge Robert with GC and EA analysis and interpretation. David Kistler is thanked for his help with digestion and measurement of copper samples, Karin Beck and Nadine Czekalski for help and discussions concerning cell count data. We thank Patrick Kathriner for his reoccurring support and inputs. Sina Hasler is appreciated for DNA extraction and following PCR to test the purity of the populations. Remo Freimann is thanked for his fruitful inputs on the analysis of the data. This study was supported by the Swiss National Science Foundation (no. 153091).

Supplementary information

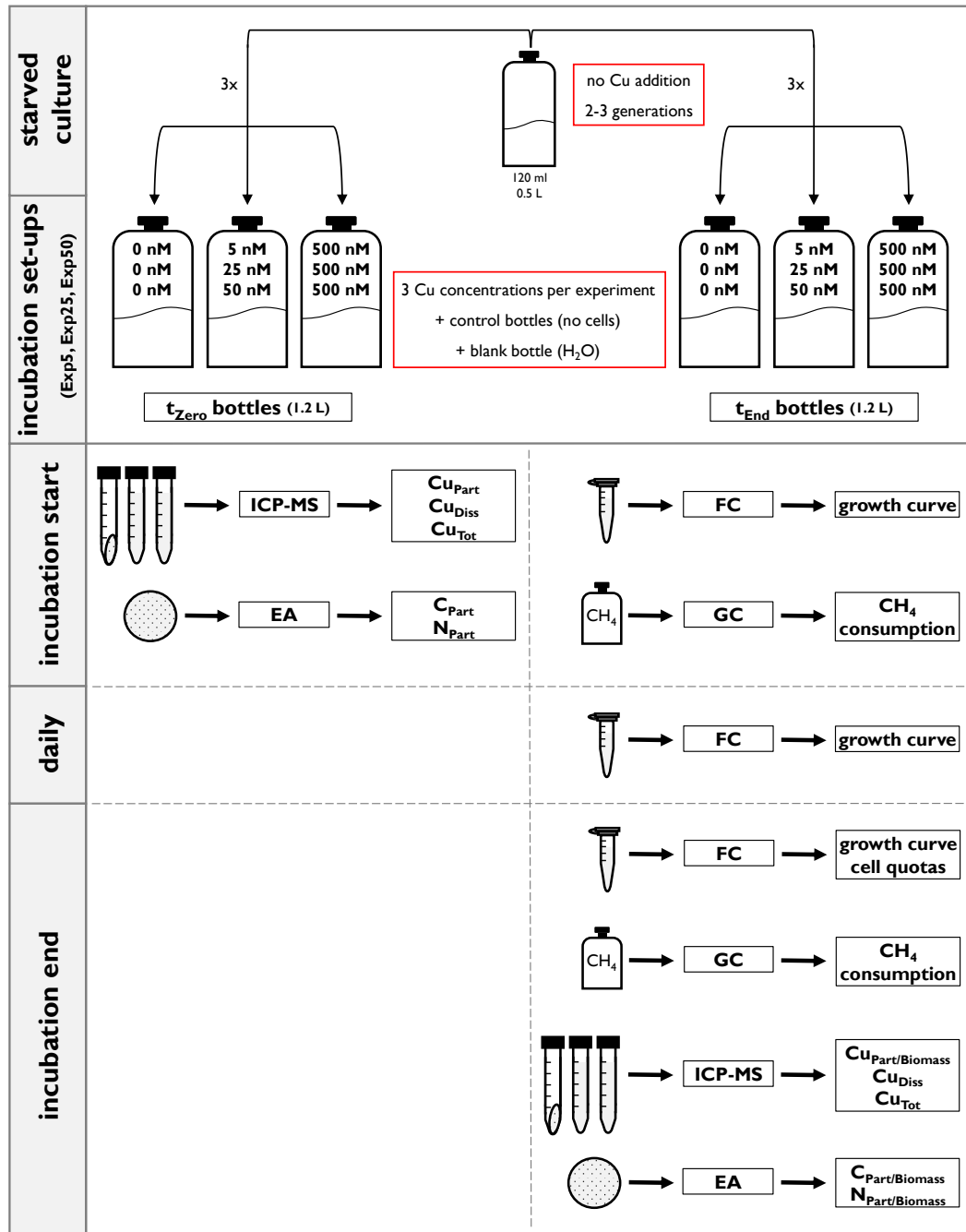


Figure S1. Schematic diagram of the incubation set-up.

M. alcaliphilum cells were grown for 2-3 generations under Cu depleted conditions. The last generation was employed as inoculum for the incubation experiments (starved culture). Three experiments (Exp5, Exp25, Exp50) were conducted with different middle concentrations (5 nM, 25 nM or 50 nM). A blank bottle (nanopure water only) ran with each experiment, as well as additional control bottles for each concentration (medium with nanopure water instead of cells). Each set-up was prepared in triplicates for two time points (t_{Zero} , t_{End}). t_{Zero} bottles were analysed immediately after culture addition, t_{End} bottles at the end of the respective incubation time (3.4-4.4 days). Cell counts were measured daily. Type of analysis: FC = Flow Cytometry, ICP-MS = Inductively Coupled Plasma Mass Spectrometry, EA = Elemental Analysis, GC = Gas Chromatography.

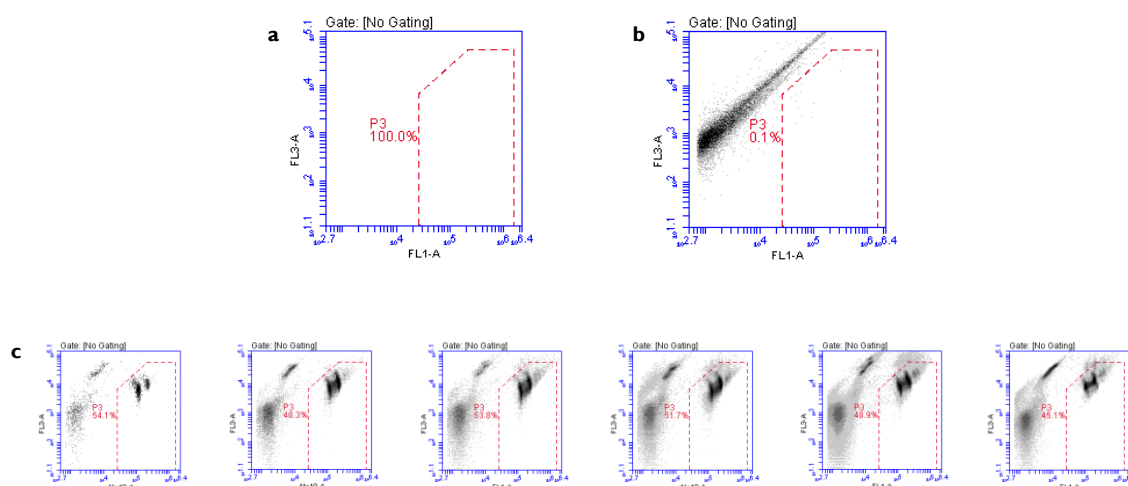


Figure S2. Gate used for evaluating flow cytometry data.

(a) Counts within gate P3 were assigned to living cells. (b) Typical medium background scatter plot of the control bottles. No living cells are depicted in P3. (c) *M. alcaliphilum* cell growth with highest copper amendment over the period of an incubation.

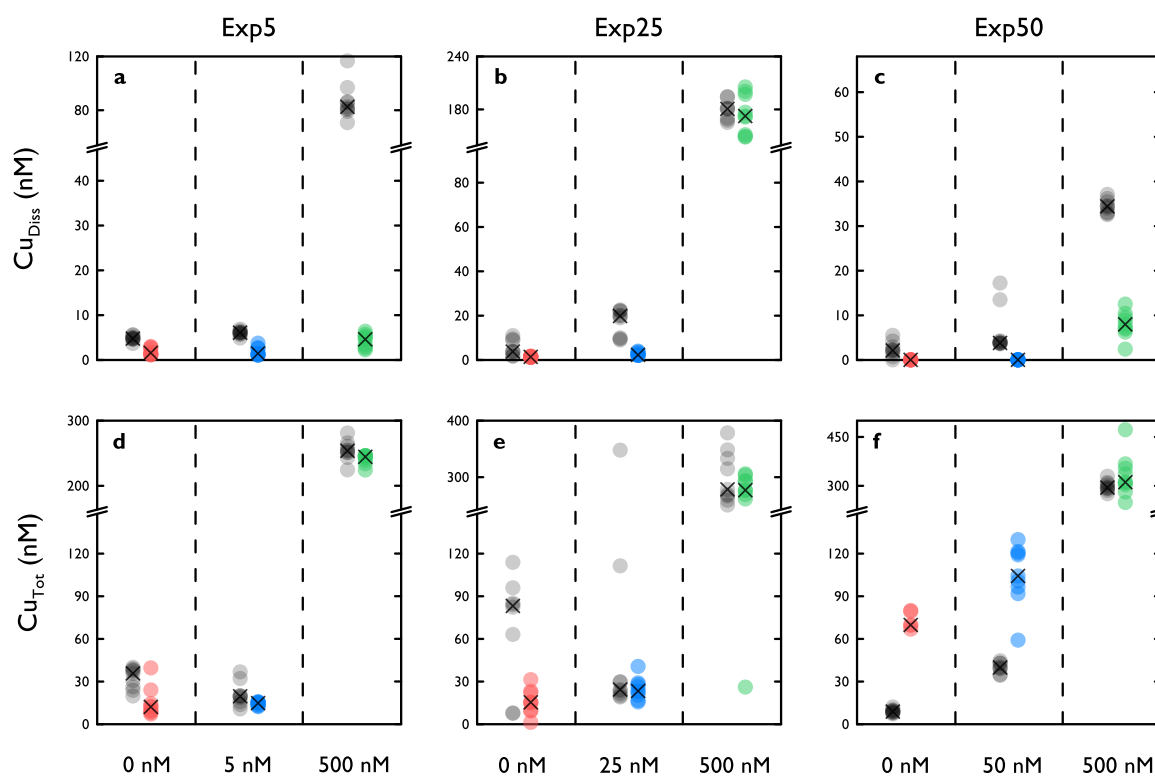


Figure S3. Measured dissolved and total copper fractions within incubation set-ups.

Measured concentrations of dissolved Cu (Cu_{Diss} , a,b,c) and total Cu (Cu_{Tot} , d,e,f) concentrations at the beginning (t_{zero} bottles, grey dots) and at the end (t_{End} bottles, coloured dots) of the respective incubation treatment (Exp5, Exp25, Exp50). Each column of the respective scatter plot belongs to a certain copper amendment (red = 0 nM, blue = 5 nM / 25 nM / 50 nM, green = 500 nM) and shows all measured samples of each incubation bottle. X represents median values. Note the different y-axis range for each plot.

Table S1. *M. alcaliphilum* 20Z maintenance. The medium was modified from DSMZ No. 1180 medium.

1. EDTA stock solution	EDTA disodium salt dihydrate	$\text{Na}_2\text{EDTA} \times 2 \text{ H}_2\text{O}$	500 mM
2. Trace element solution	Copper nitrate standard	$\text{Cu}(\text{NO}_3)_2$	0 - 500 nM
	Iron sulphate heptahydrate	$\text{FeSO}_4 \times 7 \text{ H}_2\text{O}$	7.2 mM
	Zink sulphate heptahydrate	$\text{ZnSO}_4 \times 7 \text{ H}_2\text{O}$	0.35 mM
	Nickel chloride hexahydrate	$\text{NiCl}_2 \times 6 \text{ H}_2\text{O}$	0.08 mM
	Cobalt chloride hexahydrate	$\text{CoCl}_2 \times 6 \text{ H}_2\text{O}$	0.84 mM
	Sodium molybdate dihydrate	$\text{Na}_2\text{MoO}_4 \times 2 \text{ H}_2\text{O}$	0.15 mM
	Manganese chloride tetrahydrate	$\text{MnCl}_2 \times 4 \text{ H}_2\text{O}$	0.15 mM
	Boric acid	H_3BO_3	0.49 mM
	Solution 1	EDTA stock solution	34 ml L ⁻¹
3. Salt solution	Sodium chloride	NaCl	0.51 M
	Magnesium sulphate heptahydrate	$\text{MgSO}_4 \times 7 \text{ H}_2\text{O}$	0.81 mM
	Calcium chloride dihydrate	$\text{CaCl}_2 \times 2 \text{ H}_2\text{O}$	0.14 mM
	Potassium nitrate	KNO_3	9.89 mM
	Solution 2	Trace elements	1-1.25 ml L ⁻¹
4. NaHCO_3	Sodium bicarbonate	NaHCO_3	1 M
5. Na_2CO_3	Sodium carbonate	Na_2CO_3	1 M
6. Phosphate buffer	Disodium hydrogen phosphate dihydrate	$\text{Na}_2\text{HPO}_4 \times 2 \text{ H}_2\text{O}$	83.8 mM
	Monopotassium dihydrogen phosphate	KH_2PO_4	102.9 mM
7. Serum bottles (120 ml, 0.5 L, or 1.2 L)	Solution 3	Salt solution	Headspace to liquid \approx 1:10
	Methane	CH_4	10-15% [v/v]
	Solution 4	NaHCO_3	4.15 ml L ⁻¹
	Solution 5	Na_2CO_3	0.42 ml L ⁻¹
	Solution 6	Phosphate buffer	0.33 ml L ⁻¹
	<i>Methylobacterium alcaliphilum</i> culture (autoclaved nanopure water as control)		\sim 2% [v/v]

Table S2. Statistical tests describing the differences in methane consumption rates between bottles with different copper additions within a single incubation experiment.

Exp5		Exp25		Exp50	
ANOVA	< 0.05	ANOVA	0.05	ANOVA	0.09
0 nM vs. 5 nM	0.91	0 nM vs. 25 nM	< 0.05	0 nM vs. 50 nM	0.78
0 nM vs. 500 nM	< 0.05	0 nM vs. 500 nM	0.18	0 nM vs. 500 nM	0.21
5 nM vs. 500 nM	< 0.05	25 nM vs. 500 nM	0.56	50 nM vs. 500 nM	0.09

Differences in methane consumption rates between applied copper set-ups (0 nM, 5 nM / 25 nM / 50 nM, 500 nM) of single experiments were tested by a one-way ANOVA followed by a Tukey's HSD pairwise test ($n = 2-3$). p-values < 0.05 were considered significant. Methane values were blank-corrected.

Table S3. Values of particulate carbon, nitrogen, copper, and dissolved and total copper within t_{Zero} bottles.

	Set-up	C _{Part} (mM)	N _{Part} (mM)	Cu _{Part} (nM)	Cu _{Diss} (nM)	Cu _{Tot} (nM)
Exp5	Blank			32.1 ± 16.1	6.7 ± 0.6	24.8 ± 9.7
	0 nM	0.10 ± 0.01 (0.1)	0.13 ± 0.15 (0.07)	60.5 ± 42.8 (48.8)	4.9 ± 0.6 (4.8)	32.3 ± 7.4 (35.7)
	Control 0 nM	n.a.	n.a.	26.2 ± 22.7	4.7 ± 0.3	23.5 ± 0.0
	5 nM	0.10 ± 0.01 (0.09)	0.01 ± 0.00 (0.01)	28.6 ± 21.4 (25.5)	6.0 ± 0.5 (6.1)	20.9 ± 8.4 (19.6)
	500 nM	0.18 ± 0.10 (0.14)	0.03 ± 0.03 (0.02)	32.8 ± 21.8 (22.4)	86.7 ± 13.2 (82.6)	254.1 ± 15.5 (253.9)
	Control 500 nM	n.a.	n.a.	32.1 ± 15.2	107.9 ± 2.1	234.8 ± 29.9
Exp25	Blank	0.05 ± 0.01	0.00	2.1 ± 0.7	0.8 ± 0.6	68.3 ± 31.5
	0 nM	0.08 ± 0.01 (0.07)	0.01 ± 0.00 (0.01)	3.9 ± 7.5 (1.8)	5.5 ± 3.7 (3.8)	67.5 ± 39.5 (83.2)
	Control 0 nM	0.07 ± 0.01	0.01 ± 0.01	2.5 ± 3.5	2.1 ± 0.1	8.0 ± 1.7
	25 nM	0.07 ± 0.01 (0.07)	0.01 ± 0.00 (0.01)	1.4 ± 1.5 (1.0)	17.2 ± 5.9 (19.9)	69.7 ± 108.3 (24.4)
	Control 25 nM	0.14 ± 0.12	0.03 ± 0.04	0.5 ± 1.8	12.6 ± 0.7	21.7 ± 0.2
	500 nM	0.11 ± 0.11 (0.08)	0.03 ± 0.03 (0.01)	4.3 ± 4.5 (2.3)	179.3 ± 11.2 (180.7)	299.9 ± 45.3 (278.4)
Exp50	Control 500 nM	0.05 ± 0.03	0.01	1.5 ± 0.7	143.4 ± 19.8	304.2 ± 21.8
	Blank	0.00	0.00	0.0 ± 0.0	5.4 ± 4.1	8.2 ± 0.3
	0 nM	0.13 ± 0.07 (0.16)	0.05 ± 0.01 (0.05)	0.6 ± 0.7 (0.6)	2.4 ± 1.7 (2.1)	9.1 ± 1.4 (8.9)
	Control 0 nM	0.03	0.02	2.9 ± 0.0	2.9 ± 1.5	12.3 ± 5.6
	50 nM	0.10 ± 0.06 (0.08)	0.02 ± 0.02 (0.01)	1.1 ± 1.4 (0.1)	6.4 ± 5.2 (3.8)	39.8 ± 3.7 (39.9)
	Control 50 nM	0.02	0.02	0.0 ± 0.0	4.0 ± 0.4	35.9 ± 2.2
Exp50	500 nM	0.06 ± 0.00 (0.06)	0.02 ± 0.01 (0.02)	1.3 ± 1.3 (0.7)	34.5 ± 1.5 (34.4)	298.7 ± 15.6 (394.7)
	Control 500 nM	0.00	0.00	0.0 ± 0.0	33.1 ± 0.0	288.1 ± 18.8

Particulate carbon (C_{Part}), particulate nitrogen (N_{Part}), particulate copper (Cu_{Part}), dissolved copper (Cu_{Diss}), total copper (Cu_{Tot}). Blank bottles were filled with nanopure water only. Control bottles were prepared identically to incubation bottles but received nanopure water instead of bacterial cells. Average values of triplicate samples of triplicate incubation bottles are listed. Data in brackets correspond to median values. Values of blank and control bottles with additional standard deviations represent average values of triplicate samples from the same bottle, otherwise only one sample was subducted. n.a. = not analysed.

Table S4. Average and median values of parameters in t_{End} bottles at the final time points of each incubation set-up.

	Set-up	Cell counts (cells ml ⁻¹)	CH ₄ consumption ($\mu\text{M CH}_4 \text{ h}^{-1}$)	C _{Part} (mM)	N _{Part} (mM)	Cu _{Part} (nM)	Cu _{Diss} (nM)	Cu _{Tot} (nM)	C _{Biomass} (mol cell ⁻¹)	N _{Biomass} (mol cell ⁻¹)	Cu _{Biomass} (mol cell ⁻¹)	Cu:C ($\mu\text{mol mol}^{-1}$)	Cu:N ($\mu\text{mol mol}^{-1}$)	C:N (mol mol ⁻¹)
Exp5	Blank					6.1 ± 13.5	0.5 ± 0.1	29.5 ± 4.5						
	0 nM	4.4 × 10 ⁷	43 ± 28	0.68 ± 0.10 (0.72)	0.12 ± 0.02 (0.12)	8.3 ± 11.1 (3.7)	1.9 ± 0.8 (1.6)	15.2 ± 10.4 (12.2)	1.5 × 10 ⁻¹⁴	2.7 × 10 ⁻¹⁵	1.9 × 10 ⁻¹⁹	12	69	5.7
	Control 0 nM	0.0		0.10 ± 0.01	0.01 ± 0.00	8.6 ± 7.4	8.5 ± 0.5	26.5 ± 0.1						
	5 nM	3.3 × 10 ⁷	32 ± 10	0.93 ± 0.07 (0.93)	0.15 ± 0.01 (0.15)	11.5 ± 10.5 (8.6)	1.9 ± 1.0 (1.5)	14.4 ± 1.3 (14.8)	2.8 × 10 ⁻¹⁴	4.5 × 10 ⁻¹⁵	3.5 × 10 ⁻¹⁹	12	77	6.2
	500 nM	1.9 × 10 ⁸	159 ± 52	4.42 ± 0.76 (4.61)	0.28 ± 0.05 (0.27)	179.7 ± 27.0 (176.5)	4.3 ± 1.5 (4.6)	240.7 ± 8.0 (244.5)	2.3 × 10 ⁻¹⁴	1.5 × 10 ⁻¹⁵	9.5 × 10 ⁻¹⁹	41	642	16
	Control 500 nM	0.0		0.09 ± 0.01	0.01 ± 0.00	-2.1 ± 10.6	130.5 ± 4.4	145.3 ± 12.8						
Exp25	Blank	0.0		0.05 ± 0.01	0.00	3.9 ± 1.4	2.8 ± 1.1	9.6 ± 1.2						
	0 nM	2.0 × 10 ⁶	-3 ± 12	0.17 ± 0.07 (0.15)	0.03 ± 0.02 (0.03)	8.9 ± 9.9 (6.1)	1.4 ± 0.2 (1.4)	15.9 ± 8.9 (15.4)	8.5 × 10 ⁻¹⁴	1.5 × 10 ⁻¹⁴	4.5 × 10 ⁻¹⁸	52	297	5.7
	Control 0 nM	0.0		0.05 ± 0.00	0.01 ± 0.00	2.6 ± 0.2	3.2 ± 0.2	19.6 ± 9.4						
	25 nM	6.0 × 10 ⁶	23 ± 9	0.23 ± 0.08 (0.21)	0.06 ± 0.05 (0.05)	15.9 ± 3.2 (14.2)	2.7 ± 0.8 (2.3)	24.8 ± 7.5 (23.4)	3.8 × 10 ⁻¹⁴	1.0 × 10 ⁻¹⁴	2.7 × 10 ⁻¹⁸	69	265	3.8
	Control 25 nM	0.0		0.13 ± 0.09	0.03 ± 0.03	8.0 ± 4.6	14.6 ± 0.8	17.7 ± 0.8						
	500 nM	7.4 × 10 ⁶	14 ± 9	0.30 ± 0.08 (0.32)	0.06 ± 0.02 (0.06)	45.1 ± 13.0 (47.7)	174.8 ± 22.4 (172.5)	256.2 ± 87.6 (276.9)	4.1 × 10 ⁻¹⁴	8.1 × 10 ⁻¹⁵	6.1 × 10 ⁻¹⁸	150	752	5.0
Exp50	Blank	0.0		0.05 ± 0.01	0.02 ± 0.01	26.5 ± 6.3	6.9 ± 7.3	82.0 ± 43.0						
	0 nM	1.0 × 10 ⁷	39 ± 32	0.34 ± 0.16 (0.25)	0.08 ± 0.03 (0.07)	41.6 ± 11.5 (44.2)	0.0 ± 0.0 (0.0)	73.1 ± 6.1 (69.8)	3.4 × 10 ⁻¹⁴	8.0 × 10 ⁻¹⁵	4.2 × 10 ⁻¹⁸	122	520	4.3
	Control 0 nM	0.0		0.06 ± 0.00	0.05 ± 0.01	25.6 ± 2.2	0.1 ± 0.1	72.1 ± 6.3						
	50 nM	1.3 × 10 ⁷	27 ± 11	0.65 ± 0.17 (0.57)	0.12 ± 0.04 (0.11)	86.3 ± 23.3 (82.7)	0.0 ± 0.0 (0.0)	104.8 ± 21.5 (104.3)	5.0 × 10 ⁻¹⁴	9.2 × 10 ⁻¹⁵	6.6 × 10 ⁻¹⁸	133	719	5.4
	Control 50 nM	0.0		0.06 ± 0.01	0.04 ± 0.02	68.8 ± 40.8	2.5 ± 0.1	173.0 ± 65.2						
	500 nM	2.8 × 10 ⁷	73 ± 16	0.66 ± 0.17 (0.65)	0.13 ± 0.03 (0.14)	228.1 ± 26.1 (220.1)	8.0 ± 2.9 (8.0)	331.7 ± 63.8 (311.1)	2.4 × 10 ⁻¹⁴	4.6 × 10 ⁻¹⁵	8.1 × 10 ⁻¹⁸	346	1755	5.1
Exp50	Control 500 nM	0.0		0.07 ± 0.01	0.03 ± 0.02	45.6 ± 2.3	27.4 ± 0.7	339.6 ± 17.8						

Particulate carbon (C_{Part}), particulate nitrogen (N_{Part}), particulate copper (Cu_{Part}), dissolved copper (Cu_{Diss}), total copper (Cu_{Tot}), elemental quotas (C_{Biomass}, N_{Biomass}, Cu_{Biomass}), elemental ratios (Cu:C, Cu:N, C:N). Blank bottles were filled with nanopure water only. Control bottles were prepared identically to incubation bottles but received nanopure water instead of bacterial cells. CH₄ consumption rates were calculated from blank-corrected values, other parameters were evaluated from raw values. Average (cell counts, CH₄ consumption, C_{Part}, N_{Part}, Cu_{Part}, Cu_{Diss}, Cu_{Tot}) or median (elemental quotas and ratios) values of triplicate samples of triplicate bottles are listed. Data in brackets correspond to median values.

Chapter 5

Conclusions and outlook

Conclusions and outlook

The decrease of methane via aerobic methane oxidation has been intensively studied in diverse environments. Laboratory experiments have shown that copper is a key player in the activity of aerobic methane-oxidizing bacteria (MOB) and their enzymatic pathway. With increasing methane production and emission from freshwater systems, it is important to improve our understanding of the biogeochemical role of copper on methane consuming organisms in the environment. This dissertation first aimed at providing knowledge about the lacustrine microbial methane oxidation process in the context of copper availability. In a second step, the role of other physico-chemical variables as well as the total bacterial assembly in shaping the MOB community was investigated in a freshwater lake. Finally, we tested the effect of available copper on the intra-cellular composition of a single MOB species under laboratory conditions to shed light on how MOB respond to and circumvent copper limitation. The major findings of the presented thesis are outlined below together with recommended future research directions in this field.

Monitoring copper availability in a lacustrine ecosystems

The global copper cycle combines both natural biogeochemical and anthropogenic stocks and flows, and is clearly dominated by the latter one, being in constant increase [Nriagu and Pacyna, 1988; Pacyna and Pacyna, 2001; Rauch and Graedel, 2007]. Nevertheless, copper concentrations in freshwater lakes are low compared to other trace metals (e.g. iron and manganese), and total concentrations are smaller than 50 nM on average [Wetzel, 2001c; Sigg and Stumm, 2011]. Analytical methods with low detection limits are necessary and utmost care is required during sampling and analysis to limit copper contamination.

The demand for copper as micronutrient is widespread in nature, as it is an essential trace element for various enzymatic pathways [Festa and Thiele, 2011; Solomon *et al.*, 2014]. Its uptake by organisms is coupled to copper speciation. Dissolved copper(II) is present in water in a palette of diverse species and appears to be strongly complexed to organic matter as solutes or colloids, whereas the bioavailable fraction usually remains small. We used the Diffusive Gradients in Thin film (DGT) method to gain information about the biological available copper fraction in Rotsee and quantitatively linked it with the potential of the copper-dependent

methane oxidation pathway performed by the particulate methane-monooxygenase (pMMO, Chapter 2). The DGT technique is based on diffusion characteristics of metal species through a boundary layer and the metal dissociation kinetics at an ion exchanger [Davison, 2016]. Applying DGTs in an environment allows measuring labile copper at high spatial resolution and low concentrations as it represents a passive sampling method giving rise to time-weighted average concentrations over several days. DGT samplers are relatively easy to prepare, simple to install and operate, all with reasonable expenses. However, sample preparation and handling demands trace-metal clean work to prevent contamination. Furthermore, the instability of metal species during transport and storage can introduce changes in the results.

Several other techniques for trace metal speciation analysis are used in freshwater systems [Sigg *et al.*, 2006]. The direct Voltammetric *In-situ* Profiling (VIP) system avoids limitations mentioned for the DGT method, as it performs real-time on-field monitoring and screening of the dynamic metal species smaller than 4 nm [Tercier-Waeber and Taillefert, 2008]. Voltammetric techniques are well suited for automatic and thus low cost *in-situ* metal speciation measurements, with no sample handling, which may introduce artefacts [Holmes *et al.*, 2019]. An important feature among the two measurement techniques represents the metal equilibration time that determines the time-average over which the labile species are measured [van Leeuwen *et al.*, 2005; Pesavento *et al.*, 2009]. VIP provides values in the order of minutes, while DGT gives integrated information on the time scale of days. This can result in somewhat higher concentrations measured by the DGT technique [Sigg *et al.*, 2006]. Finally applying several analytical methods (including filtration) in the same system provides a comprehensive picture in respect to the presence and distribution of various dynamic metal species and improves our understanding of biogeochemical processes.

Preliminary work on the VIP system was performed during the course of this thesis by calibrating the device in the lab and testing it in the field. However, due to the rather extended recording time per sample depth (30-45 minutes), high-resolution copper profiling along the water column as conducted by the DGT samplers is very time consuming. Moreover, the calibration of the state of the art system as well as its application in the field is not trivial and requires very experienced operators to avoid technical issues.

Competition for copper between organisms

During our four field campaigns, the copper DGT fraction in Rotsee was within the low nanomolar range. In this respect, Rotsee is comparable to other freshwater systems [Odzak *et al.*, 2002; Gimpel *et al.*, 2003; Menegário *et al.*, 2017], albeit there is little data available about copper DGT measurements in lakes (Chapter 2). In the epilimnion, the copper DGT concentrations were about tenfold smaller than the dissolved fraction, which points to the strong bonding of copper to organic complexes or colloidal species that are not detected by the DGT method. Hence, the directly available copper fraction for MOB species in Rotsee was rather low. Both fractions strongly diminished at oxic-anoxic transition zones and slightly below, where particulate copper reached maximum values. Particulate metal fractions either comprise metals bound to abiotic substances (e.g. clay minerals) or copper taken up by organisms (e.g. MOB). We found gammaproteobacterial MOB highly accumulated at similar depths as copper decline and accumulation of particulate copper. In addition, ^{13}C -methane incubations yielded highest methane oxidation rates [Oswald *et al.*, 2015]. Far higher numbers of *pmoA*, which encodes the copper-dependent pMMO, were measured compared to the iron-containing *mmoX* (sMMO functional gene). MOB have an about 10 times higher copper demand than other organisms [Semrau *et al.*, 2010], and we assumed that they account for a substantial part of the measured particulate copper. However, by calculating a copper to biomass factor (4×10^{-20} mol Cu cell $^{-1}$) for one MOB cell based on copper in pMMO, we concluded that MOB only make a small portion of the observed particulate copper peaks in Rotsee. We further discussed possible mechanisms contributing to elevated particulate copper within the oxycline of Rotsee and below, which are summarized in Figure 3 of Chapter 2. Oxygenic phototrophic organisms were abundant in similar environments than MOB. They usually require a considerably higher copper quota (10^{-16} - 10^{-18} mol Cu cell $^{-1}$) [Knauer *et al.*, 1997; Ho *et al.*, 2003; Wang, Xia *et al.*, 2017] and we suppose that they represent the most potent competitors for MOB cells in terms of copper acquisition. However, the activity of the different organisms was not explored in this thesis, and therefore we cannot conclude which uptake processes determine bioavailable copper.

In order to gain insights into the functioning of MOB and to further our understanding of their role in the biogeochemical cycling of copper, it is important to link microbial identification measurement with metabolic activity and substrate consumption. These are, for example, improving the knowledge of the exact copper

content of different environmental MOB and understanding the mechanisms of copper uptake and the role of different copper species as sources for these organisms [Knapp *et al.*, 2007; Chi Fru, 2011]. To complement the results of this thesis, future studies should perform *in-situ* or *ex-situ* enrichments to determine cell-specific metabolic rates. Besides experiments with ^{13}C -labelled methane, fractionation studies with stable copper isotopes may potentially provide valuable information of the abiotic and bacterially mediated processes happening in the highly active methane oxidation zone in Rotsee [Mathur *et al.*, 2005; Wasylenki *et al.*, 2007]. Absolute clean sample handling techniques, preferably under clean room conditions, are critical for the elemental trace determination and for precise isotope ratio determination by a HR-MC-ICP-MS (High-Resolution Multi-Collector Inductively-Coupled-Plasma Mass-Spectrometer). However, to comprehensively interpret the results of field measurements, prior rigorous calibration of copper isotopic fractionation within laboratory experiments, similar to incubations conducted in Chapter 4, is necessary. Extending copper isotope incubation treatments with the combined use of high-resolution secondary ion mass spectroscopy (NanoSIMS) and possibly synchrotron X-ray fluorescence (S-XRF) holds great promise for mechanistic, process-oriented research in environmental microbiology and biogeochemistry [Slaveykova *et al.*, 2009; Behrens *et al.*, 2012].

The benefit of copper extracellular acquisition and storage strategies

The outcomes of Chapter 2 clearly reveal that drawing direct conclusions on the relationship between *in-situ* copper concentrations and associated MOB ecology is difficult. This is not only due to the challenges in measuring the trace metal occurrence and its complex biogeochemical cycle. Moreover, environmental systems are complex in terms of interspecies interactions (Chapter 3), which can be positive, like organisms degrading copper-containing ligands, or negative in nature, like competition for copper with oxygenic phototrophs (Chapter 2). Finally, MOB have evolved strategies to increase the bioavailability of copper to overcome nutrient limitation and mediate their uptake. One example is the ability to release the biochelator methanobactin, which owns several different functions for MOB cells [Balasubramanian and Rosenzweig, 2008; DiSpirito *et al.*, 2016]. First, it generally acts as a transporter protein, which shuttles copper into the cell where it regulates pMMO expression and activity. Second, methanobactin is able to increase copper solubility and bioavailability while sequestering scarcely available copper from insoluble sources [Chi Fru *et al.*, 2011].

Lastly, methanobactin might play a role in MOB cellular copper defence as high copper concentration can be toxic to almost all organisms. To increase our understanding of copper linked to *in-situ* methane oxidation or MOB community dynamics, we should focus either on the potential capacity of MOB communities to produce methanobactin or develop methods for directly measuring methanobactin activity within the environment using genetic approaches [Kenney and Rosenzweig, 2013; Semrau *et al.*, 2013; DiSpirito *et al.*, 2016]. Up to now, methanobactin has only been detected in *ex-situ* incubation experiments with natural samples [Knapp *et al.*, 2007]. This gap needs to be filled!

Recent studies have discovered a new family of copper storage proteins (Csp), which can provide an additional strategy of MOB cells towards copper scarcity in Chapter 2 [Vita *et al.*, 2015; Dennison *et al.*, 2018]. We suggest that storage mechanisms played an important role in the laboratory incubation experiments conducted in Chapter 4. Therein, we studied the effects of copper amendments between 0-500 nanomolar copper on growth, methane consumption, and intracellular elemental stoichiometry of a single MOB species (*Methylobacterium alcaliphilum*). Although this species is not able to express the soluble methane-monooxygenase (sMMO), MOB cells demonstrated growth even at low nanomolar dissolved copper concentrations, which supports our findings in Chapter 2. Growth and methane consumption rates did not significantly vary between the experiments with added copper concentrations of two orders of magnitude difference. In contrast to rather constant biomass-bound carbon and nitrogen, copper quotas showed an increasing trend with higher copper supply, ranging from 1.9×10^{-19} to 8.1×10^{-18} mol copper cell⁻¹. Those copper per cell values (on average 3.7×10^{-18} mol Cu cell⁻¹) were approximately two orders of magnitude higher than the theoretical estimate calculated in Chapter 2 (4×10^{-20} mol Cu cell⁻¹), where only copper bound to pMMO was considered. Correspondingly, the extended cellular elemental stoichiometry (Cu:C and Cu:N) increased with increasing amounts of copper (Figure 4 in Chapter 4), and maximum values even exceeded reported ratios in phytoplankton. These results strongly support the idea that MOB can actively control their copper homeostasis while storing copper inside the cell. Additional incubations with copper isotope tracers could reveal the underlying mechanisms of MOB copper household. So far, we only conducted laboratory experiments with a single MOB species. Directly extrapolating laboratory-based studies to field conditions is difficult as environmental systems show high heterogeneity. As a next step, laboratory incubations with natural samples should be performed to further investigate the storage mechanisms of MOB. Taken together, our

results from Chapter 2 and Chapter 4 do not support the idea of a possible copper switch between pMMO and sMMO being very important in the stratified freshwater lake environment. Both, field and lab data indicate that *pmoA* driven methane oxidation remains functional and competitive under low copper conditions.

Investigating MOB community structure and niche preferences

Functional gene amplification (standard and quantitative PCR on DNA) was a crucial step in the assessment of MMO occurrence (*mmoX* and *pmoA*, see Chapter 2) and to further analyse the MOB community via high-throughput sequencing (*pmoA*, Chapter 3). We performed pre-tests with available primer sets (Table 1) for *pmoA* and *mmoX* detection of pure cultures (Chapter 2, Supplementary Table S5) to identify the most useful combination to cover a large range of *pmoA* and *mmoX* diversity in the Rotsee samples [Dumont, 2014]. *mmoX* genes were finally quantified by the primer set 536f-898r. The combination A189f-mb661 was the primer pair of choice for *pmoA* as it offered the best coverage of the axenic cultures. This primer pair is known to offer great specificity towards *pmoA* genes with less co-amplification of the *amoA* functional gene of ammonia-oxidizing bacteria. However, it fails to detect the distantly related *pxmA* gene, encoding for the pMMO homolog pXMO. Nonetheless, this primer pair is frequently used in environmental studies investigating MOB community structures [Knief, 2015].

Table 1. Tested *pmoA* and *mmoX* primer pairs by qualitative polymerase chain reaction.

Gene	Forward	Reverse	Sequences (5' to 3')
<i>pmoA</i>	A189f	mb661	GGNGACTGGGACTTCTGG / CCGMGCAACGTCYTTACC ^a
	A189f	A650r	GGNGACTGGGACTTCTGG / ACGTCCTTACCGAAGGT ^b
	A189f	682r	GGNGACTGGGACTTCTGG / GAASGCNGAGAAGAASGC ^c
<i>mmoX</i>	536f	898r	CGCTGTGGAAGGGCATGAAGCG / GCTCGACCTTGAAGTTGGAGCC ^d
	536f Deg	886r	CCNHTNTGGAAVGGNATGAA / ACCCANGGCTCGACYTTGAA ^e
	206f	886r	ATCGCBAARGAATAYGCSCG / ACCCANGGCTCGACYTTGAA ^f
	mmoXLF	mmoXLR	GAAGATTGGGGCGGCATCTG / CCCAATCATCGTGAAGGAGT ^g
	mmoX_F	mmoX_R	TCAACACCGATCTSAACAACG / TCCAGATTCCRCCCAATCC ^h

^a [Holmes *et al.*, 1995; Costello and Lidstrom, 1999] / ^b [Holmes *et al.*, 1995; Bourne *et al.*, 2001] / ^c [Holmes *et al.*, 1995] / ^d [Fuse *et al.*, 1998] / ^e 536fDeg was designed by Helmut Bürgmann, [Hutchens *et al.*, 2004] / ^f [Hutchens *et al.*, 2004] / ^g [Rahman *et al.*, 2011] / ^h [Knapp *et al.*, 2007]

Verrucomicrobial MOB and MOB belonging to NC10 both contain the gene for the pMMO enzymatic pathway. Hence, they possibly rely on copper supply to oxidize methane. In our study, we did not apply primers to detect those MOB species. To comprehensively encompass MOB diversity in natural systems, and quantitatively link it to copper biogeochemistry, it will be beneficial to include these species in the molecular analysis. There are primer pairs available, which cover the *pmoA* gene of verrucomicrobial and NC10-like MOB [Luesken *et al.*, 2011; Sharp *et al.*, 2014] and can be used in future studies. Recently, a new set of primers was published, which looks very promising [Ghashghavi *et al.*, 2017]. It has the ability to amplify genes of alpha- and gammaproteobacterial MOB, together with MOB of *Verrucomicrobia* and NC10, and has already been tested on pure and enrichment cultures, as well as environmental samples.

Maximum MOB abundance in Rotsee was usually located at the oxic-anoxic transitions, in accordance to where methane consumption was most intense (Chapter 2 and 3). MOB were also found in the epi- and hypolimnion of Rotsee, where methane oxidation could also have taken place. We identified a clear prevalence of MOB belonging to *Gammaproteobacteria* throughout the water column in all field campaigns, besides the oxygenated epilimnion, which was inhabited by alphaproteobacterial MOB (*Methylocystis*). These species were embedded in a surrounding with low amount of methane (0.12-1.07 μM), but highest available and dissolved copper. Some members of *Methylocystis* (and *Methylosinus*) are true oligotrophs as they have the competitive advantage of using pMMO₂, which has a significantly higher affinity for methane than pMMO and can even oxidize methane at atmospheric level [Baani and Liesack, 2008]. However, cells are exposed to intense light and high oxygen concentrations, which can hamper methane oxidation activity [Murase and Sugimoto, 2005]. The herein used primer pair for *pmoA* detection is less adequate for *pmoCAB2* detection, the gene operon encoding pMMO₂ [Ricke *et al.*, 2004]. It would be interesting to investigate the potential *in-situ* occurrence and activity of the *pmoCAB2* gene in accordance to epilimnetic methane oxidation dynamics.

In addition to detected methane consumption at the oxycline and immediately below, we saw methane slightly decreasing within the anoxic hypolimnion, which besides general physical diffusion could highlight methane oxidation. This is also apparent in the slight changes to isotopically heavy methane in August 2013 and September 2014 [Oswald *et al.*, 2015, 2017]. MOB appeared at those depths and corresponding copies of *pmoA* genes were detected via qPCR. The applied methodology in this thesis focused on the total MOB community reflecting the genetic potential of the investigated sites, and the differences in structure and

abundance, but does not necessarily mirror the pool of active species. During the last years, several studies reported the presence of MOB (especially *Methylobacter* types) in deeper anoxic layers of lakes [Chistoserdova, 2015]. The results of Chapter 2 and 3 add to these findings and raise the questions if MOB are active in the hypolimnion of Rotsee, and if so, how they pursue methane oxidation and acquire copper for the expression of pMMO. Hence, besides analysing the active MOB population at the oxic-anoxic interface and immediately above and below, we should investigate their potential activity also in the deeper hypolimnion. Activity studies at some discrete depths in the hypolimnion of Rotsee have already been conducted by FISH/NanoSIMS [Oswald *et al.*, 2015] and cDNA sequencing [Mayr *et al.*, submitted]. Nevertheless, mechanistic understanding of involved processes is still lacking. Some suggested explanations of MOB occurrence at depths depleted in oxygen and without light penetration are discussed in the results section of Chapter 2 and discussion of Chapter 3. Anyway, this topic needs more research in the future. One possible approach are enrichment, isolation, and cultivation studies depending on appropriate growth media and incubation conditions. This could help to better understand MOB electron-accepting capacity under controlled laboratory conditions ultimately unravelling correlations from actual causalities. Furthermore, if MOB are active at greater depths, and employing the pMMO pathway, it raises the question how they secure their copper requirement. This would bring us back to the discussion mentioned earlier about MOB exhibiting the ability to release extracellular copper binding proteins.

Besides aerobic methane oxidation, anaerobic methane-oxidizing archaea (ANME) could play a role in consuming methane at greater depths. They were not detected in August 2013 by the CARD-FISH method between 8 and 11 m depths [Oswald *et al.*, 2015]. Nevertheless, this hybridisation technique only covers the detection of known targeted organisms, whereas non-cultivated microorganisms are likely to be overlooked. Hence, besides already offering high throughput sample analysis, expanding the sequencing technique by considering the detection of ANME would offer a more comprehensive picture of the present methane oxidizing community [Klindworth *et al.*, 2013].

Completing the picture - total bacterial community as a significant driver of MOB community structure

Until now, studies of MOB diversity have principally focussed on the influence of physico-chemical variables shaping MOB community structures. Apart from abiotic factors, the microbial environment can additionally affect MOB occurrence and linked ecosystem functioning, such as methane removal within freshwater lakes. In Chapter 3, we applied high throughput sequencing paired with statistical modelling to investigate the interactions of MOB, their environments, as well as the associated bacterial communities to gain a more holistic view on the underlying mechanisms of methane oxidation in freshwater systems. MOB in Rotsee were well integrated in a correlational network of physico-chemical variables and the bacterial community. Whereas abiotic drivers alone only counted for 2% of the variability, interactions with co-occurring organisms had a significant impact on the MOB distribution (22%). Considering both relationships we could explain up to 60% of MOB occurrence in Rotsee (Figure 7 in Chapter 3). Herein, we focused on positive inter-correlations, which show species co-existence based on synergism (i.e. win-win situation), mutualism (i.e. cooperation), and shared niche preferences (neutral effects). We additionally cover positive feedback loops between MOB and total bacterial community interacting with their environment. Several mechanistic interactions are proposed in the discussion of Chapter 3, and explain part of the complexity of the studied system. However, the mode of action underlying the mentioned correlations have not been unambiguously unravelled in this study. Conducting an investigation of Rotsee over a whole year with high spatio-temporal resolution would add to the models and ultimately help to better understand the dynamics of the MOB community. Furthermore, including metagenome, metatranscriptome and even metaproteomic data would largely help to uncovering the interdependencies forming the metabolic potential of MOB communities. Predictive modelling of bacterial community functionality based on 16S rRNA sequencing is likely to help unravel if bacterial and MOB co-occurrence are based on actual interactions or on similar niche preferences [Langille *et al.*, 2013].

In conclusion, the results of this thesis show that MOB are not solely dependent on their direct copper supply to oxidize methane, but are rather embedded in a complex network with many abiotic and biotic parameters, which influence their performance. Additionally, they evolved strategies to escape limiting copper conditions, which significantly complicates the story. In the future, it will be important to combine

geochemical analysis and established molecular techniques together with imaging methods and metagenomics to get a quantitative picture of how environmental and biological interactions act together. As omics technologies become cheaper and more accessible, it is likely that a synthesis of these techniques will ultimately give us a more precise understanding of the mechanisms shaping MOB communities and their provided ecosystem functions.

Bibliography

- Akberdin, IR, Thompson, M, Hamilton, R, Desai, N, Alexander, D, Henard, CA, et al. (2018) Methane utilization in *Methylobacterium alcaliphilum* 20ZR: a systems approach. *Sci. Rep.* **8**: 10.1038/s41598-018-20574-z.
- Allan, W, Struthers, H, and Lowe, DC (2007) Methane carbon isotope effects caused by atomic chlorine in the marine boundary layer: global model results compared with Southern Hemisphere measurements. *J. Geophys. Res. Atmos.* **112**: 10.1029/2006JD007369.
- Amann, RI, Ludwig, W, and Schleifer, K-H (1995) Phylogenetic identification and in situ detection of individual microbial cells without cultivation. *Microbiol. Rev.* **59**: 143–169.
- Anderson, MJ, Ellingsen, KE, and McArdle, BH (2006) Multivariate dispersion as a measure of beta diversity. *Ecol. Lett.* **9**: 683–693.
- Annett, AL, Lapi, S, Ruth, TJ, and Maldonado, MT (2008) The effects of Cu and Fe availability on the growth and Cu:C ratios of marine diatoms. *Limnol. Oceanogr.* **53**: 2451–2461.
- Aronson, EL, Allison, SD, and Helliker, BR (2013) Environmental impacts on the diversity of methane-cycling microbes and their resultant function. *Front. Microbiol.* **4**: 10.3389/fmicb.2013.00225.
- Baani, M and Liesack, W (2008) Two isozymes of particulate methane monooxygenase with different methane oxidation kinetics are found in *Methylocystis* sp. strain SC2. *Proc. Natl. Acad. Sci.* **105**: 10203–10208.
- Balasubramanian, R, Kenney, GE, and Rosenzweig, AC (2011) Dual pathways for copper uptake by methanotrophic bacteria. *J. Biol. Chem.* **286**: 37313–37319.
- Balasubramanian, R and Rosenzweig, AC (2008) Copper methanobactin: a molecule whose time has come. *Curr. Opin. Chem. Biol.* **12**: 245–249.
- Balasubramanian, R and Rosenzweig, AC (2007) Structural and mechanistic insights into methane oxidation by particulate methane monooxygenase. *Acc. Chem. Res.* **40**: 573–580.
- Balasubramanian, R, Smith, SM, Rawat, S, Yatsunyk, LA, Stemmler, TL, and Rosenzweig, AC (2010) Oxidation of methane by a biological dicopper centre. *Nature* **465**: 115–119.
- Bar-Or, I, Elvert, M, Eckert, W, Vigderovich, H, Zhu, Q, Ben-Dov, E, and Sivan, O (2017) Iron-coupled anaerobic oxidation of methane performed by a mixed bacterial-archaeal community based on poorly reactive minerals. *Environ. Sci. Technol.* **51**: 12293–12301.
- Baslé, A, El Ghazouani, A, Lee, J, and Dennison, C (2018) Insight into metal removal from peptides that sequester copper for methane oxidation. *Chem. - Eur. J.* **24**: 4515–4518.
- Bastian, M, Heymann, S, and Jacomy, M (2009) Gephi: an open source software for exploring and manipulating networks. In, *Proceedings of the Third International AAAI Conference on Weblogs and Social Media*. San Jose, CA, pp. 361–362.
- Bastviken, D, Cole, JJ, Pace, M, and Tranvik, LJ (2004) Methane emissions from lakes: dependence of lake characteristics, two regional assessments, and a global estimate. *Global Biogeochem. Cycles* **18**: GB4009; 10.1029/2004GB002238.
- Bastviken, D, Cole, JJ, Pace, ML, and Van de Bogert, MC (2008) Fates of methane from different lake habitats: connecting whole-lake budgets and CH₄ emissions. *J. Geophys. Res.* **113**: G02024; 10.1029/2007JG000608.
- Bastviken, D, Ejlertsson, J, Sundh, I, and Tranvik, LJ (2003) Methane as a source of carbon and energy for lake pelagic food webs. *Ecology* **84**: 969–981.
- Bastviken, D, Ejlertsson, J, and Tranvik, LJ (2002) Measurement of methane oxidation in lakes: a comparison of methods. *Environ. Sci. Technol.* **36**: 3354–3361.
- Bastviken, D, Tranvik, LJ, Downing, JA, Crill, PM, and Enrich-Prast, A (2011) Freshwater methane emissions offset the continental carbon sink. *Science* **331**: 50.
- Begonja, A and Hrsak, D (2001) Effect of growth conditions on the expression of soluble methane monooxygenase. *Food Technol. Biotechnol.* **39**: 29–35.
- Behrens, S, Kappler, A, and Obst, M (2012) Linking environmental processes to the in situ functioning of microorganisms by high-resolution secondary ion mass spectrometry (NanoSIMS) and scanning transmission X-ray microscopy (STXM). *Environ. Microbiol.* **14**: 2851–2869.
- Berney, M, Hammes, FA, Bosshard, F, Weilenmann, H-U, and Egli, T (2007) Assessment and interpretation of bacterial viability by using the LIVE/DEAD BacLight kit in combination with flow cytometry. *Appl. Environ. Microbiol.* **73**: 3283–3290.
- Bidre-Petit, C, Jézéquel, D, Dugat-Bony, E, Lopes, F, Kuever, J, Borrel, G, et al. (2011) Identification of microbial communities involved in the methane cycle of a freshwater meromictic lake. *FEMS Microbiol. Ecol.* **77**: 533–545.
- Blees, J, Niemann, H, Wenk, CB, Zopfi, J, Schubert, CJ, Kirf, MK, et al. (2014) Micro-aerobic bacterial methane oxidation in the chemocline and anoxic water column of deep south-Alpine Lake Lugano (Switzerland). *Limnol. Oceanogr.* **59**: 311–324.
- Bloesch, J (1974) Sedimentation und Phosphorhaushalt im Vierwaldstättersee (Horwer Bucht) und im Rotsee. *Hydrology* **36**: 71–186.
- van Bodegom, PM, Stams, F, Mollema, L, Bockel, S, and Leffelaar, P (2001) Methane oxidation and the competition for oxygen in the rice rhizosphere. *Appl. Environ. Microbiol.* **67**: 3586–3597.

- Bogard, MJ, del Giorgio, PA, Boutet, L, Garcia Chaves, MC, Prairie, YT, Merante, A, and Derry, AM (2014) Oxidic water column methanogenesis as a major component of aquatic CH₄ fluxes. *Nat. Commun.* **5**: 5350; 10.1038/ncomms6350.
- Bornemann, M, Bussmann, I, Tichy, L, Deutzmann, JS, Schink, B, and Pester, M (2016) Methane release from sediment seeps to the atmosphere is counteracted by highly active Methylococcaceae in the water column of deep oligotrophic Lake Constance. *FEMS Microbiol. Ecol.* **92**: 10.1093/femsec/fiw123.
- Borrel, G, Jézéquel, D, Biderre-Petit, C, Morel-Desrosiers, N, Morel, JP, Peyret, P, et al. (2011) Production and consumption of methane in freshwater lake ecosystems. *Res. Microbiol.* **162**: 833–847.
- Bourne, DG, McDonald, IR, and Murrell, JC (2001) Comparison of pmoA PCR primer sets as tools for investigating methanotrophic diversity in three Danish soils. *Appl. Environ. Microbiol.* **67**: 3802–3809.
- Bowman, JP (2014) The family Methylococcaceae. In: Rosenberg, E., DeLong, E.F., Lory, S., Stackebrandt, E., and Thompson, F. (eds), *The Prokaryotes - Gammaproteobacteria*. Springer-Verlag Berlin Heidelberg, pp. 411–441.
- Bowman, JP (2006) The methanotrophs - The families Methylococcaceae and Methylocystaceae. In: Dworkin, M., Falkow, S., Rosenberg, E., Schleifer, K.-H., and Stackebrandt, E. (eds), *The Prokaryotes*. Springer, New York, NY, pp. 82–100.
- Brand, A, Bruderer, H, Oswald, K, Guggenheim, C, Schubert, CJ, and Wehrli, B (2016) Oxygenic primary production below the oxycline and its importance for redox dynamics. *Aquat. Sci.* **78**: 727–741.
- Burrows, KJ, Cornish, A, Scott, D, and Higgins, IJ (1984) Substrate specificities of the soluble and particulate methane mono-oxygenases of *Methylosinus trichosporium* OB3b. *J. Gen. Microbiol.* **130**: 3327–3333.
- Cantera, S, Lebrero, R, García-Encina, PA, and Muñoz, R (2016) Evaluation of the influence of methane and copper concentration and methane mass transport on the community structure and biodegradation kinetics of methanotrophic cultures. *J. Environ. Manage.* **171**: 11–20.
- Cao, L, Caldararu, O, Rosenzweig, AC, and Ryde, U (2018) Quantum refinement does not support dinuclear copper sites in crystal structures of particulate methane monooxygenase. *Angew. Chemie Int. Ed.* **1**: 162–166.
- Carini, S, Bano, N, LeClerc, G, and Joye, SB (2005) Aerobic methane oxidation and methanotroph community composition during seasonal stratification in Mono Lake, California (USA). *Environ. Microbiol.* **7**: 1127–1138.
- Chang, J, Gu, W, Park, D, Semrau, JD, and DiSpirito, AA (2018) Methanobactin from *Methylosinus trichosporium* OB3b inhibits N₂O reduction in denitrifiers. *ISME J.* **12**: 2086–2089.
- Chen, Y, Crombie, A, Rahman, MT, Dedysh, SN, Liesack, W, Stott, MB, et al. (2010) Complete genome sequence of the aerobic facultative methanotroph *Methylocella silvestris* BL2. *J. Bacteriol.* **192**: 3840–3841.
- Chen, Y, Dumont, MG, Cébron, A, and Murrell, JC (2007) Identification of active methanotrophs in a landfill cover soil through detection of expression of 16S rRNA and functional genes. *Environ. Microbiol.* **9**: 2855–2869.
- Chi Fru, E (2011) Copper biogeochemistry: a cornerstone in aerobic methanotrophic bacterial ecology and activity? *Geomicrobiol. J.* **28**: 601–614.
- Chi Fru, E, Gray, ND, McCann, C, Baptista, JDC, Christgen, B, Talbot, HM, et al. (2011) Effects of copper mineralogy and methanobactin on cell growth and sMMO activity in *Methylosinus trichosporium* OB3b. *Biogeosciences* **8**: 2887–2894.
- Chidambarampadmavathy, K, Karthikeyan, OP, Huerlimann, R, Maes, GE, and Heijmans, K (2017) Responses of mixed methanotrophic consortia to variable Cu²⁺/Fe²⁺ ratios. *J. Environ. Manage.* **197**: 159–166.
- Chistoserdova, L (2015) Methylophilic in natural habitats: current insights through metagenomics. *Appl. Microbiol. Biotechnol.* **99**: 5763–5779.
- Chistoserdova, L (2011) Methylophilic in a lake: from metagenomics to single-organism physiology. *Appl. Environ. Microbiol.* **77**: 4705–4711.
- Chistoserdova, L and Kalyuzhnaya, MG (2018) Current trends in methylophilic. *Trends Microbiol.* **26**: 703–7014.
- Chistoserdova, L and Lidstrom, ME (2013) Aerobic methylophilic prokaryotes. In: Rosenberg, E., DeLong, E.F., Thompson, F., Lory, S., and Stackebrandt, E. (eds), *The Prokaryotes - Prokaryotic Physiology And Biochemistry*. Springer-Verlag, pp. 267–285.
- Choi, DW, Bandow, NL, McEllistrem, MT, Semrau, JD, Antholine, WE, Hartsel, SC, et al. (2010) Spectral and thermodynamic properties of methanobactin from γ -proteobacterial methane oxidizing bacteria: a case for copper competition on a molecular level. *J. Inorg. Biochem.* **104**: 1240–1247.
- Choi, DW, Kunz, RC, Boyd, ES, Semrau, JD, Antholine, WE, Han, J-I, et al. (2003) The membrane-associated methane monooxygenase (pMMO) and pMMO-NADH: quinone oxidoreductase complex from *Methylococcus capsulatus* Bath. *J. Bacteriol.* **185**: 5755–5764.
- Ciais, P, Sabine, C, Bala, G, Bopp, L, Brovkin, V, Canadell, JG, et al. (2013) Carbon and other biogeochemical cycles. In: Stocker, T.F., Qin, D., Plattner, G.-K., Tignor, M., Allen, S.K., Boschung, A., et al. (eds), *Climate Change 2013: The Physical Science Basis. Contribution of Working Group I to the Fifth Assessment Report of the Intergovernmental Panel on Climate Change*. Cambridge University Press, Cambridge, United Kingdom and New York, NY, USA, pp. 465–570.
- Cicerone, RJ and Oremland, RS (1988) Biogeochemical aspects of atmospheric methane. *Global Biogeochem. Cycles* **2**: 299–327.
- Cline, JD (1969) Spectrophotometric determination of hydrogen sulfide in natural waters. *Limnol. Oceanogr.* **14**: 454–458.
- Colby, J, Stirling, DI, and Dalton, H (1977) The soluble methane mono-oxygenase of *Methylococcus capsulatus* (Bath). Its ability to oxygenate n-alkanes, n-alkenes, ethers, and alicyclic, aromatic and heterocyclic compounds. *Biochem. J.* **165**: 395–402.
- Comte, J, Lovejoy, C, Crevecoeur, S, and Vincent, WF (2016) Co-occurrence patterns in aquatic bacterial communities across changing permafrost landscapes. *Biogeosciences* **13**: 175–190.
- Conrad, R (2007) Microbial ecology of methanogens and methanotrophs. In: Sparks, D. (ed), *Advances in Agronomy*. Elsevier, pp. 1–63.

- Conrad, R (2009) The global methane cycle: recent advances in understanding the microbial processes involved. *Environ. Microbiol. Rep.* **1**: 285–292.
- Costello, AM and Lidstrom, ME (1999) Molecular characterization of functional and phylogenetic genes from natural populations of methanotrophs in lake sediments. *Appl. Environ. Microbiol.* **65**: 5066–5074.
- Cotner, JB, Hall, EK, Scott, JT, and Heldal, M (2010) Freshwater bacteria are stoichiometrically flexible with a nutrient composition similar to seston. *Front. Microbiol.* **1**: 10.3389/fmicb.2010.00132.
- Crowe, SA, Katsev, S, Leslie, K, Sturm, A, Magen, C, Nomosatryo, S, et al. (2011) The methane cycle in ferruginous Lake Matano. *Geobiology* **9**: 61–78.
- Crowe, SA, O'Neill, AH, Katsev, S, Hehanussa, P, Haffner, GD, Sundby, B, et al. (2008) The biogeochemistry of tropical lakes: a case study from Lake Matano, Indonesia. *Limnol. Oceanogr.* **53**: 319–331.
- Csárdi, G and Nepusz, T (2006) The igraph software package for complex network research. *InterJournal Complex Syst.* **1695**: 1–9.
- Cui, M, Ma, A, Qi, H, Zhuang, X, and Zhuang, G (2014) Anaerobic oxidation of methane: an “active” microbial process. *Microbiol. Open* **4**: 10.1002/mbo3.232.
- Culpepper, MA and Rosenzweig, AC (2012) Architecture and active site of particulate methane monooxygenase. *Crit. Rev. Biochem. Mol. Biol.* **47**: 483–492.
- Curry, CL (2007) Modeling the soil consumption at atmospheric methane at the global scale. *Global Biogeochem. Cycles* **21**: 10.1029/2006GB002818.
- Dassama, LMK, Kenney, GE, Ro, SY, Zielazinski, EL, and Rosenzweig, AC (2016) Methanobactin transport machinery. *Proc. Natl. Acad. Sci.* **113**: 13027–13032.
- Dassama, LMK, Kenney, GE, and Rosenzweig, AC (2017) Methanobactins: from genome to function. *Metallomics* **9**: 7–20.
- Davison, W (2016) Diffusive Gradients in Thin-Films for Environmental Measurements Cambridge University Press.
- Davison, W and Zhang, H (1994) In situ speciation measurements of trace components in natural waters using thin-film gels. *Nature* **367**: 546–548.
- Davison, W and Zhang, H (2012) Progress in understanding the use of diffusive gradients in thin films (DGT) - Back to basics. *Environ. Chem.* **9**: 1–13.
- Dedysh, SN, Dunfield, PF, and Trotsenko, YA (2004) Methane utilization by Methylobacterium species: new evidence but still no proof for an old controversy. *Int. J. Syst. Evol. Microbiol.* **54**: 1919–1920.
- Denfeld, BA, Ricão Canelhas, M, Weyhenmeyer, GA, Bertilsson, S, Eiler, A, and Bastviken, D (2016) Constraints on methane oxidation in ice-covered boreal lakes. *J. Geophys. Res. Biogeosciences* **121**: 1924–1933.
- Deng, Y, Cui, X, Lüke, C, and Dumont, MG (2013) Aerobic methanotroph diversity in Riganqiao peatlands on the Qinghai-Tibetan Plateau. *Environ. Microbiol. Rep.* **5**: 566–74.
- Dennison, C, David, S, and Lee, J (2018) Bacterial copper storage proteins. *J. Biol. Chem.* **293**: 4616–4627.
- Devlin, SP, Saarenheimo, J, Syväranta, J, and Jones, RI (2015) Top consumer abundance influences lake methane efflux. *Nat. Commun.* **6**: 8787.
- DiSpirito, AA, Semrau, JD, Murrell, JC, Gallagher, WH, and Dennison, C (2016) Methanobactin and the link between copper and bacterial methane oxidation. *Microbiol. Mol. Biol. Rev.* **80**: 387–409.
- Dlugokencky, EJ (2017) NOAA/ESRL. www.esrl.noaa.gov/gmd/ccgg/trends_ch4/ (accessed December 10, 2017).
- Donis, D, Flury, S, Stöckli, A, Spangenberg, JE, Vachon, D, and McGinnis, DF (2017) Full-scale evaluation of methane production under oxic conditions in a mesotrophic lake. *Nat. Commun.* **8**: 1661; 10.1038/s41467-017-01648-4.
- Downing, JA, Prairie, YT, Cole, JJ, Duarte, CM, Tranvik, LJ, Striegl, RG, et al. (2006) The global abundance and size distribution of lakes, ponds, and impoundments. *Limnol. Oceanogr.* **51**: 2388–2397.
- Dumont, MG (2014) Primers: functional marker genes for methylophiles and methanotrophs. In, McGenity, T.J., Timmis, K.N., and Nogales, B. (eds), *Hydrocarbon and Lipid Microbiology Protocols*. Springer-Verlag Berlin Heidelberg, pp. 57–77.
- Dumont, MG, Lüke, C, Deng, Y, and Frenzel, P (2014) Classification of pmoA amplicon pyrosequences using BLAST and the lowest common ancestor method in MEGAN. *Front. Microbiol.* **5**: 10.3389/fmicb.2014.00034.
- Dunfield, PF, Khmelenina, VN, Suzina, NE, Trotsenko, YA, and Dedysh, SN (2003) Methylocella silvestris sp. nov., a novel methanotroph isolated from an acidic forest cambisol. *Int. J. Syst. Evol. Microbiol.* **53**: 1231–1239.
- Ehhalt, DH (1974) The atmospheric cycle of methane. *Tellus A* **26**: 1–2.
- Encinas Fernandez, J, Peeters, F, and Hofmann, H (2014) Importance of the autumn overturn and anoxic conditions in the hypolimnion for the annual methane emissions from a temperate lake. *Environ. Sci. Technol.* **48**: 7297–7304.
- Erikstad, HA, Jensen, S, Keen, TJ, and Birkeland, N-K (2012) Differential expression of particulate methane monooxygenase genes in the verrucomicrobial methanotroph “Methylacidiphilum kamchatkense” Kam1. *Extremophiles* **16**: 405–409.
- Etioppe, G and Klusman, RW (2002) Geologic emissions of methane to the atmosphere. *Chemosphere* **49**: 777–789.
- Ettwig, KF, Butler, MK, Le Paslier, D, Pelletier, E, Mangenot, S, Kuypers, MMM, et al. (2010) Nitrite-driven anaerobic methane oxidation by oxygenic bacteria. *Nature* **464**: 543–548.
- Farhan Ul-Haque, M, Gu, W, Baral, BS, DiSpirito, AA, and Semrau, JD (2017) Carbon source regulation of gene expression in Methylosinus trichosporium OB3b. *Appl. Microbiol. Biotechnol.* **101**: 3871–3879.

- Faust, K and Raes, J (2012) Microbial interactions: from networks to models. *Nat. Rev. Microbiol.* **10**: 538–550.
- Fergala, A, AlSayed, A, and Eldyasti, A (2018) Behavior of type II methanotrophic bacteria enriched from activated sludge process while utilizing ammonium as a nitrogen source. *Int. Biodeterior. Biodegradation* **130**: 8–16.
- Festa, RA and Thiele, DJ (2011) Copper: an essential metal in biology. *Curr. Biol.* **21**: 877–883.
- Fuse, H, Ohta, M, Takimura, O, Murakami, K, Inoue, H, Yamaoka, Y, et al. (1998) Oxidation of trichloroethylene and dimethyl sulfide by a marine *Methylobacterium* strain containing soluble methane monooxygenase. *Biosci. Biotechnol. Biochem.* **62**: 1925–1931.
- Gallego, V, García, MT, and Ventosa, A (2005) *Methylobacterium variabile* sp. nov., a methylotrophic bacterium isolated from an aquatic environment. *Int. J. Syst. Evol. Microbiol.* **55**: 1429–1433.
- Geider, R and La Roche, J (2002) Redfield revisited: variability of C:N:P in marine microalgae and its biochemical basis. *Eur. J. Phycol.* **37**: 10.1017/S0967026201003456.
- Ghashghavi, M, Jetten, MSM, and Lüke, C (2017) Survey of methanotrophic diversity in various ecosystems by degenerate methane monooxygenase gene primers. *AMB Express* **7**: 10.1186/s13568-017-0466-2.
- Gilman, A, Fu, Y, Hendershott, M, Chu, F, Puri, AW, Smith, AL, et al. (2017) Oxygen-limited metabolism in the methanotroph *Methylobacterium buryatense* 5GB1C. *PeerJ* **5**: e3945; 10.7717/peerj.3945.
- Gimpel, J, Zhang, H, Davison, W, and Edwards, AC (2003) In situ trace metal speciation in lake surface waters using DGT, dialysis, and filtration. *Environ. Sci. Technol.* **37**: 138–146.
- Glass, JB and Orphan, VJ (2012) Trace metal requirements for microbial enzymes involved in the production and consumption of methane and nitrous oxide. *Front. Microbiol.* **3**: 61; 10.3389/fmicb.2012.00061.
- Gotelli, NJ, Hart, EM, and Ellison, AM (2015) Package “EcoSimR” - Null model analysis for ecological data. R package version 0.1.0.
- Gotelli, NJ and Ulrich, W (2012) Statistical challenges in null model analysis. *Oikos* **121**: 171–180.
- Graf, JS, Mayr, MJ, Machant, HK, Tienken, D, Hach, PF, Brand, A, et al. (2018) Bloom of a denitrifying methanotroph, “*Candidatus Methyloirabilis limnetica*”, in a deep stratified lake. *Environ. Microbiol.* **20**: 2598–2614.
- Grob, C, Ostrowski, M, Holland, RJ, Heldal, M, Norland, S, Erichsen, ES, et al. (2013) Elemental composition of natural populations of key microbial groups in Atlantic waters. *Environ. Microbiol.* **15**: 3054–3064.
- Grossart, H-P, Frindte, K, Dziallas, C, Eckert, W, and Tang, KW (2011) Microbial methane production in oxygenated water column of an oligotrophic lake. *Proc. Natl. Acad. Sci.* **108**: 19657–19661.
- Gu, W, Farhan Ul-Haque, M, Baral, BS, Turpin, EA, Bindow, NL, Kremmer, E, et al. (2016) A TonB-dependent transporter is responsible for methanobactin uptake by *Methylosinus trichosporium* OB3b. *Appl. Environ. Microbiol.* **82**: 1917–1923.
- Gu, W, Farhan Ul-Haque, M, and Semrau, JD (2017) Characterization of the role of copCD in copper uptake and the “copper-switch” in *Methylosinus trichosporium* OB3b. *FEMS Microbiol. Lett.* **364**: 10.1093/femsle/fnx094.
- Gu, W and Semrau, JD (2017) Copper and cerium-regulated gene expression in *Methylosinus trichosporium* OB3b. *Appl. Microbiol. Biotechnol.* **101**: 8499–8516.
- Guggenheim, C, Brand, A, Bürgmann, H, Sigg, L, and Wehrli, B (2019) Aerobic methane oxidation under copper scarcity in a stratified lake. *Sci. Rep.* **9**: doi.org/10.1038/s41598-019-40642-2.
- van der Ha, D, Vanwonterghem, I, Hoefman, S, De Vos, P, and Boon, N (2013) Selection of associated heterotrophs by methane-oxidizing bacteria at different copper concentrations. *Antonie Van Leeuwenhoek* **103**: 527–537.
- Hakemian, AS and Rosenzweig, AC (2007) The biochemistry of methane oxidation. *Annu. Rev. Biochem.* **76**: 223–241.
- Hakemian, AS, Tinberg, CE, Kondapalli, KC, Telser, J, Hoffman, BM, Stemmler, TL, and Rosenzweig, AC (2005) The copper chelator methanobactin from *Methylosinus trichosporium* OB3b binds copper(I). *J. Am. Chem. Soc.* **127**: 17142–17143.
- Hamilton-Taylor, J, Smith, EJ, Davison, W, and Sugiyama, M (2005) Resolving and modeling the effects of Fe and Mn redox cycling on trace metal behavior in a seasonally anoxic lake. *Geochim. Cosmochim. Acta* **69**: 1947–1960.
- Hammes, F, Berney, M, Wang, Y, Vital, M, and Egli, T (2008) Flow-cytometric total bacterial cell counts as a descriptive microbiological parameter for drinking water treatment processes. **42**: 269–277.
- Hanson, RS and Hanson, TE (1996) Methanotrophic bacteria. *Microbiol. Rev.* **60**: 439–471.
- Hao, WM and Ward, DE (1993) Methane production from global biomass burning. *J. Geophys. Res.* **98**: 20657.
- He, R, Wooller, MJ, Pohlman, JW, Catranis, C, Quensen, J, Tiedje, JM, and Leigh, MB (2012) Identification of functionally active aerobic methanotrophs in sediments from an arctic lake using stable isotope probing. *Environ. Microbiol.* **14**: 1403–1419.
- He, S, Stevens, SL, Chan, L-K, Bertilsson, S, Glavina del Rio, T, Tringe, SG, et al. (2017) Ecophysiology of freshwater Verrucomicrobia inferred from metagenome-assembled genomes. *mSphere* **2**: 5; 10.1128/mSphere.00277-17.
- He, Z, Cai, C, Wang, J, Xu, X, Zheng, P, Jetten, MSM, and Hu, B (2016) A novel denitrifying methanotroph of the NC10 phylum and its microcolony. *Sci. Rep.* **6**: 10.1038/srep32241.
- Hedderich, R and Whitman, WB (2013) Physiology and biochemistry of the methane-producing archaea. In: Rosenberg, E., DeLong, E.F., Lory, S., Stackebrandt, E., and Thompson, F. (eds), *The Prokaryotes: Prokaryotic Physiology and Biochemistry*. Springer Berlin Heidelberg, pp. 635–662.

- Hengy, MH, Horton, DJ, Uzarski, DG, and Learman, DR (2017) Microbial community diversity patterns are related to physical and chemical differences among temperate lakes near Beaver Island, MI. *PeerJ* **5**: 10.7717/peerj.3937.
- Henneberger, R, Chiri, E, Bodelier, PLE, Frenzel, P, Lüke, C, and Schroth, MH (2015) Field-scale tracking of active methane-oxidizing communities in a landfill cover soil reveals spatial and seasonal variability. *Environ. Microbiol.* **17**: 1721–1737.
- Herlemann, DP, Labrenz, M, Jürgens, K, Bertilsson, S, Waniek, JJ, and Andersson, AF (2011) Transitions in bacterial communities along the 2000 km salinity gradient of the Baltic Sea. *ISME J.* **5**: 1571–1579.
- Ho, A, Angel, R, Veraart, AJ, Daebeler, A, Jia, Z, Kim, SY, et al. (2016) Biotic interactions in microbial communities as modulators of biogeochemical processes: methanotrophy as a model system. *Front. Microbiol.* **7**: 10.3389/fmicb.2016.01285.
- Ho, A, Kerckhof, F-M, Lüke, C, Reim, A, Krause, S, Boon, N, and Bodelier, PLE (2013) Conceptualizing functional traits and ecological characteristics of methane-oxidizing bacteria as life strategies. *Environ. Microbiol. Rep.* **5**: 335–345.
- Ho, A, Lüke, C, Reim, A, and Frenzel, P (2013) Selective stimulation in a natural community of methane oxidizing bacteria: effects of copper on pmoA transcription and activity. *Soil Biol. Biochem.* **65**: 211–216.
- Ho, A, de Roy, K, Thas, O, De Neve, J, Hoefman, S, Vandamme, P, et al. (2014) The more, the merrier: heterotroph richness stimulates methanotrophic activity. *ISME J.* **8**: 1945–1948.
- Ho, T-Y, Quigg, A, Finkel, Z V., Milligan, AJ, Wyman, K, Falkowski, PG, and Morel, FMM (2003) The elemental composition of some marine phytoplankton. *J. Phycol.* **39**: 1145–1159.
- Ho, T and Lee, D (2007) The trace-metal composition of size-fractionated plankton in the South China Sea: biotic versus abiotic sources. *Limnol. Oceanogr.* **52**: 1776–1788.
- Hofmann, H, Federwisch, L, and Peeters, F (2010) Wave-induced release of methane: littoral zones as source of methane in lakes. *Limnol. Oceanogr.* **55**: 1990–2000.
- Holgerson, MA and Raymond, PA (2016) Large contribution to inland water CO₂ and CH₄ emissions from very small ponds. *Nat. Geosci.* **9**: 222–226.
- Holmes, AJ, Costello, AM, Lidstrom, ME, and Murrell, JC (1995) Evidence that particulate methane monooxygenase and ammonia monooxygenase may be evolutionarily related. *FEMS Microbiol. Lett.* **132**: 203–208.
- Holmes, J, Pathirathna, P, and Hashemi, P (2019) Trends in analytical chemistry novel frontiers in voltammetric trace metal analysis: towards real time, on-site, in situ measurements. *Trends Anal. Chem.* **111**: 206–219.
- Hugert, LW, Larsson, J, Alneberg, J, Lindh, M V, Legrand, C, Pinhassi, J, and Andersson, AF (2015) Metagenome-assembled genomes uncover a global brackish microbiome. *Genome Biol.* **16**: 279; 10.1186/s13059-015-0834-7.
- Hutchens, E, Radajewski, S, Dumont, MG, McDonald, IR, and Murrell, JC (2004) Analysis of methanotrophic bacteria in Movile Cave by stable isotope probing. *Environ. Microbiol.* **6**: 111–120.
- Iguchi, H, Yurimoto, H, and Sakai, Y (2015) Interactions of methylotrophs with plants and other heterotrophic bacteria. *Microorganisms* **3**: 137–151.
- Im, J, Lee, S, Yoon, S, DiSpirito, AA, and Semrau, JD (2011) Characterization of a novel facultative Methylocystis species capable of growth on methane, acetate and ethanol. *Environ. Microbiol. Rep.* **3**: 174–181.
- Johnson, KA, Ve, T, Larsen, Ø, Pedersen, RB, Lillehaug, JR, Jensen, HB, et al. (2014) CorA is a copper repressible surface-associated copper(I)-binding protein produced in Methylobacterium album BG8. *PLoS One* **9**: 2; 10.1371/journal.pone.0087750.
- Jones, RI and Grey, J (2011) Biogenic methane in freshwater food webs. *Freshw. Biol.* **56**: 213–229.
- Jones, SE and Lennon, JT (2009) Evidence for limited microbial transfer of methane in a planktonic food web. *Aquat. Microb. Ecol.* **58**: 45–53.
- Ju, F, Xia, Y, Guo, F, Wang, Z, and Zhang, T (2014) Taxonomic relatedness shapes bacterial assembly in activated sludge of globally distributed wastewater treatment plants. *Environ. Microbiol.* **16**: 2421–2432.
- Kalidass, B, Farhan Ul-Haque, M, Baral, BS, DiSpirito, AA, and Semrau, JD (2015) Competition between metals for binding to methanobactin enables expression of soluble methane monooxygenase in the presence of copper. *Appl. Environ. Microbiol.* **81**: 1024–1031.
- Kalyuzhnaya, MG, Gomez, OA, and Murrell, JC (2019) The methane-oxidizing bacteria (methanotrophs). In, McGenity T. (ed), *Taxonomy, Genomics and Ecophysiology of Hydrocarbon-Degrading Microbes. Handbook of Hydrocarbon and Lipid Microbiology*. Springer Cham, pp. 1–34.
- Kalyuzhnaya, MG, Khmelenina, V, Eshinimaev, B, Sorokin, D, Fuse, H, Lidstrom, M, and Trotsenko, YA (2008) Classification of halo(alkali)philic and halo(alkali)tolerant methanotrophs provisionally assigned to the genera Methylobacterium and Methylobacter and emended description of the genus Methylobacterium. *Int. J. Syst. Evol. Microbiol.* **58**: 591–596.
- Kalyuzhnaya, MG, Yang, S, Rozova, ON, Smalley, NE, Clubb, J, Lamb, A, et al. (2013) Highly efficient methane biocatalysis revealed in a methanotrophic bacterium. *Nat. Commun.* **4**: 1–7.
- Kelly, DP, McDonald, IR, and Wood, AP (2014) The family Methylobacteriaceae. In, Rosenberg, E., DeLong, E.F., Lory, S., Stackebrandt, E., and Thompson, F. (eds), *The Prokaryotes: Alphaproteobacteria and Betaproteobacteria*. Springer-Verlag Berlin Heidelberg, pp. 313–340.
- Kembel, SW, Cowan, PD, Helmus, MR, Cornwell, WK, Morlon, H, Ackerly, DD, et al. (2010) Picante: R tools for integrating phylogenies and ecology. *Bioinformatics* **26**: 1463–1464.
- Kenney, GE and Rosenzweig, AC (2013) Genome mining for methanobactins. *BMC Biol.* **11**: 10.1186/1741-7007-11-17.
- Kenney, GE and Rosenzweig, AC (2018) Methanobactins: maintaining copper homeostasis in methanotrophs and beyond. *J. Biol. Chem.* **293**: 4606–4615.

- Kenney, GE, Sadek, M, and Rosenzweig, AC (2016) Copper-responsive gene expression in the methanotroph *Methylosinus trichosporium* OB3b. *Metallomics* **8**: 931–940.
- Khadem, AF, Pol, A, Wiczeorek, A, Mohammadi, SS, Francoijs, KJ, Stunnenberg, HG, et al. (2011) Autotrophic methanotrophy in verrucomicrobia: *Methyloacidiphilum fumariolicum* SolV uses the calvin-benson-bassham cycle for carbon dioxide fixation. *J. Bacteriol.* **193**: 4438–4446.
- Kim, HJ, Graham, DW, DiSpirito, AA, Alterman, MA, Galeva, N, Larive, CK, et al. (2004) Methanobactin, a copper-acquisition compound from methane-oxidizing bacteria. *Science* **305**: 1612–1615.
- King, GM (1992) Ecological aspects of methane oxidation, a key determinant of global methane dynamics. In, Marshall, K.C. (ed), *Advances in Microbial Ecology*. Plenum Press, New York, pp. 431–468.
- Kirf, MK, Dinkel, C, Schubert, CJ, and Wehrli, B (2014) Submicromolar oxygen profiles at the oxic-anoxic boundary of temperate lakes. *Aquat. Geochemistry* **20**: 39–57.
- Kirschke, S, Bousquet, P, Ciais, P, Saunio, M, Canadell, JG, Dlugokencky, EJ, et al. (2013) Three decades of global methane sources and sinks. *Nat. Geosci.* **6**: 813–823.
- Kitmitto, A, Myronova, N, Basu, P, and Dalton, H (2005) Characterization and structural analysis of an active particulate methane monooxygenase trimer from *Methylococcus capsulatus* (Bath). *Biochemistry* **44**: 10954–10965.
- Kits, KD, Campbell, DJ, Rosana, AR, and Stein, LY (2015) Diverse electron sources support denitrification under hypoxia in the obligate methanotroph *Methylobacterium album* strain BG8. *Front. Microbiol.* **6**: 10.3389/fmicb.2015.01072.
- Kits, KD, Klotz, MG, and Stein, LY (2015) Methane oxidation coupled to nitrate reduction under hypoxia by the Gammaproteobacterium *Methylomonas denitrificans*, sp. nov. type strain FJG1. *Environ. Microbiol.* **17**: 3219–3232.
- Klindworth, A, Pruesse, E, Schweer, T, Peplies, J, Quast, C, Horn, M, and Glöckner, FO (2013) Evaluation of general 16S ribosomal RNA gene PCR primers for classical and next-generation sequencing-based diversity studies. *Nucleic Acids Res.* **41**: 10.1093/nar/gks808.
- Knapp, CW, Fowle, DA, Kulczycki, E, Roberts, JA, and Graham, DW (2007) Methane monooxygenase gene expression mediated by methanobactin in the presence of mineral copper sources. *Proc. Natl. Acad. Sci.* **104**: 12040–12045.
- Knauer, K, Behra, R, and Sigg, L (1997) Effects of free Cu^{2+} and Zn^{2+} ions on growth and metal accumulation in freshwater algae. *Environ. Toxicol. Chem.* **16**: 220–229.
- Knief, C (2015) Diversity and habitat preferences of cultivated and uncultivated aerobic methanotrophic bacteria evaluated based on pmoA as molecular marker. *Front. Microbiol.* **6**: 1346; 10.3389/fmicb.2015.01346.
- Knief, C and Dunfield, PF (2005) Response and adaptation of different methanotrophic bacteria to low methane mixing ratios. *Environ. Microbiol.* **7**: 1307–1317.
- Knoblauch, C, Spott, O, Evgrafova, S, Kutzbach, L, and Pfeiffer, EM (2015) Regulation of methane production, oxidation, and emission by vascular plants and bryophytes in ponds of the northeast Siberian polygonal tundra. *J. Geophys. Res. Biogeosciences* **120**: 2525–2541.
- Kohler, H-P, Åhring, B, Albella, C, Ingvorsen, K, Keweloh, H, Laczkó, E, et al. (1984) Bacteriological studies on the sulfur cycle in the anaerobic part of the hypolimnion and in the surface sediments of Rotsee in Switzerland. *FEMS Microbiol. Lett.* **21**: 279–286.
- Kolb, S, Knief, C, Stubner, S, and Conrad, R (2003) Quantitative detection of methanotrophs in soil by novel pmoA- targeted real-time PCR assays. *Appl. Environ. Microbiol.* **69**: 2423–2429.
- Kraemer, SM, Duckworth, OW, Harrington, JM, and Schenkeveld, WDC (2015) Metallophores and trace metal biogeochemistry. *Aquat. Geochemistry* **21**: 159–195.
- Kroneck, PMH and Sosa Torres, ME (2015) Sustaining Life on Planet Earth: Metalloenzymes Mastering Dioxygen and Other Chewy Gases Sigel, A., Sigel, H., and Sigel, R.K.O. (eds) Springer.
- Kulczycki, E, Fowle, D a., Kenward, P a., Leslie, K, Graham, DW, and Roberts, J a. (2011) Stimulation of methanotroph activity by Cu-substituted borosilicate glass. *Geomicrobiol. J.* **28**: 10.1080/01490451003614971.
- Kumar, S, Stecher, G, Li, M, Knyaz, C, and Tamura, K (2018) MEGA X: molecular evolutionary genetics analysis across computing platforms. *Mol. Biol. Evol.* **35**: 1547–1549.
- Lane, DJ (1991) 16S/23S rRNA sequencing. In, Stackebrandt, E. and Goodfellow, M. (eds), *Nucleic Acid Techniques in Bacterial Systematics*. John Wiley & Sons, New York, pp. 115–175.
- Langille, MGI, Zaneveld, J, Caporaso, JG, McDonald, D, Knights, D, Reyes, JA, et al. (2013) Predictive functional profiling of microbial communities using 16S rRNA marker gene sequences. *Nat. Biotechnol.* **31**: 814–821.
- Lawton, TJ, Ham, J, Sun, T, and Rosenzweig, AC (2015) Structural conservation of the B subunit in the ammonia monooxygenase/particulate methane monooxygenase superfamily. *Proteins* **82**: 2263–2267.
- Lawton, TJ, Kenney, GE, Hurley, JD, and Rosenzweig, AC (2016) The CopC family: structural and bioinformatic insights into a diverse group of periplasmic copper binding proteins. *Biochemistry* **55**: 2278–2290.
- Leak, DJ and Dalton, H (1986a) Growth yields of methanotrophs - 1. Effect of copper on the energetics of methane oxidation. *Appl. Microbiol. Biotechnol.* **23**: 470–476.
- Leak, DJ and Dalton, H (1986b) Growth yields of methanotrophs - 2. A theoretical analysis. *Appl. Microbiol. Biotechnol.* **23**: 477–481.
- Lee, S-W, Keeney, DR, Lim, DH, DiSpirito, AA, and Semrau, JD (2006) Mixed pollutant degradation by *Methylosinus trichosporium* OB3b expressing either soluble or particulate methane monooxygenase: can the tortoise beat the hare. *Appl. Environ. Microbiol.* **72**: 7503–7509.

- van Leeuwen, HP, Town, RM, Buffle, J, Cleven, RFMJ, Davison, W, Puy, J, et al. (2005) Dynamic speciation analysis and bioavailability of metals in aquatic systems. *Environ. Sci. Technol.* **39**: 8545–8556.
- Lelieveld, J, Crutzen, PJ, and Dentener, FJ (1998) Changing concentration, lifetime and climate forcing of atmospheric methane. *Tellus, Ser. B Chem. Phys. Meteorol.* **50**: 128–150.
- Lieberman, RL and Rosenzweig, AC (2004) Biological methane oxidation: regulation, biochemistry, and active site structure of particulate methane monooxygenase. *Crit. Rev. Biochem. Mol. Biol.* **39**: 147–164.
- Lieberman, RL and Rosenzweig, AC (2005) Crystal structure of a membrane-bound metalloenzyme that catalyses the biological oxidation of methane. *Nature* **434**: 177–182.
- Liebner, S and Svenning, MM (2013) Environmental transcription of mmoX by methane-oxidizing Proteobacteria in a subarctic peatland. *Appl. Environ. Microbiol.* **79**: 701–706.
- Lloyd, JS, De Marco, P, Dalton, H, and Murrell, JC (1999) Heterologous expression of soluble methane monooxygenase genes in methanotrophs containing only particulate methane monooxygenase. *Arch. Microbiol.* **171**: 364–370.
- Lombardi, A (2015) Metalloproteins: simple structure, complex function. *Nat. Chem. Biol.* **11**: 760–761.
- Lontoh, S and Semrau, JD (1998) Methane and trichloroethylene degradation by *Methylosinus trichosporium* OB3b expressing particulate methane monooxygenase. *Appl. Environ. Microbiol.* **64**: 1106–1114.
- Lotter, AF (1988) Paläoökologische und paläolimnologische Studie des Rotsees bei Luzern.
- Loulergue, L, Schilt, A, Spahni, R, Masson-Delmotte, V, Blunier, T, Lemieux, B, et al. (2008) Orbital and millennial-scale features of atmospheric CH₄ over the past 800,000 years. *Nature* **453**: 383–386.
- Luesken, FA, Zhu, B, van Alen, TA, Butler, MK, Rodriguez Diaz, M, Song, B, et al. (2011) pmoA primers for detection of anaerobic methanotrophs. *Appl. Environ. Microbiol.* **77**: 3877–3880.
- Lüke, C and Frenzel, P (2011) Potential of pmoA amplicon pyrosequencing for methanotroph diversity studies. *Appl. Environ. Microbiol.* **77**: 6305–6309.
- Mansilla-Rivera, I and Nriagu, JO (1999) Copper chemistry in freshwater ecosystems: an overview. *J. Great Lakes Res.* **25**: 599–610.
- Marin, I and Ruiz Arahal, D (2014) The family Beijerinckiaceae. In: Rosenberg, E., DeLong, E.F., Lory, S., Stackebrandt, E., and Thompson, F. (eds), *The Prokaryotes - Alphaproteobacteria and Betaproteobacteria*. Springer-Verlag Berlin Heidelberg, pp. 115–133.
- Martin, H and Murrell, JC (1995) Methane monooxygenase mutants of *Methylosinus trichosporium* constructed by marker-exchange mutagenesis. *FEMS Microbiol. Lett.* **127**: 243–248.
- Martinez-Cruz, K, Sepulveda-Jauregui, A, Walter Anthony, K, and Thalasso, F (2015) Geographic and seasonal variation of dissolved methane and aerobic methane oxidation in Alaskan lakes. *Biogeosciences* **12**: 4595–4606.
- Martinho, M, Choi, DW, DiSpirito, AA, Antholine, WE, Semrau, JD, and Münck, E (2007) Mössbauer studies of the membrane-associated methane monooxygenase from *Methylococcus capsulatus* Bath: evidence for a diiron center. *J. Am. Chem. Soc. Chem. Soc.* **129**: 15783–15785.
- Mason, RP (2013) Trace Metals in Aquatic Systems Wiley-Blackwell, Oxford.
- Mathur, R, Ruiz, J, Titley, S, Liermann, L, Buss, H, and Brantley, S (2005) Cu isotopic fractionation in the supergene environment with and without bacteria. *Geochim. Cosmochim. Acta* **69**: 5233–5246.
- Mayr, MJ, Zimmermann, M, Guggenheim, C, Brand, A, and Bürgmann, H Niche partitioning of methane-oxidizing bacteria along the oxygen-methane counter gradient of stratified lakes. *Submitt. to ISME J.*
- McDonald, IR, Bodrossy, L, Chen, Y, and Murrell, JC (2008) Molecular ecology techniques for the study of aerobic methanotrophs. *Appl. Environ. Microbiol.* **74**: 1305–1315.
- McMurdie, PJ and Holmes, SP (2013) Phyloseq: an R package for reproducible interactive analysis and graphics of microbiome census data. *PLoS One* **8**: 4; 10.1371/journal.pone.0061217.
- Menegário, AA, Marques Yabuki, LN, Luko, KS, Williams, PN, and Blackburn, DM (2017) Use of diffusive gradient in thin films for in situ measurements: a review on the progress in chemical fractionation, speciation and bioavailability of metals in waters. *Anal. Chim. Acta* **983**: 54–66.
- Merkx, M, Kopp, DA, Sazinsky, MH, Blazyk, JL, Müller, J, and Lippard, SJ (2001) Dioxygen activation and methane hydroxylation by soluble methane monooxygenase: a tale of two irons and three proteins. *Angew. Chemie Int. Ed.* **40**: 2782–2807.
- Meyer, TE and Cusanovich, MA (2003) Discovery and characterization of electron transfer proteins in the photosynthetic bacteria. *Photosynth. Res.* **76**: 111–126.
- Milucka, J, Kirf, MK, Lu, L, Krupke, A, Lam, P, Littmann, S, et al. (2015) Methane oxidation coupled to oxygenic photosynthesis in anoxic waters. *ISME J.* **9**: 1991–2002.
- Montzka, SA, Dlugokencky, EJ, and Butler, JH (2011) Non-CO₂ greenhouse gases and climate change. *Nature* **476**: 43–50.
- Morana, C, Borges, A V., Roland, FAE, Darchambeau, F, Descy, J-P, and Bouillon, S (2015) Methanotrophy within the water column of a large meromictic tropical lake (Lake Kivu, East Africa). *Biogeosciences* **12**: 2077–2088.
- Morel, FMM (2008) The co-evolution of phytoplankton and trace element cycles in the oceans. *Geobiology* **6**: 318–324.

- Morris, BEL, Henneberger, R, Huber, H, and Moissl-Eichinger, C (2013) Microbial syntrophy: interaction for the common good. *FEMS Microbiol. Rev.* **37**: 384–406.
- Morrison, JM, Šimek, K, Baker, KD, Zamor, RM, Nikolai, S, Elshahed, S, and Youssef, NH (2017) Spatiotemporal analysis of microbial community dynamics during seasonal stratification events in a freshwater lake. *PLoS One* **12**: 5; 10.1371/journal.pone.177488.
- Morton, JD, Hayes, KF, and Semrau, JD (2000) Effect of copper speciation on whole-cell soluble methane monooxygenase activity in *Methylosinus trichosporium* OB3b. *Appl. Environ. Microbiol.* **66**: 1730–1733.
- Murase, J, Sakai, Y, Kametani, A, and Sugimoto, A (2005) Dynamics of methane in mesotrophic Lake Biwa, Japan. *For. Ecosyst. Environ.* **143**: 143–151.
- Murase, J and Sugimoto, A (2005) Inhibitory effect of light on methane oxidation in the pelagic water column of a mesotrophic lake (Lake Biwa, Japan). *Limnol. Oceanogr.* **50**: 1339–1343.
- Murrell, JC (2010) The aerobic methane oxidizing bacteria (methanotrophs). In, Timmis, K.N. (ed), *Handbook of Hydrocarbon and Lipid Microbiology*. Springer-Verlag Berlin Heidelberg, pp. 1953–1966.
- Murrell, JC, Gilbert, B, and McDonald, IR (2000) Molecular biology and regulation of methane monooxygenase. *Arch. Microbiol.* **173**: 325–332.
- Murrell, JC, McDonald, IR, and Gilbert, B (2000) Regulation of expression of methane monooxygenases by copper ions. *Trends Microbiol.* **8**: 221–225.
- Murrell, JC and Smith, TJ (2010) Biochemistry and molecular biology of methane monooxygenase. In, Timmis, K.N. (ed), *Handbook of Hydrocarbon and Lipid Microbiology*. Springer-Verlag Berlin Heidelberg, pp. 1045–1055.
- Myhre, G, Shindell, DT, Bréon, F-M, Collins, W, Fuglestad, J, Huang, J, et al. (2013) Anthropogenic and natural radiative forcing. In, Stocker, T.F., Qin, D., Plattner, G.-K., Tignor, M., Allen, S.K., Boschung, J., et al. (eds), *Climate Change 2013: The Physical Science Basis. Contribution of Working Group I to the Fifth Assessment Report of the Intergovernmental Panel on Climate Change*. Cambridge University Press, Cambridge, United Kingdom and New York, NY, USA, pp. 659–740.
- Nazarides, L, Murrell, JC, Millard, P, Baggs, L, and Singh, BK (2013) Methane, microbes and models: fundamental understanding of the soil methane cycle for future predictions. *Environ. Microbiol.* **15**: 2395–2417.
- Nei, M and Kumar, S (2000) *Molecular Evolution and Phylogenetics* Oxford University Press.
- Nielsen, AK, Gerdes, K, and Murrell, JC (1997) Copper-dependent reciprocal transcriptional regulation of methane monooxygenase genes in *Methylococcus capsulatus* and *Methylosinus trichosporium*. *Mol. Microbiol.* **25**: 399–409.
- Nihous, GC (2010) Notes on the temperature dependence of carbon isotope fractionation by aerobic CH₄-oxidising bacteria. *Isotopes Environ. Health Stud.* **46**: 133–140.
- Nikaido, H (2003) Molecular basis of bacterial outer membrane permeability revisited. *Microbiol. Mol. Biol. Rev.* **67**: 593–656.
- Nisbet, EG, Dlugokencky, EJ, and Bousquet, P (2014) Methane on the rise - again. *Science* **343**: 493–495.
- Nisbet, EG, Dlugokencky, EJ, Manning, MR, Lowry, D, Fisher, RE, France, JL, et al. (2016) Rising atmospheric methane: 2007–2014 growth and isotopic shift. *Global Biogeochem. Cycles* **30**: 1356–1370.
- Noinaj, N, Guillier, M, Barnard, TJ, and Buchanan, SK (2010) TonB-dependent transporters: regulation, structure, and function. *Annu. Rev. Mi* **64**: 43–60.
- Nriagu, JO and Pacyna, JM (1988) Quantitative assessment of worldwide contamination of air, water and soils by trace metals. *Nature* **333**: 134–139.
- Odzak, N, Kistler, D, Xue, H, and Sigg, L (2002) In situ trace metal speciation in a eutrophic lake using the technique of diffusion gradients in thin films (DGT). *Aquat. Sci.* **64**: 292–299.
- Oksanen, AJ, Blanchet, FG, Kindt, R, Legendre, P, Minchin, PR, Hara, RBO, et al. (2018) vegan: community ecology package. R package version 2.4-4.
- Op den Camp, HJM, Islam, T, Stott, MB, Harhangi, HR, Hynes, A, Schouten, S, et al. (2009) Environmental, genomic and taxonomic perspectives on methanotrophic Verrucomicrobia. *Environ. Microbiol. Rep.* **1**: 293–306.
- Oshkin, IY, Beck, DAC, Lamb, AE, Tchesnokova, V, Benuska, G, McTaggart, TL, et al. (2015) Methane-fed microbial microcosms show differential community dynamics and pinpoint taxa involved in communal response. *ISME J.* **9**: 1119–1129.
- Oswald, K, Graf, JS, Littmann, S, Tienken, D, Brand, A, Wehrli, B, et al. (2017) Crenothrix are major methane consumers in stratified lakes. *ISME J.* **11**: 2124–2140.
- Oswald, K, Jegge, C, Tischer, J, Berg, J, Brand, A, Miracle, MR, et al. (2016) Methanotrophy under versatile conditions in the water column of the ferruginous meromictic Lake La Cruz (Spain). *Front. Microbiol.* **7**: 10.3389/fmicb.2016.01762.
- Oswald, K, Milucka, J, Brand, A, Hach, P, Littmann, S, Wehrli, B, et al. (2016) Aerobic gammaproteobacterial methanotrophs mitigate methane emissions from oxic and anoxic lake waters. *Limnol. Oceanogr.* **61**: 101–118.
- Oswald, K, Milucka, J, Brand, A, Littmann, S, Wehrli, B, Kuypers, MMM, and Schubert, CJ (2015) Light-dependent aerobic methane oxidation reduces methane emissions from seasonally stratified lakes. *PLoS One* **10**: 7; 10.1371/journal.pone.0132574.
- Pacyna, JM and Pacyna, EG (2001) An assessment of global and regional emissions of trace metals to the atmosphere from anthropogenic sources worldwide. *Environ. Rev.* **9**: 269–298.
- Peres-Neto, PR and Jackson, DA (2001) How well do multivariate data sets match? The advantages of a procrustean superimposition approach over the Mantel test. *Oecologia* **129**: 169–178.

- Pesavento, M, Alberti, G, and Biesuz, R (2009) Analytical methods for determination of free metal ion concentration, labile species fraction and metal complexation capacity of environmental waters: a review. *Anal. Chim. Acta* **631**: 129–141.
- Pesch, M-L, Hoffmann, M, Christl, I, Kraemer, SM, and Kretzschmar, R (2012) Competitive ligand exchange between Cu-humic acid complexes and methanobactin. *Geobiology* **11**: 44–54.
- Prior, SD and Dalton, H (1985) The effect of copper ions on membrane content and methane monooxygenase activity in methanol-grown cells of *Methylococcus capsulatus* (Bath). *J. Gen. Microbiol.* **131**: 155–163.
- Quigg, A, Finkel, Z V., Irwin, AJ, Rosenthal, Y, Ho, T-Y, Reinfelder, JR, et al. (2003) The evolutionary inheritance of elemental stoichiometry in marine phytoplankton. *Nature* **425**: 291–294.
- Rahman, MT, Crombie, AT, Moussard, H, Chen, Y, and Murrell, JC (2011) Acetate repression of methane oxidation by supplemental *Methylocella silvestris* in a peat soil microcosm. *Appl. Environ. Microbiol.* **77**: 4234–4236.
- Rasigraf, O, Kool, DM, Jetten, MSM, Damsté, SS, and Ettwig, KF (2014) Autotrophic carbon dioxide fixation via the Calvin-Benson-Bassham cycle by the denitrifying methanotroph “*Candidatus Methyloirabilis oxyfera*.” *Appl. Environ. Microbiol.* **80**: 2451–2460.
- Rasilo, T, Prairie, YT, and del Giorgio, PA (2015) Large-scale patterns in summer diffusive CH₄ fluxes across boreal lakes, and contribution to diffusive C emissions. *Glob. Chang. Biol.* **21**: 1124–1139.
- Rauch, JN and Graedel, TE (2007) Earth’s anthropobiogeochemical copper cycle. *Global Biogeochem. Cycles* **21**: 10.1029/2006GB002850.
- Redfield, AC (1934) On the proportions of organic derivatives in sea water and their relation to the composition of plankton. In, Daniel, R.J. (ed), *James Johnstone Memorial Volume*. Liverpool University Press, pp. 176–192.
- Redfield, AC (1958) The biological control of chemical factors in the environment. *Am. Sci.* **46**: 205–221.
- Reeburgh, WS (2007) Oceanic methane biogeochemistry. *Chem. Rev.* **107**: 486–513.
- Reisinger, A, Meinshausen, M, Manning, M, and Bodeker, G (2010) Uncertainties of global warming metrics: CO₂ and CH₄. *Geophys. Res. Lett.* **37**: 2–7.
- Rhee, TS, Kettle, AJ, and Andreae, MO (2009) Methane and nitrous oxide emissions from the ocean: a reassessment using basin-wide observations in the Atlantic. *J. Geophys. Res. Atmos.* **114**: 10.1029/2008JD011662.
- Ricke, P, Erkel, C, Kube, M, Liesack, W, and Reinhardt, R (2004) Comparative analysis of the conventional and novel pmo (particulate methane monooxygenase) operons from *Methylocystis* strain SC2. *Appl. Environ. Microbiol.* **70**: 3055–3063.
- Rigby, M, Montzka, SA, Prinn, RG, White, JWC, Young, D, O’Doherty, S, et al. (2017) Role of atmospheric oxidation in recent methane growth. *Proc. Natl. Acad. Sci.* **114**: 5373–5377.
- Rohart, F, Gautier, B, Singh, A, and Lê Cao, K-A (2017) mixOmics: An R package for ‘omics feature selection and multiple data integration. *PLOS Comput. Biol.* **13**: 11; 10.1371/journal.pcbi.1005752.
- Rosenberg, E, DeLong, EF, Lory, S, Stackebrandt, E, and Thompson, F (2014a) The Prokaryotes - Alphaproteobacteria and Betaproteobacteria Rosenberg, E., DeLong, E.F., Lory, S., Stackebrandt, E., and Thompson, F. (eds) Springer-Verlag Berlin Heidelberg.
- Rosenberg, E, DeLong, EF, Lory, S, Stackebrandt, E, and Thompson, F (2014b) The Prokaryotes - Gammaproteobacteria 4th ed. Rosenberg, E., DeLong, E.F., Lory, S., Stackebrandt, E., and Thompson, F. (eds) Springer-Verlag Berlin Heidelberg.
- Roslev, P and King, GM (1994) Survival and recovery of methanotrophic bacteria starved under oxic and anoxic conditions. *Appl. Environ. Microbiol.* **60**: 2602–2608.
- Ross, MO and Rosenzweig, AC (2016) A tale of two methane monooxygenases. *J. Biol. Inorg. Chem.* **22**: 307–319.
- Rudd, JWM and Hamilton, RD (1975) Factors controlling rates of methane oxidation and the distribution of the methane oxidizers in a small stratified lake. *Arch. Hydrobiol.* **75**: 522–538.
- Salawitch, RJ, Canty, TP, Hope, AP, Tribett, WR, and Bennett, BF (2017) Paris Climate Agreement: Beacon of Hope.
- Samad, MS and Bertilsson, S (2017) Seasonal variation in abundance and diversity of bacterial methanotrophs in five temperate lakes. *Front. Microbiol.* **8**: 10.3389/fmicb.2017.00142.
- Sanseverino, AM, Bastviken, D, Sundh, I, Pickova, J, and Enrich-Prast, A (2012) Methane carbon supports aquatic food webs to the fish level. *PLoS One* **7**: 8; 10.1371/journal.pone.0042723.
- Sapart, C-J, Monteil, G, Prokopiou, M, van de Wal, RSW, Kaplan, JO, Sperlich, P, et al. (2013) Natural and anthropogenic variations in methane sources during the past two millennia. *Nature* **490**: 85–88.
- Saunois, M, Bousquet, P, Poulter, B, Peregon, A, Ciais, P, Canadell, JG, et al. (2016) The global methane budget 2000-2012. *Earth Syst. Sci. Data* **8**: 697–751.
- Sazinsky, MH and Lippard, SJ (2015) Methane monooxygenase: functionalizing methane at iron and copper. In, Kroneck, P.M.H. and Sosa Torres, M.E. (eds), *Sustaining Life On Planet Earth: Metalloenzymes Mastering Dioxygen And Other Chewy Gases*, Metal Ions in Life Sciences. Springer International, pp. 205–256.
- Scally, S, Davison, W, and Zhang, H (2006) Diffusion coefficients of metals and metal complexes in hydrogels used in diffusive gradients in thin films. *Anal. Chim. Acta* **558**: 222–229.
- Scanlan, J, Dumont, MG, and Murrell, JC (2009) Involvement of MmoR and MmoG in the transcriptional activation of soluble methane monooxygenase genes in *Methylosinus trichosporium* OB3b. *FEMS Microbiol. Lett.* **301**: 181–187.

- Schaefer, H, Fletcher, SEM, Veidt, C, Lassey, KR, Brailsford, GW, Bromley, TM, et al. (2016) A 21st-century shift from fossil-fuel to biogenic methane emissions indicated by $\delta^{13}\text{C}$. *Science* **352**: 2–7.
- Schmidt, ML, White, JD, and Denef, VJ (2016) Phylogenetic conservation of freshwater lake habitat preference varies between abundant bacterioplankton phyla. *Environ. Microbiol.* **18**: 1212–1226.
- Schubert, CJ, Coolen, MJL, Nelson, KE, Schippers, A, Abbas, B, Durisch-Kaiser, E, et al. (2006) Aerobic and anaerobic methanotrophs in the Black Sea water column. *Environ. Microbiol.* **8**: 1844–1856.
- Schubert, CJ, Diem, T, and Eugster, W (2012) Methane emissions from a small wind shielded lake determined by Eddy covariance, flux chambers, anchored funnels, and boundary model calculations: a comparison. *Environ. Sci. Technol.* **46**: 4515–4522.
- Schubert, CJ, Lucas, FS, Durisch-Kaiser, E, Stierli, R, Diem, T, Scheidegger, O, et al. (2010) Oxidation and emission of methane in a monomictic lake (Rotsee, Switzerland). *Aquat. Sci.* **72**: 455–466.
- Semrau, JD (2011) Bioremediation via methanotrophy: overview of recent findings and suggestions for future research. *Front. Microbiol.* **2**: 1–7.
- Semrau, JD, Chistoserdov, A, Lebron, J, Costello, AM, Davagnino, J, Kenna, E, et al. (1995) Particulate methane monooxygenase genes in methanotrophs. *J. Bacteriol.* **177**: 3071–3079.
- Semrau, JD, DiSpirito, AA, and Vuilleumier, S (2011) Facultative methanotrophy: false leads, true results, and suggestions for future research. *FEMS Microbiol. Lett.* **323**: 10.1111/j.1574-6968.2011.02315.x.
- Semrau, JD, DiSpirito, AA, and Yoon, S (2010) Methanotrophs and copper. *FEMS Microbiol. Rev.* **34**: 496–531.
- Semrau, JD, Jagadevan, S, DiSpirito, AA, Khalifa, AYZ, Scanlan, J, Bergman, BH, et al. (2013) Methanobactin and MmoD work in concert to act as the “copper-switch” in methanotrophs. *Environ. Microbiol.* **15**: 3077–3086.
- Shaked, Y, Erel, Y, and Sukenik, A (2004) The biogeochemical cycle of iron and associated elements in Lake Kinneret. *Geochim. Cosmochim. Acta* **68**: 1439–1451.
- Sharp, CE, Smirnova, A V., Graham, JM, Stott, MB, Khadka, R, Moore, TR, et al. (2014) Distribution and diversity of Verrucomicrobia methanotrophs in geothermal and acidic environments. *Environ. Microbiol.* **16**: 1867–1878.
- Sigg, L, Black, F, Buffle, J, Cao, J, Cleven, RFMJ, Davison, W, et al. (2006) Comparison of analytical techniques for dynamic trace metal speciation in natural freshwaters. *Environ. Sci. Technol.* **40**: 1934–1941.
- Sigg, L and Stumm, W (2011) *Aquatische Chemie: Einführung in die Chemie natürlicher Systeme* Vdf, UTB, Zurich.
- Siljanen, HMP, Saari, A, Bodrossy, L, and Martikainen, PJ (2012) Effects of nitrogen load on the function and diversity of methanotrophs in the littoral wetland of a boreal lake. *Front. Microbiol.* **3**: 10.3389/fmicb.2012.00039.
- Sirajuddin, S and Rosenzweig, AC (2015) Enzymatic oxidation of methane. *Biochemistry* **54**: 2283–2294.
- Slaveykova, VI, Guignard, C, Eybe, T, Migeon, HN, and Hoffmann, L (2009) Dynamic NanoSIMS ion imaging of unicellular freshwater algae exposed to copper. *Anal. Bioanal. Chem.* **393**: 583–589.
- Solomon, EI, Heppner, DE, Johnston, EM, Ginsbach, JW, Cirera, J, Qayyum, M, et al. (2014) Copper active sites in biology. *Chem. Rev.* **114**: 3659–3853.
- Spearman, C (2010) The proof and measurement of association between two things. *Am. J. Psychol.* **39**: 1137–1150.
- Stadelmann, P (1980) Der Zustand des Rotsee bei Luzern. In: *Maihof Rotsee. Geschichte und Eigenart eines Quartiers*. Quartierverein Maihof, pp. 54–61.
- Stafford, GP, Scanlan, J, McDonald, IR, and Murell, JC (2003) rpoN, mmoR and mmoG, genes involved in regulating the expression of soluble methane monooxygenase in *Methylosinus trichosporium* OB3b. *Microbiology* **149**: 1771–1784.
- Stanley, SH, Prior, SD, Leak, DJ, and Dalton, H (1983) Copper stress underlies the fundamental change in intracellular location of methane monooxygenase in methane-oxidizing organisms: studies in batch and continuous cultures. *Biotechnol. Lett.* **5**: 487–492.
- Sterner, RW and Elser, JJ (2002) *Ecological Stoichiometry: The Biology of Elements from Molecules to the Biosphere*. Princeton University Press, New Jersey.
- Stock, M, Hoefman, S, Kerckhof, F-M, Boon, N, De Vos, P, De Baets, B, et al. (2013) Exploration and prediction of interactions between methanotrophs and heterotrophs. *Res. Microbiol.* **164**: 1045–1054.
- Stocker, TF, Dahe, Q, Plattner, G-K, Alexander, L V., Allen, SK, Bindoff, NL, et al. (2013) Technical summary. In: Stocker, T.F., Qin, D., Plattner, G.-K., Tignor, S.K., Boschung, J., Nauels, A., et al. (eds), *Climate Change 2013: The Physical Science Basis. Contribution of Working Group I to the Fifth Assessment Report of the Intergovernmental Panel on Climate Change*. Cambridge University Press, Cambridge, United Kingdom and New York, NY, USA.
- Stolper, DA, Lawson, M, Davis, CL, Ferreira, AA, Santos Neto, E V., Ellis, GS, et al. (2014) Formation temperatures of thermogenic and biogenic methane. *Science* **344**: 12–14.
- Stolyar, S, Costello, AM, Peeples, TL, and Lidstrom, ME (1999) Role of multiple gene copies in particulate methane monooxygenase activity in the methane-oxidizing bacterium *Methylococcus capsulatus* Bath. *Microbiology* **145**: 1235–1244.
- Stolyar, S, Franke, M, and Lidstrom, ME (2001) Expression of individual copies of *Methylococcus capsulatus* Bath particulate methane monooxygenase genes. *J. Bacteriol.* **183**: 1810–1812.
- Sundh, I, Bastviken, D, and Tranvik, LJ (2005) Abundance, activity, and community structure of pelagic methane-oxidizing bacteria in temperate lakes. *Appl. Environ. Microbiol.* **71**: 6746–6752.

- Taillefert, M and Gaillard, JF (2002) Reactive transport modeling of trace elements in the water column of a stratified lake: iron cycling and metal scavenging. *J. Hydrol.* **256**: 16–34.
- Takai, K and Horikoshi, K (2000) Rapid detection and quantification of members of the archaeal community by quantitative PCR using fluorogenic probes. *Appl. Environ. Microbiol.* **66**: 5066–5072.
- Tang, KW, McGinnis, DF, and Grossart, H-P (2016) Methane production in oxic lake waters potentially increases aquatic methane flux to air. *Environ. Sci. Technol. Lett.* **3**: 227–233.
- Tavormina, PL, Orphan, VJ, Kalyuzhnaya, MG, Jetten, MSM, and Klotz, MG (2011) A novel family of functional operons encoding methane/ammonia monooxygenase-related proteins in gammaproteobacterial methanotrophs. *Environ. Microbiol. Rep.* **3**: 91–100.
- van Teeseling, MCF, Pol, A, Harhangi, HR, van der Zwart, S, Jetten, MSM, Op den Camp, HJM, and van Niftrik, L (2014) Expanding the verrucomicrobial methanotrophic world: description of three novel species of *Methylococcoides* gen. nov. *Appl. Environ. Microbiol.* **80**: 6782–6791.
- Tercier-Waeber, M-L and Taillefert, M (2008) Remote in situ voltammetric techniques to characterize the biogeochemical cycling of trace metals in aquatic systems. *J. Environ. Monit.* **10**: 30–54.
- Tinberg, CE and Lippard, SJ (2011) Dioxygen activation in soluble methane monooxygenase. *Acc. Chem. Res.* **44**: 280–288.
- Tissot, BP and Welte, DH (1984) Petroleum Formation and Occurrence Tissot, B.P. and Welte, D.H. (eds) Springer-Verlag Berlin Heidelberg New York Tokyo.
- Trotsenko, YA and Khmelenina, VN (2002) Biology of extremophilic and extremotolerant methanotrophs. *Arch. Microbiol.* **177**: 123–131.
- Trotsenko, YA and Murrell, JC (2008) Metabolic aspects of aerobic obligate methanotrophy. In, *Advances in Applied Microbiology*, pp. 183–229.
- Tsutsumi, M, Iwata, T, Kojima, H, and Fukui, M (2011) Spatiotemporal variations in an assemblage of closely related planktonic aerobic methanotrophs. *Freshw. Biol.* **56**: 342–351.
- Twining, BS and Baines, SB (2013) The trace metal composition of marine phytoplankton. *Ann. Rev. Mar. Sci.* **5**: 191–215.
- Ve, T, Mathisen, K, Helland, R, Karlsen, OA, Fjellbirkeland, A, Røhr, ÅK, et al. (2012) The *Methylococcus capsulatus* (Bath) secreted protein, MopE*, binds both reduced and oxidized copper. *PLoS One* **7**: 8; 10.1371/journal.pone.0043146.
- Větrovský, T and Baldrian, P (2013) The variability of the 16S rRNA gene in bacterial genomes and its consequences for bacterial community analyses. *PLoS One* **8**: 2; 10.1371/journal.pone.0057923.
- Vigliotta, G, Nutricati, E, Carata, E, Tredici, SM, De Stefano, M, Pontieri, P, et al. (2007) *Clonothrix fusca* Roze 1896, a filamentous, sheathed, methanotrophic γ -proteobacterium. *Appl. Environ. Microbiol.* **73**: 3556–3565.
- Vita, N, Landolfi, G, Baslé, A, Platsaki, S, Lee, J, Waldron, KJ, and Dennison, C (2016) Bacterial cytosolic proteins with a high capacity for Cu(I) that protect against copper toxicity. *Sci. Rep.* **6**: 39065.
- Vita, N, Platsaki, S, Baslé, A, Allen, SJ, Paterson, NG, Crombie, AT, et al. (2015) A four-helix bundle stores copper for methane oxidation. *Nature* **525**: 140–143.
- Vorobev, A V., Baani, M, Doronina, N V., Brady, AL, Liesack, W, Dunfield, PF, and Dedysh, SN (2011) *Methyloferula stellata* gen. nov., sp. nov., an acidophilic, obligately methanotrophic bacterium that possesses only a soluble methane monooxygenase. *Int. J. Syst. Evol. Microbiol.* **61**: 2456–2463.
- Vuilleumier, S, Khmelenina, VN, Bringel, F, Reshetnikov, AS, Lajus, A, Mangenot, S, et al. (2012) Genome Sequence of the Haloalkaliphilic Methanotrophic Bacterium *Methylococcoides alcaliphilum* 20Z. *J. Bacteriol.* **194**: 551–552.
- Waller, BJ and Lipscomb, JD (1996) Dioxygen activation by enzymes containing binuclear non-heme iron clusters. *Chem. Rev.* **96**: 2625–2658.
- Wang, D, Xia, W, Kumar, KS, and Gao, K (2017) Increasing copper alters cellular elemental composition (Mo and P) of marine diatom. *Ecol. Evol.* **7**: 3362–3371.
- Wang, VC-C, Maji, S, Chen, PPY, Lee, HK, Yu, SSF, and Chan, SI (2017) Alkane oxidation: methane monooxygenases, related enzymes, and their biomimetics. *Chem. Rev.* **117**: 8574–8621.
- Wang, Y, Naumann, U, Wright, ST, and Warton, DI (2012) Mvabund- an R package for model-based analysis of multivariate abundance data. *Methods Ecol. Evol.* **3**: 471–474.
- Warnken, KW, Zhang, H, and Davison, W (2006) Accuracy of the diffusive gradients in thin-films technique: diffusive boundary layer and effective sampling area considerations. *Anal. Chem.* **78**: 3780–3787.
- Wasylenko, LE, Anbar, AD, Liermann, L, Mathur, R, Gordon, GW, and Brantley, S (2007) Isotope fractionation during microbial metal uptake measured by MC-ICP-MS. *J. Anal. At. Spectrom.* **22**: 905–910.
- Webb, CO, Ackerly, DD, Mcpeek, MA, and Donoghue, MJ (2002) Phylogenies and community ecology. *Annu. Rev. Ecol. Syst.* **33**: 475–505.
- Webb, HK, Ng, HJ, and Ivanova, EP (2014) The family Methylocystaceae. In, Rosenberg, E., DeLong, E.F., Lory, S., Stackebrandt, E., and Thompson, F. (eds), *The Prokaryotes - Alphaproteobacteria and Betaproteobacteria*. Springer-Verlag Berlin Heidelberg, pp. 341–347.
- Weiss, S, Treuren, W Van, Lozupone, C, Faust, K, Friedman, J, Deng, Y, et al. (2016) Correlation detection strategies in microbial data sets vary widely in sensitivity and precision. *ISME J.* **10**: 1669–1681.
- Wen, X, Yang, S, and Liebner, S (2016) Evaluation and update of cutoff values for methanotrophic pmoA gene sequences. *Arch. Microbiol.* **198**: 629–636.

- Wetzel, RG (2001a) 14 – Iron, sulfur, and silica cycles. In, *Limnology - Lake and River Ecosystems*. Academic Press, pp. 289–330.
- Wetzel, RG (2001b) 21 – Sediments and microflora. In, *Limnology - Lake and River Ecosystems*. Academic Press, pp. 631–664.
- Wetzel, RG (2001c) *Limnology: Lake and River Ecosystems* Wetzel, R.G. (ed) Academic Press.
- Whittenbury, R, Phillips, KC, and Wilkinson, JF (1970) Enrichment, isolation and some properties of methane-utilizing bacteria. *J. Gen. Microbiol.* **61**: 205–218.
- Wiesenburg, DA and Guinasso Jr., NL (1979) Equilibrium solubilities of methane, carbon monoxide, and hydrogen in water and sea water. *J. Chem. Eng. Data* **24**: 356–360.
- Wuebbles, DDJ, Hayhoe, K, and K, H (2002) Atmospheric methane and global change. *Earth-Science Rev.* **57**: 177–210.
- Xing, Z, Zhao, T, Zhang, L, Gao, Y, Liu, S, and Yang, X (2018) Effects of copper on expression of methane monooxygenases, trichloroethylene degradation, and community structure in methanotrophic consortia. *Eng. Life Sci.* **18**: 236–243.
- Xue, H, Gächter, R, and Sigg, L (1997) Comparison of Cu and Zn cycling in eutrophic lakes with oxic and anoxic hypolimnion. *Aquat. Sci.* **59**: 176–189.
- Xue, H and Sigg, L (2002) A review of competitive ligand-exchange-voltammetric methods for speciation of trace metals in freshwater. *Environ. Electrochem.* **811**: 336–370.
- Yimga, MT, Dunfield, PF, Rieke, P, and Liesack, W (2003) Wide distribution of a novel pmoA-like gene copy among type II methanotrophs, and its expression in *Methylocystis* strain SC2. *Appl. Environ. Microbiol.* **69**: 5593–5602.
- Zahn, JA and DiSpirito, AA (1996) Membrane-associated methane monooxygenase from *Methylococcus capsulatus* (Bath). *J. Bacteriol.* **178**: 1018–1029.
- Zhang, H and Davison, W (1995) Performance characteristics of diffusion gradients in thin films for the in situ measurement of trace metals in aqueous solution. *Anal. Chem.* **67**: 3391–3400.
- Zhang, H and Davison, W (2015) Use of diffusive gradients in thin-films for studies of chemical speciation and bioavailability. *Environ. Chem.* **12**: 85–101.
- Zigah, PK, Oswald, K, Brand, A, Dinkel, C, Wehrli, B, and Schubert, CJ (2015) Methane oxidation pathways and associated methanotrophic communities in the water column of a tropical lake. *Limnol. Oceanogr.* 553–572.

Acknowledgements

This dissertation chronicles a crucial part of my life. I have discovered new facades of my nature, which will benefit my future. I would like to thank a few people.

First and foremost I would like to express my gratitude to my main supervisor Bernhard Wehrli. Thank you Bernhard for giving me the chance to dive deep into a completely new world - the world of applied science and more particularly in Aquatic Chemistry. Thank you for your trust, the fundamental freedom of research, for your open door and for your inputs within my thesis. I very much admire your incredible general knowledge. The get-togethers organized by you and Tine at your home and your birthday celebration on top of Rigi were great and always filled with warmth.

Secondly, but not less importantly, I would like to thank my second supervisor Helmut Bürgmann. Helmut, I very much appreciate that you have opened your doors and invited me to be part of your Microbial Ecology group. As a chemist by training with only minor knowledge of microorganisms, it was a pleasure to sense your spark and enormous enthusiasm about this research field. This has inspired me and automatically carried me along. Besides microbiology, you have also taught me many new words, like for example “nadir”, and broadened my English writing tremendously.

I would like to express my gratitude to my third supervisor Laura Sigg. Laura, you are a great expert in trace metal chemistry, and I was very thankful that you introduced me to the complex world of small molecules. Many thanks for taking care of me at my first conference abroad (I remember well the hot and full train ride), your great inputs, regular supportive e-mails and for asking upon my wellbeing. I very much appreciate that you supervised me, even though you were getting to the time of retirement. All the best for the next chapter of your life.

Thanks to Carsten Schubert for his supervision in terms of methane and elemental analysis. This has given great additional value to my thesis. Particularly in the last phase of my PhD, your funny emails always enlightened a hard day of writing. Great thanks also go to Geri Furrer for taking particular care of our Aquatic Chemistry group far away from Kastanienbaum, your scientific, administrative, as well as life support. I wish

to extend my thanks to Martin Ackermann for being in my committee and for co-examining this thesis. I very much appreciate the good discussion we had before Christmas to get to know each other.

Without our field and lab support, our administrative staff and our major of technical service in Kastanienbaum, this thesis would have never been possible. Andreas Brand, Chregu Dinkel, and Wisi Zwysig, I would like to thank you for all your help and effort in coordinating the logistics of the field campaigns along with your support during field work and for continuously discussing data with me. It was always a great pleasure and fun with you on the boat. Thank you very much Karin Beck for your immense persistence in teaching me about micro- and molecular biology. The nice rides between Kastanienbaum and Zurich were always a great end to a hard day of work. Serge Robert and Patrick Kathriner, thank you very much for your great help in the lab, your open ears for discussions and input on my sampling strategies and data. Many thanks also go to Gijs Nobbe for his assistance in the methane lab in the beginning of my thesis. Rest in peace! A big thank you David Kistler in Dübendorf, for your continuous support and willingness to analyse my tremendous amount of copper samples and always welcoming me in your office. Luzia Fuchs, Patricia Achleitner and Eliane Scharmin, you all played a crucial role for facilitating my overnight stays in Kastanienbaum, but also in the overall administrative work, you made my life much easier. Last but not least, Beat Kienholz, without you, Kastanienbaum would not be what it is. You were always willing to help me with any kind of problem, even when you were overloaded with work. Thanks for the great talks and for always dropping me off at the station.

Thanks go to Niksa Odzak for mentoring me with the use of the DGT method and helping me constructing the units. It was an honour to learn from you and to have lively discussions about data and life. I would like to thank Mary-Lou Tercier-Waeber for introducing me to the VIP technique and always answering my questions with great detail. Ruth Henneberger, without you I could have never managed these small beasts. Thank you for the endless discussions about MOB maintenance and molecular analysis.

The scope of this work would have not been possible without my Bachelor student Tanja Beck, my HiWi Nora Minas and my scientific assistant Karolin Kleffel. Thanks so much for all your hard work, inputs, and the time and energy you put into this project.

Special thanks go to my present and past ETH office crew: Marie, Elisa, Désirée, Scott – Juliana, Till, Stephanie, Tim, Alissa, Nathalie, Nina, Marie-Ève, Sébastien, Jasmin, Nuttakan, and Tonya. Thanks for

sharing the office space, coffee and ice cream breaks, lunches on the rooftop, dinners at home, and much more. It was always fun to work in such a nice environment.

Many thanks to the group in Kastanienbaum: Ulrike, Nadine, Kirsten, Magdalena, Ulrika, Typhaine, Franzi, Bene, Fabian, Adrien (R.I.P.), Oli, David, Raoul, Matthias, Patrick, Philipp, Jaime and Gabriel. The daily lunches were always a relaxing break. I enjoyed the warm and welcoming atmosphere during all the special activities: Badehüsli and Christmas parties, BBQs, 100 year anniversary, Poker nights, and many more. Special thanks go to Rohini, my office mate in Kastanienbaum. We have undergone many ups and downs together, and I am glad to have had you always by my side.

To my most amazing friends Sibylle and Lucie. I am happy to have had you in my life for such a long time and for sharing this experience of doing a PhD. Thank you very much for your endless support. Dilia, Nicole, Salomé, Fanny, Livia, Tamara, Betty, Rebi, Gabriela, Evelin, Anna, Sandra, Yael, Bianca, Simi, Martina, Ruth, Anne-Sophie, Maria, Jussi, Ben, Christoph, Simon, Hans and Andreas. Thank you very much for your friendship, for always being here for me and I am looking forward to spending more time with you again.

I am very fortunate to have my parents, Silvia and Raymond, and my brothers, Alain and Dennis. You are such an important part of my life. Thanks for your dedicated support and your encouragement during not only my dissertation, but my whole life, for your pride and for standing behind me in all my decisions.

Very special thanks go to my beloved Remo. Without you, this thesis would have not been finished. Thanks for standing always by my side, your everlasting patience, for your dedicated research enthusiasm and great help concerning my data.